31 OCTOBER 1967

K-14-67-3

FINAL REPORT

A STUDY OF CRYOGENIC CONTAINER THERMODYNAMICS DURING PROPELLANT TRANSFER

VOLUME II | FINAL ENGINEERING REPORT

X68-10447
(ACCESSION NUMBER)
(THRU)
307
(PAGES)
50
(CODE)
CR#90352
(NASA CR OR TMX OR AD NUMBER)
33
(CATEGORY)
FF No. 602(D)
AVAILABLE TO U.S. GOVERNMENT AGENCIES AND CONTRACTORS ONLY

CRYOGENIC STAGE PROGRAMS

LOCKHEED MISSILES & SPACE COMPANY / SUNNYVALE, CALIFORNIA

K-14-67-3

A STUDY OF CRYOGENIC CONTAINER THERMODYNAMICS DURING PROPELLANT TRANSFER

VOLUME II FINAL ENGINEERING REPORT

Contract NAS 8-20362

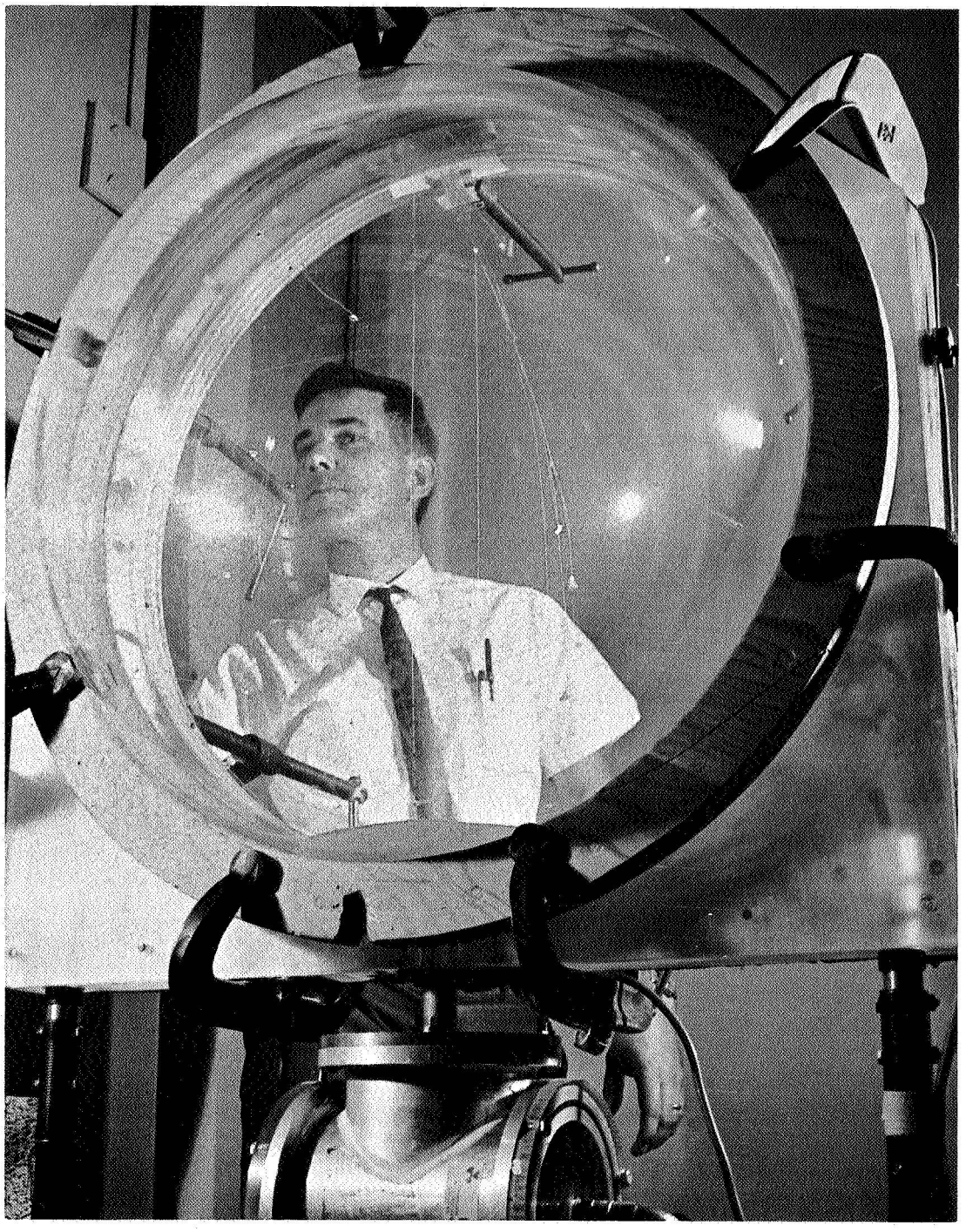
Prepared for
GEORGE C. MARSHALL SPACE FLIGHT CENTER
HUNTSVILLE, ALABAMA

R. M. VERNON
PROJECT LEADER

J. J. BROGAN
PROGRAM MANAGER

CRYOGENIC STAGE PROGRAMS

LOCKHEED MISSILES & SPACE COMPANY
SUNNYVALE, CALIFORNIA



Two-Foot Diameter Transparent Tank

FOREWORD

This report was prepared by the Cryogenic Stage Programs organization of the Research and Development Division, Lockheed Missiles & Space Company, (LMSC) for the George C. Marshall Space Flight Center (MSFC) of the National Aeronautics and Space Administration (NASA).

The work reported herein was performed under NASA Contract NAS 8-20362, "Study of Cryogenic Container Thermodynamics During Propellant Transfer", under the technical direction of the NASA Contract Monitor, Mr. Howard F. Trucks of the Fluid Mechanics and Thermodynamics Branch, Propulsion and Vehicle Engineering Laboratory, NASA/MSFC.

This report describes the major results of the subject study. This report is the second of six volumes comprising the contract final report. The titles of the individual volumes are as follows:

Volume I	Summary
Volume II	Final Engineering Report
Volume III	Transfer Line Thermodynamic Analysis
Volume IV	Receiver Tank Thermodynamic Analysis
Volume V	Complete System Thermodynamic Analysis
Volume VI	Test Data Summary

Primary contributors to the study were:

● Literature Survey and Preliminary Calculations	T. C. Fugate G. D. Bizzell
● Transfer Line Analysis	M. M. McNally
● Tank Fill Analysis	S. E. Hurd
● Flow Phenomena Tests	G. C. Vliet
● Scaling Law Verification and Complete System Tests	J. H. Young

Close coordination was maintained during this study with Mr. W. G. Steward of the National Bureau of Standards, Institute for Materials Research, Cryogenics Division, where a related analytical and experimental program on transfer line chill-down is in progress. The assistance of Mr. Steward and his associates in the performance of this work is gratefully acknowledged.

R. M. Vernon
Project Leader

J. J. Brogan
Program Manager

CONTENTS

Section		Page
1	INTRODUCTION	1
2	SUMMARY OF RESULTS	5
3	TRANSFER LINE ANALYSIS	15
4	TANK FILL ANALYSIS	17
5	DIMENSIONAL ANALYSIS	19
6	COMPUTER PROGRAMMING	21
7	MODELING LAWS STUDY	23
8	FLOW PHENOMENA TESTS	31
9	SCALING LAW VERIFICATION TESTS & COMPLETE SYSTEMS TESTS	153
10	IMPLOSION-PREVENTION TECHNIQUES	211
11	CONCLUSIONS	253
12	REFERENCES	257
APPENDIX A	CALIBRATION OF LIQUID VOLUME FRACTION METER	259
APPENDIX B	LITERATURE SURVEY AND PRELIMINARY CALCULATIONS	273
INDEX		287
ILLUSTRATIONS		291
TABLES		301

Section 1

INTRODUCTION

1.1 PROGRAM OBJECTIVES AND APPROACH

This report describes the results of a study of cryogenic container thermodynamics during propellant transfer. The purpose of this study is to provide analytical and empirical descriptions of the transient phenomena occurring in cryogenic transfer lines and receiver tanks during initial propellant transfer. A further basic objective is to identify those conditions which give rise to the possibility of tank implosion, and to establish the procedures and/or systems necessary to eliminate this possibility. These objectives have been accomplished by the following approach:

1. Derive scaling laws and investigate the feasibility of using data from small-scale experiments to verify solutions of potential problems associated with cryogenic transfer to large-scale (S-IC, S-II, S-IVB, and MMM) tanks. Perform small-scale tank experiments to verify scaling laws and other analytical procedures.

2. Perform a detailed analysis to predict the variation of parameters affecting transfer line cooldown during propellant transfer, and specify inlet conditions to the receiver tank as a function of time. Construct experimental models to verify the analysis. Establish procedures which will produce rapid chilldown with minimum oscillatory flow.

3. Perform analyses to predict internal thermodynamics of LO_2 and LH_2 receiver tanks during initial propellant transfer.

At the beginning of this study this basic procedure was analyzed and subdivided into a number of specific tasks. These tasks are summarized in the next paragraph; detailed objectives of each task and the results obtained in the course of this study are presented in Sections 2 through 13.

1.2 TASK SUMMARY

A brief summary of the study tasks to be performed is presented below:

1. Survey the literature concerning transfer line and receiver tank thermodynamics and receiver tank implosion
2. Perform preliminary hand calculations of the bulk exchange of energy and mass in receiver tank and transfer line
3. Derive the equations governing the processes of mass, momentum, and energy exchange in a cryogenic transfer line
4. Formulate equations governing the processes of mass, momentum, and energy exchange in a cryogenic receiver tank
5. Derive the dimensionless parameters which characterize the transport of mass, momentum, and energy in cryogenic transfer lines and receiver tanks during propellant transfer
6. Write and debug digital (or analog) computer programs for the numerical solution of equations resulting from the transfer line and receiver tank thermodynamic analyses
7. Develop practical modeling rules for planning and evaluating flow phenomena and scaling tests
8. Prepare a test plan and perform tests to investigate the flow phenomena occurring in a cryogenic transfer line during propellant transfer.

9. Prepare a test plan and perform tests to investigate the flow phenomena occurring in a cryogenic receiver tank during propellant transfer

10. Plan and perform tests to verify experimentally the results of the scaling law and modeling analyses (Tasks 5 and 7)

11. Plan and perform complete system tests to verify the coupled line-receiver tank analytical model during transient fill conditions.

12. Perform an analysis to describe those conditions under which receiver tank implosion will occur and design methods of preventing implosion

13. Plan and perform tests to demonstrate the effectiveness and confirm the predicted performance of the implosion-prevention techniques evolved in Task 12.

Section 2

SUMMARY OF RESULTS

Lockheed Missiles & Space Company has conducted a comprehensive study of the transient thermodynamic processes occurring when cryogenic fluid is transferred from one vessel to another through a cryogenic transfer line. A major goal of this study was the prediction of the pressure change within the tank being filled with the cryogenic fluid and, in particular, the specification of fill conditions which result in a pressure drop in this tank.

The following brief summary of results is provided as a synopsis of conclusions which are discussed in detail in later sections of this volume. For a general summary of the methods used and the conclusions obtained throughout the course of the study, the reader is referred to Volume I of this report.

As illustrated by the task summaries in Section 1, the approach used to study the fluid transfer problem in this program was to analyze the thermodynamic processes occurring in a cryogenic transfer line separately from those occurring in a tank which is being filled by a cryogenic fluid. Upon confirmation of the adequacy of the analytical models (by comparison with test data on transfer line chilldown and tank fill data) the computer programs describing these models were coupled to simulate a complete fluid transfer system and the analytical results compared with data from tests on complete fill systems using both small and large size tanks.

A summary of the capabilities of the three computer analyses developed during this study is given in Table 1.

2.1 TRANSFER LINE CHILLDOWN

A computer analysis of the processes of heat, mass and momentum exchange occurring during transfer line chilldown has been derived and results of the analysis compared with test data.

Very good agreement was obtained between measured temperature-time histories, particularly for long transfer lines. Predictions of overall chilldown time within $\pm$ 15% of the data were obtained. These correlations were obtained for line diameters of 1/2 inch and 5/8 inch and line lengths of 200, 28 and 16 feet. Data were correlated for both liquid hydrogen and liquid nitrogen in the long (200-foot) transfer line, and for nitrogen only in the shorter lines. (A long transfer here is defined as one whose length-to-diameter ratio is greater than 3800 when the flowing fluid is liquid hydrogen and 475 when the fluid is liquid nitrogen or oxygen). As the length-to-diameter (L/D) ratio is decreased, the transient chilldown process is increasingly dominated by pressure and flowrate surges in the fluid. An analytical method of predicting the frequency and magnitude of these oscillations has also been derived; agreement between predicted and measured values of the frequency and magnitude of these oscillations was generally between $\pm$ 10% of the measured values.

2.2 TANK FILL THERMODYNAMICS

A computer analysis of the processes of mass, momentum and energy exchange occurring during tank fill has been derived and results of the analysis compared with test data. The results of these comparisons showed that

TABLE 1 SUMMARY OF COMPUTER PROGRAM CHARACTERISTICS

	Transfer Line Chilldown Program (FLOW)
Data Input	Fluid Inlet Pressure and Temperature; Fluid Properties, Line Dimensions and Material Properties; Exist Pressure. Number of Nodal Divisions to be used in the Finite Difference Approximation; Total Run Time , Initial Conditions.
Output	Position of Liquid, Two-Phase and Vapor Interfaces as a function of time; Line Temperature History and Fluid Temperature, Pressure, and Velocity History at each node; Heat Rate at Each Node; Vapor quality at each Node in Two-Phase Region.
Assumptions and Restrictions	Inlet and Exit conditions must be constant with time; Fluid may not be saturated at a pressure higher than the inlet pressure (i.e., no inlet pressure drop is computed); Line is assumed to be perfectly insulated. Surging parameters not computed. Choking in the gas region is accounted for, but not in the two-phase region.
	Tank Fill Computer Program (TNKFIL)
Data Input	Inlet mass flowrate, quality and temperature; Fluid and tank wall material properties; Heat transfer correlations for varying fluids, Tank vent rate, characteristic droplet diameter; Initial conditions and Total Run Time.
Output	Tank Ullage Pressure, Fluid Mass Distribution, Fluid Temperature Distribution and Tank Wall Temperature Distribution; all as a function of time.
Assumption and Restrictions	Separate heat transfer correlations required for varying fluid orientations and gravity levels; however, there is no restriction on program capability if these qualities are specified. Fluid inlet flowrate, quality temperature and vent rate may be varied with time if desired.

LOCKHEED MISSILES & SPACE COMPANY

Table 1 (Concluded)

Complete Fill System Computer Program (FILL)	
Data Input	Fluid inlet pressure and temperature. Pressure as a function of time at the end of the first pipe node if inlet pressure drop is desired. Fluid properties, Line Dimensions, Material properties, Total number of pipe nodes, Tank vent rate, Characteristic Droplet diameter, Initial Conditions and Total Run Time.
Output	Position of liquid, two-phase and vapor regions as a function of time, line temperature, fluid temperature, pressure and velocity, all as a function of time for each node in the line, mass flowrate at inlet to the line and inlet to the tank, heat rate to the fluid in the line, vapor quality distribution in the two-phase region, tank ullage pressure, temperature and fluid mass distribution, tank wall temperature distribution, line surge pressure and frequency as a function of time.
Assumptions and Restrictions	Inlet pressure must be constant with time, but an option is provided to allow the fluid to flash across a specified pressure drop at the inlet to the pipe. Surge pressures and frequencies are computed but are not used in the line chilldown computations. Choking conditions in both the vapor and two-phase regions is accounted for. Pressure buildup due to fill of initial, warm gas is also accounted for.

LOCKHEED MISSILES & SPACE COMPANY

the initial tank pressure response was highly dependent on a droplet diameter which characterizes the distribution of droplet sizes in the fluid spray entering the tank. Prior to attempts at test data correlation, neither an analytical nor an empirical method of predicting this parameter was available. As a result of comparisons between analytical predictions and test data, an empirical method of specifying the characteristic droplet diameter was obtained.

By specifying the correct value for the characteristic droplet diameter, agreement between measured and predicted tank pressures during fill within $\pm$ 0.15 psia were obtained in fill tests with nitrogen. Corresponding values of ullage vapor temperatures were predicted within about $\pm$ 5% of the absolute values of the measured temperatures.

Similar predictions of tank pressure response and ullage temperature distribution during fill were also obtained for tests on both large-and small-size tanks when the inlet was covered with a screen or a flat-plate baffle. A substantial correlation (using the TNKFIL program) of test data for liquid hydrogen was not possible. This was due to the large flowrate of gas evolved by rapid boiling of the hydrogen in the transfer line during testing.

The tank-fill analysis may also be used, with some modifications, for predictions of tank pressure response and temperature distributions for fluid transfer under varying gravitational accelerations and with fluid entering the tank from various orientations with respect to the direction of acceleration.

2.3 THERMODYNAMIC ANALYSES OF A COMPLETE FILL SYSTEM

The Complete Fill System Computer program combines the capabilities of line-chilldown and tank-fill programs, as indicated in Table 1.

During execution of this program the conditions at the exit of the transfer line are provided as inputs to the tank-fill program; conversely, as new values of tank pressures are computed, they are communicated to the line-chilldown program. The complete program thus simulates the operation of a complete fill system.

However, in addition to the capabilities of the separate programs, several additional features were added to the Complete Fill System Computer Program during the course of data correlation for complete system tests. These features include a provision for an inlet pressure drop (as would be experienced across an inlet valve) with or without subcooled inlet fluid conditions. Thus the possibility of the fluid flashing into a two-phase mixture at the inlet to the line (as observed in several complete system tests) is accounted for. Also, fluid flowrates are limited when a two-phase fluid as well as a vapor, experiences choking conditions within the transfer line. Computations of surge frequency and surge pressure are also performed, but are not used in the chilldown computations.

As indicated above, the modifications to allow for an inlet pressure drop, as well as choking in the two-phase region, were found to be required to obtain agreement with data obtained during complete system fill tests.

Comparisons with test data from four complete system tests were made and the agreement between predictions and test data is quite good. During three of the four runs for which correlations were attempted, an implosion condition (drop in tank pressure below its initial valve) was observed. The predicted pressure response for these tests is generally within 1 psi of the

measured values.

The complete fill system computer program, like the tank-fill program, may be used for fill from varying orientations and at any gravity level.

2.4 TEST PROGRAM

A total of 50 tests were performed throughout the course of the study. The type of test, the apparatus used, and the number of runs for which data were obtained and reduced is summarized in Table 1a . The type of tests performed are classified as Flow Phenomena Tests, Scaling Law Verification Complete System Tests, and Implosion Prevention Techniques Tests.

The purpose of the flow phenomena tests was to record observations of the phenomena occurring within a tank during the initial phases of fill and in a transfer line during the chilldown process. These tests were performed on the line and tank separately in order to provide data against which the separate analytical models could be checked. A primary goal of this testing was to provide sufficiently detailed measurements of the pertinent variables so that the mechanisms assumed to control the processes of mass and energy transfer in the analytical models could be verified. Thus, for the tank fill tests, measurements were made of the ullage pressure, inlet flowrate and quality, and the temperature distribution throughout the tank. In addition, high speed movies were made of the flow inside the tank. During the transfer line tests measurements were made of the pipe-wall temperature distribution, fluid

TABLE 1a TEST PROGRAM SUMMARY

Type of Test	Test Apparatus	Test Fluid	Total Number of Runs
Flow Phenomena Testing-Quasi-Steady-State Tank Fill	Two-Foot Diameter Plexiglas Tank	Liquid Nitrogen	9
Flow Phenomena Testing-Transfer Line Chilldown	Half-Inch Diameter Copper Transfer Line (L/D=672)	Liquid Nitrogen	9
Scaling Law Verification and Complete System Testing	Half-Inch Line Coupled to Two-Foot Tank	Liquid Nitrogen	1
	Three-Inch Copper Transfer Line Coupled to Five-Foot Diameter Aluminum Tank	Liquid Nitrogen	4
		Liquid Hydrogen	4
Implosion Prevention Techniques Testing	Half-Inch Line Coupled to Two-Foot Tank	Liquid Nitrogen	4
	Three-Inch Line (L/D=53) Coupled to Five-Foot Tank	Liquid Nitrogen	7
		Liquid Hydrogen	12

temperature distribution, pressure distribution and fluid quality and flowrate.

The evolution of the tank-fill and line-chilldown analytical models was clearly a result of this test philosophy.

The tank-fill analytical model, for example, was initially formulated using a single ullage vapor region having a uniform temperature. In attempting to correlate data from initial flow phenomena tests, it was found that data for the vapor region were not well represented by the single ullage vapor region model.

Consequently, a new analytical model was devised in which the vapor region was divided into three zones, with mass and energy balances being performed separately on each zone. The revised model was provided results which were in much better agreement with the flow phenomena test data.

The major purpose of the Scaling Law Verification and Complete System Tests was to provide data on large-and small-size apparatus for comparison with results of the tank-fill model and the complete-fill system computer model. An additional objective was the verification of model laws for the tank-fill and transfer-line chilldown processes. The instrumentation for these tests was essentially the same as that for the flow phenomena tests. One test only was run on the small-size apparatus due to failure of the test tank during the first run. The remaining tests were run on a large-size (five-foot diameter) tank

using both liquid nitrogen and liquid hydrogen.

The objective of the implosion prevention techniques tests was to demonstrate the effect of a device for suppressing any tendency for an ullage pressure drop during the initial phases of the fill process, and to provide data for comparison with the analytical model. The device selected, a flat, disk-shaped baffle, was successful in completely suppressing any tendency for a drop in ullage pressure during these tests. In addition to the baffle tests, the effect of a screen over the inlet on the tank pressure response was also investigated. Tests with both nitrogen and hydrogen showed that the screen produced a greater drop in tank ullage pressure, for similar fill conditions, than was observed with tests with an unobstructed inlet.

Section 3

TRANSFER LINE ANALYSES

The objective of this task is to formulate the equations governing the processes of mass, momentum, and energy exchange in a cryogenic transfer line and, by using appropriate simplifying assumptions, obtain a reduced form of the equations suitable for analog computer solution or numerical solution on a digital computer.

These objectives have been completely accomplished and are described in detail in Volume III of this report. A brief discussion of the major results of this task will be presented here.

The literature search has indicated that analysis of the unsteady two-phase flow phenomena associated with transfer line chilldown has been attacked in two general ways: (1) examination of the flow oscillations via a pseudo spring-mass analogy, and (2) examination of the overall chilldown process by a conservation law approach. The analytical approach which has been evolved in this study has been directed toward the following major goals:

- An investigation of flow oscillations occurring during the chilldown process
- The construction of a transfer line chilldown computer model utilizing a finite-difference procedure applied directly to the heat, mass, and momentum balances on the fluid flowing in the transfer line.

- An investigation of the feasibility of a general solution to the conservation law equations.

A digital computer program has been completed which calculates fluid and pipe-wall temperatures at any point along the line as a function of time, as well as fluid pressure, heat transfer rates, and the thermodynamic state of the fluid for the averaged, quasi-steady progression of the fluid down the tube. This program is described in Volume III of this report.

Superimposed on the mean chilldown process are the oscillatory processes. These oscillations, while complicated and influenced by many variables, have been successfully interpreted by a mechanical analog model. The solution to the equations describing the oscillatory processes in the line during chilldown has been programmed into the Complete System Computer Program described in Volume V of this report. The correlation between analytical results obtained from the line chilldown program and the complete system computer program are described in Sections 8, 9 and 10 of this volume.

An investigation of the feasibility of a general solution to the convervation law equations desclosed that such a solution was apparently beyond the capability of present numerical solution techniques. Although several methods of integrating the general conservation equations were investigated, a satisfactory method was not uncovered, and an investigation of the rapid oscillatory fluid motion was performed separately from the more gradual chilldown process, as described above.

Section 4

TANK FILL ANALYSIS

The objectives of this task are to formulate the equations governing the processes of mass,momentum, and energy exchange in a cryogenic receiver tank and to reduce these equations to a form suitable for analog or digital computer solution.

These objectives have been accomplished and are described in detail in Volume IV of this report. As indicated in Section 2, the model used in this analysis evolved as a result of attempts to correlate test data on small-size test tanks. This model is designed so that a proper accounting of mass and energy transfer within the tank is in accordance with these test data. The resultant analysis is capable of predicting (with certain restrictions) the temperature and pressure distribution in a tank being filled with a fluid, given the initial state of the fluid within the tank.

Very good predictions of tank pressure response, as well as ullage temperature distribution during fill, have been obtained for both large-and small-size tanks. The results of the comparison between this analysis and test data for a variety of fill conditions are described in Sections, 9,10 and 11 of this volume.

Section 5
DIMENSIONAL ANALYSIS

The objective of this task is to specify those dimensionless parameters which characterize the transport of mass, momentum, and energy in cryogenic transfer lines and receiver tanks during propellant transfer, and to investigate the significance of these dimensionless groups in modeling transfer line and receiver tank phenomena.

The results of the transfer line dimensional analyses are presented in Volume III of this report.

The results of the receiver tank general scaling law analysis are presented in Appendix A to this Volume, as are the results of the scaling rules for the specialized analyses of the receiver tank fill.

The latter analysis refers to the assumption that the tank fill process may be divided into four sequential phases, as illustrated in Fig. 1. The application of the results of the dimensional analyses to scale modeling of the phenomena occurring during transfer line chilldown and tank fill is described in Section 7.

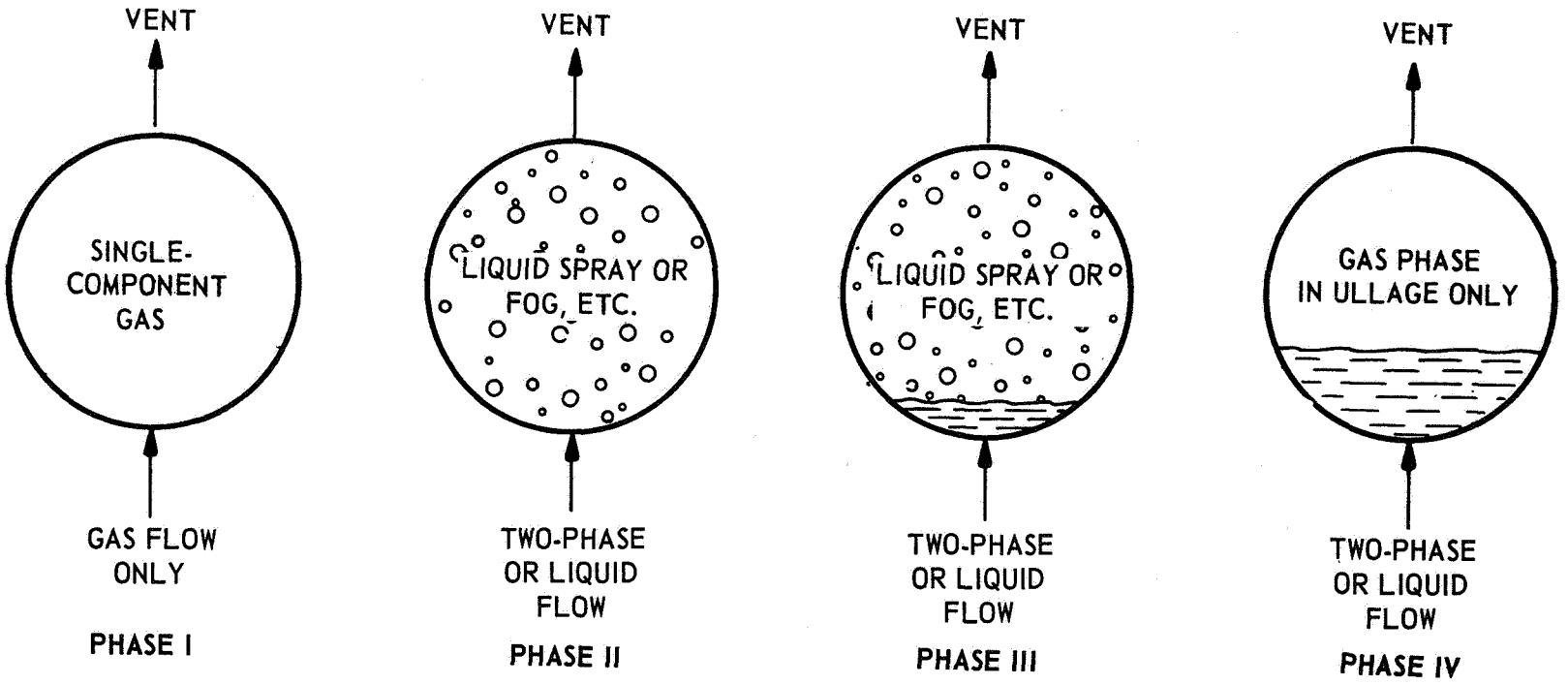


Fig. 1 Sequence of Tank Fill Conditions

Section 6

COMPUTER PROGRAMMING

The objective of this task is to write and debug computer programs for the numerical solution of equations resulting from the transfer line and receiver tank analyses. As a result of this effort, three completely operational computer programs have been developed. The function of these programs is as follows:

- The computation of the wall temperature distribution, fluid temperature distribution, and pressure distribution in a cryogenic transfer line during the chilldown process.
- The computation of the tank wall temperature distribution, fluid temperature distribution and fluid pressure in a tank being filled with a cryogenic fluid.
- The performance of all the above functions, as well as the computation of the period, amplitude and magnitude of pressure oscillations in the transfer line.

The first of these computer programs is titled FLOW, and is described in detail in Volume III of this report. The second of these programs is titled TNKFIL, and is described in Volume IV of this report. The third program, which combines the functions of transfer line chilldown and tank fill programs, is titled FILL, and is described in Volume V of this report. All of these programs were used in the correlation of data presented in Sections 9, 10, and 11 of this volume.

Section 7

MODELING LAWS

The objective of this task is to establish practical modeling rules for planning and evaluating flow phenomena tests, and to provide additional insight into the processes occurring in transfer line chilldown and the tank filling processes.

7.1 TANK FILL MODELING

Typical Saturn V transfer line diameters, fill rates, and vent rates have been used to evaluate the dimensionless groups obtained from the tank fill scaling analysis (see Appendix A to Volume IV of this report). The results of this evaluation are shown in Figs. 2, 3 and 4 . For example, if it is desired that a test be run with nitrogen in a 24-in.-diameter tank to simulate conditions during fill of the S-IVB tank with hydrogen, Fig. 2 can be used. It can be seen that the required test fill rates should range from 2.8 to 17 lb/sec. Fig. 4 is used in the same manner to size the experimental fill line. For example, if simulation of the S-II tank fill line with the 60-in. tank is desired, a fill line diamteter of 1.85 in. should be used.

The results of the scaling analysis have been extended further to provide test conditions for small-diameter tanks using fluids other than nitrogen. The results of this analysis are shown in Table 2, wherein property ratios

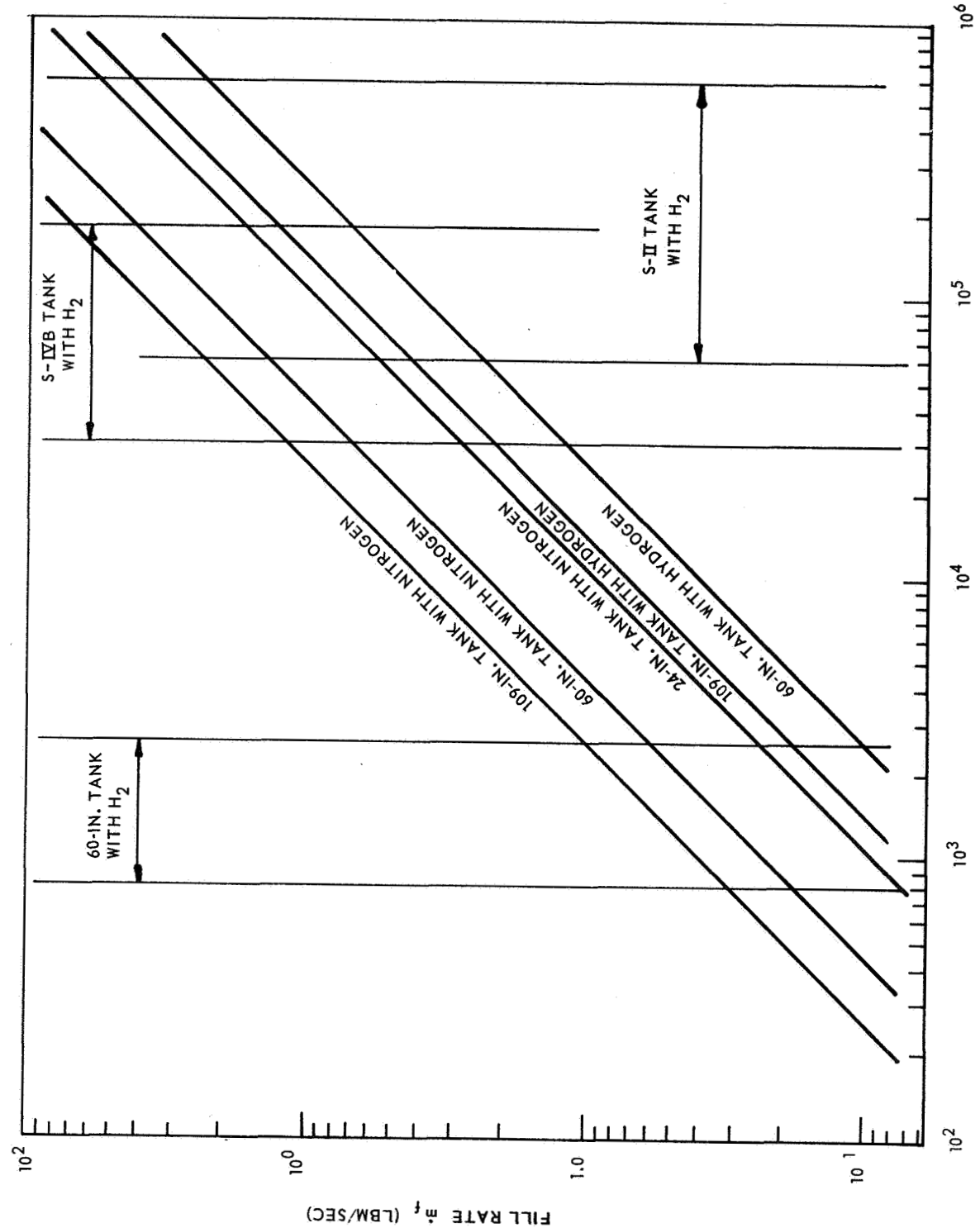


Fig. 2 Fill Rates Required to Simulate Full-Size Tanks

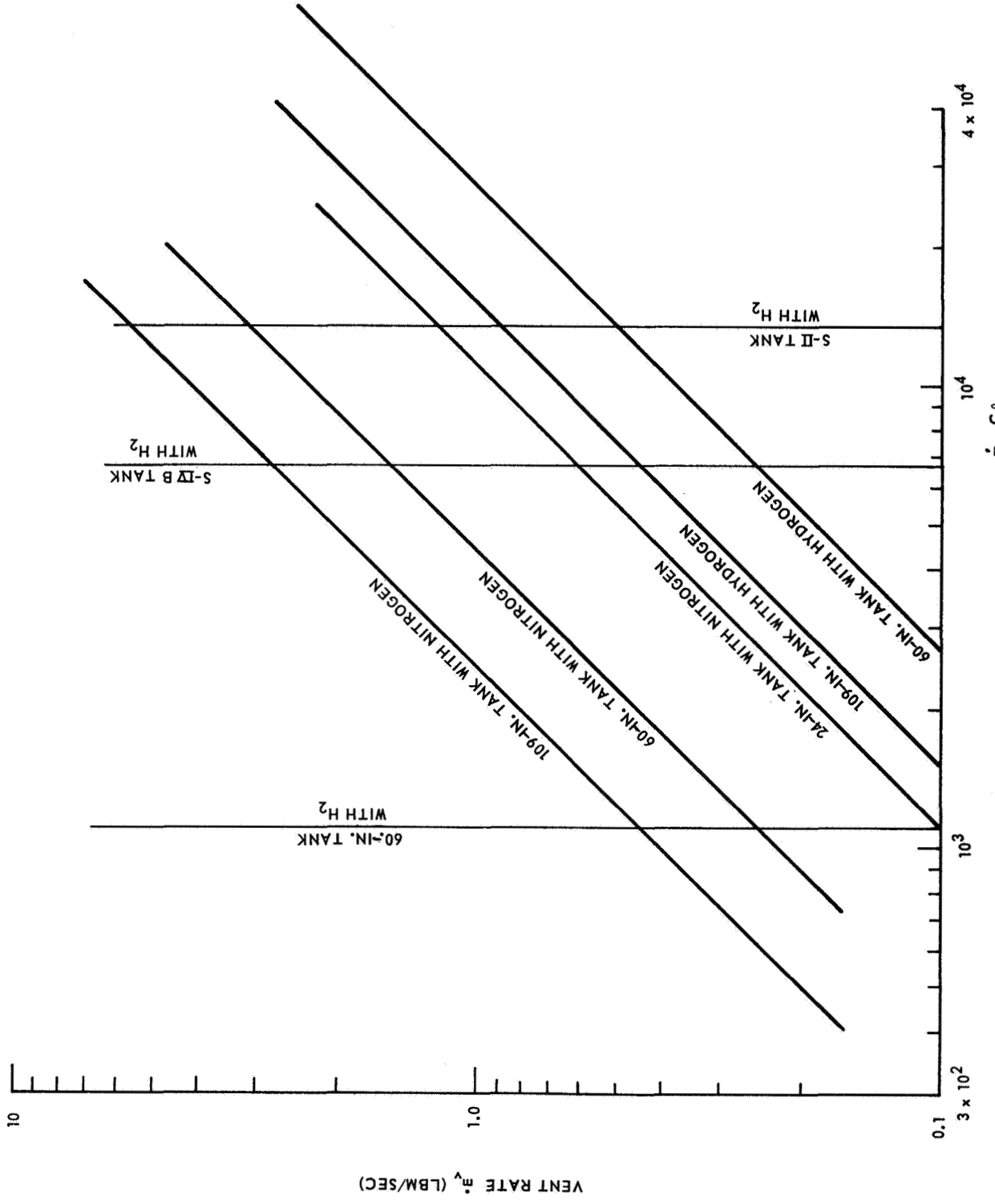


Fig. 3 Vent Rates Required to Simulate Full-Size Tanks

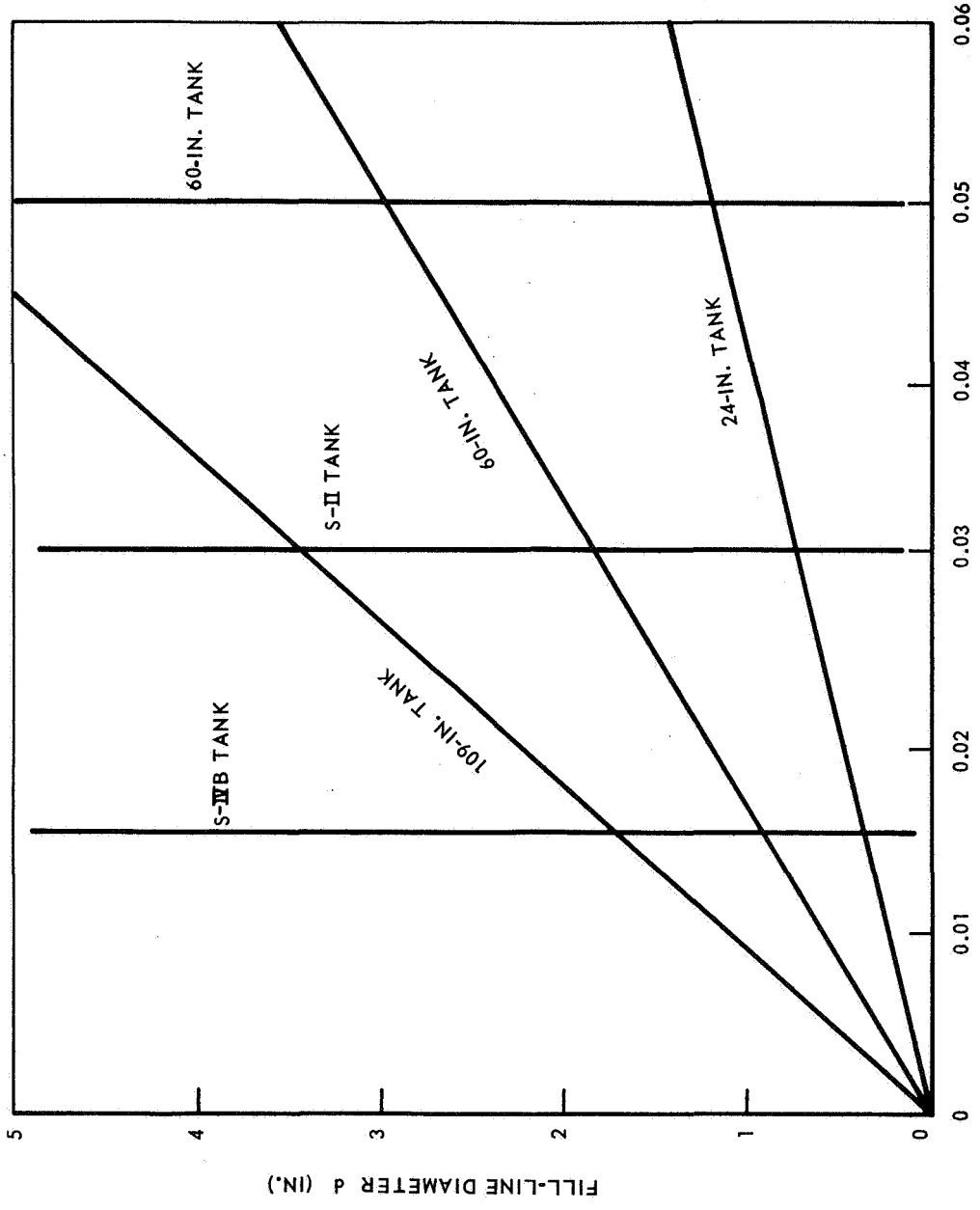


Fig. 4 Full-Line Diameter Required to Simulate Full-Size Tanks

Table 2

Comparison of Fluid Modeling Parameters

Fluid	Symbol	Boiling Point (°R at 1 atm.)	Freezing Point (°R at 1 atm.)	R (Btu/lbm-°R)	C_{p_v} (Btu/lbm-°R)	C_ℓ (Btu/lbm-°R)	k_v (Btu/hr-ft-°F)	k_ℓ (Btu/hr-ft-°F)	μ_v (lbm/hr-ft)	λ (Btu/lbm)	ρ_v (lbm/ft³)	ρ_ℓ (lbm/ft³)	Pr_v	$\frac{R}{C_{p_v}}$	$\frac{C_\ell}{C_{p_v}}$	$\frac{k_v}{k_\ell}$	$\frac{\lambda}{C_\ell}$	$\frac{\rho_v}{\rho_\ell}$
Hydrogen	H_2	(1)37.03	(1)25.2	0.984	(5)2.45	(2)2.33	(5)0.0098	(6)0.069	(6)0.00262	(5)190.4	(8)0.0830	(8)4.43	0.655	0.401	0.951	0.142	81.8	0.0187
Oxygen	O_2	(1)162.6	(1)98.6	0.0621	(5)0.219	(2)0.398	(5)0.0048	(12)0.085	(6)0.0170	(5) 91.7	(6)0.276	(6)71	0.775	0.284	1.82	0.0565	230	0.00388
Helium	He	(1)7.59	(1) 1.7	0.497	(7)1.5	(6)1.11	(6)0.0051	(6)0.0158	(6)0.00485	(5) 8.8	(7)1.04	(7)7.77	1.43	0.331	0.740	0.333	7.93	0.134
Nitrogen	N_2	(1)139.2	(1)113.8	0.071	(5)0.25	(2)0.475	(1)0.0043	(6)0.0805	(6)0.0131	(5)85.2	(6)0.29	(6)50.4	0.761	0.284	1.90	0.0534	179	0.00575
Hexane	$C_6 H_{14}$	(1)515.9	(1)322.0	0.0218	(10)0.365[f]	(2)0.531	(2)0.0077	(2)0.081	(2)0.0145	(2)158	(10)0.245	(1)41.1	0.686	0.0587	1.45	0.0950	297	0.00595
Pentane	$C_5 H_{12}$	(1)557.1	(1)256.3	0.0264	(10)0.409[g]	(11)0.54[b]	(2)0.0090	(2)0.0775	(2)0.0150	(2)145	(10)0.187	(1)39.2	0.683	0.0646	1.32	0.116	268	0.00477
Ethyl Chloride	$C_2 H_5 Cl$	(1)514.5	(1)242.0	0.0306	(3)0.275	(2)0.375	(2)0.0059	(14)0.074	(2)0.0223	(2)161	(9)0.175	(1)56.4	1.04	0.111	1.36	0.084	430	0.00310
N-Butane	$C_4 H_{10}$	(1)490.9	(1)248.7	0.0330	(9)0.391[a]	(2)0.549	(2)0.0078	–	(3)0.0191	(1)165.5	(1)0.169	(1)37.5	0.956	0.0845	1.40	–	302	0.00451
Sulfur Dioxide	SO_2	(1)474.0	(1)356.1	0.0300	(2)0.151	(2)0.312	(2)0.00475	(2)0.126	(2)0.0266	(1)167	(1)0.194	(1)91.2	0.845	0.199	2.06	0.0377	535	0.00213
Iso-Butane	$C_4 H_{10}$	(1)470.0	(1)230.7	0.0336	(9)0.355[c]	(2)0.549	(2)0.0074	–	(3)0.0161	(1)158.5	(1)0.174	(1)37.2	0.773	0.0946	1.55	–	288	0.00467
Methyl Chloride	$CH_3 Cl$	(1)448.6	(1)315.6	0.0396	(9)0.199[c]	(2)0.364	(2)0.00445	(1)0.111	(3)0.0214	(1)184.2	(1)0.155	(1)62.6	0.955	0.199	1.83	0.0400	506	0.00248
Freon 11	$C Cl_3 F$	(4)534.8	(4)292	0.0143	(4)0.135	(4)0.209	(4)0.00452	(4)0.0545	(4)0.0263	(4) 78.4	(4)0.360	(4)92.4	0.785	0.106	1.55	0.0830	375	0.00390
Freon 12	$C Cl_2 F_2$	(4)438.4	(4)212.3	0.0155	(4)0.134	(4)0.240[f]	(4)0.00448	(4)0.0527	(4)0.0263	(1) 71.8	(1)0.404	(4)92.6	0.787	0.115	1.79	0.0850	299	0.00436
Freon 22	$CH Cl F_2$	(4)418.6	(4)204	0.0219	(4)0.152[f]	(4)0.335[f]	(4)0.0049	(4)0.069	(4)0.0254	(4)100.7	(13)0.300	(13)88.0	0.788	0.144	2.20	0.0710	300	0.00341
Freon 113	$C_2 Cl_3 F_3$	(4)577.6	(4)428	0.0102	(4)0.158	(4)0.224	(4)0.00502	(4)0.040	(4)0.0262	(4) 63.1	(4)0.465	(4)94.3	0.823	0.0646	1.42	0.125	282	0.00493
Ammonia	NH_3	(1)432	(1)351.6	0.115	(2)0.49	(2)1.08	(2)0.0105	(2)0.29	(2)0.0194	(1)589.3	(1)0.0555	(1)42.7	0.905	0.235	2.20	0.0362	545	0.00130
Propane	$C_3 H_8$	(1)416	(1)154.6	0.0456	(9)0.389[a]	(2)0.576	(2)0.0063	–	(2)0.0157	(1)183	(1)0.145	(1)36.4	0.970	0.117	1.42	–	318	0.00399
Carbon Dioxide	CO_2	(1)350.7	(1)391[i]	0.0365	(2)0.2	(3)0.457	(2)0.0053	(1)0.042	(2)0.0242	(2)170	(1)0.214	(1)68.8	(2)0.75	0.182	2.28	0.126	372	0.00311
Ethane	$C_2 H_6$	(1)332.5	(1)161.9	0.0640	(2)0.33	1.15[h]	(2)0.0057	–	(2)0.0140	(2)235	(9)0.129	(1)35.7	0.810	0.194	3.48	–	204	0.00361
Ethylene	$C_2 H_4$	(1)305.3	(1)187.1	0.0692	(2)0.29	0.92[h]	(2)0.0048	–	(2)0.0152	(9)207.9	(9)0.130	(9)35.4	0.920	0.238	3.18	–	226	0.00367
Methane	CH_4	(1)201.1	(1)163.2	0.114	(3)0.505	(2)0.83	(2)0.00685	(6)0.110	(3)0.0102	(6)219	(6)0.12	(1)25.9	(2)0.75	0.266	1.64	0.0624	264	0.00463
Methyl Alcohol	$CH_3 OH$	(1)609	(1)316	0.0592	(10)0.390[e]	(3)0.632	(2)0.012	(1)0.10	(2)0.0266	(2)460	(10)0.0763	(1)49.4	0.867	0.152	1.62	0.120	728	0.00155

- Unless otherwise noted, all properties are evaluated at saturation for a pressure of one atmosphere.
- Numbers in parentheses denote references.

Notes:

(a) Evaluated at 60°F
(b) Evaluated at 68°F
(c) Evaluated at 77°F
(d) Evaluated at 86°F
(e) Evaluated at 171°F
(f) Evaluated at 176°F
(g) Evaluated at 187°F
(h) C_ℓ calculated using Kopp's Rule (Ref. 10)
(i) Evaluated at 5.2-atm. pressure

References:

(1) "Handbook of Chemistry and Physics," The Chemical Rubber Co., Cleveland, Ohio (1966)
(2) McAdams, W.H., "Heat Transmission," McGraw-Hill Book Co., N.Y. (1954)
(3) "International Critical Tables, National Research Council of USA," McGraw-Hill Book Co., N.Y. (1929)
(4) Data for various Freons supplied by the DuPont deNemours and Co., Wilmington, Del.
(5) "Handbook of Thermal Design Data for Multilayer Insulation Systems," LMSC-A742592-VI (1965)
(6) Johnson, V.J., "A Compendium of the Properties of Materials at Low Temperature (Phase I), Part I, Properties of Fluids," WADD TR60-56, Wright-Patterson AFB, Ohio, (1960)
(7) "The Thermodynamic Properties of Helium from 3 to 300°K Between 0.5 and 100 Atmospheres," NBS TN154 (1962)
(8) "A Tabulation of the Thermodynamic Properties of Normal Hydrogen from Low Temperatures to 540°R and from 10 to 1500 psia," NBS TN120A (1962)
(9) Matheson Gas Data Book, The Matheson Company, Inc., Ontario, Canada (1966)
(10) Lange, N., "Handbook of Chemistry," McGraw-Hill Book Co., N.Y. (1961)
(11) Marsden, C., "Solvents Guide," John Wiley and Sons Inc., N.Y. (1963)
(12) Seader, J.D., et al., "Boiling Heat Transfer for Cryogenics," NASA CR243 (1965)
(13) ASHRAE Guide and Data Book, Fundamentals and Equipment for 1965 and 1966, ASHRAE, N.Y.
(14) Tsederberg, N.V., "Thermal Conductivity of Gases and Liquids," The MIT Press, Cambridge, Mass. (1965)

for 22 different fluids are compared. The last six columns of this table contain the pertinent property ratios for the various fluids (Pr_v, μ/C_{p_v}, C_v/C_{p_v}, k_v/k_ℓ, λ/C_ℓ, and ρ_v/ρ_ℓ). Numerical equality of values of these quantities for two different fluids implies that, for the purpose of receiver tank testing, one fluid may be replaced by the other. A significant result of this comparison is that liquid oxygen, a relatively hazardous test fluid, may be very closely modeled by liquid nitrogen or Freon 22.

7.2 LINE CHILLDOWN MODELING

The transfer line dimensional* analyses has produced five dimensionless groups whose values must be equal in a model and prototype transfer line. They are

$$\frac{\rho u D}{\mu} = Re \;, \quad \frac{CT}{u^2} = \frac{Pr}{Br} \;, \quad \frac{\rho C u D}{k} = RePr$$

$$\frac{\rho C T D}{\mu u} = \frac{RePr}{Br} \;, \quad \frac{\rho u^2}{P_{EXIT}}$$

If heat production by viscous dissipation is assumed negligible compared to the heat transport by convection and conduction, equality of the Brinkman number

$$Br = \frac{\mu u^2}{k T}$$

may be waived, and the scaling conditions may be satisfied by equality of the Reynold's number, Prandtl number, and the quantity $\rho u^2/p_{exit}$ between model and prototype. Using the subscripts M and P for model and prototype, respectively, the modeling laws for transfer line chilldown may be written as follows:

*(described in Volume III of this report)

$$\frac{(\rho/\mu)_m}{(\rho/\mu)_p} = \frac{(uD)_p}{(uD)_m}$$

and

$$\left(\frac{Ck}{\mu}\right)_m = \left(\frac{Ck}{\mu}\right)_p$$

$$\left(\frac{P_{EXIT}}{u^2}\right)_m \Big/ \left(\frac{P_{EXIT}}{u^2}\right)_p = \frac{\rho_m}{\rho_p}$$

It should be noted that the fluid properties above refer to both liquid and vapor properties.

7.3 "LONG" TRANSFER LINES

Recently Steward (Ref. 17) has developed an alternative form of chilldown analysis which is applicable to relatively long transfer lines. From a knowledge of the pipe size, change in fluid and pipe enthalpy, and the density and velocity of sound in the warm gas, this method allows one to quickly calculate the cooldown time for a simple system. The method gives a rapid means of estimating cooldown times for long, well-insulated transfer lines, and is based on an analysis which assumes zero heat transfer to the gas region and that only liquid and gaseous phases exist within the pipe during chilldown. Using these assumptions, among others, Steward indicates a dependence of the form

$$\frac{\theta u_g^+}{\phi L} = f\left(\frac{\bar{f}L}{D}, \frac{p_i}{p_{EXIT}}\right) \qquad (2)$$

where u_g^+ = velocity of sound in the gas

$\bar{f}$ = average friction factor in gas region

and

$$\phi = 1 + \frac{\rho_w A_w \Delta h_w - \rho_\ell A \Delta h_\ell}{\rho_{gi} A (\Delta h_\ell + \Delta h_{tot})}$$

where ρ_{gi} = density of the gas at the inlet pressure

$\Delta h_{tot} = h_g - h_{\ell s}$ and θ = chilldown time.

Thus, for "long", well-insulated transfer lines with no appreciable heat leaks, constrictions or concentrated thermal masses, chilldown times may be scaled using Eq. (2). A "long" line is defined as one whose L/D is greater than 3800 for liquid hydrogen and 475 for liquid nitrogen.

Section 8

FLOW PHENOMENA TESTING

Flow phenomena testing in a small size facility was conducted to provide:

- Insight into the mechanisms which influence the implosion problems.
- Quantitative data for a small scale geometry.
- Assistance in planning tests in the larger scale complete system tests.

As originally planned, the emphasis was to be placed on insight into the implosion problem; however, considerable useful quantitative data was obtained which was used for comparison with the receiver tank and transfer line analyses. The experiments were conducted using a two-foot-diameter transparent Plexiglas sphere as the receiver tank and a one-half-inch diameter transfer line of 28 ft maximum length. Instrumentation included a turbine liquid flowmeter, a nuclear void fraction meter, and pressure and temperature sensors. Photographic coverage was made of both receiver tank and transfer line flow phenomena; liquid nitrogen was used in all tests.

Three types of tests were performed: (1) tank fill tests in which the flow conditions at the receiver inlet were maintained "quasi-steady," (2) transfer line tests in which the transfer line vented to atmosphere and (3) limited testing with the tank and instrumented transfer line coupled. The emphasis in this experimental portion of the program was placed on the tank fill thermodynamics for two-phase discharge into the vessel. This was necessitated by the lack of available experimental data on these phenomena;

whereas, considerable experimental data were available on feed line thermodynamics. Further, in the present tests particular emphasis was placed on obtaining quasi-steady inlet flow conditions.

The quasi-steady inlet flow tests were planned to:

- Obtain insight into the gross flow phenomena occurring during the fill process in order to verify the adequacy of the lumped tank fill analytical model (or, alternatively, to indicate the necessity of breaking down the model into subregions).
- Study details of the flow to assist in the formulation or modification of the analytical model and verify the adequacy of assumptions used in the analysis.
- Permit low vapor quality inlet flow conditions which may not be achieved in the transparent Plexiglas vessel because of pressure limitations (approximately 10 psig) when coupled to a long transfer line where the initial flow is mainly vapor.
- Provide quantitative experimental data for more idealized boundary conditions so that the results could be compared with those from the analysis.

The uncoupled transfer line tests were performed to provide:

(a) Better understanding of the nature of the transient flow

(b) Quantitative data for comparison with the analytical transfer line model.

The coupled transfer line-receiver tests were conducted to provide quantitative data for comparison with the coupled analytical models. These tests are described in subsequent sections under the three categories: Receiver Tank Quasi-Steady Inlet Flow Tests, Uncoupled Transfer Line Tests, and Coupled Transfer Line-Receiver Tests.

8.1 QUASI-STEADY-STATE TANK FILL TESTS

The quasi-steady-state tank fill tests were performed with the apparatus shown schematically in Fig. 5 . The apparatus consists of the transparent Plexiglas tank, an LN_2 supply vessel coupled to a short transfer line, a flow meter, void fraction meter, and pressure and temperature instrumentation.

The 2-ft diameter Plexiglas test sphere (Fig. 6) consists of two hemispheres, approximately 0.2 in. thick, welded to two Plexiglas flanges 1/2 and 2 in. thick, respectively. The thicker flange incorporates the main inlet port for the fill line, as well as ports for purging, venting, quick pressure relief, thermocouples, and a pressure transducer. The sphere has an internal pressure limit of approximately 10 psig and its optical properties are remarkably good. A photograph of the sphere prior to thermocouple instrumentation is shown in Fig. 7 .

The sphere was instrumented with a 0-30 psia pressure transducer and 15 copper-constantan (3 mil) thermocouples (5 distributed in the vapor along the vessel axis, 3 in the vapor offset from the axis, 4 on the inside of the vessel wall, and 3 on the outside of the vessel wall) in one plane as indicated in Fig. 7 . The 8 thermocouples in the vapor allow the temperature

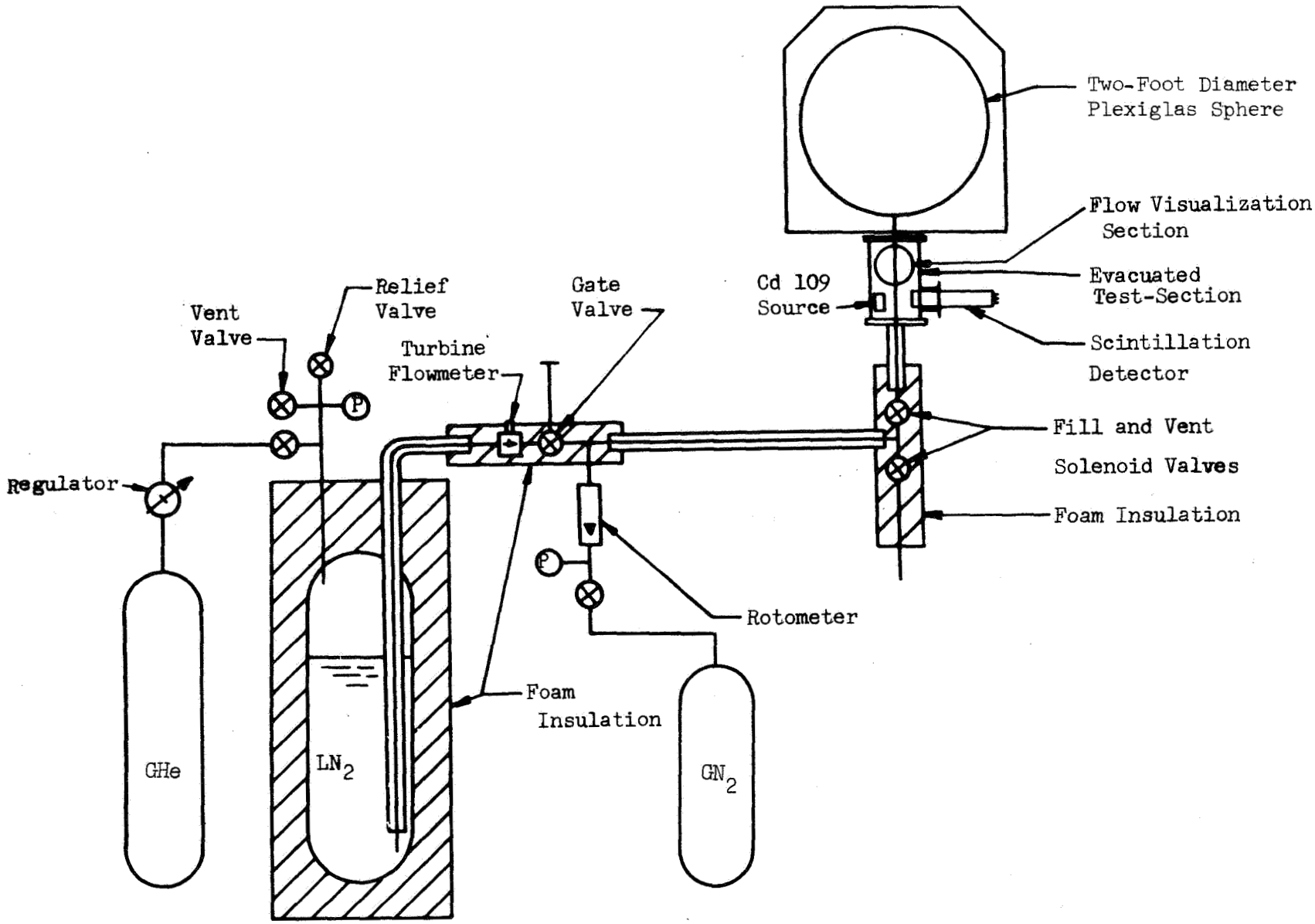


Fig. 5 Test Set-up of Quasi-Steady-State Tests

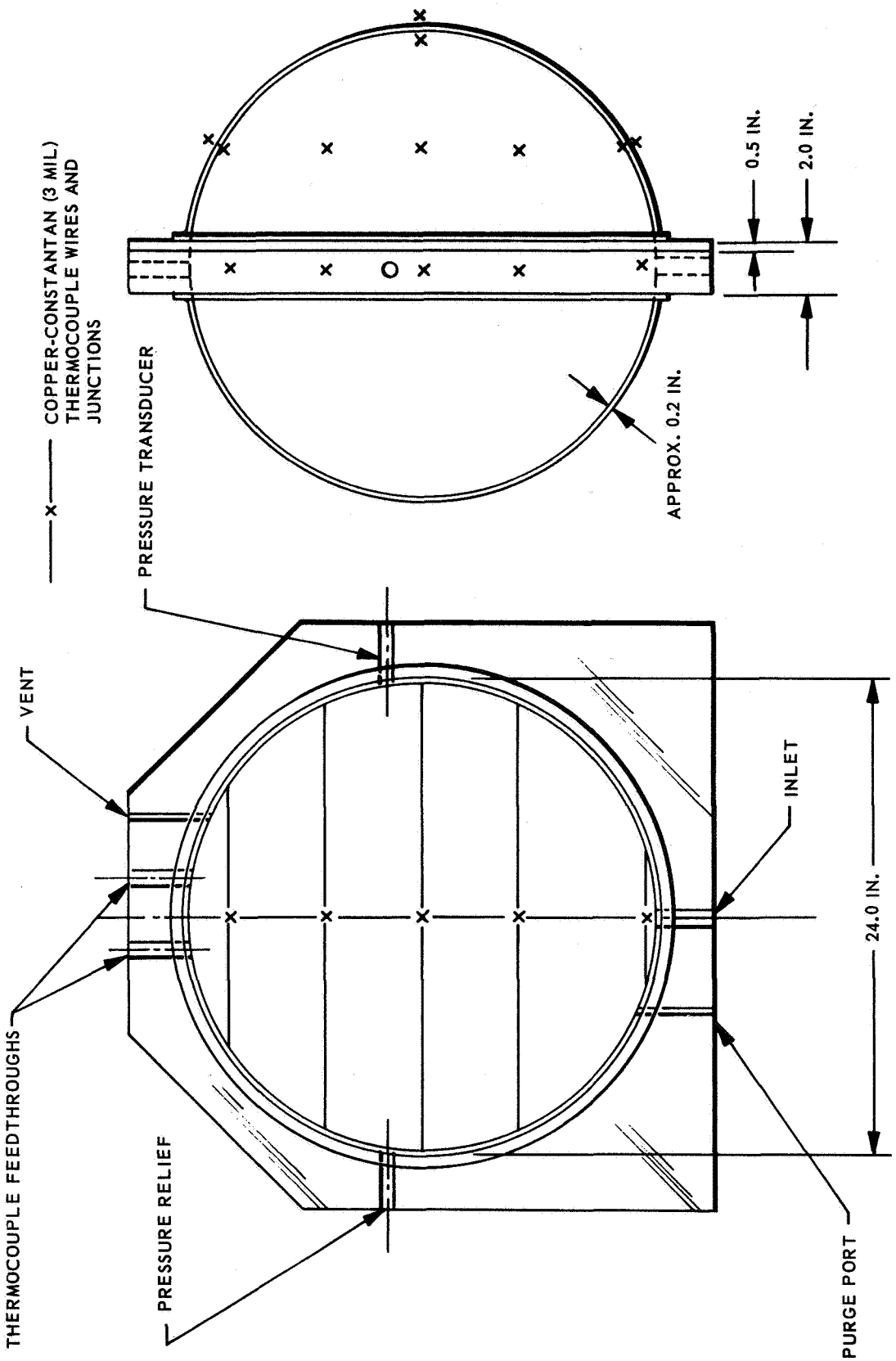


Fig. 6 Transparent Two-Ft. Diameter Test Sphere

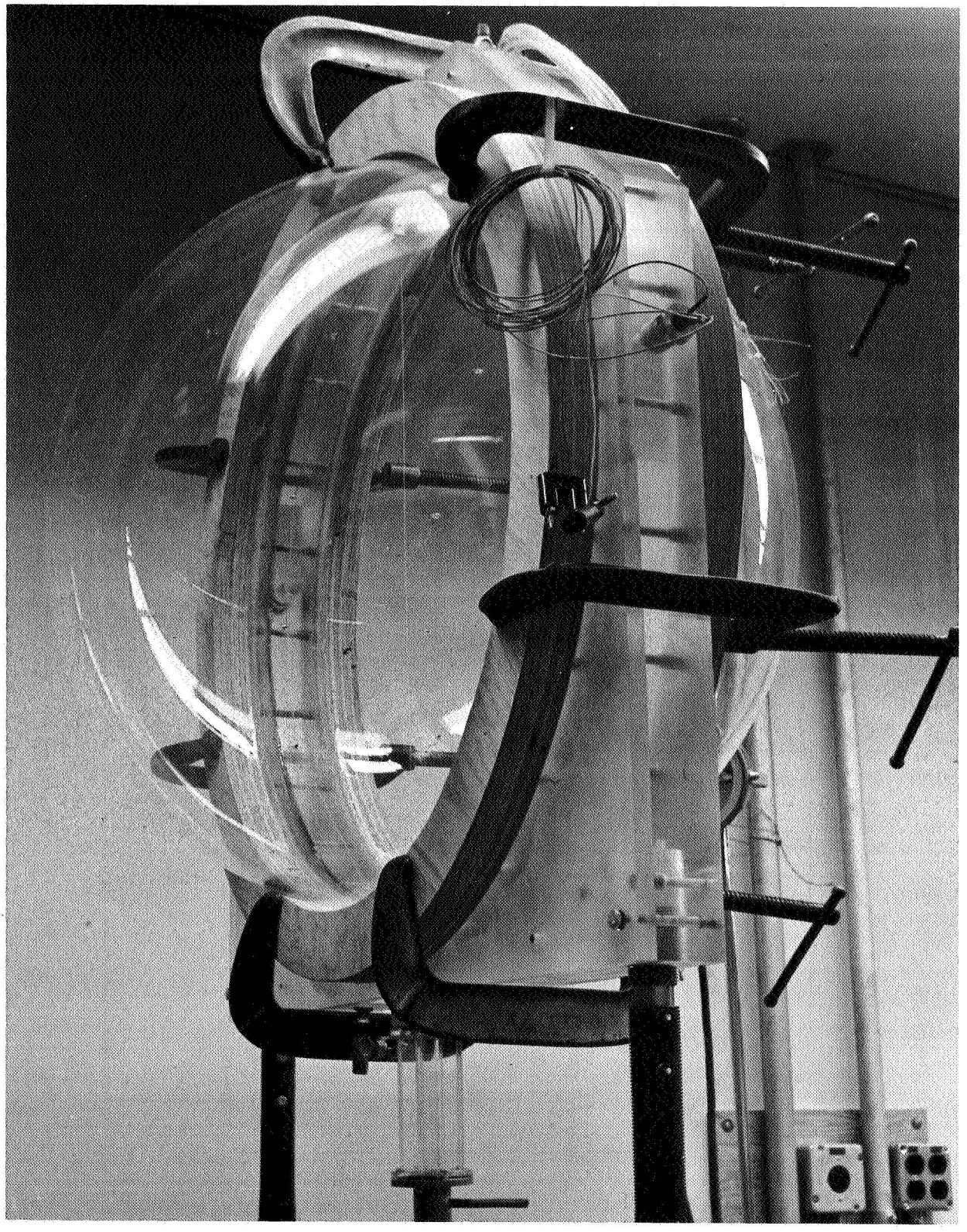


Fig. 7 Transparent Tank Ready for Instrumentation

nonuniformity of the vapor to be continuously measured and the 6 wall thermocouples, similarly, permit measurement of the wall response. The thermocouples in the vapor are positioned by stringing the thermocouple wires across the vessel and attaching them to the walls, with the junctions near the center to minimize their effect on the flow. Pressure and temperature measurements were recorded on oscillograph recorders.

The insulated cryogen supply vessel of approximately 15 gallon capacity is normally prefilled from a 160 liter LN_2 dewar. It includes a vacuum jacketed 3/4-inch liquid withdrawal line and ports for fill and for pressurization from an external helium gas supply. LN_2 flow rate is measured with a 1/2-in. Fisher-Porter turbine flow meter (calibrated in LMSC flow calibration laboratory) and regulated downstream of the meter with a 5/8-in. Goddard cryogenic gate valve. Room temperature GN_2 from a pressurized supply and measured with a Fisher-Porter rotometer may be introduced downstream of the gate valve. The 1/2-inch-diameter vacuum jacketed transfer line of approximately 3 ft, leads to the fill and vent solenoids. The vent and fill legs are of approximately equal length (20 inches). The vertical fill leg also of 1/2-inch diameter includes the nuclear void fraction meter and a transparent flow visualization section mounted in an evacuated tee. The tee is located as near to the inlet as possible, as indicated in Fig. 8 , i.e., the mid-points of the 5-inch-long aluminum section (void fraction station) and 4-inch long glass section (visualization station) are 14-1/2 and 9 inches from the inlet respectively. A complete description of the nuclear void fraction meter and its calibration appears in Appendix A.

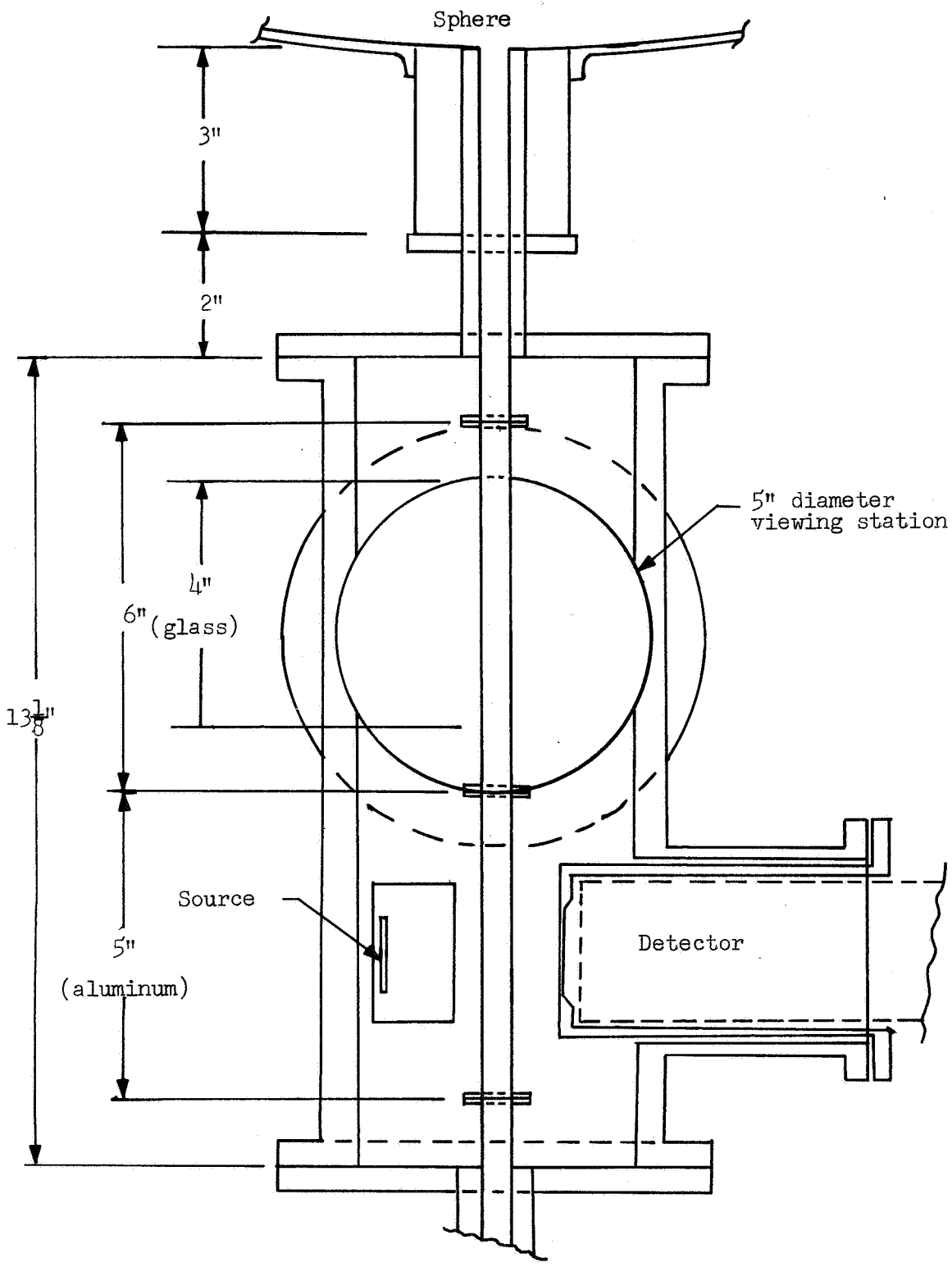


Fig. 8 - Viewing and Void Fraction Measurement System

Measured flows of LN_2 and GN_2 from pressurized supply vessels were combined, passed through a short insulated transfer line section and vented to atmosphere through the vent solenoid for a short period of time until the line had chilled down and the flow was steady. The fill and vent valves were then simultaneously opened and closed respectively to initiate the flow into the sphere. To attempt to achieve reasonably steady flow, the line capacitance between the fill solenoid and the sphere was minimized by minimizing both length and wall thickness and the supplies were pressurized sufficiently to prevent significant flow variation due to variation with receiver pressure during the test. Because of the necessity of installing the nuclear void fraction meter and a transparent viewing section near the receiver inlet, the above mentioned wall thermal capacitance was sufficient to make the inlet flow variations significant; however, tests over a wide variation of flow conditions were permitted before the pressure limitations of the receiver were exceeded.

The nuclear void fraction meter was not received and calibrated until well into the contract and as a result was not available prior to the tests dated 3-30. For these earlier tests, a pre-inlet section with a transparent section, as sketched in Fig. 9 , was used. During these tests an attempt was made to prechill the pre-inlet section with LN_2 immediately prior to the test to achieve more steady inlet conditions; however, these attempts were unsuccessful.

8.1.1 Photographic Coverage

Observations of flow geometry and drop-size distributions with the receiver

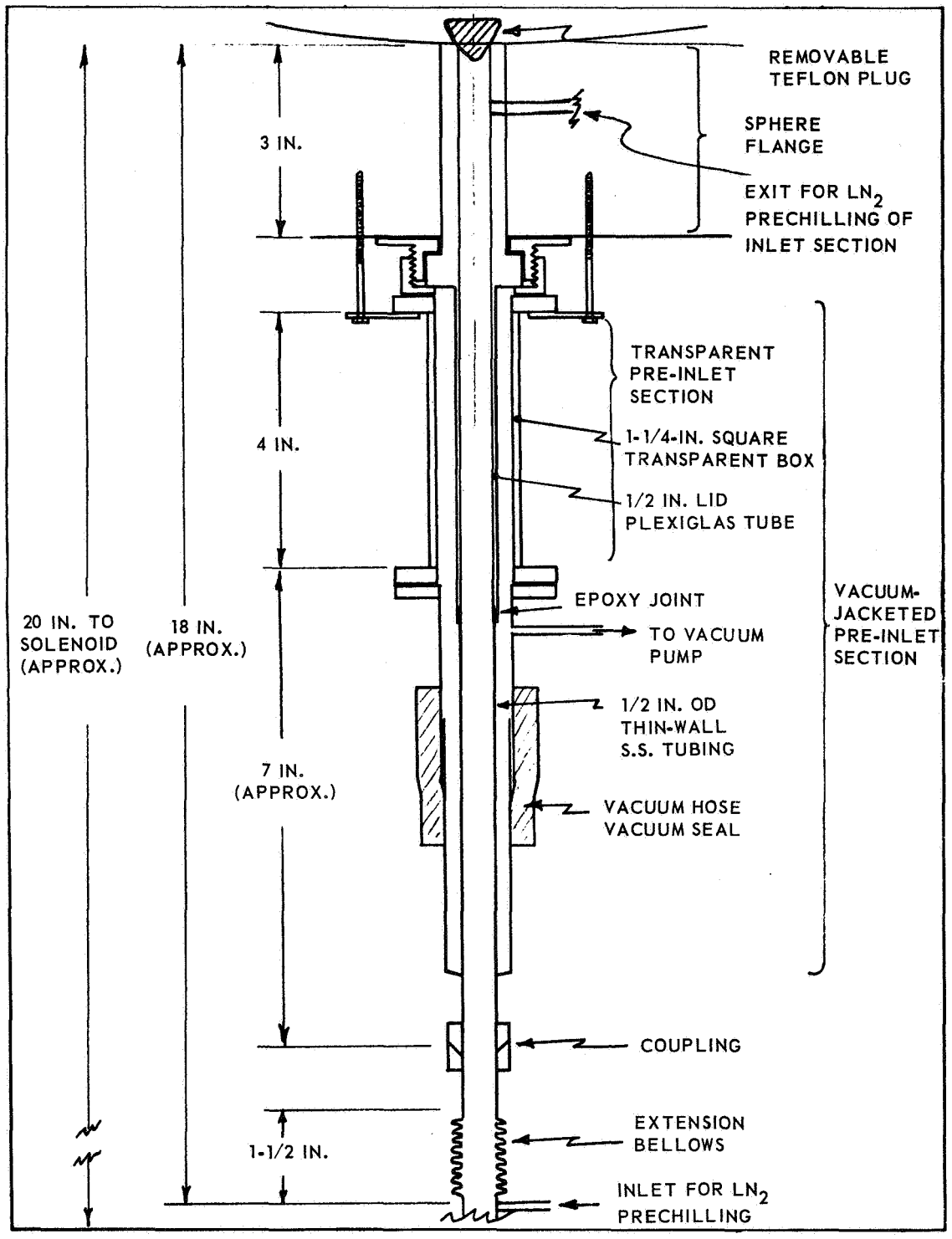


Fig. 9 Early Version of Pre-Inlet Section

tank provide essential data for verification of the tank fill analysis; therefore, considerable attention was devoted to the development of satisfactory motion picture techniques. The objective of these efforts was to take simultaneous, highspeed, closeup motion pictures of the pre-inlet and post-inlet flow and also moderate-speed pictures of the overall flow in the sphere under lighting conditions optimized for all three views. Direct lighting techniques were found to be inadequate for detailed examination of both pre- and post-inlet flows; however, for pictures of the flow in the entire sphere, direct lighting is adequate. In both cases, good contrast between the lighted droplets and the background is necessary. The liquid droplets act as lenses, so that an inverted image of the background is seen, as illustrated in Fig. 10 . Because liquid nitrogen has a low index of refraction (n = 1.20) compared to water (n = 1.33), the back angle Θ between the droplet and the viewing line must be small in order to obtain a sufficiently large lighted image area.

For water, the angle Θ can be as large as 43 deg for $\delta/r = 0.10$; for liquid nitrogen, Θ must be reduced to 31 deg in order to obtain the same image size. Adequate observation of a large field of droplets contrasted against a uniform background is therefore made more difficult. As a result, direct lighting of the overall sphere was used, while a separate, diffusely lighted background was provided for the small pre- and post-inlet flow areas. The latter consists of a diffusely lighted opal glass background with the field contrasted against blacked-out areas as illustrated in Fig. 11. A 40-in.-diameter black disk is positioned 28 in. behind the center of the sphere with eight quartz lamps for direct lighting of the overall sphere. An 18-by-24-in. opal glass sheet, lighted from behind with four quartz lamps, is located behind the pre-

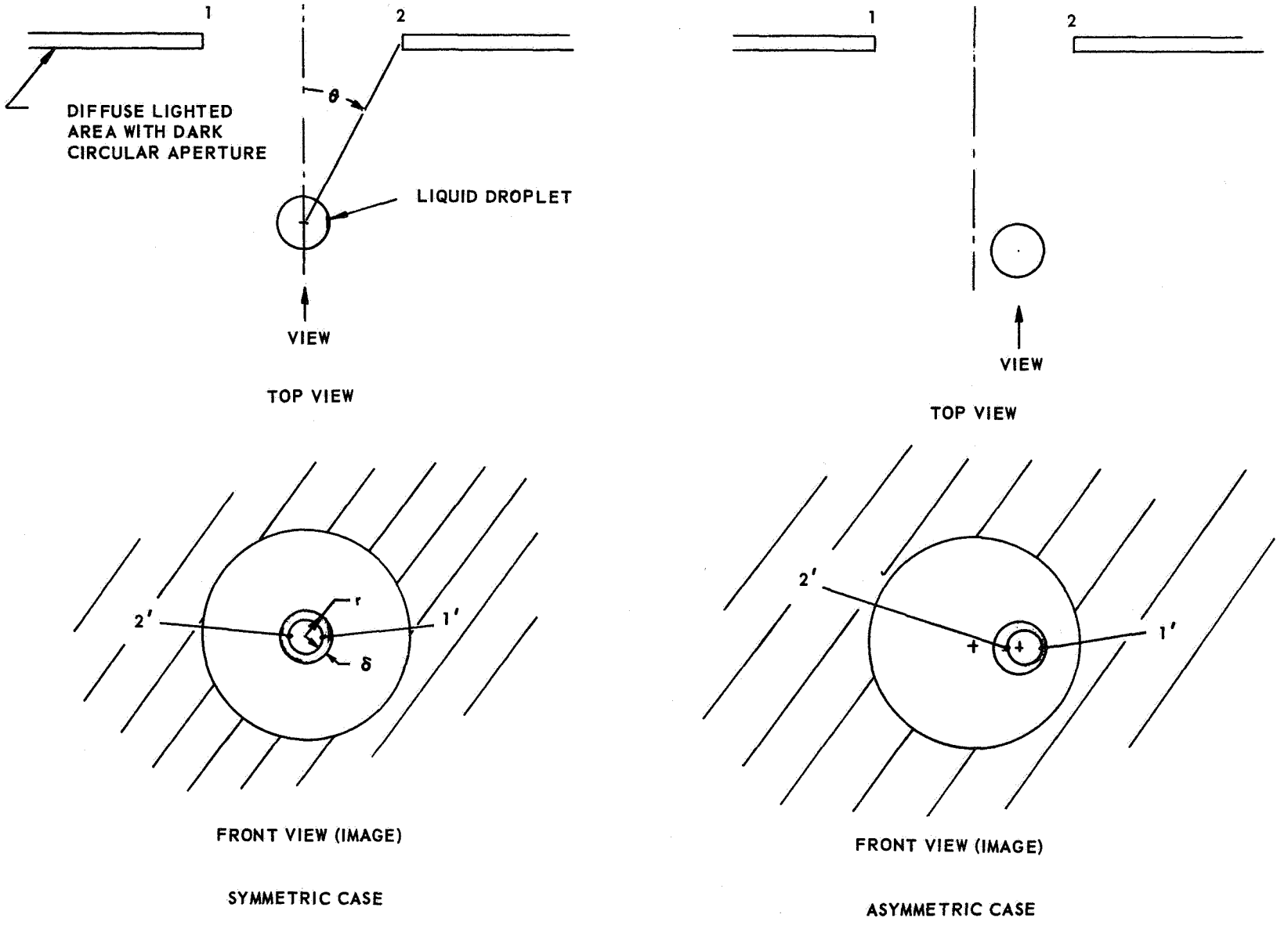


Fig. 10 Image in Spherical Liquid Droplets

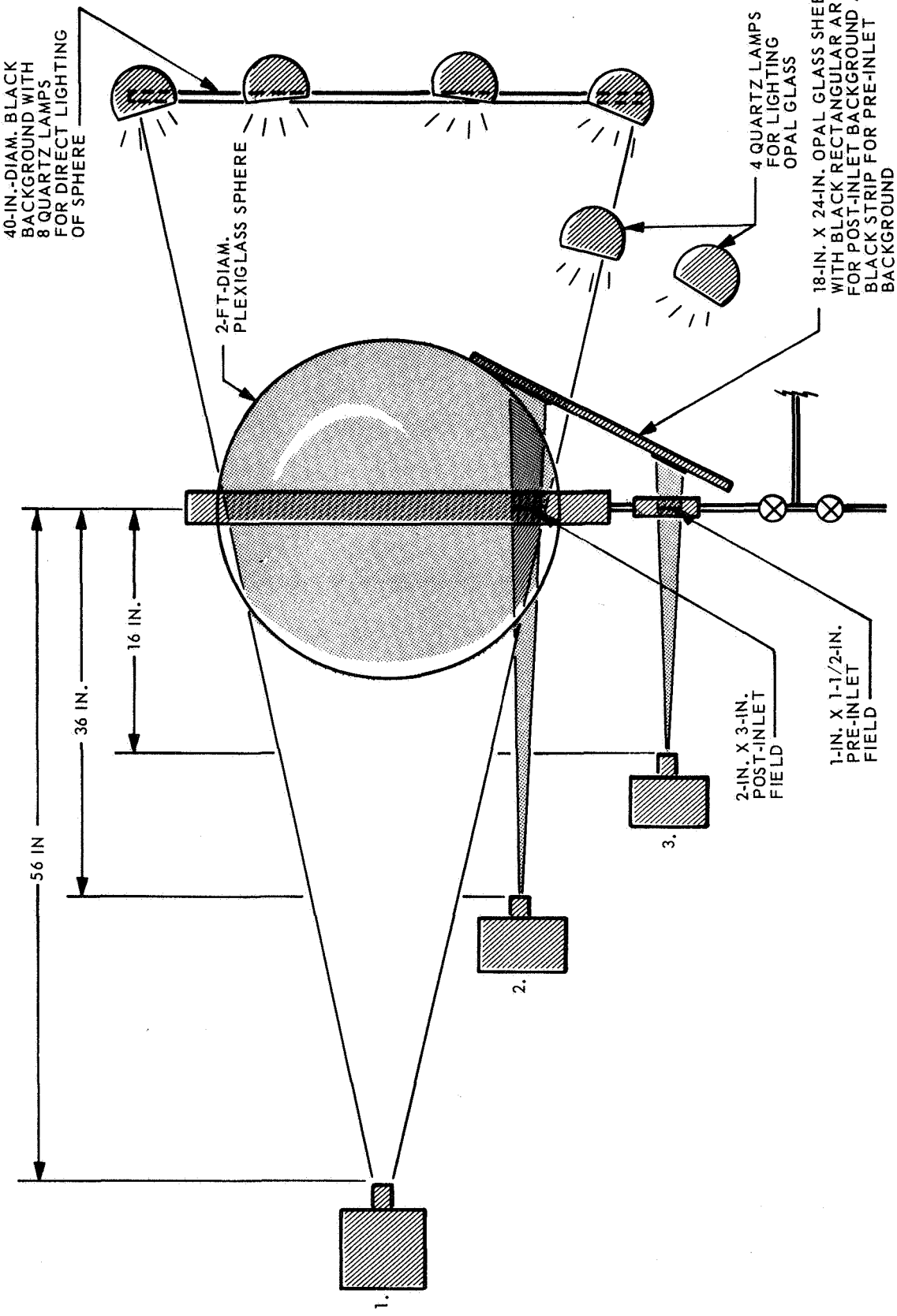


Fig. 11 Photographic and Lighting Set-Up

and post-inlet areas with small blacked-out areas positioned to provide a contrasting background for the pre-inlet and post-inlet regions respectively. The field of view in the post-inlet area is approximately 2 in. high by 3 in. wide, and it is positioned 1 in. above the inlet. The pre-inlet field-of-view is approximately 1 in. wide by 1-1/2 in. high. The lighting system described provides good contrast in all the areas covered, with the exception of the lower 15 percent of the sphere as viewed with the camera looking at the entire sphere. In the post-inlet flows, the two-phase jet appears against a black rectangular background, with the outer portion of the liquid droplets lighted and with only a small rectangular black image in the droplets. In the pre-inlet flow, a horizontal black background strip on the opal glass is used, resulting in lighted droplets (with a thin horizontal black strip) against a black background. A black strip across the opal glass was required to prevent light reflections on the lucite inlet tube. The results obtained through use of this lighting technique were found to be very good. The overall test setup is shown in Fig. 12.

8.1.2 Results of Quasi-Steady-State Fill Tests

The results and conditions for all of the tank-fill tests conducted and which are discussed below are summarized in Table 3. In each case, both photographic and duplicate tests were performed. All pressure, temperature and flow rate measurements presented are for the duplicate tests. (described below)

8.1.2.1 Tests Prior to Installation of Void Fraction Meter

The results of a detailed analysis of Run 1-18-2, are presented in Figs. 13 through 18. This particular test is discussed in some detail; however, the

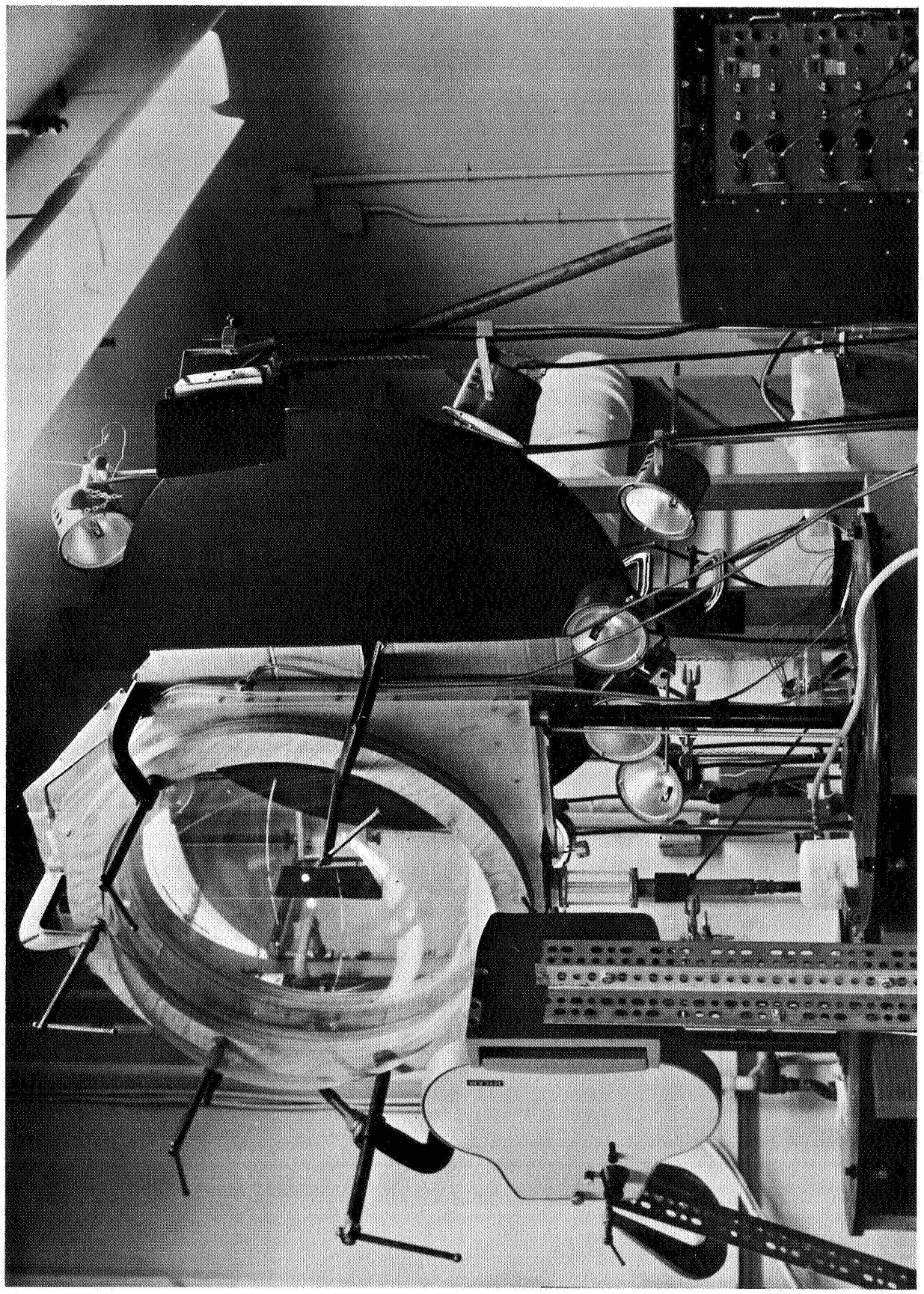


Fig. 12 Flow Phenomena Test Setup

Table 3

Summary of Quasi-Steady-State Tank Fill Tests

Test No.	Fill Duration (sec)	Initial[1] Flowrate (lbm/sec)	Final[1] Flowrate (lbm/sec)	Initial Pressure (psia)	Final Pressure (psia)	REMARKS
1-18-2	9.0	0.036	0.033	14.70	18.75	Quality found from movie data
2-17-1	10.0	0.036	0.032	14.70	19.52	"Low" Vapor Quality[2]
2-17-2	10.0	0.0386	0.0346	14.70	18.42	"Low" Vapor Quality (2)
2-17-3	10.0	0.1729	0.1537	14.70	18.84	"High" Vapor Quality,[2] Combined LN_2 - GN_2 flow. High Initial Flow Velocity.
3-30-1	8.0	0.0662	0.0572	14.70	21.10	$(F_\ell)_{max} = 0.134$[3]
3-30-2	12.5	0.0358	0.0301	14.70	21.10	$(F_\ell)_{max} = 0.137$[3]
3-30-3	12.5	0.0364	0.0296	14.70	21.10	Combined LN_2- GN_2 Flow, $(F_\ell)_{max} = 0.063$[3]
3-30-4	12.5	0.0354	0.0288	14.70	21.25	Combined LN_2- GN_2 Flow, $(F_\ell)_{max} = 0.056$[3]
3-30-5	6.5	0.0681	0.0557	14.70	22.25	Combined LN_2 - GN_2 Flow, $(F_\ell)_{max} = 0.063$[3]

Note: (1) Flowmeter data

(2) Void Fraction Measurement System not used

(3) F_ℓ = Liquid Volume Fraction

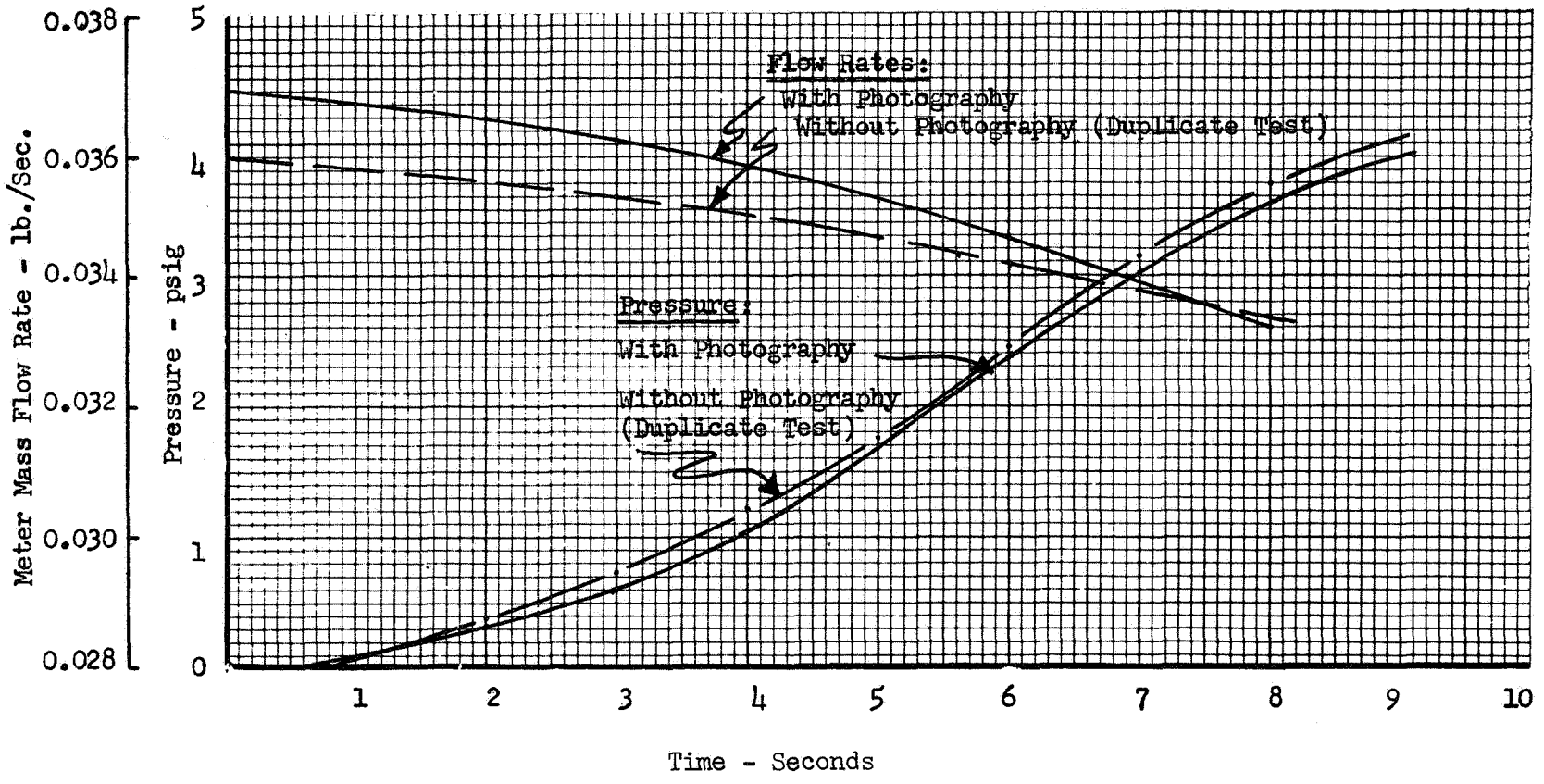


FIGURE 13 - LIQUID FLOW RATES AND PRESSURES

Run No. 2 January 18, 1967

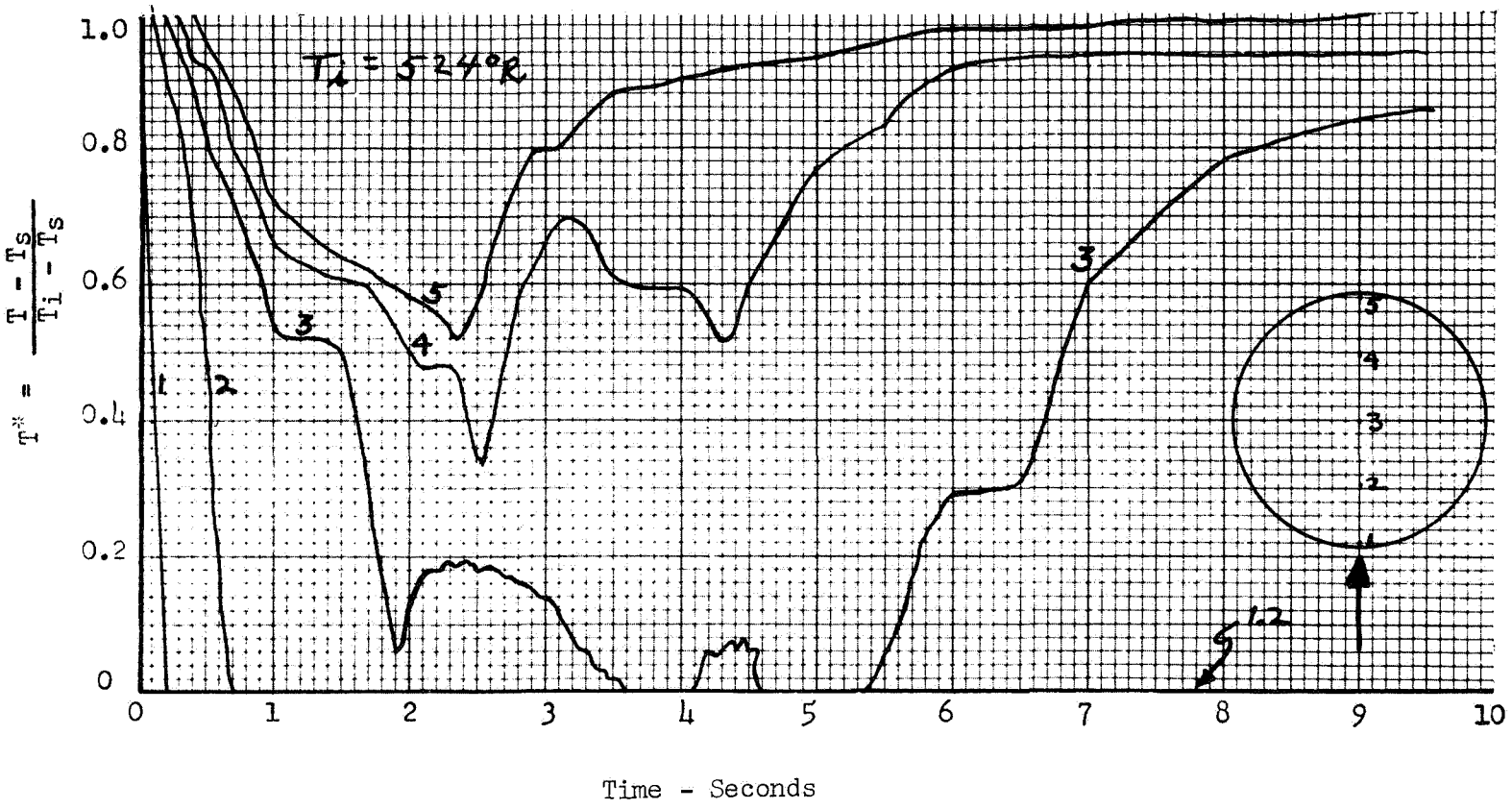


FIGURE 14 - CENTER LINE TEMPERATURES

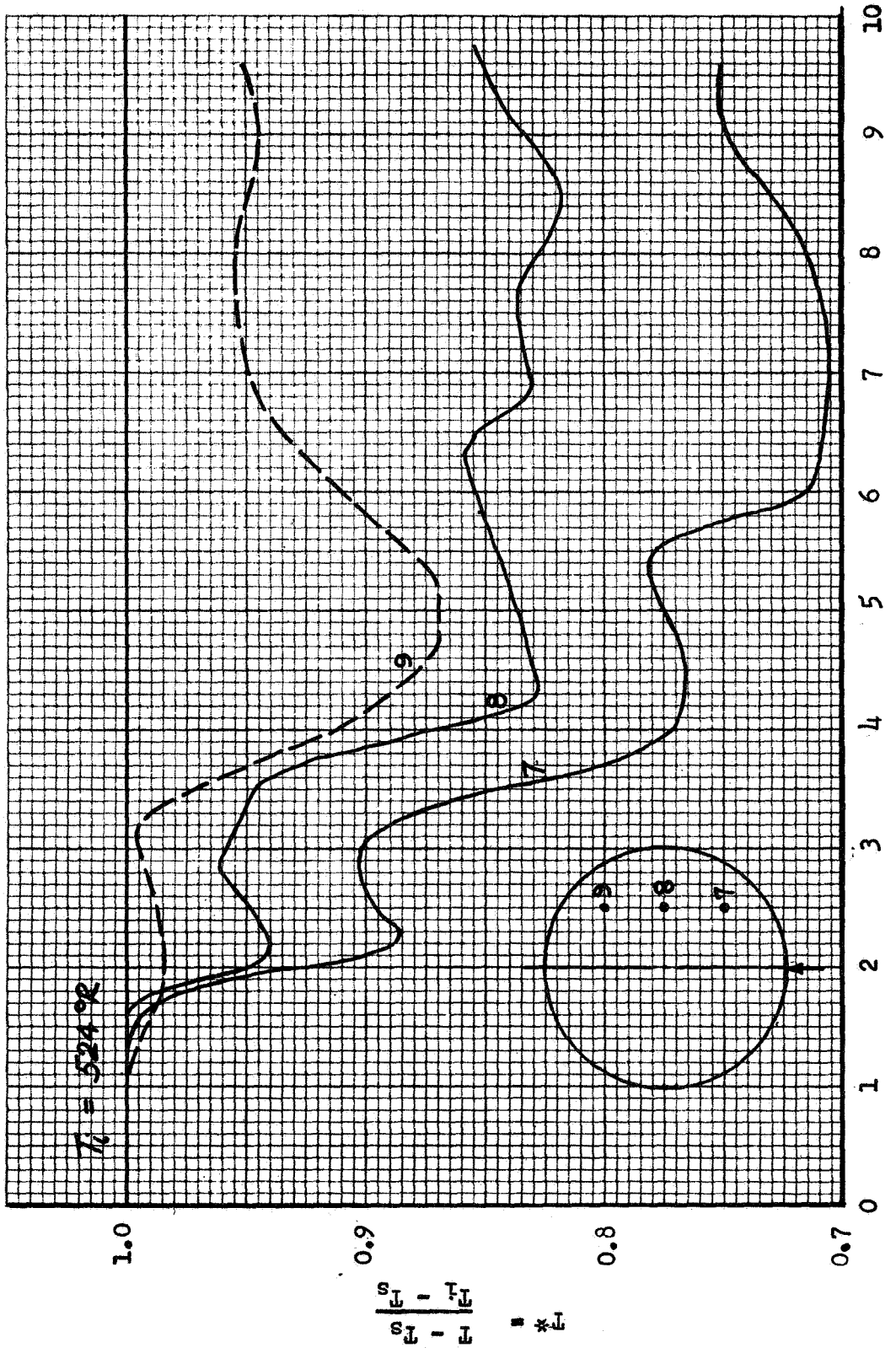


FIGURE 15 - OFF-CENTER TEMPERATURES

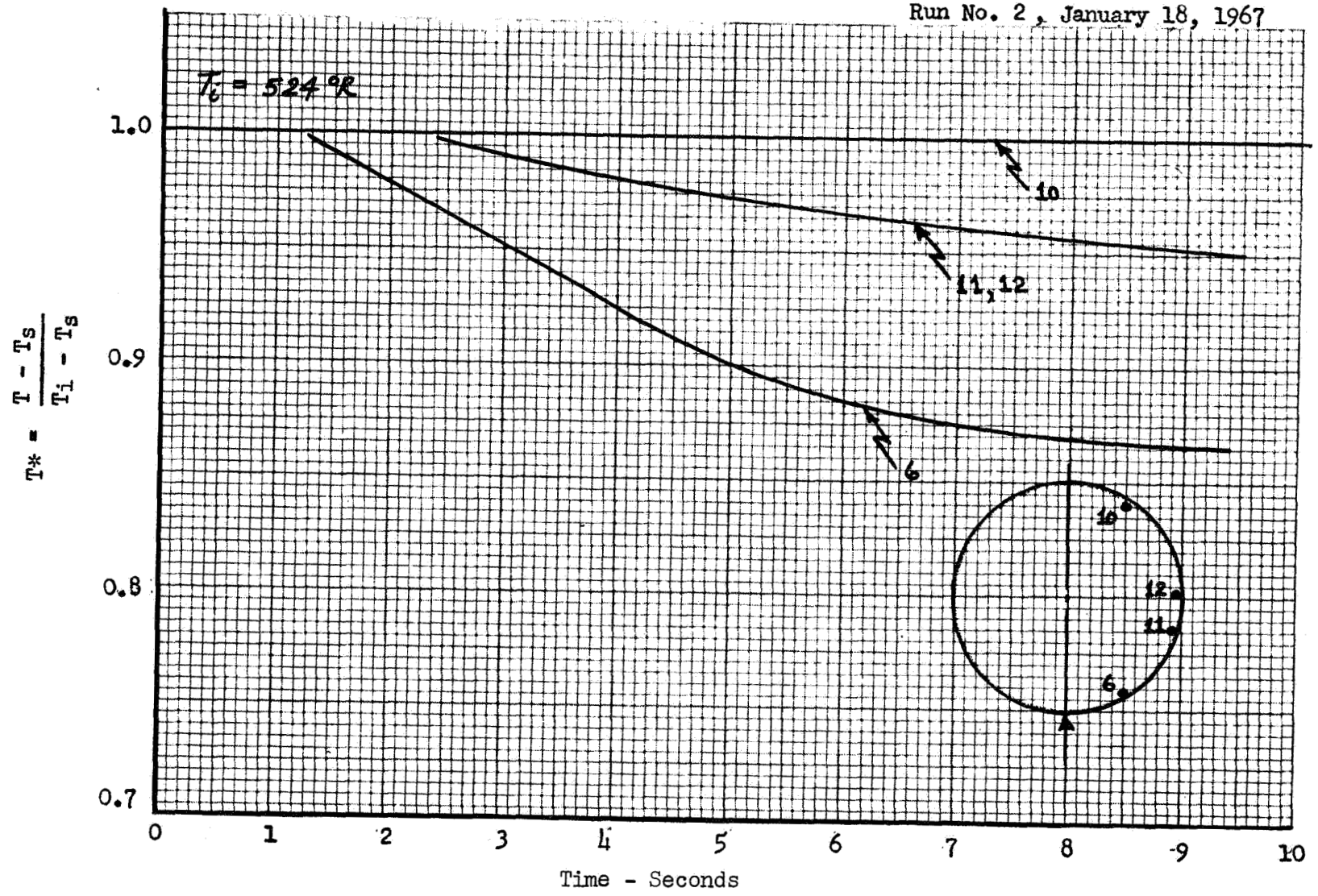


FIGURE 16 - INSIDE WALL TEMPERATURES

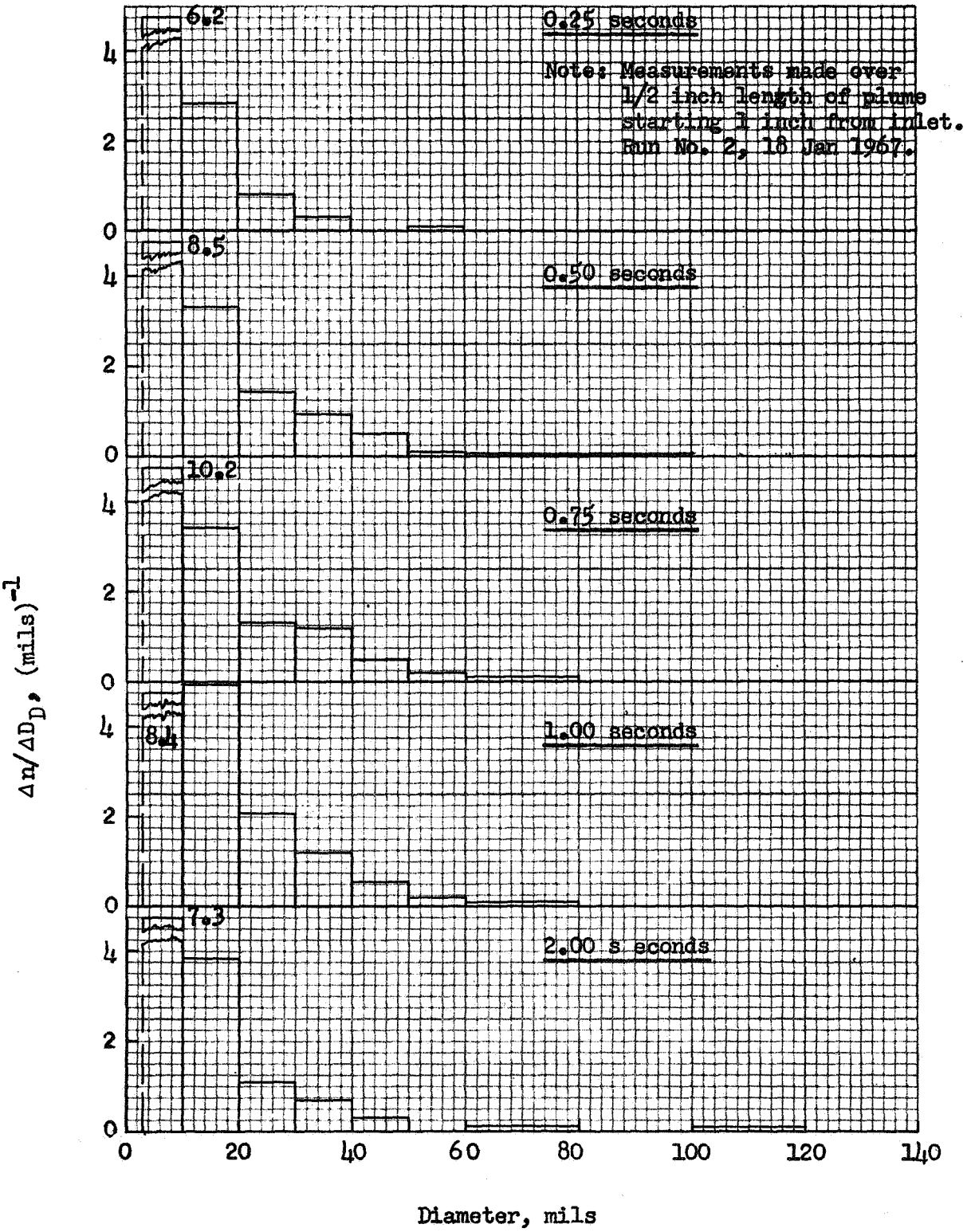


FIGURE 17 - Drop-Diameter Histogram for Post-Inlet Flow

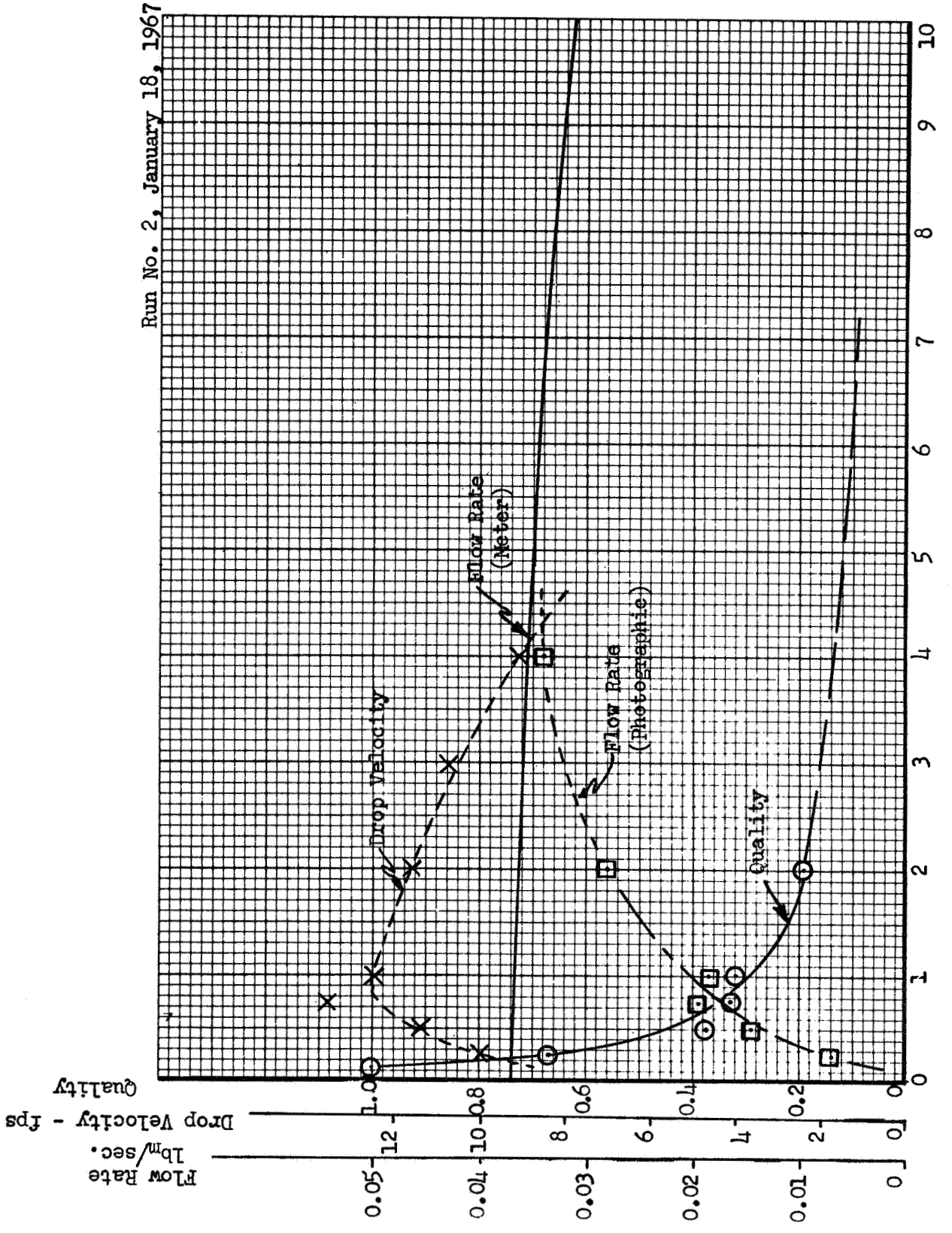


FIGURE 18 - REDUCED FLOW, QUALITY AND DROP VELOCITY DATE

description of subsequent tests are brief, pointing out mainly the salient features of each test. For test 1-18-2 the transparent inlet section used was that shown in Fig. 9 . The transfer line length was approximately 6 feet and there was no GN_2 flow. It was found that the lighting required for photography significantly affected the thermocouples in the vessel and on the walls, and it was decided that for each successful test involving photographic coverage, a "duplicate," non-photographic test (without lighting) would be conducted. Figure 13 shows the flowrate and pressure response of the sphere for both the photographic and duplicate tests. The repeatability is seen to be very good. Initial conditions within the sphere and transfer line were approximately identical. The test procedure involved establishing the desired flowrate while diverting the flow through the vent solenoid and then switching the flow into the receiver tank. Over the duration of the test, approximately 8 to 9 seconds, the pressure is seen to show a shallow, then later a steeper increase, while the flowrate is seen to drop approximately 10%. This decrease in flowrate is a result of the pressure rise in the sphere, which is vented through a relief valve at about 6 psig.

Figures 14 , 15 and 16 show the measured temperature response of thermocouples within the sphere for the duplicate test. The dimensionless temperature T* is plotted against time (T_R = initial or room temperature and T_S = liquid nitrogen saturation temperature). The centerline thermocouples are shown on Figure 14 , the off-center thermocouples on Figure 15 , and the inside wall thermocouples on Figure 16 . Thermocouples on the outside of the wall were unaffected. The centerline thermocouples (Fig. 14) respond quickly to the flow; however, after approximately 2 seconds, the

upper thermocouples respond and the thermocouple No. 3 also starts rising after approximately 5 seconds. The off-center thermocouples respond after 1-1/2 seconds but Nos. 8 and 9 show responses similar to Nos. 4 and 5 on the center toward the end of the test, while No. 7 in the lower region, tends to level out at a somewhat lower temperature. These results correspond to photographic data, which show that the plume impinges off the top of the vessel for about the first 2 seconds (i.e., Froude No. > 2). Thereafter the plume height decreases, and toward the end of the test, the height was approximately 1/4 to 1/2 of the vessel diameter. Although no distinct regions in the vessel are apparent, the lower regions are much colder, suggesting significant interaction between the plume and the vapor around it. Figure 16 shows the response of the inner wall thermocouples (note change of temperature scale), where No. 10 shows little wall cooling, Nos. 11 and 12 somewhat more, and No. 6 exhibits significant wall cooling, undoubtedly due to liquid droplets falling to the vessel bottom.

An analysis of the photographic data was also made. Histograms of the droplet size distribution, measured one inch above the inlet, are shown in Figure 17 for five times. The resolution of droplets was estimated to be about 3 mils, as indicated by the dashed line in Figure 17 . Actual droplet diameter could be measured down to approximately 10 mil size, but between 3 and 10 mils, only a count of droplets was made. The distributions appear to be quite consistent and are typical of two-phase droplet (mist) flows; however, the resolution does not permit extending the histogram below 3 mils where droplet population may still increase with decreasing diameter. In general, a peak occurs at very low diameter, below which population decreases; however,

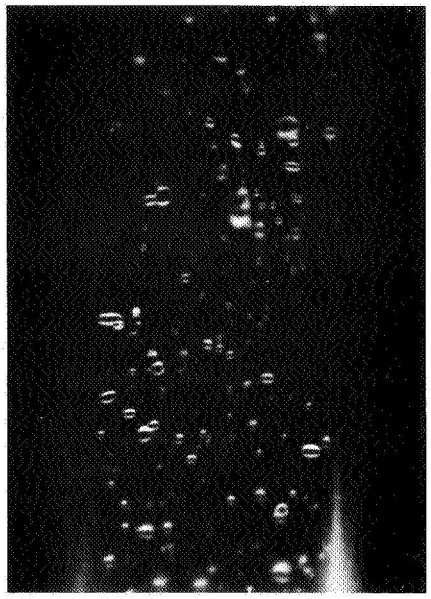
data in this range is difficult to obtain. Although the histograms appear much the same, the few droplets of large diameter at 2 sec. represent the major contributions to the flow quality and mass flow rate.

Figure 18 shows mean drop velocity, quality, and flowrate as determined from photographic analysis as well as flowrate from the turbine flowmeter. Drop velocities for a range of sizes were found to be surprisingly constant at any particular time, showing a mean deviation of less than 10% and no apparent variation attributable to difference in droplet size. This indicates that the slip velocity is small, otherwise there would be a large variation in velocity between small and large droplets. The data of Figure 18 shows that the velocity peaks around 13 ft/sec (Froude No. = 2.6) near 1 sec and thereafter decreases, being approximately 8 ft/sec (Froude No. = 1.0) near 4-1/2 sec. These values are in qualitative agreement with the photographs which indicate that the plume rises to the vessel top up to approximately 2 to 3 seconds.

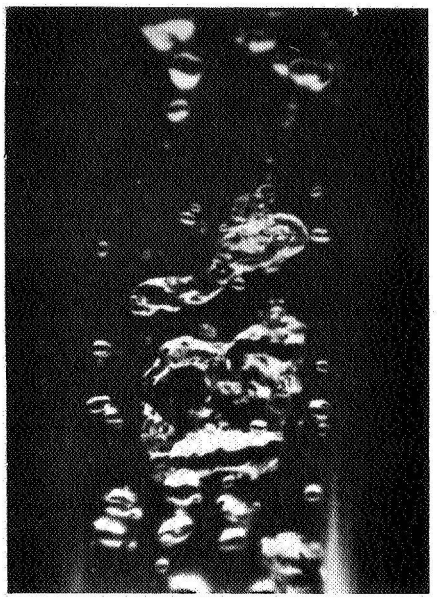
The quality and flowrate were computed by integrating the histogram data and assuming average velocities for the liquid droplets. These calculations were made only out to 2 seconds since, by that time, falling droplets were observed to appear in the post-inlet field of view, causing difficulty in determining which droplets were indeed associated with the inlet plume. Furthermore, by one second the quality had decreased sharply and the large irregular liquid droplets present were difficult to measure accurately. The flow, although not pulsating greatly, did exhibit a rather unsteady overall quality which made it difficult to discern a true average quality. These flowrate and

quality measurements are shown on Figure 18 , where the turbine meter flowrate is shown for comparison with the photographically measured flowrate. The large initial difference in these two flowrates is attributed to unsteady flow in the transfer line between the turbine flowmeter and the fill-solenoid, a distance of approximately 6 feet. Upon opening the fill-solenoid, the acceleration of the vaporizing flow in the warm inlet section upstream of the receiver tank causes a temporary accumulation of mass in the transfer line due to compression of the vapor phase. The "photographic" flowrate curve (extrapolated) is seen to approach the flowmeter curve within approximately 10% after 4 seconds; however, it is felt that the photographic flow rate measurements made at 1 and 2 sec. could be low due to the reasons given above. Thus the flow indicated by the meter may be approached more rapidly. Similarly, the quality curve is probably high after approximately one second. Comparisons of this data with the receiver tank computer model are made in section 8.2 of this report.

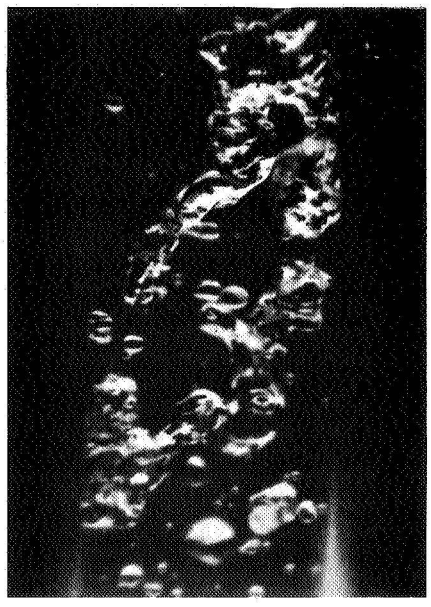
Typical single-frame prints of the pre- and post-inlet flows at 1/2, 1, 2 and 3 seconds are shown in Figures 19 and 20 , respectively. These movies were obtained with a Hycam camera at a film speed of 2500 frames/sec, with a frame-to-exposure-time ratio of 10:1. In Fig. 19 , the flow is vertically upward through the 1/2-inch inside diameter tube where the resulting field-of-view is approximately 1-1/2 in. high by 1 in. wide. The droplets are seen as light areas (spheres or distorted shapes), each containing a small horizontal black strip which is the image of the black background strip. The flow is relatively low quality, and the resulting droplets are generally quite large. Droplet diameters in the pre-inlet flow could be resolved to approxi-



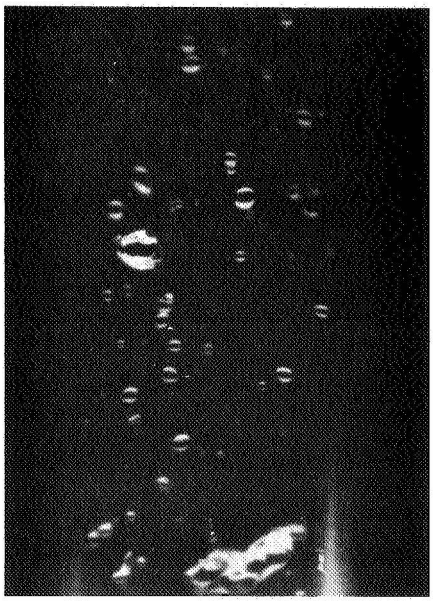
a. 1/2 SEC



b. 1 SEC

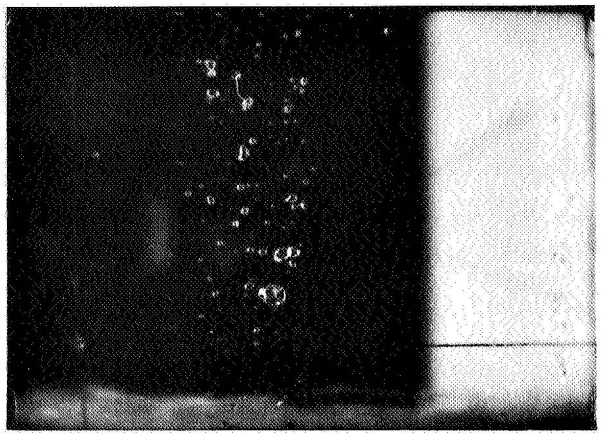


c. 2 SEC



d. 3 SEC

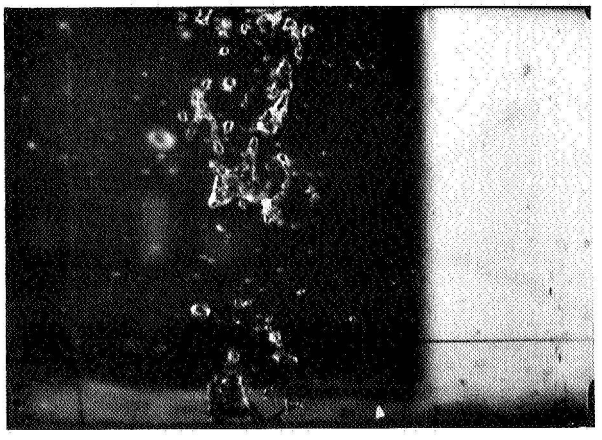
Fig. 19 Pre-Inlet Flow (Flow From Bottom to Top)



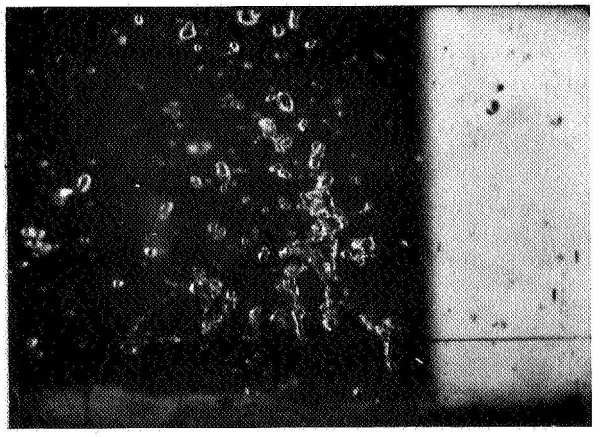
a. 1/2 SEC



b. 1 SEC



c. 2 SEC



d. 3 SEC

Fig. 20 Post-Inlet Flow (Flow From Bottom to Top)

mately 5 mils with an estimated uncertainty, for a drop 5 mils in diameter, of approximately 10 percent.

In Fig. 20 , showing the post-inlet flow, the flow direction is again vertically upward; the distance between the marks on the nylon thread to the left of the flow is 1/2 in. The overall field-of-view in the post-inlet flow is thus approximately 2 in. high by 3 in. wide (twice the size of the pre-inlet field). The droplets appear as light areas against a black background, with a small black image of the background in the center of each droplet (the light area to the right is part of the lighted opal screen). The faint horizontal line at the bottom is the lower thermocouple wire (thermocouple 1) which is approximately 1 in. above the inlet. These post-inlet frames are close to, but do not correspond exactly to, the corresponding frames of Fig. 19 for the pre-inlet flow. The resolution of liquid droplet diameter in the post-inlet flow is better than 10 mils, with an estimated uncertainty in a 10-mil diameter of approximately 10 percent.

Additional receiver tank tests were run in which the transfer line was shortened from 6 to approximately 3 feet, and the pre-inlet transparent section was removed such that the pre-inlet length was approximately 6 inches in an attempt to achieve more constant inlet flow conditions. For these tests - 2-17-1, 2-17-2, and 2-17-3 only post-inlet and overall photographic coverage was made. The results of these three additional tests are presented in Figures 21 through 32 . The first two tests (No. 2-17-1 in Figures 21 - 24 and No. 2-17-2 in Figures 25 - 29 were for "moderate" and "low" liquid nitrogen flow rates, respectively, and compared to very low

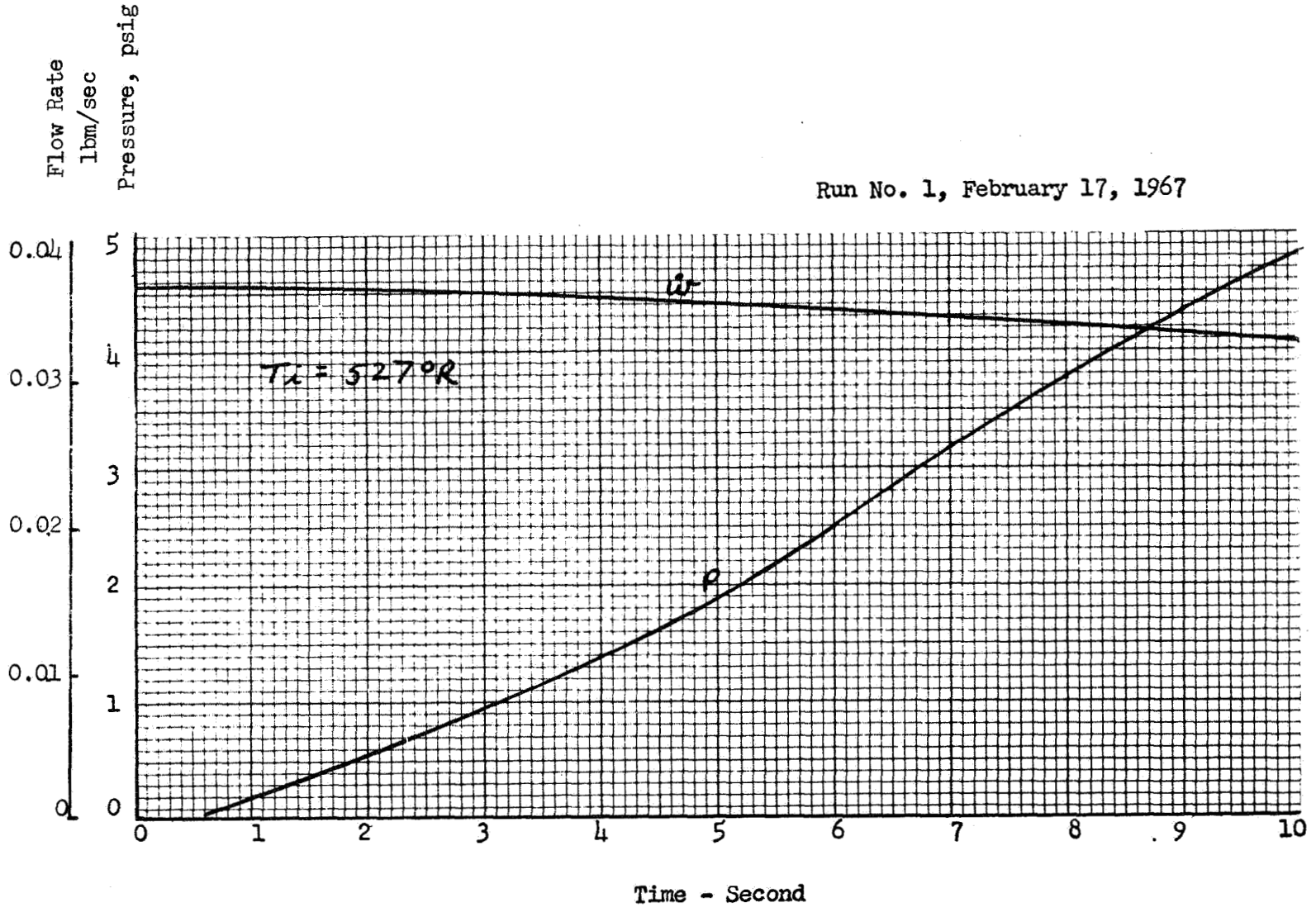


FIGURE 21 - LIQUID FLOW RATE & PRESSURE DATA

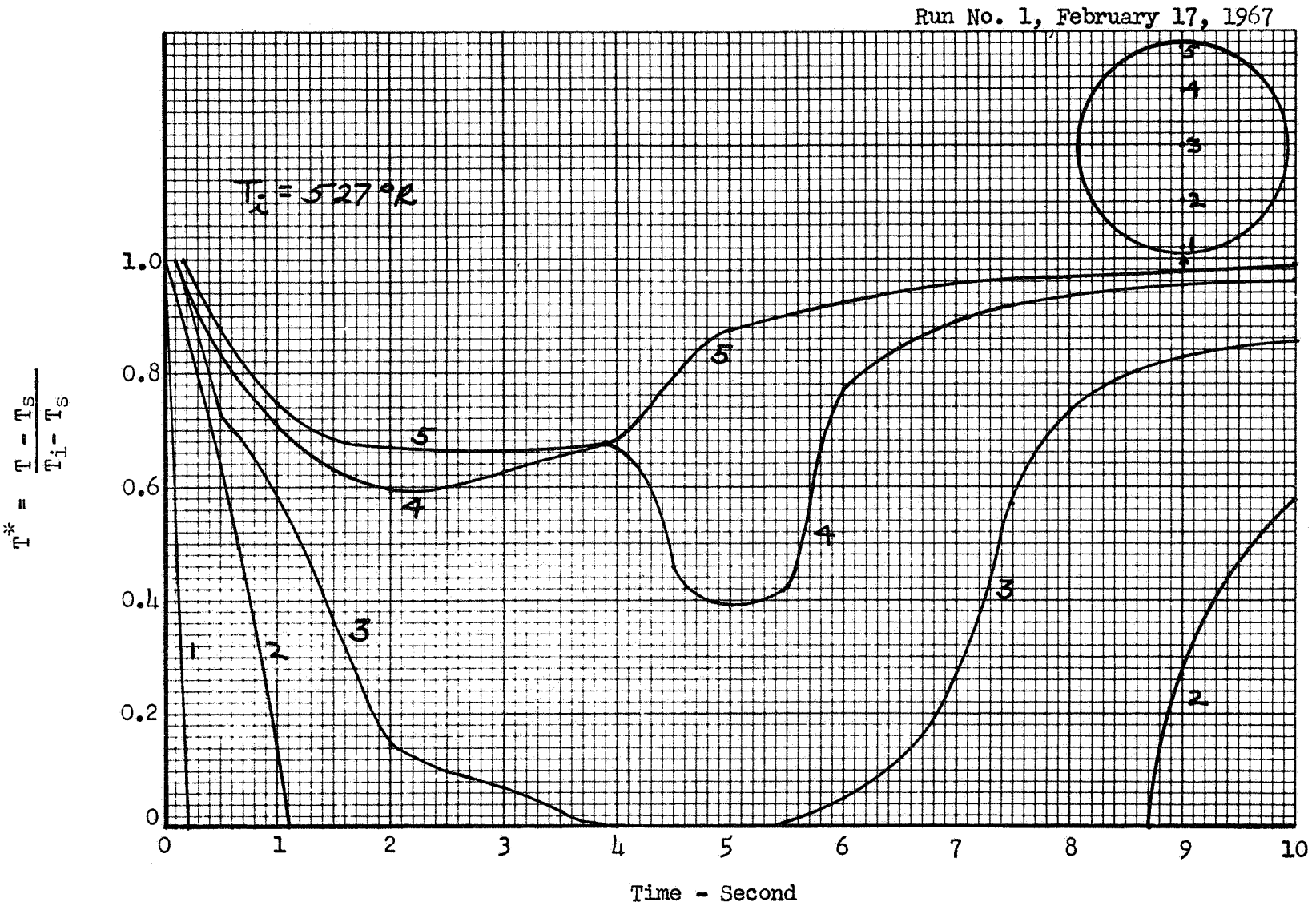


FIGURE 22 - CENTER LINE TEMPERATURES

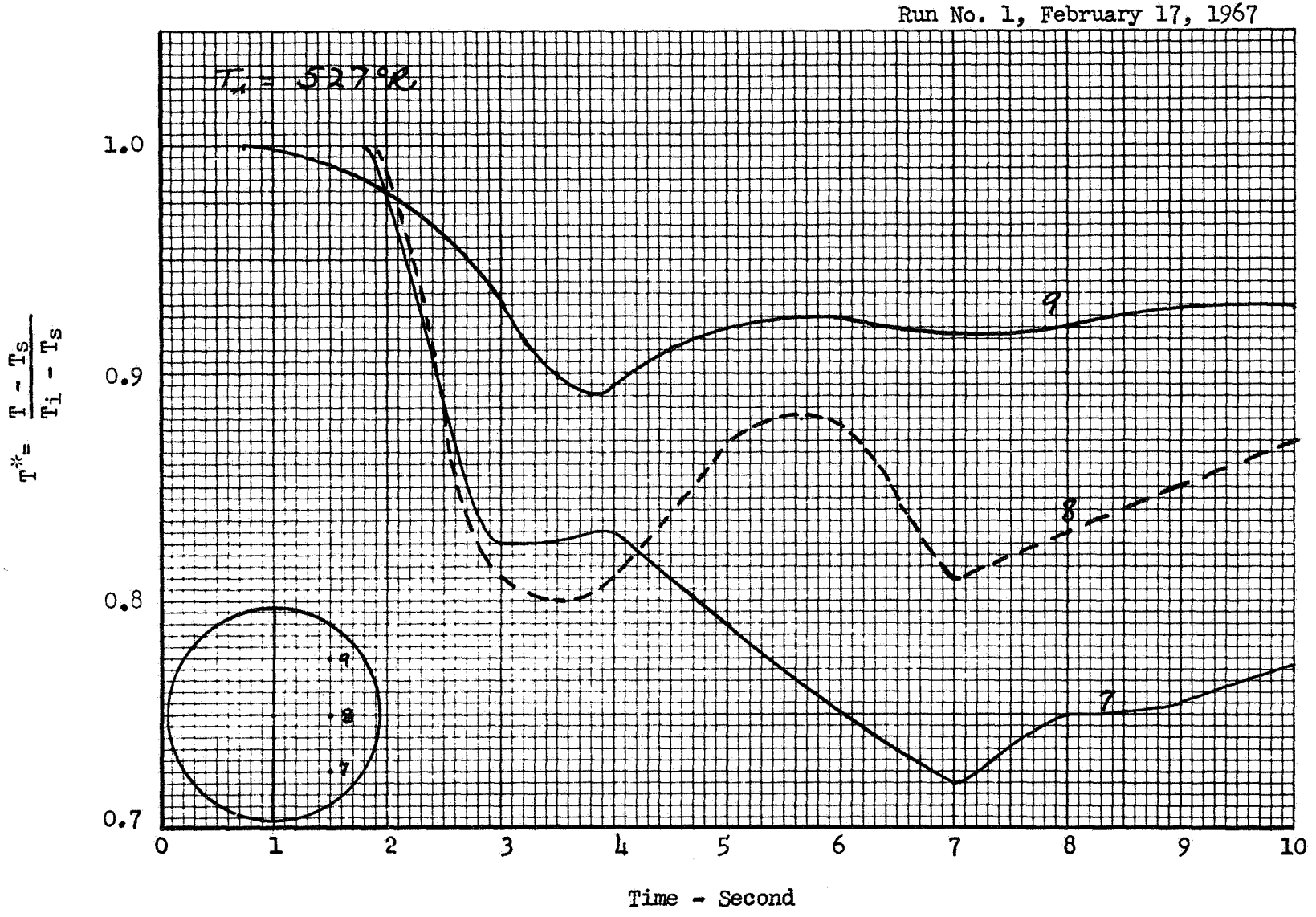


FIGURE 23 OFF-CENTER TEMPERATURES

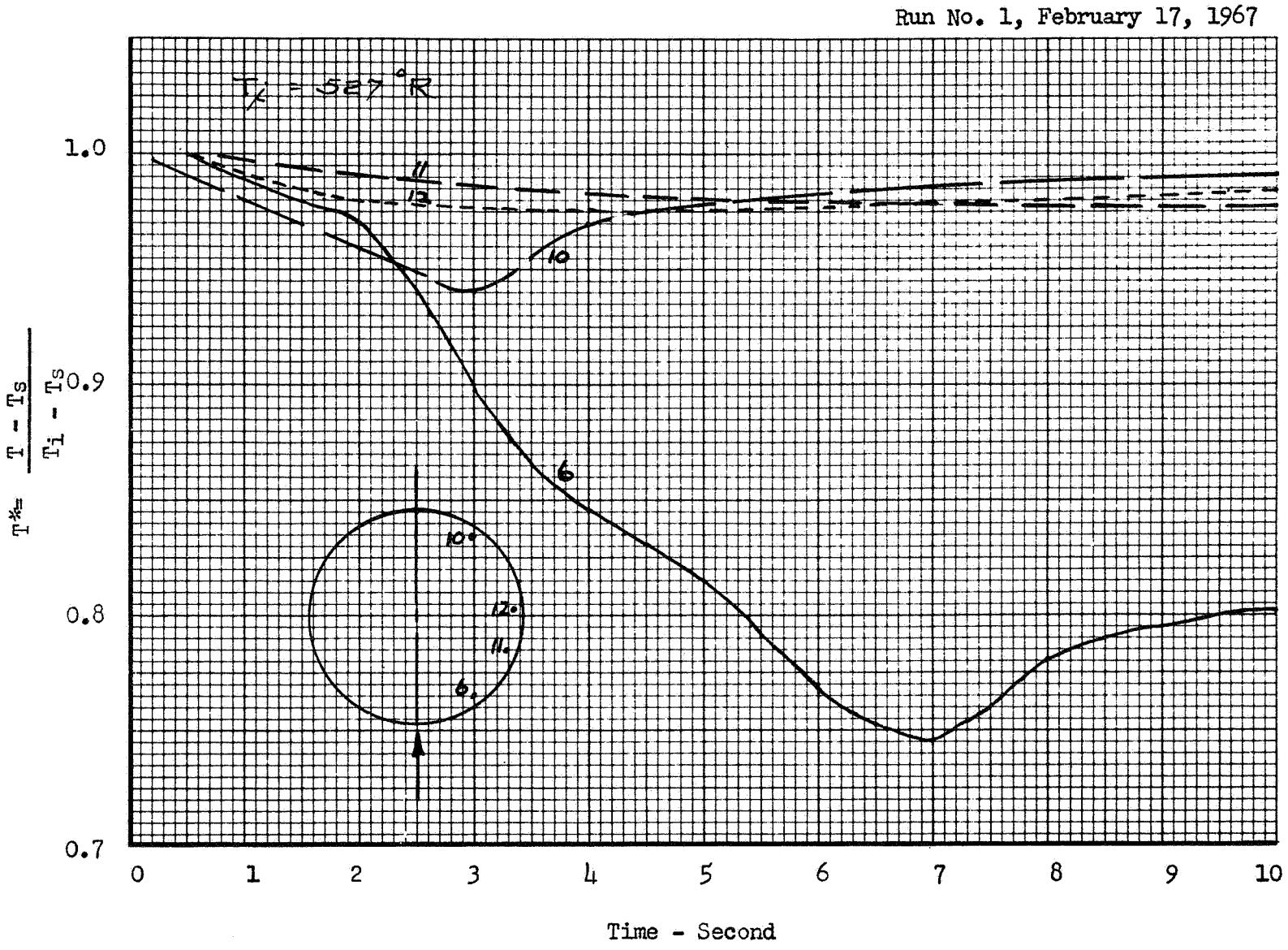


FIGURE 24 - INSIDE WALL TEMPERATURES

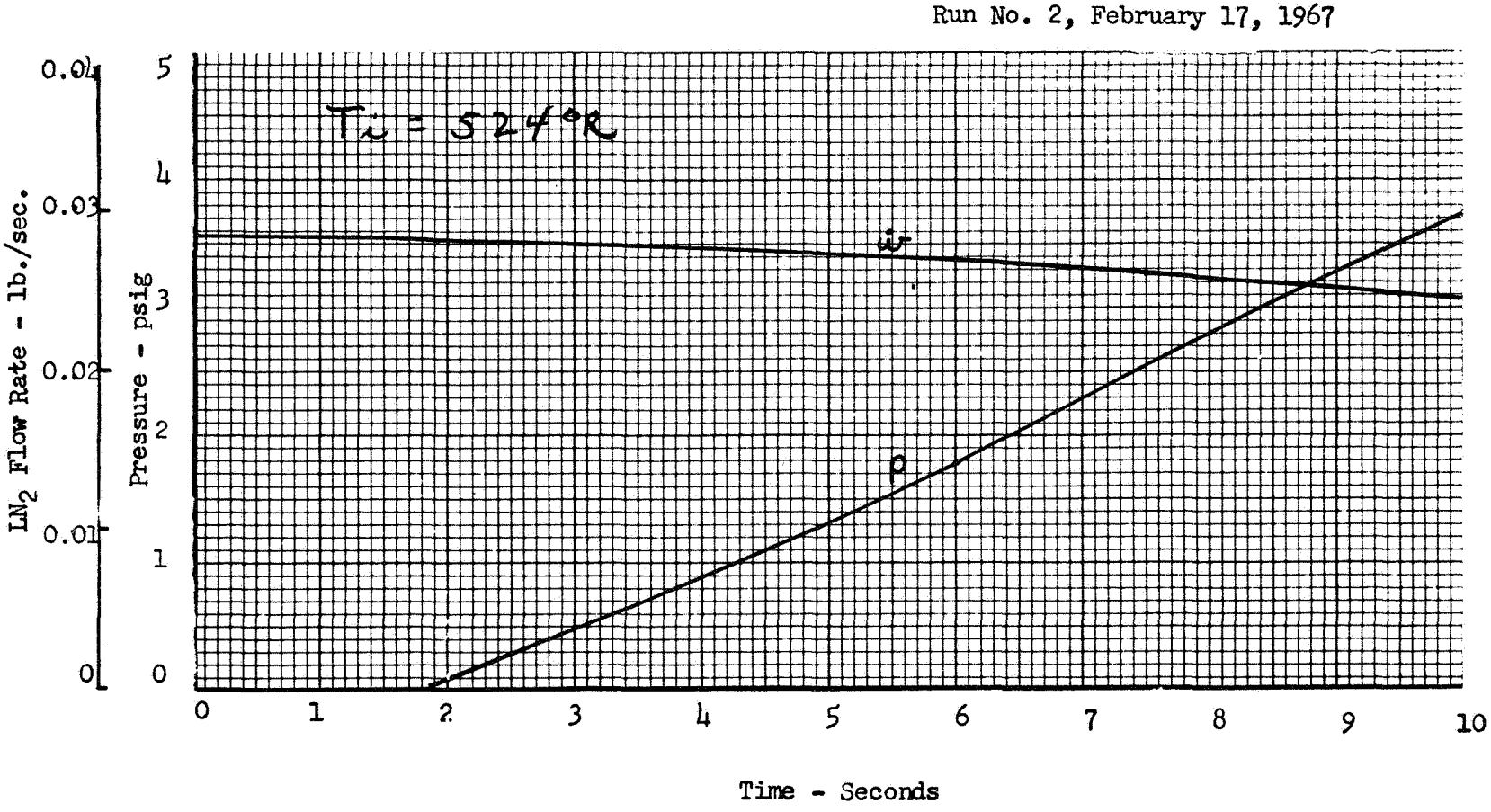


FIGURE 25 - LIQUID FLOW RATE AND PRESSURE DATA

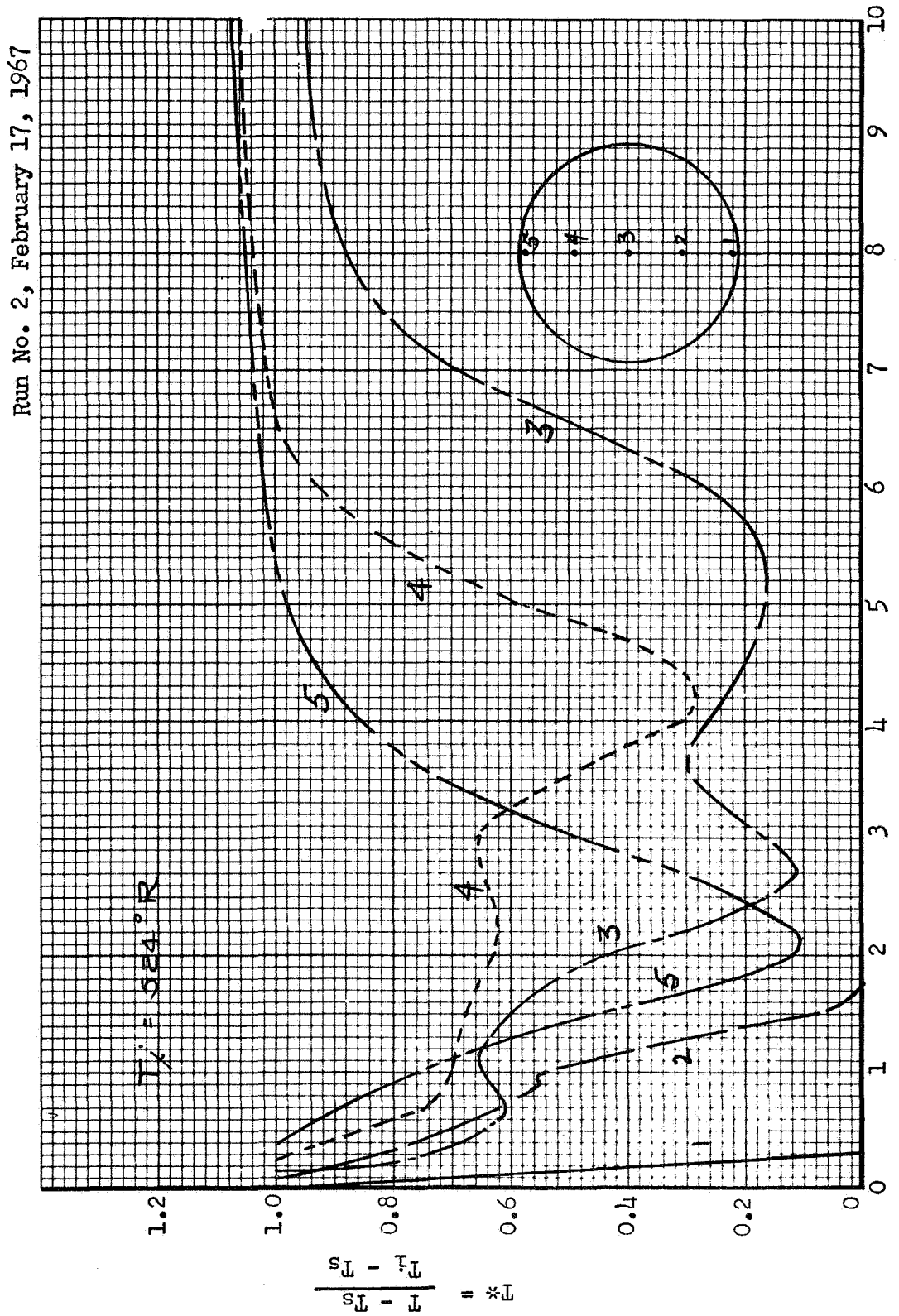


FIGURE 26 - CENTER-LINE TEMPERATURES

Run No. 2, February 17, 1967

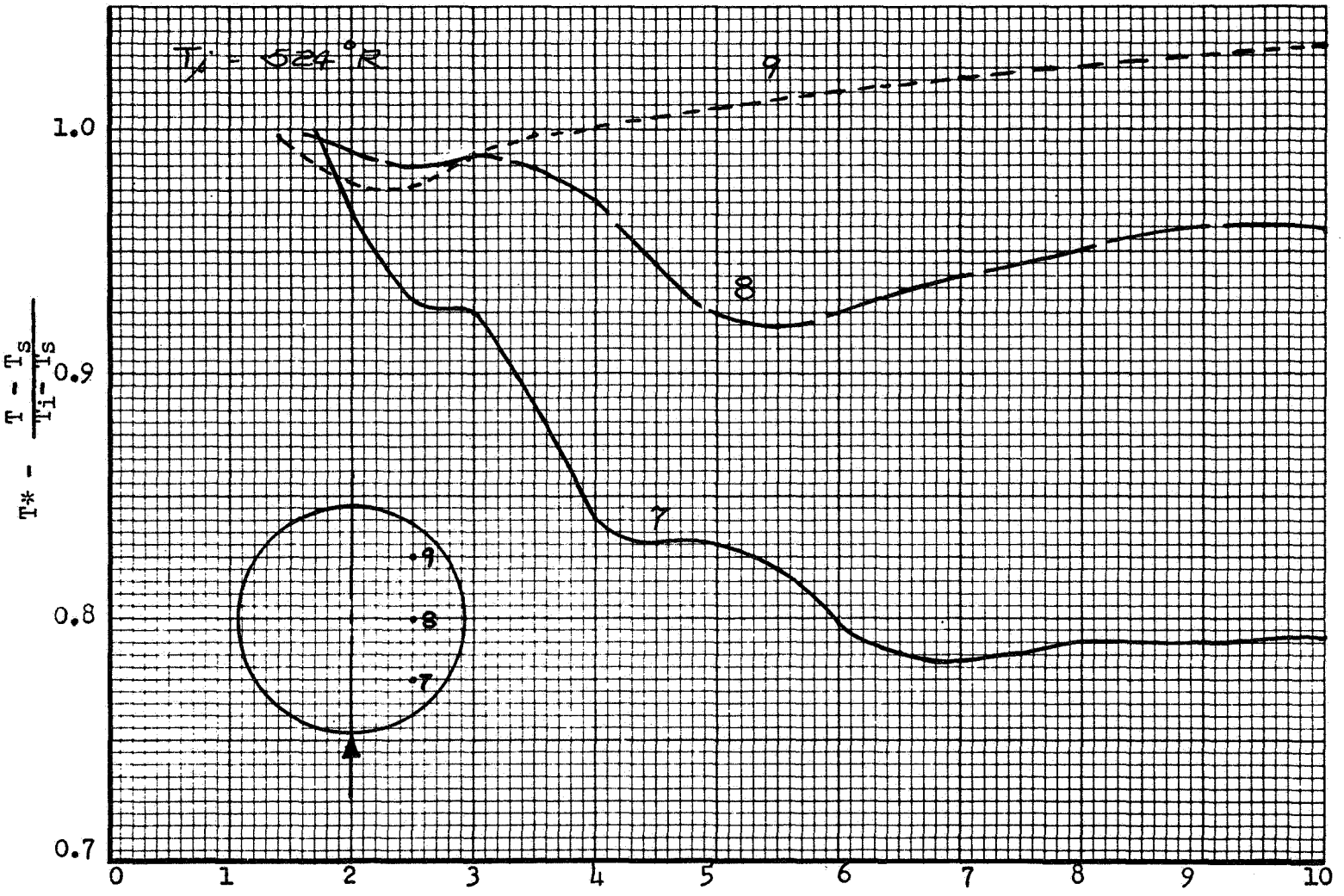


FIGURE 27 - OFF-CENTER TEMPERATURES

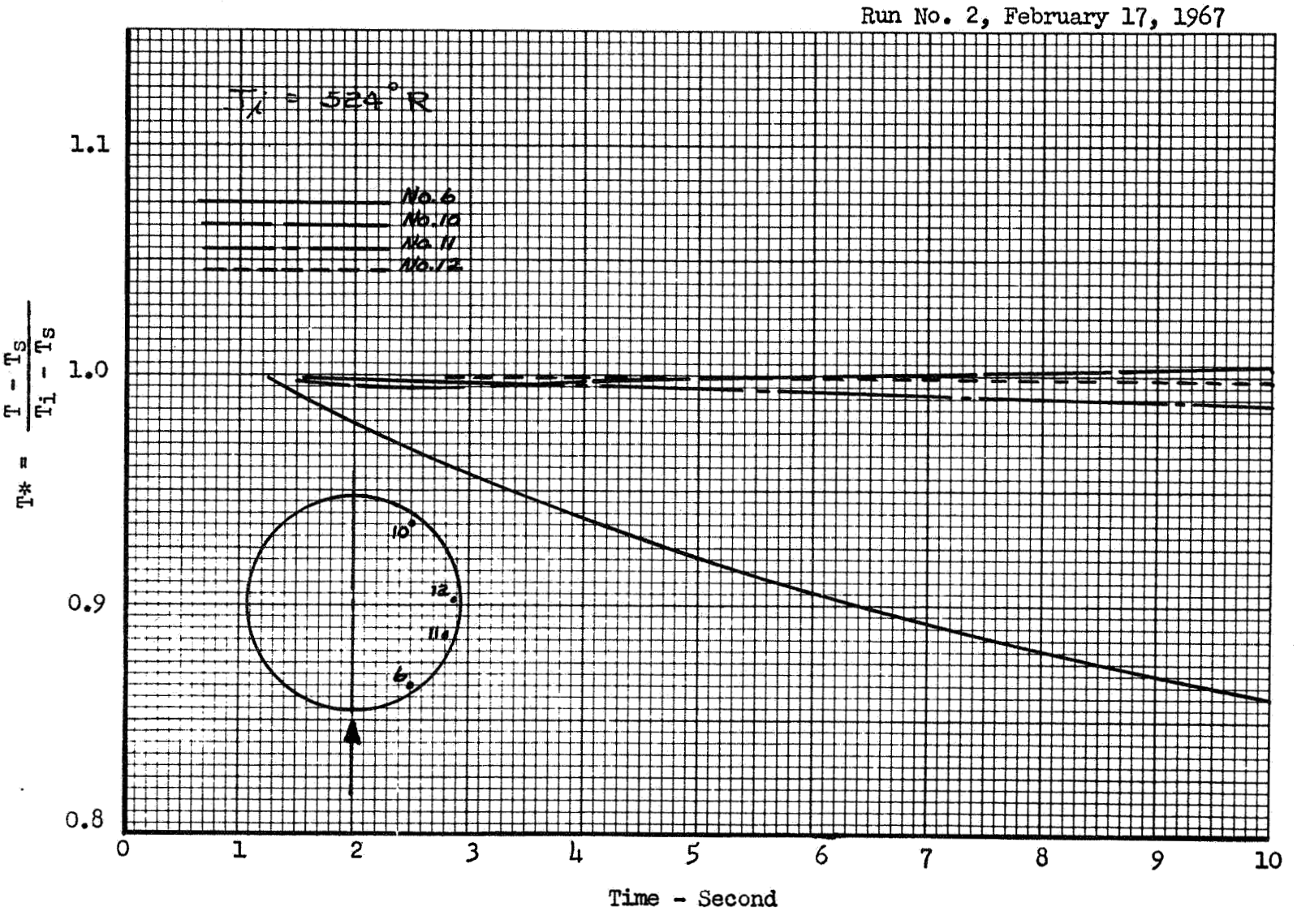


FIGURE 28 - INSIDE WALL THERMOCOUPLES

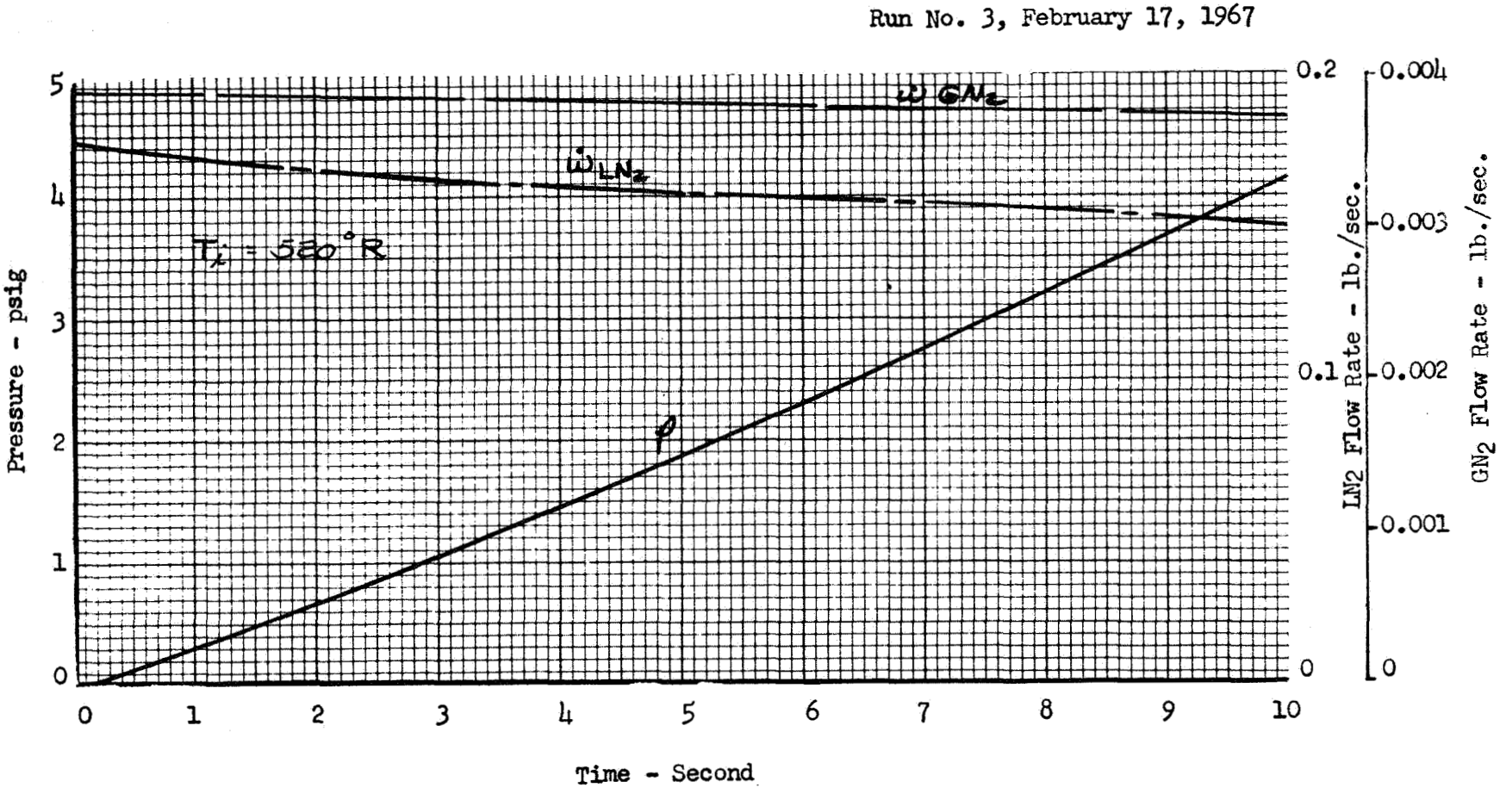


FIGURE. 29 - FLOW RATES AND PRESSURE DATA

Run No. 3, February 17, 1967

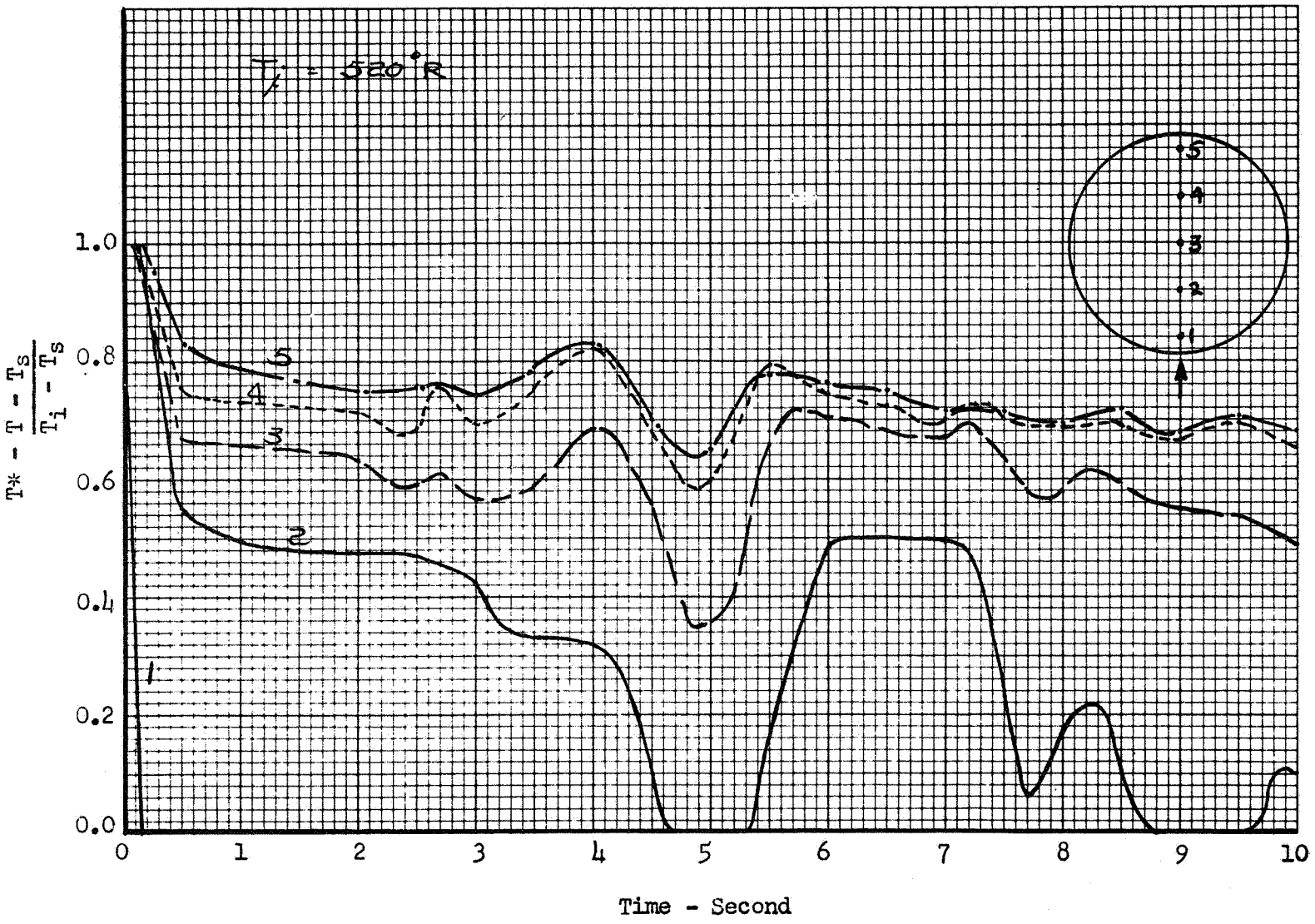


FIGURE 30- CENTER-LINE TEMPERATURES

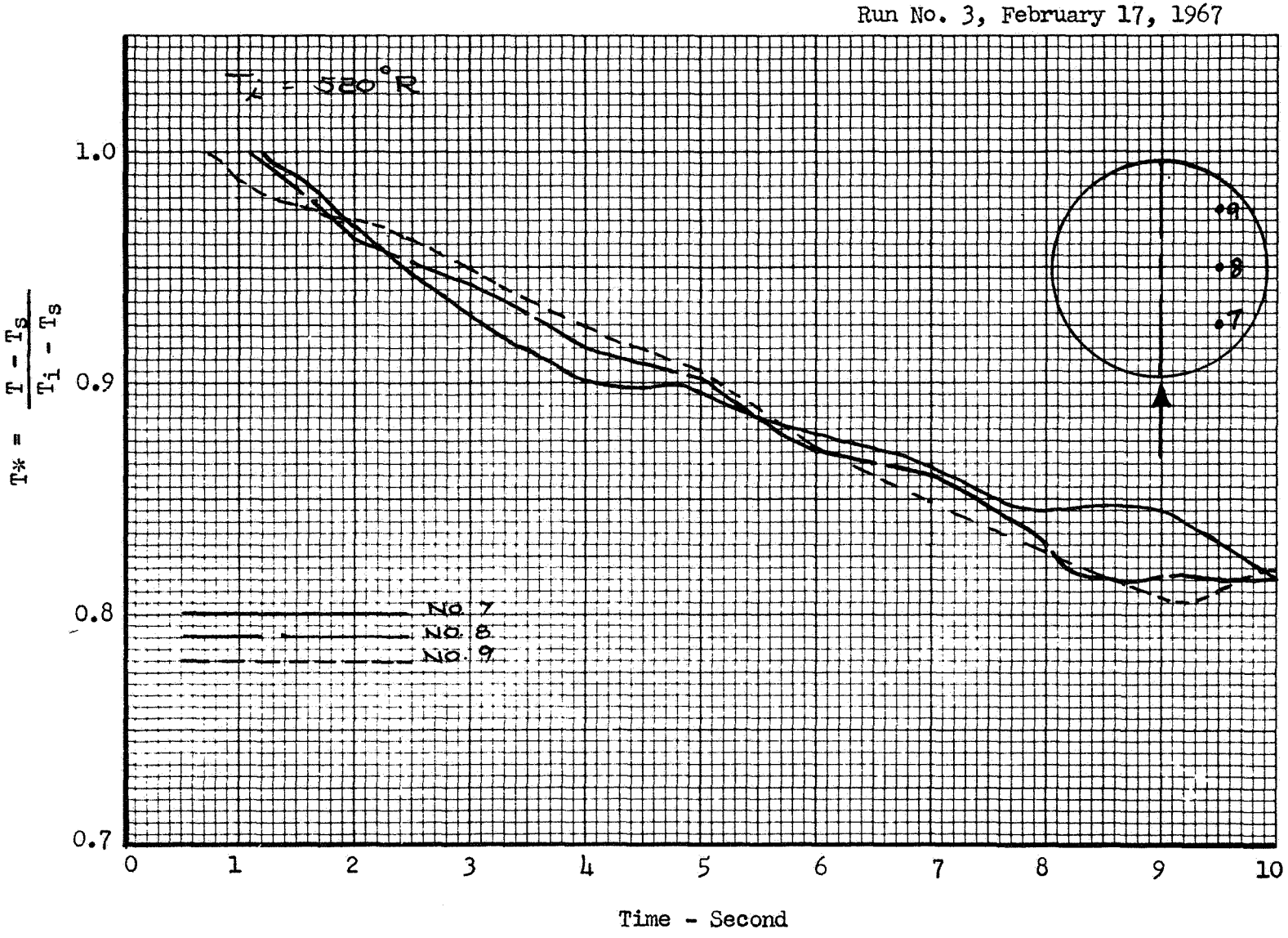


FIGURE 31 - OFF-CENTER TEMPERATURES

Run No. 3, February 17, 1967

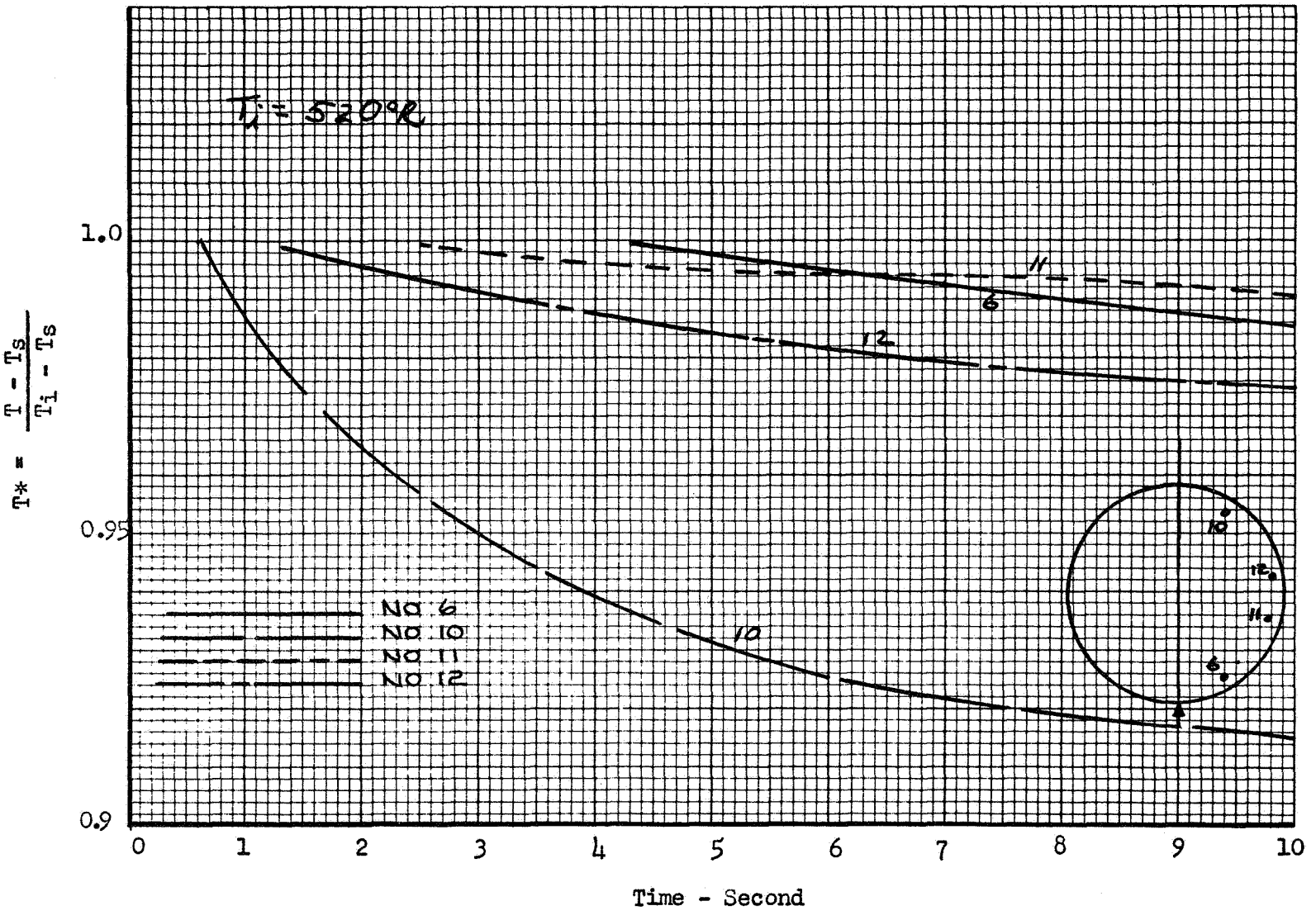


FIGURE 32 - INSIDE WALL TEMPERATURES

vapor qualities. In both tests the plume initially rose to the vessel top, but thereafter, receded (more rapidly for the low flow rate - test No. 2-17-2) due to the pressure rise in the vessel. The temperature rise above the initial temperature for the upper thermocouples later in the tests, particularly for test No. 2-17-2, is a result of the approximate isentropic compression of the gas in the upper region of the vessel. Later in the tests, there is little interaction with the two-phase jet. The temperature variation indicated by the off-center thermocouples is seen to be approximately linear. No implosion condition was observed during either of these tests.

The third test (No. 2-17-3 in Figures 29 - 32) consists of combining GN_2 and LN_2 fluid streams just downstream of the Goddard valve as shown in Fig. 5 (a Fischer-Porter rotometer is used to measure gas flow rate). Figure 29 shows the resulting pressure variation, and the liquid and gas flow rates. Figures 30 to 32 show the measured temperature distribution. Several rather significant features indicate the difference between this and prior low quality tests which used only an LN_2 supply. First, the centerline thermocouples show a much more spatially and temporally uniform temperature distribution; secondly, the off-center thermocouples indicate a very nearly uniformly mixed condition throughout the sphere outside of the jet; and finally the wall near the top exhibits the greatest cooling. In previous tests the wall at the bottom exhibited the greatest cooling. However, an implosion condition was not evident in this test.

Little data reduction of the photographic coverage of any of the above three tests has been done. However, in test No. 3 the liquid droplet size was ob-

served to be significantly smaller than in previous tests and the initial jet velocity was approximately 50 fps (Fr $\approx$ 40) compared to approximately 10 fps (Fr $\approx$ 1 to 2) in previous low vapor quality tests. The more uniform temperature distribution observed in the last test is probably strongly dependent on the considerably higher inlet velocities and greater drop dispersion.

8.1.2.2 Tests Using Liquid Volume Fraction Meter

Since the liquid volume fraction meter has been calibrated, additional tests were performed with the meter mounted in the evacuated tee section as illustrated in Figs. 5 and 8. . These tests partially duplicate the previous tests performed; however, they are more extensive and do include the liquid fraction data.

They include tests with both LN_2 flow only and also tests with combined GN_2 and LN_2 flows to provide variations in inlet velocity and quality as summarized below.

No. 3-30-1	LN_2 only	($\approx$ 0.067 lb/sec)
No. 3-30-2	LN_2 only	($\approx$ 0.035 lb/sec)
No. 3-30-3	Combined LN_2 and GN_2 (0.00128 lb/sec) flows	($\approx$ 0.036 lb/sec)
No. 3-30-4	Combined LN_2 and GN_2 (0.00339 lb/sec) flows	($\approx$ 0.035 lb/sec)
No. 3-30-5	Combined LN_2 and GN_2 (0.00616 lb/sec) flows	($\approx$ 0.067 lb/sec)

The liquid volume fractions measured at the location of the meter (approximately 14-1/2 inches upstream of the sphere inlet) are presented for run 3-30-3 in Fig. 33. In general, the liquid fraction is relatively low; however, the vapor

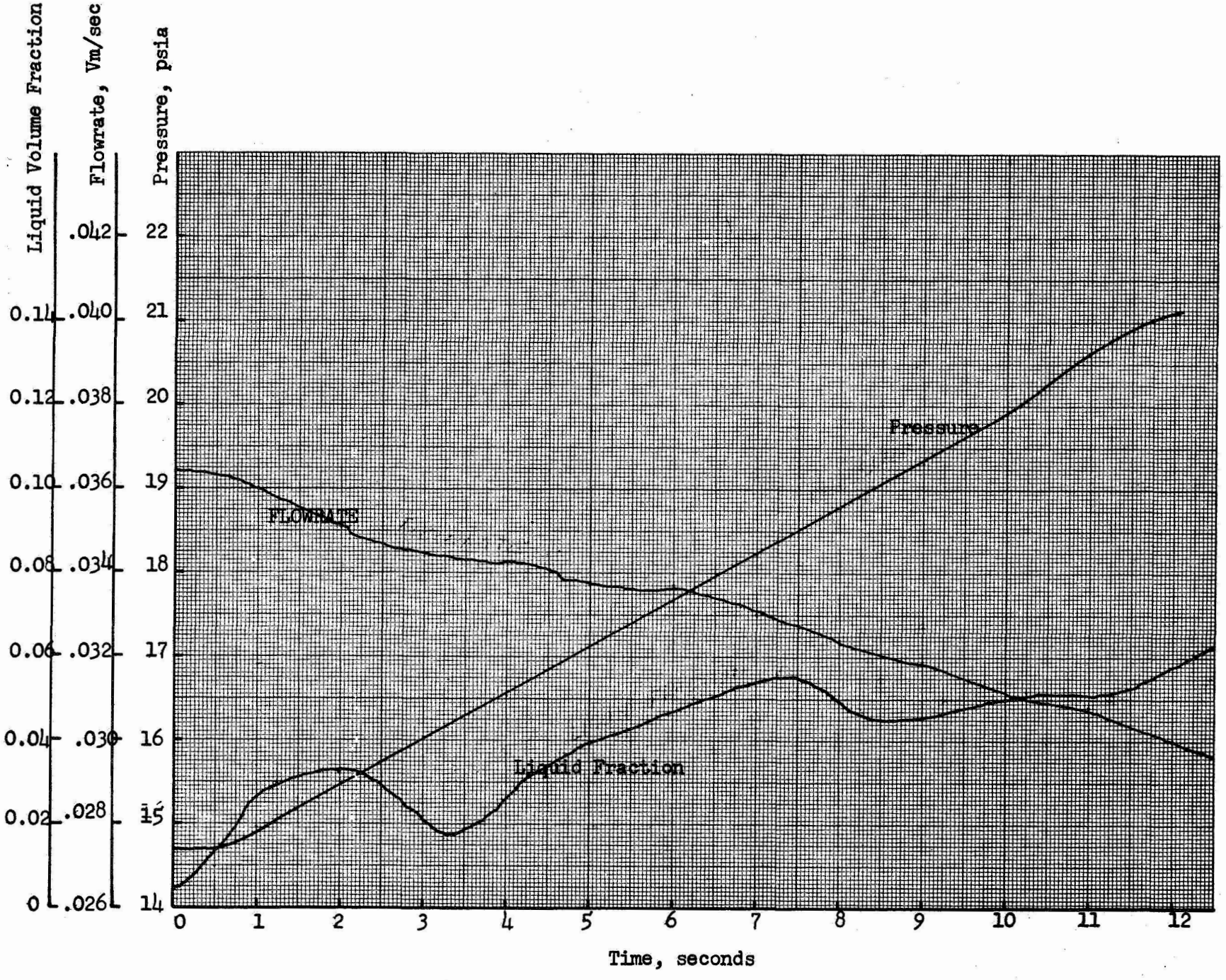


FIGURE 33 - PRESSURE, LIQUID FRACTION AND FLOWRATE RUN 3-30-3

quality drops quickly to a very low value. The vapor quality is defined as

$$X = \frac{1}{1 + \frac{F_\ell}{1-F_\ell}\frac{\rho_\ell}{\rho_g}} \approx \frac{\rho_g}{\rho_g + \rho_\ell F_\ell} \quad \text{(for } F_\ell \text{ small)}$$

For zero slip velocity, where F_ℓ is the liquid volume fraction. The temperature behavior for tests 3-30-1 and 3-30-2 are similar to those in Figs. 14 to 16 ; i.e., there are no distinct thermal regions within the sphere, and the off-center line thermocouples show an approximately linear variation. In contrast, tests 3-30-3, -4, and -5 for combined gas-liquid flow, where the inlet velocities are much greater, exhibit a more uniform temperature within the sphere (See Figs. 34 - 36). In general, the lower portions of the wall (thermocouple No. 6) exhibits greater effects for the LN_2 runs than the upper portion of the wall (thermocouple No. 10) due to the considerable liquid falling to and collecting near the bottom. For the combined LN_2-GN_2 flow tests -3, -4 and -5, the upper portions of the wall (thermocouple No. 10) responds considerably more due to the impingement of the higher velocity plume at the top of the vessel. The increase in temperature above the initial temperature toward the end of the test (particularly for No. 2) is a result of the approximate isentropic compression of the gas near the top of the sphere as the pressure continues to increase and the plume height recedes. For none of these tests, even though inlet conditions were varied considerably, did an implosion pressure drop occur. There was a very short period for some tests when the pressure responded only after a fraction of a second.

$$T^* = \frac{T - T_s}{T_i - T_s}$$

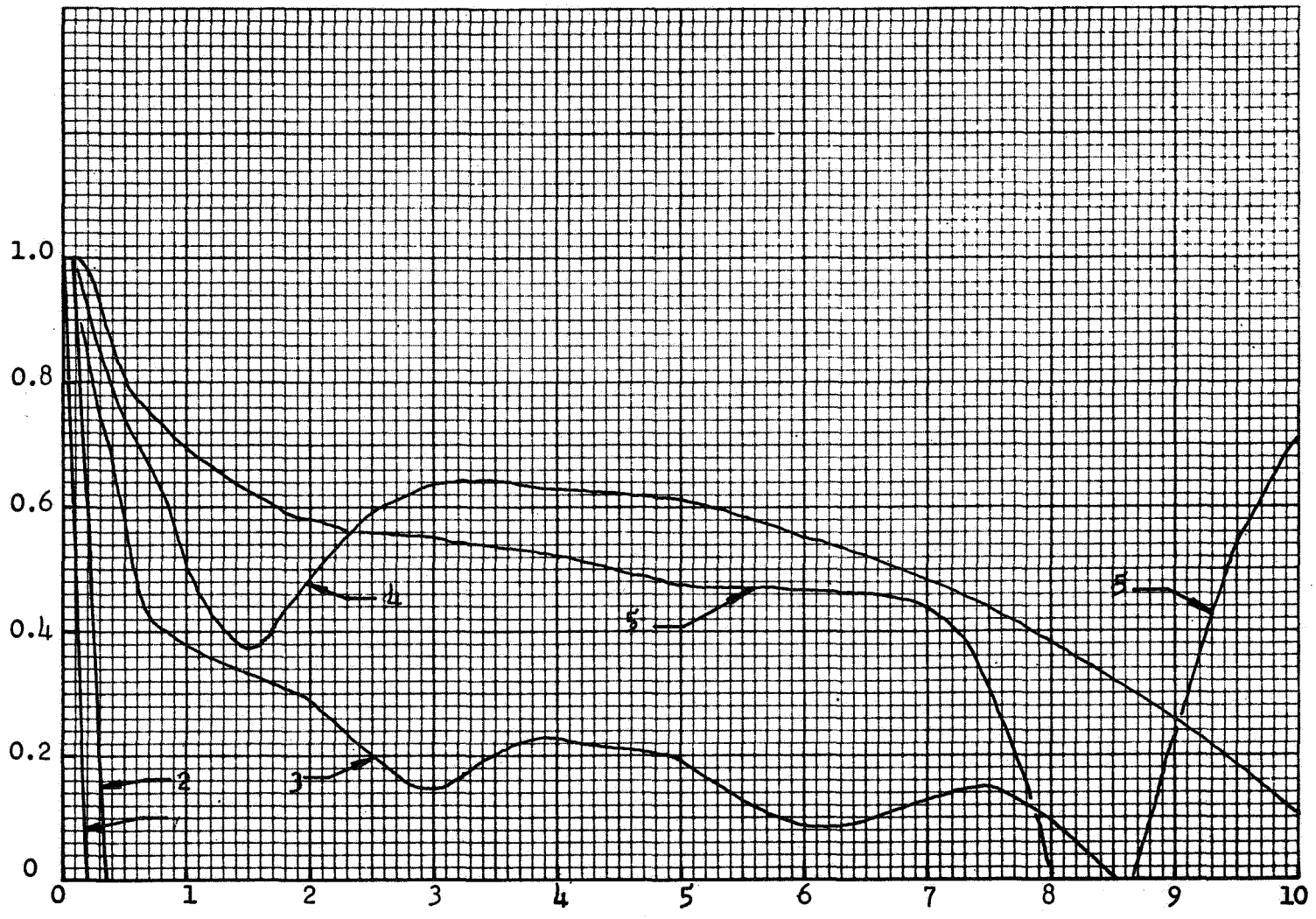


FIGURE 34 CENTERLINE TEMPERATURES RUN 3-30-3

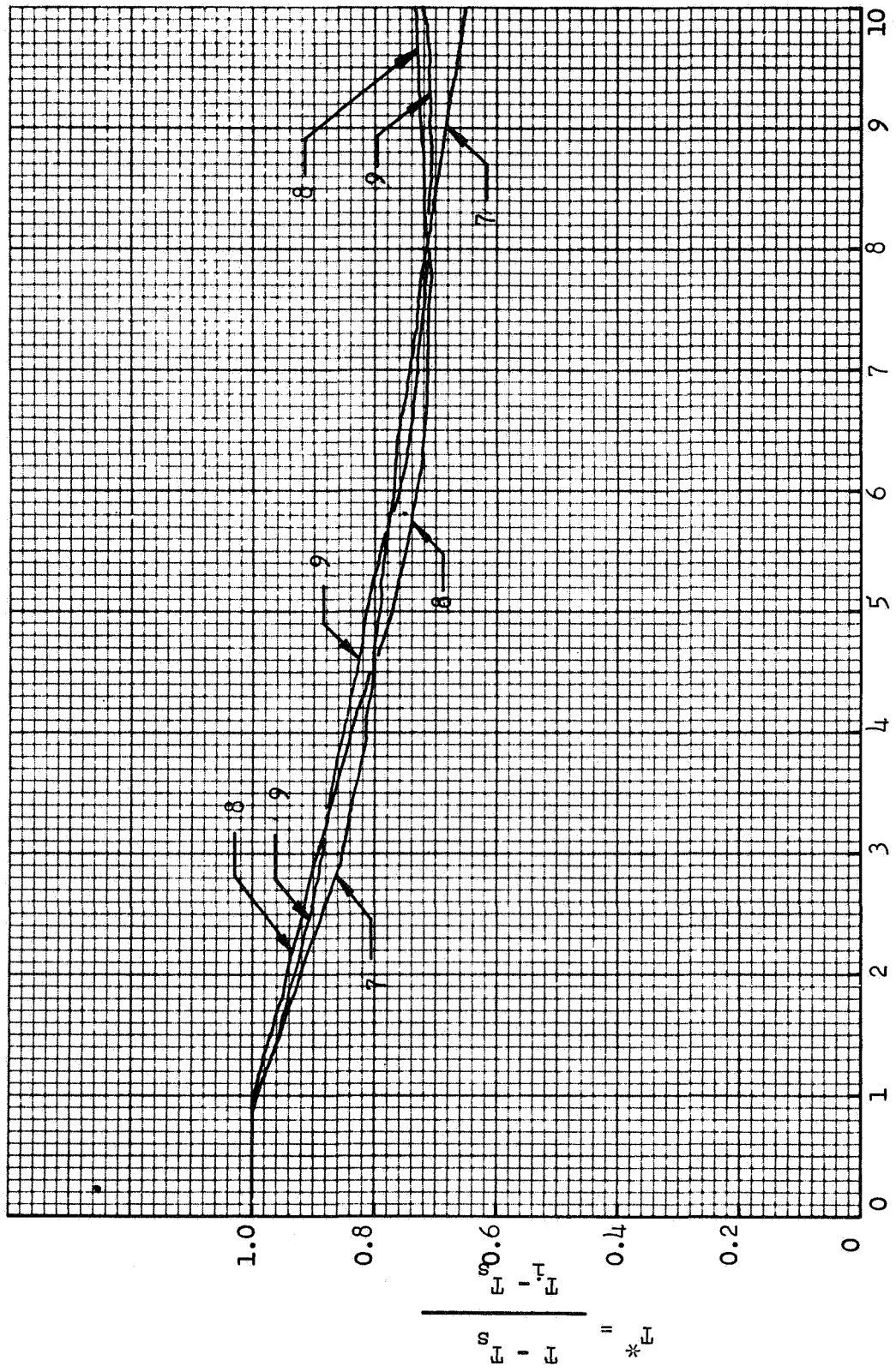


FIGURE 35 - OFFCENTER TEMPERATURES RUN 3-30-3

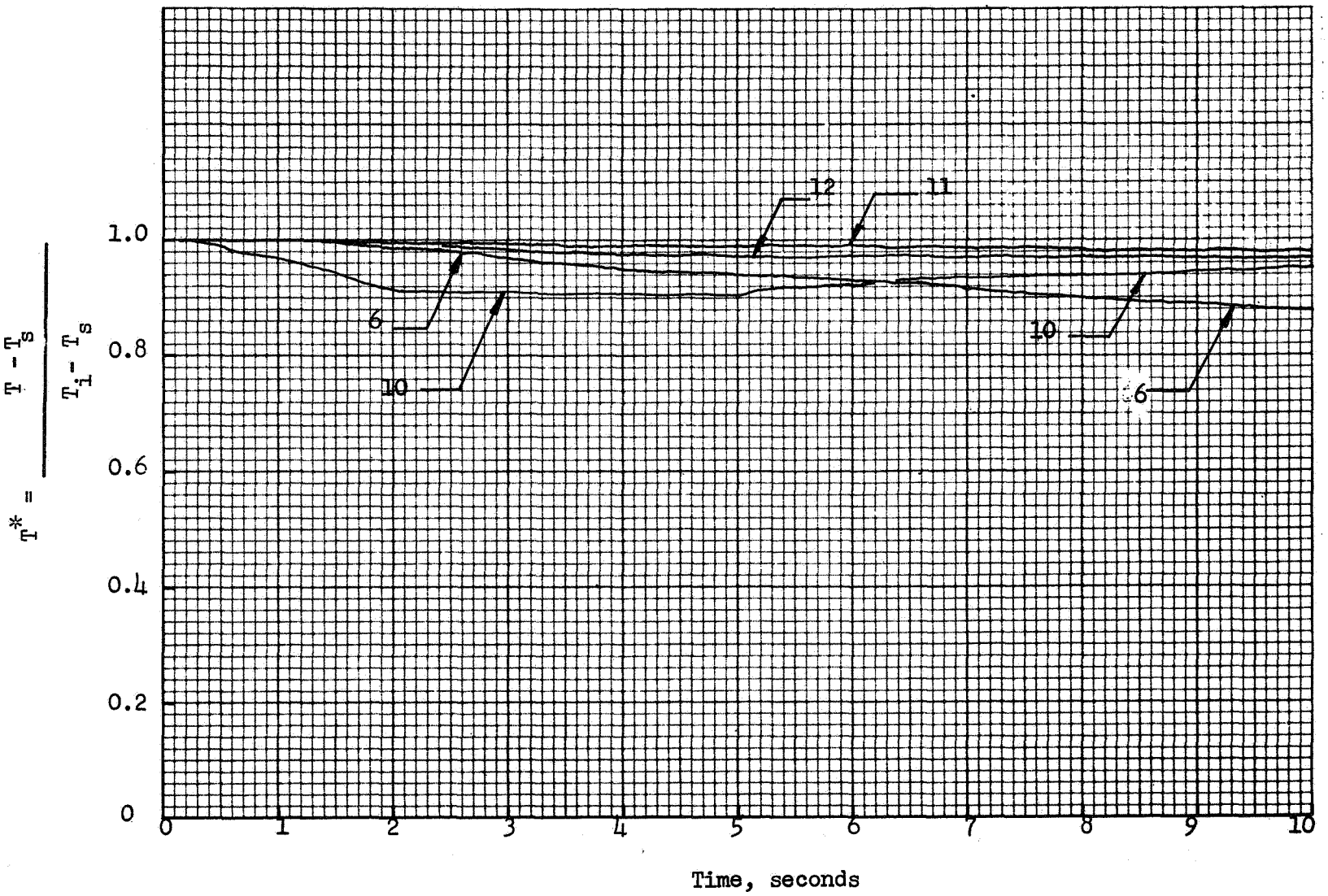


FIGURE 36 - INSIDE WALL TEMPERATURES RUN 3-30-3

8.2 COMPARISON OF ANALYTICAL PREDICTIONS WITH EXPERIMENTAL DATA

As discussed earlier, one objective of the quasi-steady-state tests was to provide as nearly constant inlet flow conditions as possible. For most of the tests, the transfer line coupling the supply dewar and the test tank were prechilled up to the tank inlet. Thus, with the exception of an initial transient, the inlet flowrate dropped slowly throughout the test as the tank pressure rose.

For one test, Run 1-18-2, quality data were obtained from high-speed movies of the flow just inside the tank inlet (see Figure 17). These data were obtained as a function of time by measuring droplet volumes from the movie film using a precision film reader. For the other runs, quality histories at the inlet were obtained from measurements made with a void fraction measurement system.

8.2.1. Tank Pressure Response

The tank-fill computer program, which is described in detail in Volume III of this report, relies on certain auxiliary analyses (performed in a subroutine) to provide the transport coefficients and fluid mechanical parameters required in the main computation procedure. In the tank fill model analysis it is assumed that two-phase fluid entering the tank forms a two-phase (liquid-vapor) jet containing liquid droplets as the dispersed phase. As a result, specification of the size of these droplets is required. In a typical jet the size distribution of droplets as a function of time may be characterized by a reference drop diameter D_D'. If a histogram, or size frequency distribution, is drawn for the droplets at the tank inlet, this char-

acteristic diameter is just the droplet diameter (at a given instant of time) at the peak of the histogram. An analysis which would specify D_D' would have to specify the fluid flow geometry at the end of the transfer line, and would need to include the effect of line geometry (valves, bends, flow obstructions) and orientation. In addition, the incoming fluid configuration may be broken up upon entering the tank if the flow stability is affected by the sudden enlargement in flow area. In view of the difficulties involved in attempting to predict D_D' and the limited utility of any specialized results which would be obtained, no such analyses was attempted.

An attempt was made to measure the characteristic droplet diameter from histograms prepared from droplet diameters measured from films of the post-inlet flow for Run 1-18-2. However, sufficiently small drop diameters could not be resolved from the film to define a peak in the histogram. The minimum measurable diameter was about 2.8×10^{-4} feet, so it could only be concluded that D_D' was less than this value.

Figure 37 shows the pressure predictions for Run 1-18-2 for a range of values of D_D'. The predictions agree best with these data when a value of D_D' of about 1.66×10^{-4} feet is used. When smaller values are used for D_D' the pressure may drop below its initial value because most of the incoming droplets evaporate in the gas. For larger values of D_D', more droplets evaporate on the tank wall producing a greater rate of pressure rise. As the droplets become very large ($D_D' = 4 \times 10^{-4}$ ft or larger) almost all of the evaporation occurs at the tank wall and the pressure approaches a limiting upper value. This is found because the larger droplets fall quickly

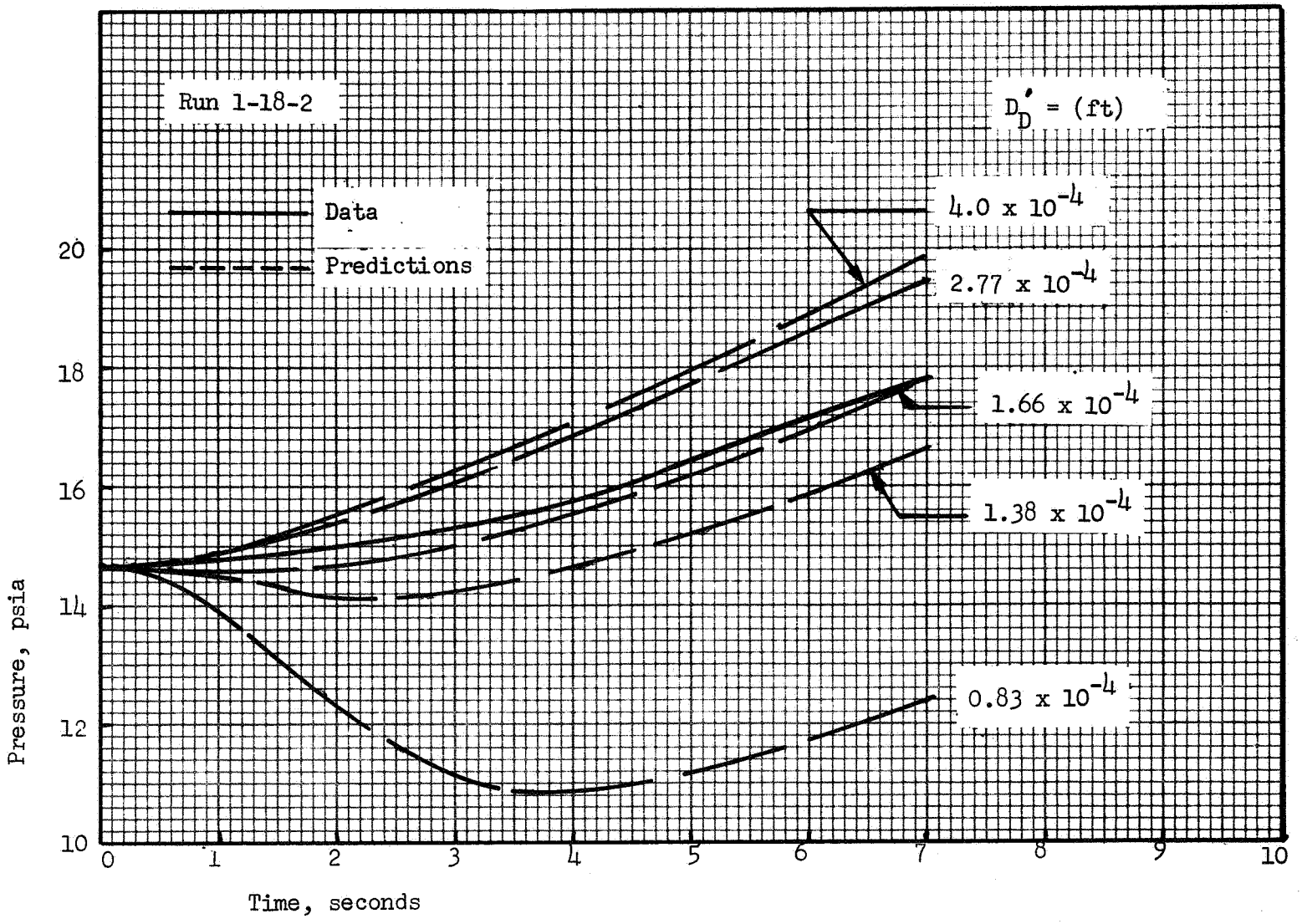


Fig. 37 Comparison of Pressure Data with Predictions --- Two-ft Transparent Tank

through the ullage vapor and on to the tank wall where rapid boiling occurs. Thus, for the larger droplets, a greater amount of energy is absorbed from the tank wall during evaporation than from the ullage vapor. Small droplets fall more slowly through the ullage vapor and extract more energy from the vapor than from the tank wall, producing a smaller rate of pressure rise, or even a pressure drop.

The results shown in Figure 37 indicate that the data for this run can be matched quite closely if the proper value for D'_D is used. Data for the other runs, shown in Figures 38 through 47 , do not match the predictions regardless of the value used for D'_D. This is because the value of D'_D does not have a significant effect on the rate of pressure rise once the initial transient is past. As the ullage vapor cools below the temperature of the tank wall, the rate of heat transfer between the ullage vapor and the wall increases. Thus, after the initial portion of the fill process, the value of h^*_{WU} has an increasingly greater effect on the rate of pressure rise. This effect is illustrated in Figures 43 and 44 wherein analytical predictions are shown for two cases. In the first case values of h^*_{WU} were computed as usual from the auxiliary analysis to the main computation procedure; in the second case, the value of h^*_{WU} is set equal to zero. As shown in Figures 43 and 44 , the computed value of h^*_{WU} is much too high. This is due to the fact that, in the auxiliary analysis, the value of h^*_{WU} (the forced-convection heat transfer coefficient between the ullage vapor and the tank wall) is computed using the average velocity of the fluid in the jet at the center of the tank. In reality, the gas velocity near the tank wall is probably an order of magnitude less than in the jet. In addition, the analytical

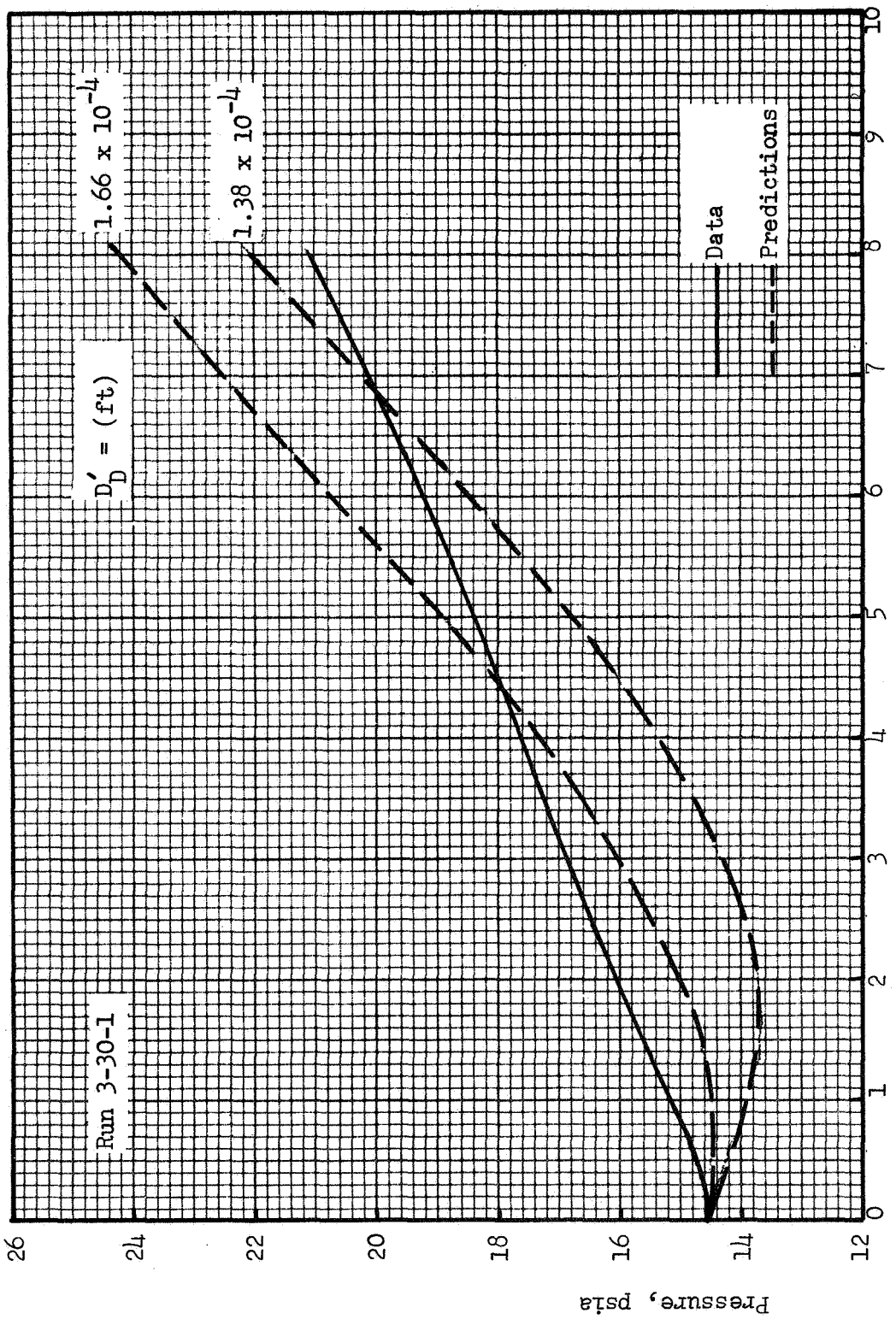


Fig. 38-Comparison of Pressure Data with Predictions --- Two-ft Transparent Tank

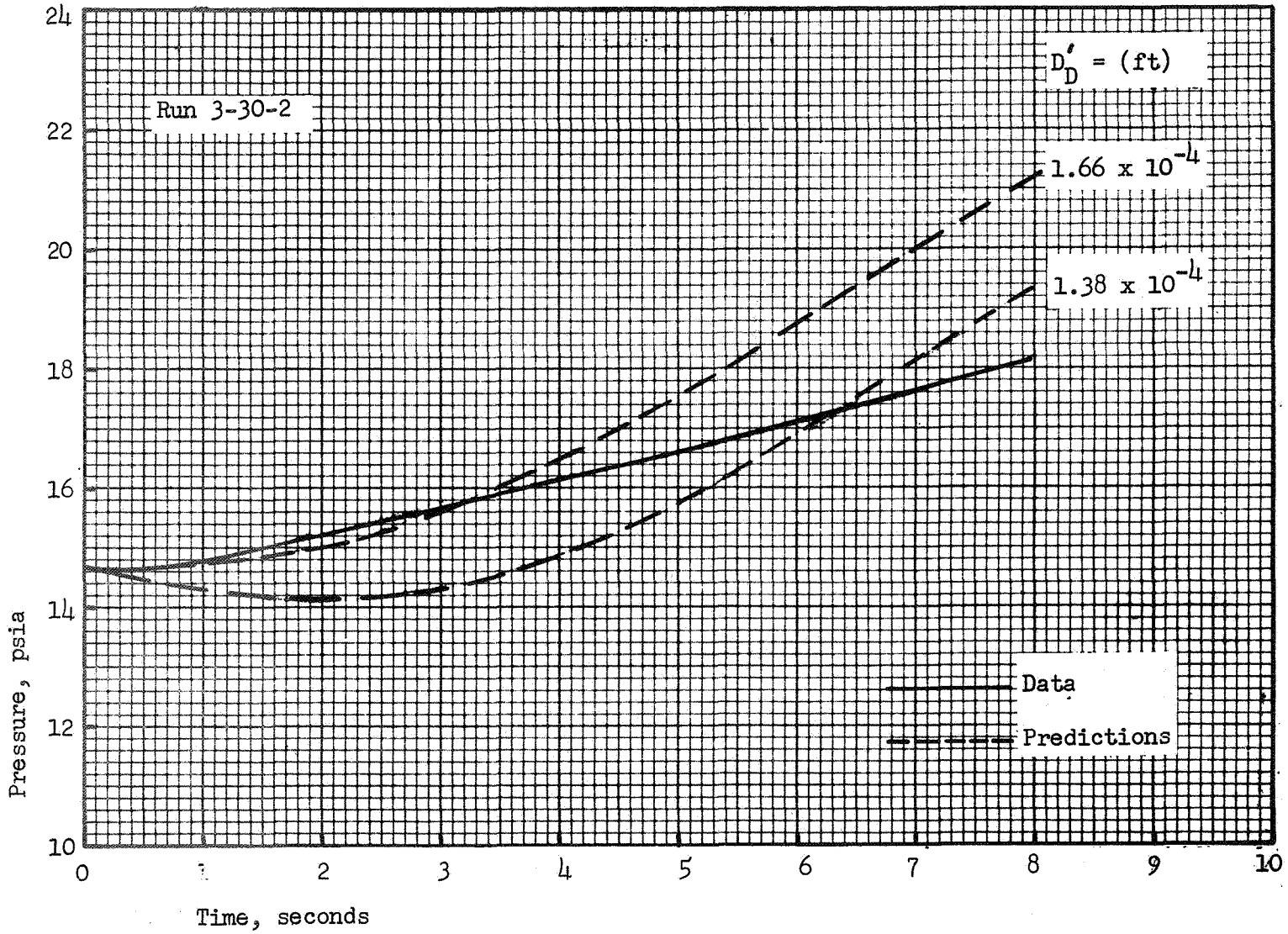


Fig. 39-Comparison of Pressure Data with Predictions --- Two-ft Transparent Tank

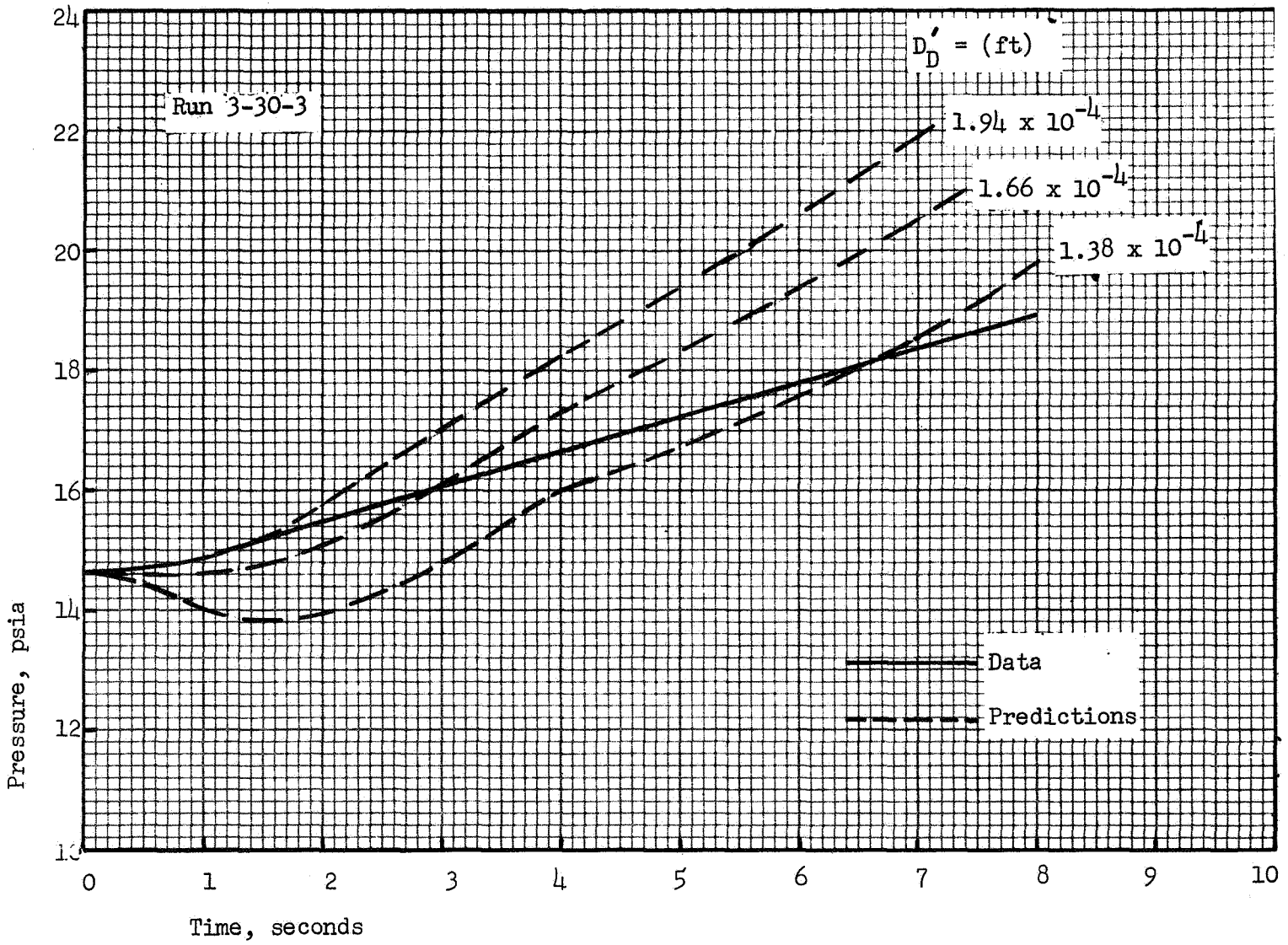


Fig. 40 Comparison of Pressure Data with Predictions --- Two-ft Transparent Tank

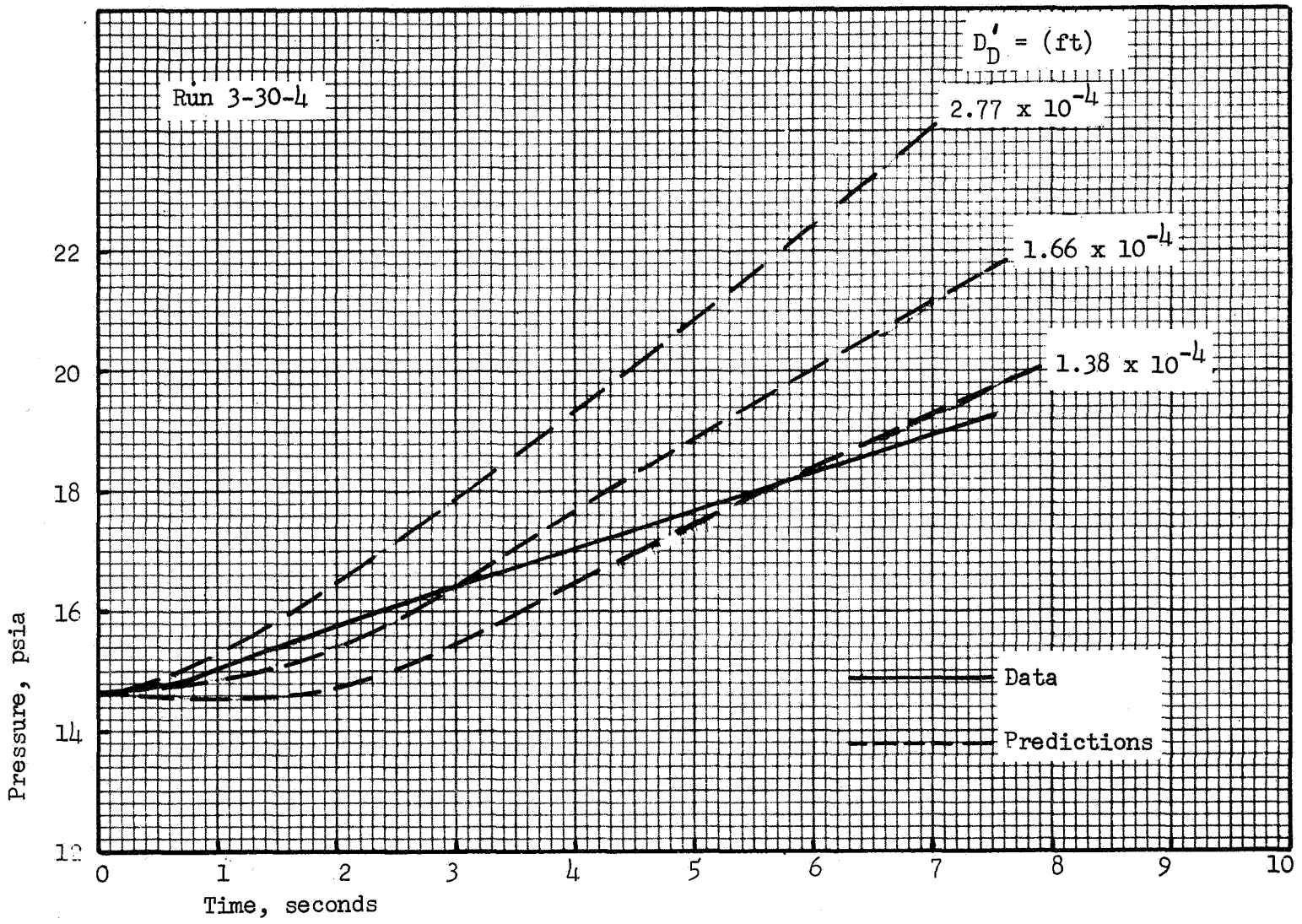


Fig. 41- Comparison of Pressure Data with Predictions --- Two-ft Transparent Tank

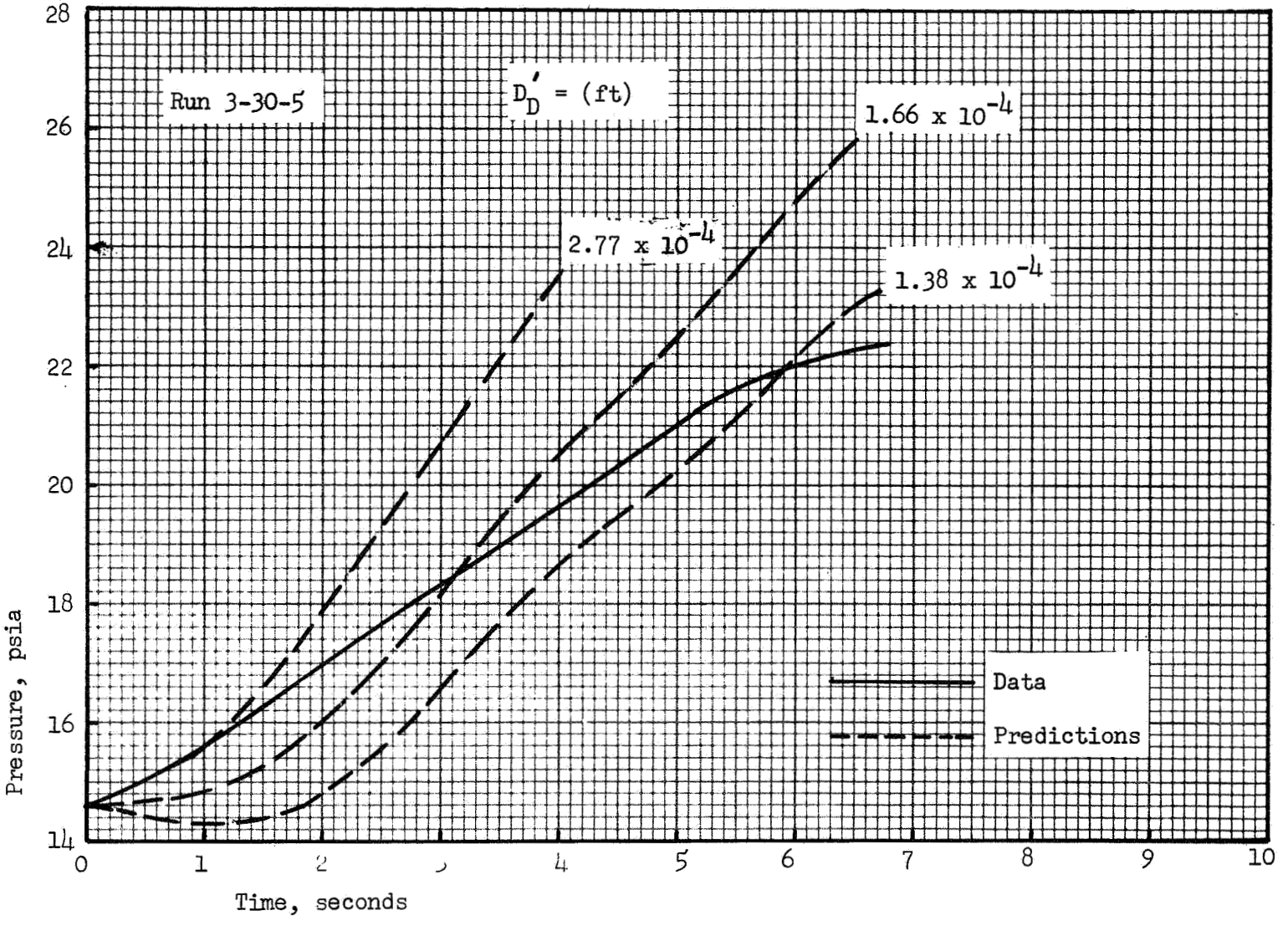


Fig. 42- Comparison of Pressure Data with Predictions --- Two-ft Transparent Tank

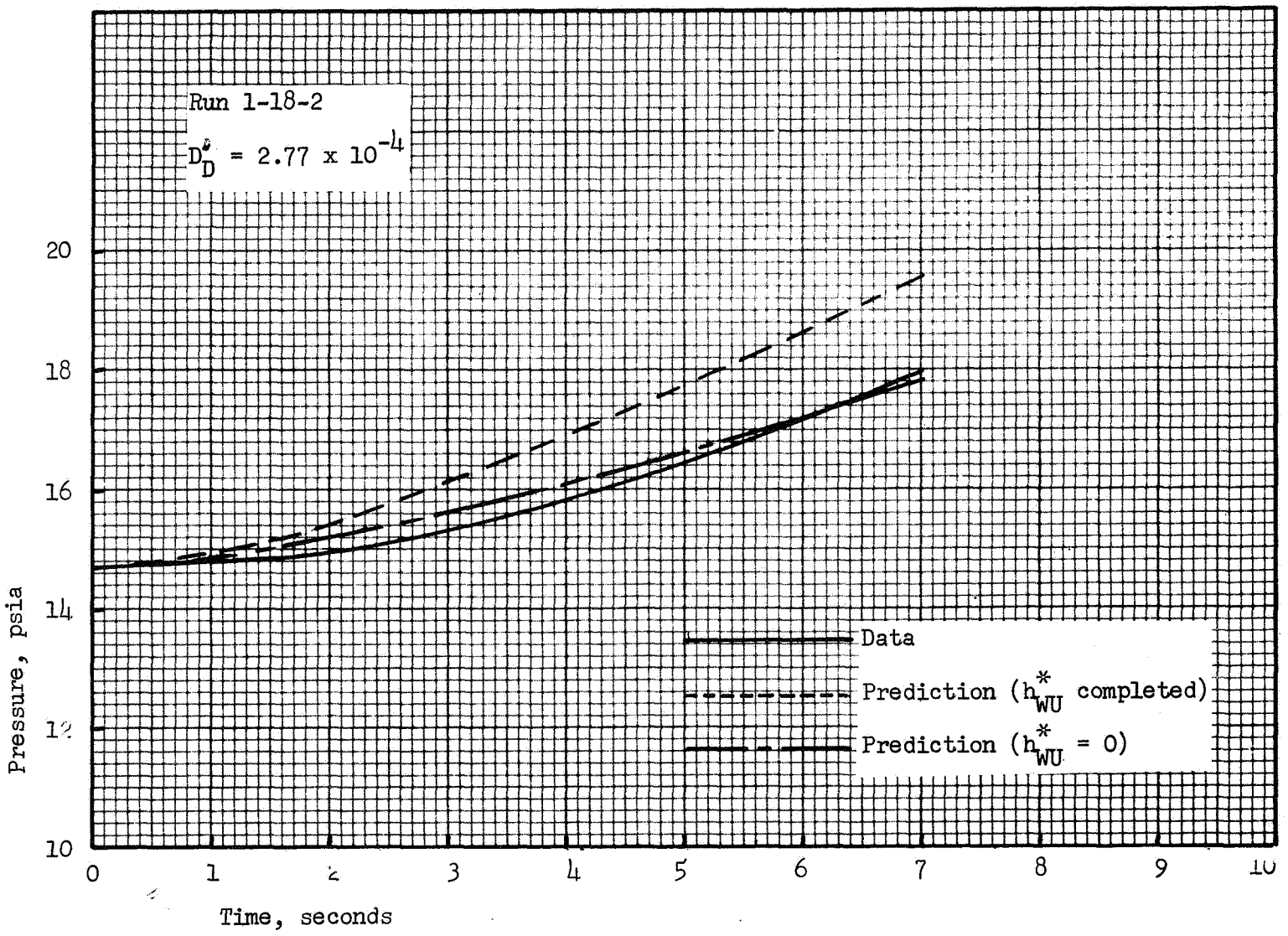


Fig. 43-Comparison of Pressure Data with Predictions --- Two-ft Transparent Tank

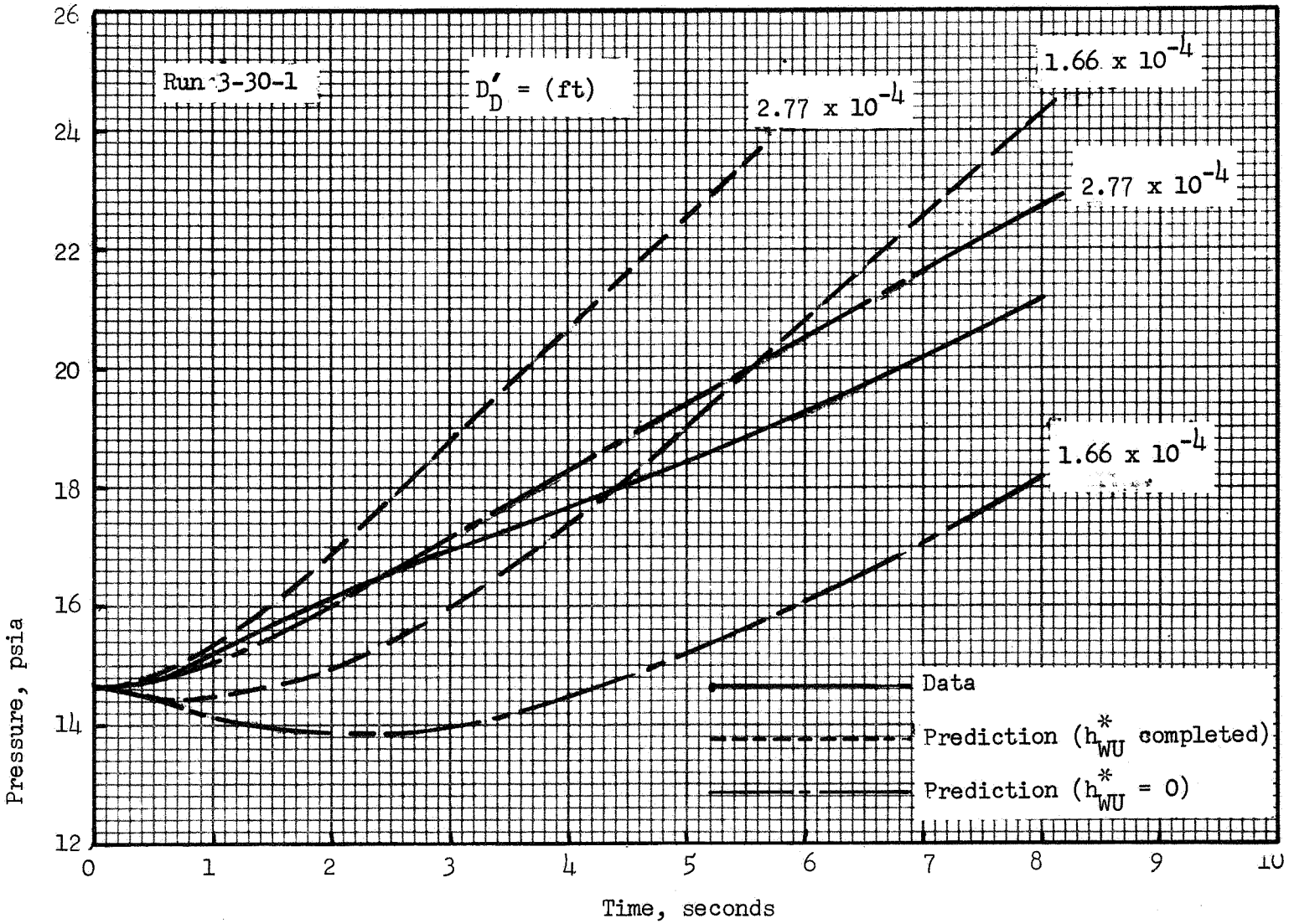


Fig. 44 - Comparison of Pressure Data with Predictions --- Two-ft Transparent Tank

model assumes uniformly mixed gas regions whereas, in actuality, the gas near the wall is relatively warm and acts to reduce heat transfer between the wall and ullage vapor.

It should be pointed out that the relative importance of heat transfer from the wall to the gas becomes less as the tank size is increased. The ratio of wall area to tank volume is a direct measure of the influence of heat transfer between the wall and the ullage vapor. For a sphere, for example, the relative importance of h^*_{WU} is inversely proportional to the tank diameter. This effect is illustrated below in section 9.2 , where data from tests on the five-foot diameter tank are compared with analytical predictions.

An attempt was not made to improve the analytical prediction of h^*_{WU} because an accurate description of the flow in the tank would be required. Since h^*_{WU} is not important for large tanks, the effect of h^*_{WU} on the small tank results is adequately illustrated with the limiting values as shown. The comparison shown in Figure 43 indicates that the predicted rate of pressure rise with a zero value of h^*_{WU} is slightly less than that indicated by the test data. However, the comparison shown for Run 3-30-1 (Figure 44) shows that the predicted equilibrium rate of pressure rise is very close to that shown by the test data. Thus, in most cases, a good prediction of the rate of pressure rise can be obtained with h^*_{WU} set equal to zero.

8.2.2 Ullage Vapor Temperature Distribution

In Figures 45 , 46 , and 47 , measured temperature data are compared with predictions using $D'_D = 1.66 \times 10^{-4}$ ft. Figure 45 shows the data measured

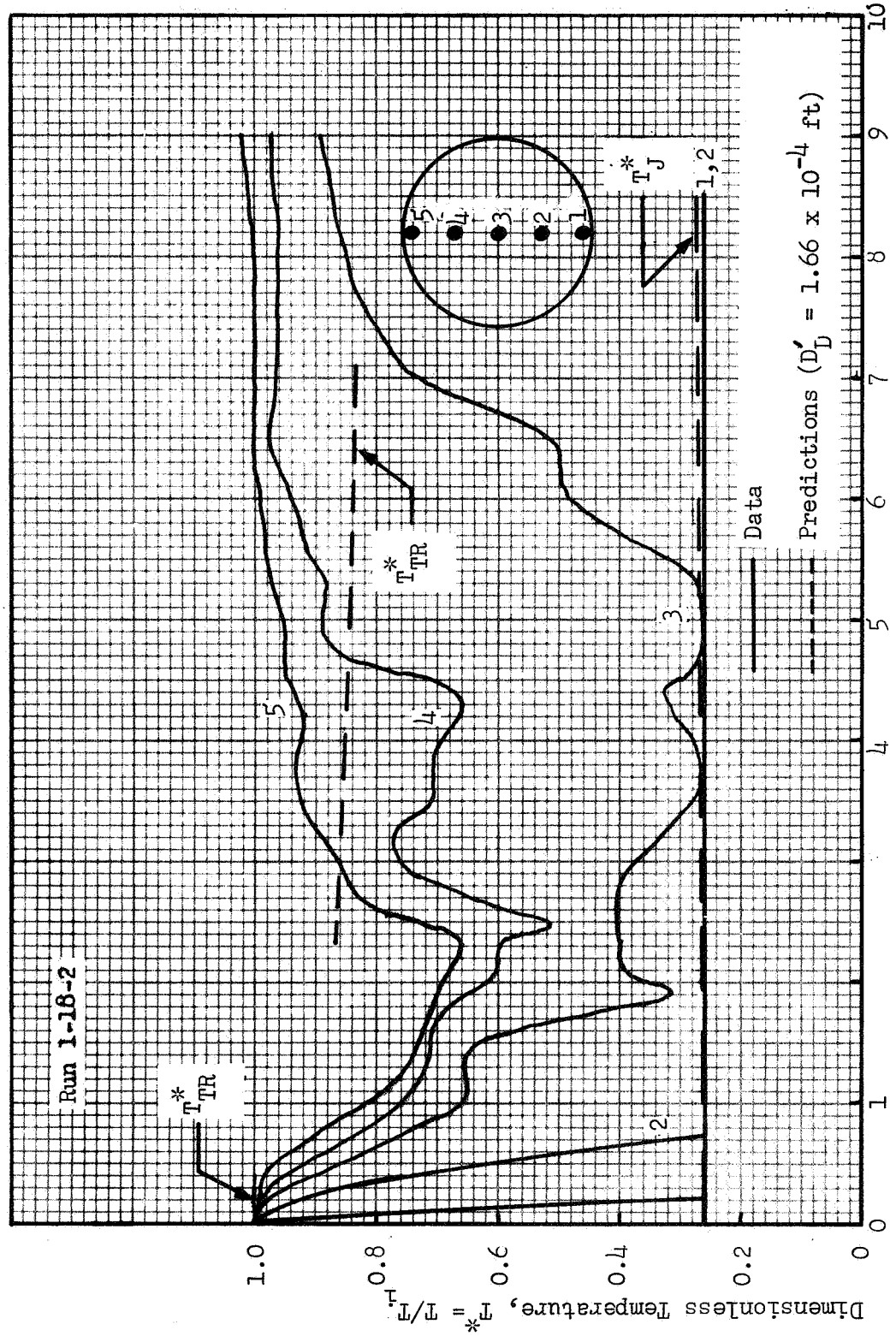


Fig. 45 -Comparison of Temperature Data with Predictions --- Two-ft Transparent Tank

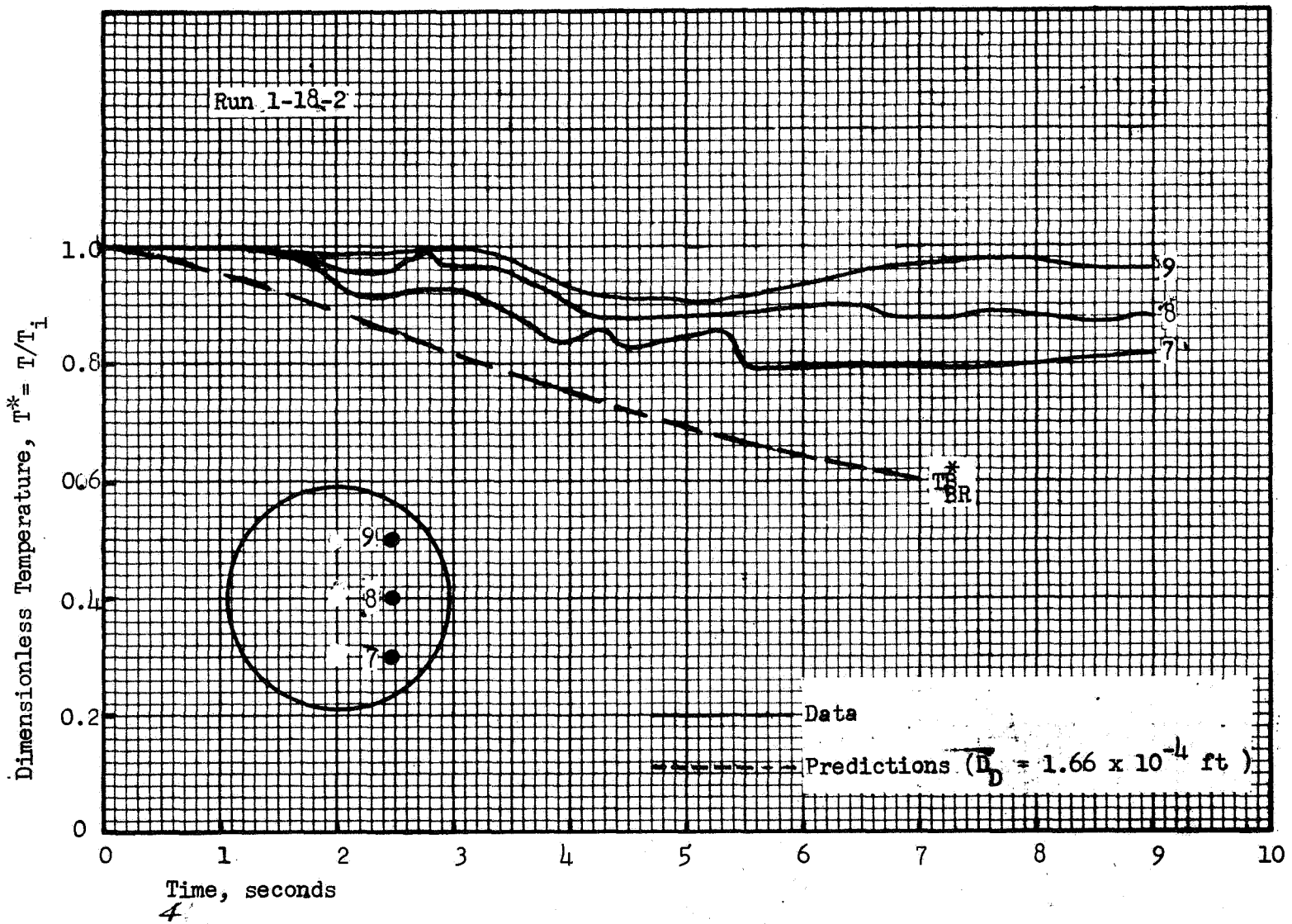


Fig. 46 Comparison of Temperature Data with Predictions --- Two-ft Transparent Tank

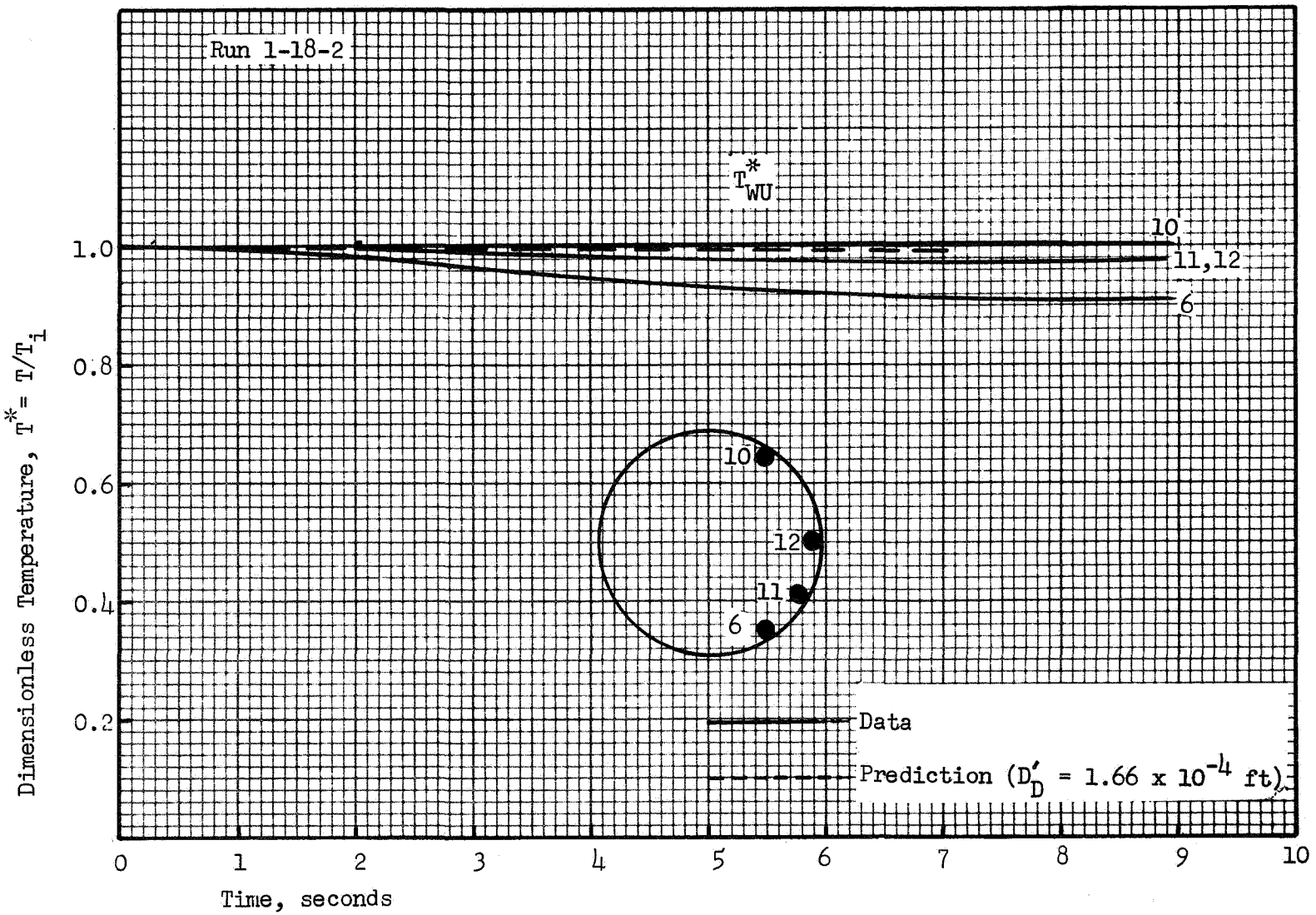


Fig.47 - Comparison of Temperature Data with Predictions --- Two-ft Transparent Tank

at five locations along the centerline of the tank. As the cold jet rises to the top of the tank (during the initial transient flow surge), the thermocouples are progressively submerged in cold gas. At approximately two seconds after initiation of flow, the jet begins to fall away from the top of the tank and continues to decrease in height as the velocity at the inlet decreases. When the jet drops below a given thermocouple the temperature at that location begins to rise. It was observed that the top of the jet never dropped below the level of thermocouple 2; therefore, thermocouples 1 and 2 remain in the jet for the remainder of the test duration and register the saturation temperature. As shown in Figure 45, the predicted jet temperature is very close to the saturation temperature throughout the entire test; this agrees very well with observed results.

The "top" region is that spherical sector of the tank above the top of the jet. This implies that during the time when the jet impinges on the top of the tank, the volume of the "top" region is zero; or, more accurately, the top region is undefined. (See Vol. III of this report for an exact description of the geometry used in the analyses.) Therefore, the predicted top region temperature is undefined between about 0.4 and 2.4 seconds from the start of fill. Since the volume occupied by the top region is changing with time (i.e., it increases from zero to some finite value as the top of the jet drops from the top of the tank to a point near the center of the tank), the value of the temperature of the top region, T^*_{TR}, represents a "mass-average temperature" of the fluid in the top region. Although the data have not been compared with the prediction on this basis, the values of T^*_{TR} and their variations with time appear to be quite reasonable.

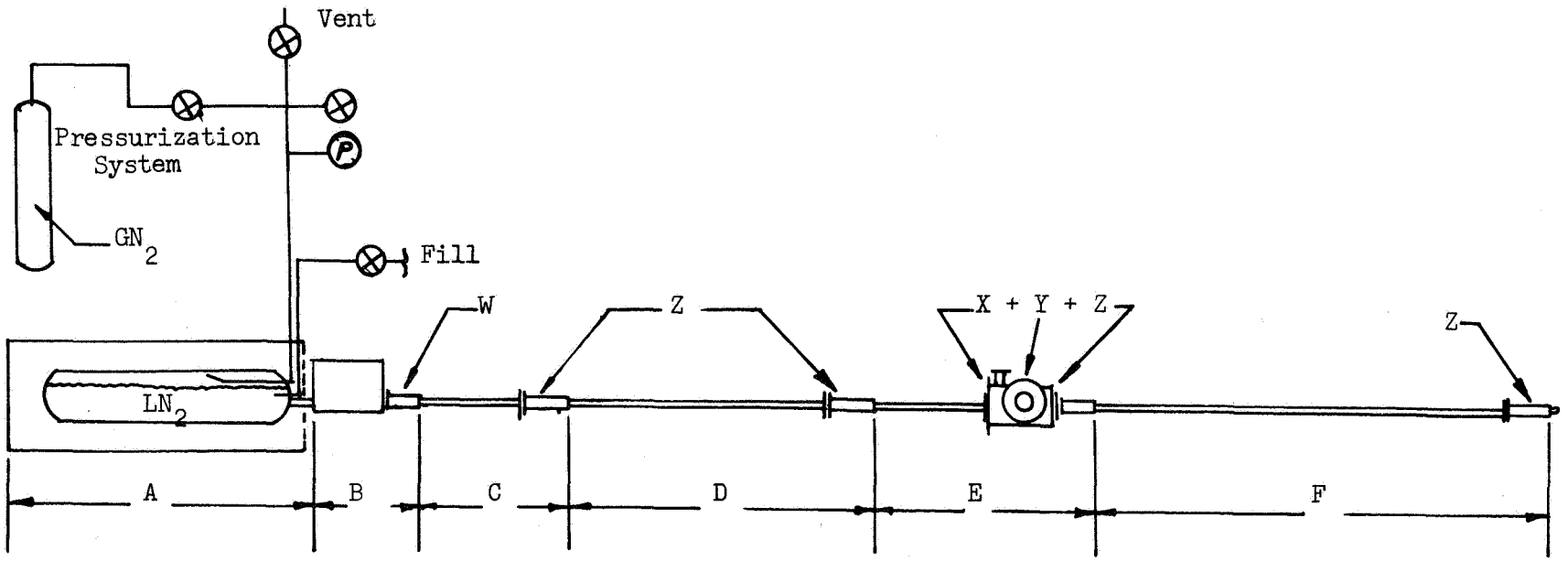
Experimental data and predicted values of the "bottom region" temperatures, T^*_{BR}, are shown in Figure 46. This comparison shows that the predicted values for T^*_{BR} are lower than the measured data. This is probably due to the fact that the temperatures recorded by thermocouples 7, 8, and 9 do not represent a proper average gas temperature in the bottom region. Near the jet the bottom region temperatures approach the saturation temperature since there is mixing between the gas jet and the bottom region.

In Figure 47 the computed and measured values of the tank wall inner surface temperatures are shown. The predicted values are very close to those measured by thermocouples 11 and 12.

8.3 TRANSFER LINE TESTS

The transfer line assembly is shown in Figure 48 . It consists of the LN_2 supply vessel, the control box, four transfer line sections of different lengths and associated instrumentation. The inner transfer line is 1/2-inch I.D. by 5/8-inch O.D. copper, with an outer 1-1/8-inch vacuum jacket. Each transfer line section has an instrumentation station at the downstream end for pressure and temperature measurements and also has thermocouples at intervals along the section. One section includes, in addition, the liquid volume fraction measuring and flow visualization stations. The control box also has an instrumented area. Line expansion or contraction is allowed for only at one location - in the inner line at the supply tank exit.

The LN_2 supply tank is a foam-insulated cylindrical vessel mounted horizontally and having a capacity of approximately 16 gallons. The vessel may be actively pressurized with helium; a transducer is used to monitor the



A - Insulated Liquid Nitrogen Supply Tank
B - Control Box and Instrumented Upstream Area
C - Three-ft. Standard Instrumented Transfer Line Section
D - Seven-ft. Standard Instrumented Transfer Line Section
E - Five and one-half ft. Visual and Instrumented Transfer Line Sections
F - Eleven-ft. standard Instrumented Transfer Line Section
W - Upstream Instrumentation Station
X - Liquid Volume Fraction Measuring Station
Y - Transparent Visualization Station
Z - Standard Instrumentation Station

NOTE: Line Segments can be arranged in any order.

FIG 48 Assembly Drawing for One-half Inch Transfer Line

pressure supply.

The control box as shown in Figure 49 includes the expansion bellows which allows for the entire line expansion, a platinum resistor, the turbine flow meter, the throttling valve, and the full open solenoid valve followed by an instrumentation area including fluid and wall temperature thermocouples (chromel-constantan) and one static and three stagnation probes (two for forward flow and one for reverse flow). In addition, an LN_2 vent line between the valves permits complete chilldown of the line upstream of the solenoid. The short thin-walled stainless-steel section between the solenoid and beginning of the copper transfer line reduces heat transfer from the copper line prior to initiation of flow. The various line sections are joined with copper sweat couplings.

Figure 50 shows a standard instrumentation station which includes the wall and fluid temperature thermocouples (3 mil chromel-constantan), a static pressure tap and two forward stagnation probes, one being on the centerline and the other at mid-radius. Two differential pressure transducers and one absolute pressure transducer are located within the jacket, and all electrical wires feed through the upstream flange. The expanded vacuum-jacketed section accommodates the instrumentation and connects the vacuum jacket together with "O" ring seals. For the upstream instrumentation area (Fig. 49), there is additionally a "downstream facing" pitot tube and an additional differential pressure transducer. In the design of the line expansion and contraction can occur only at the upstream end of the line. During the course of testing it was found there was a 1-inch relative displacement of

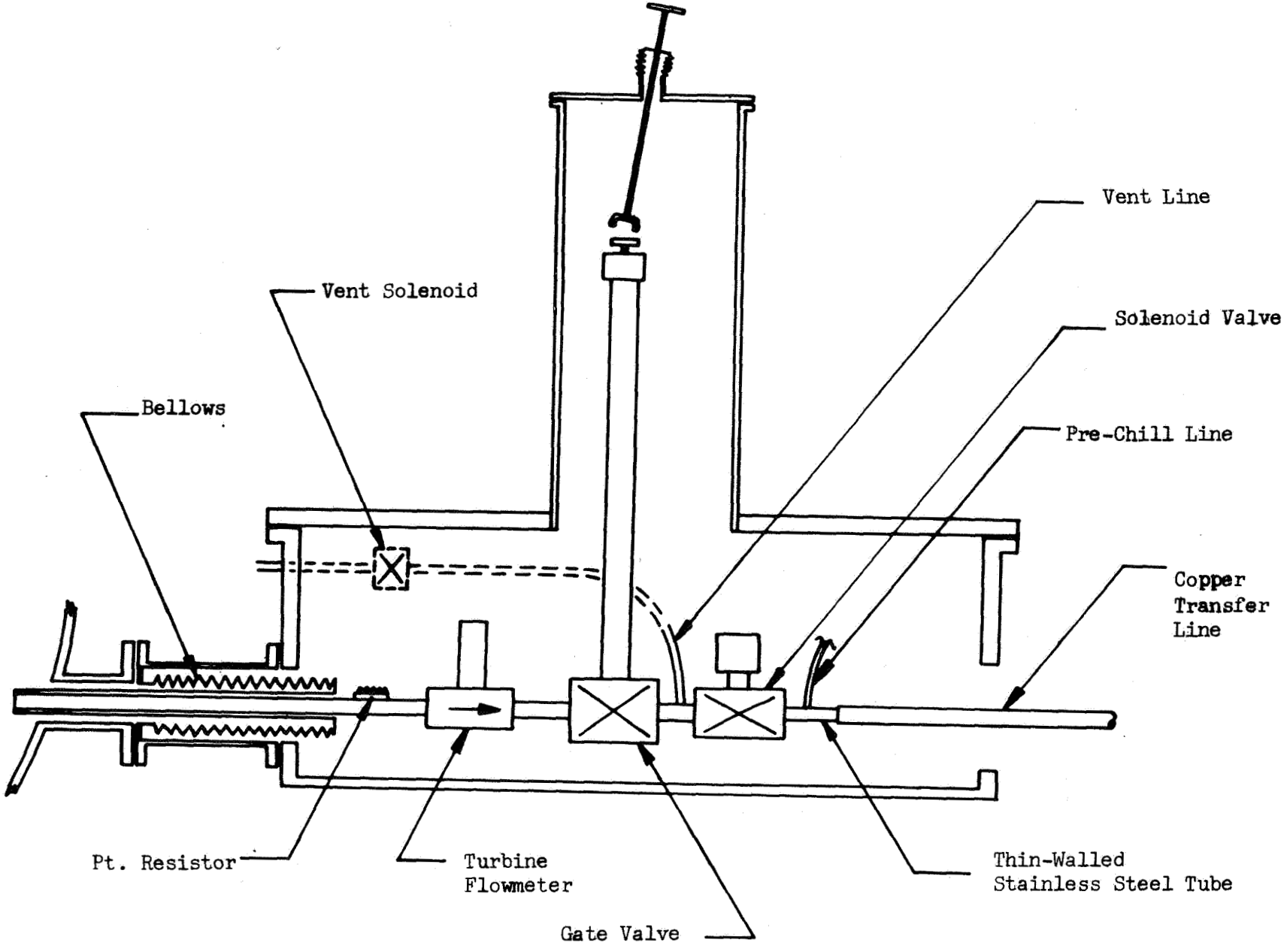


FIG 49 UPSTREAM CONTROL BOX

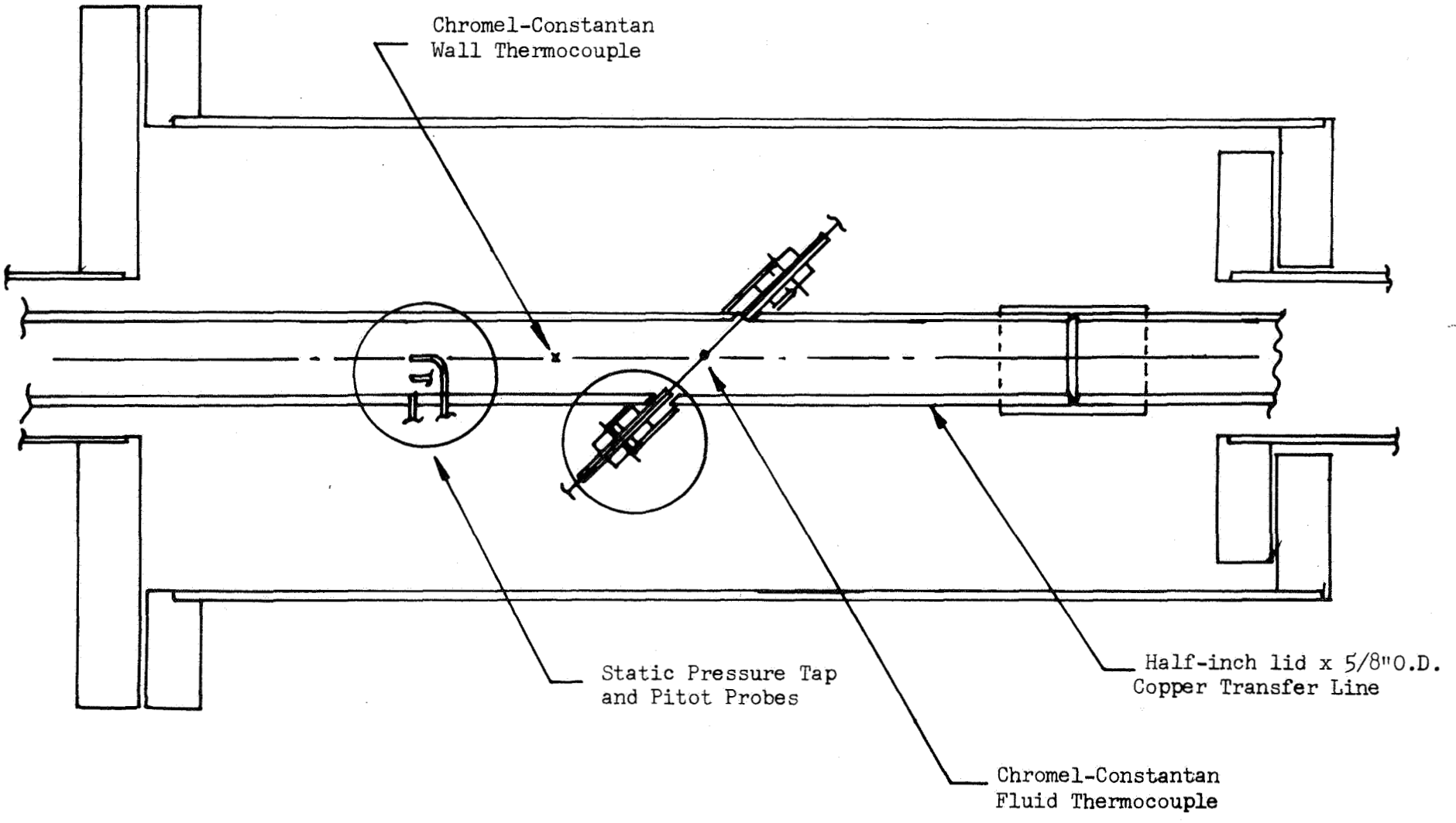


FIG 50 Standard Instrumentation Section

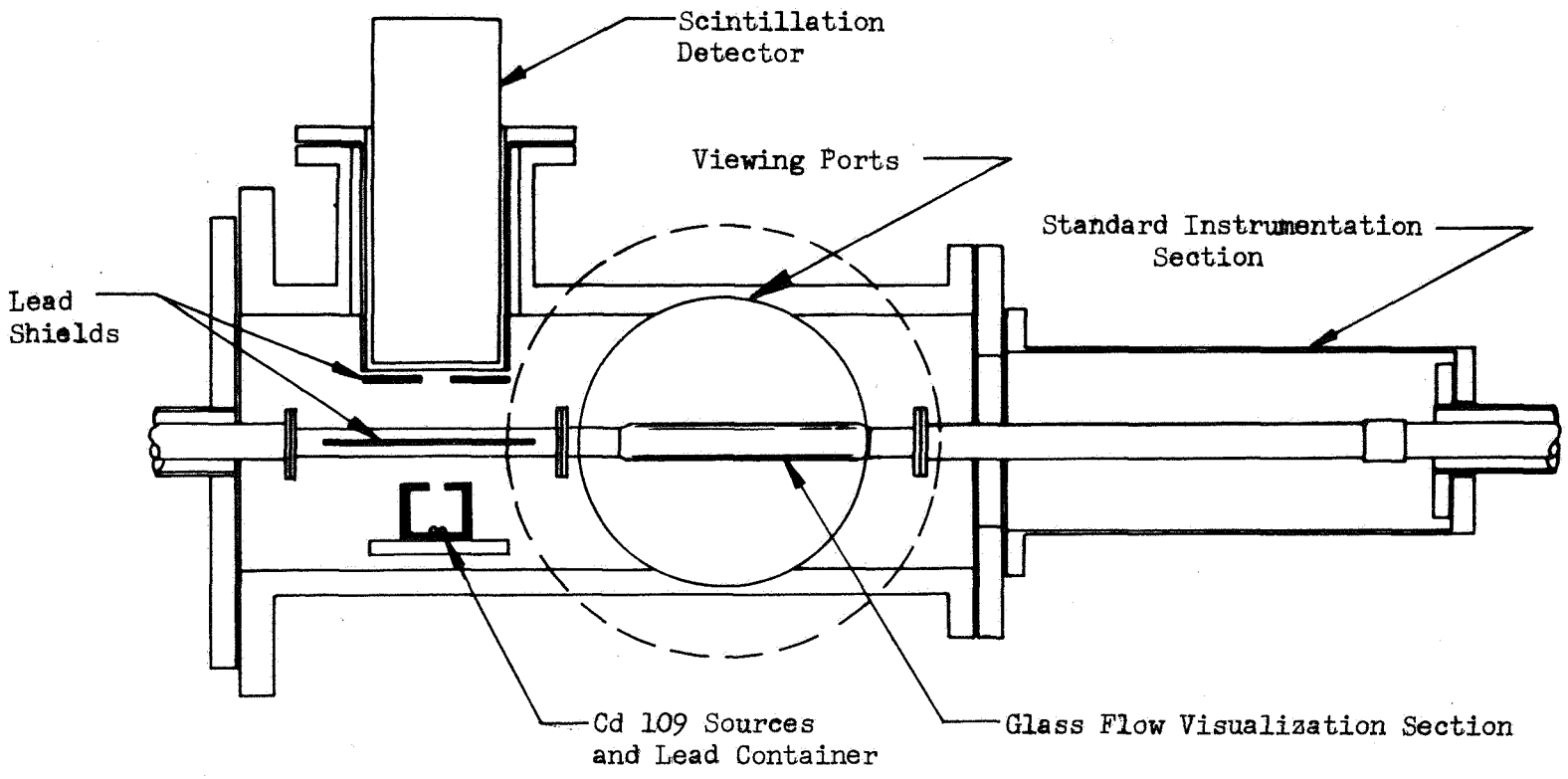


Fig. 51 - Liquid Volume Fraction Measuring Section, Flow Visualization Section and Standard Instrumentation Section for 5½ Foot Line Section

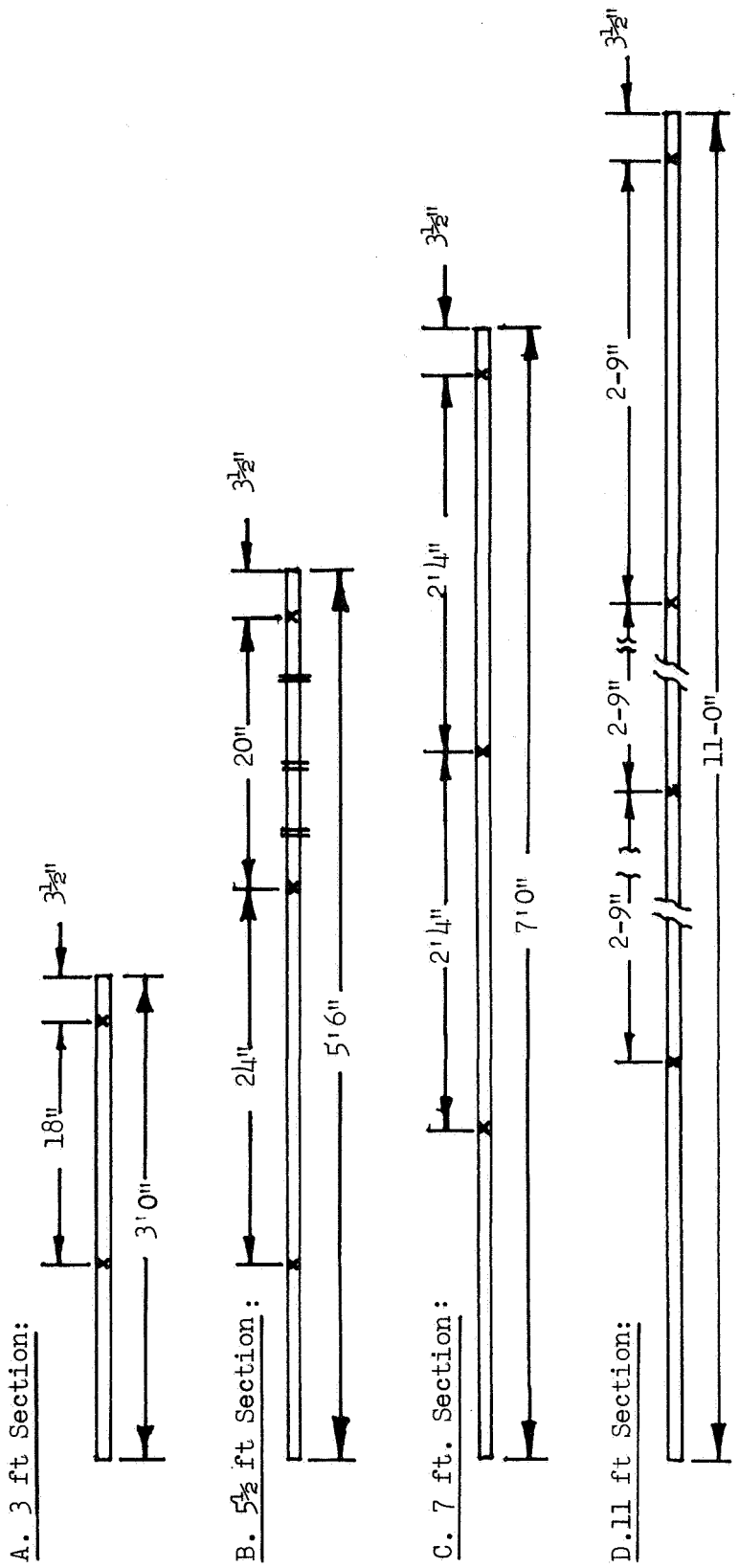


Fig. 52- Location of Wall Thermocouples on Transfer Line Sections

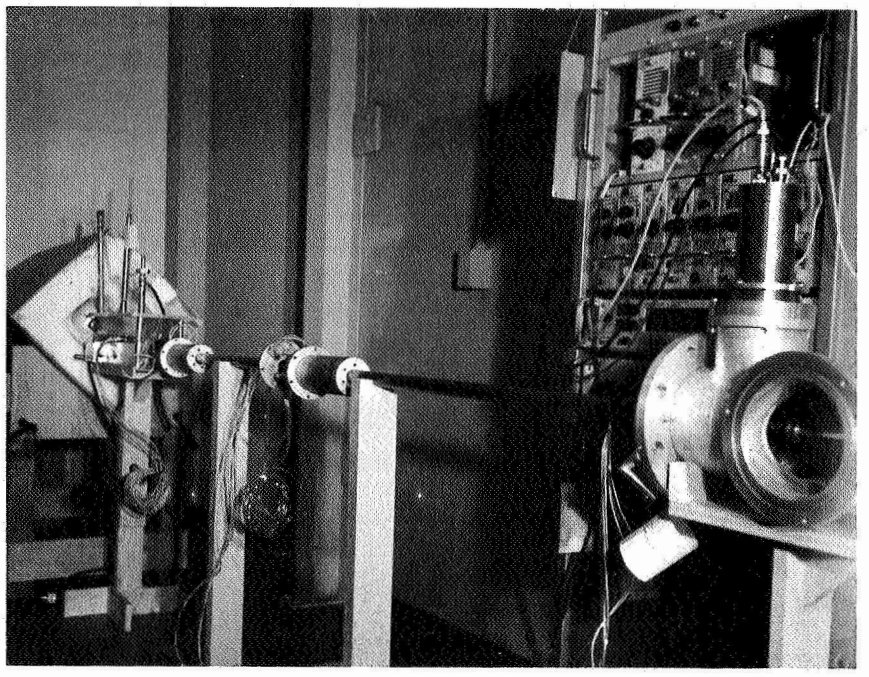


Fig. 53 View of Supply Tank, Control Box and Two Transfer Line Sections

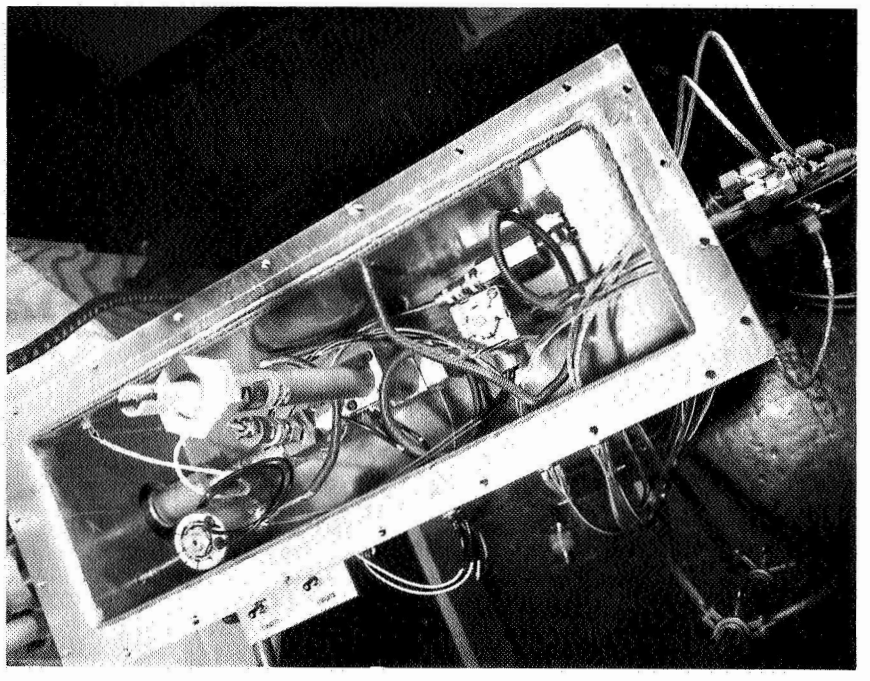


Fig. 54 View of Inside of Control Box

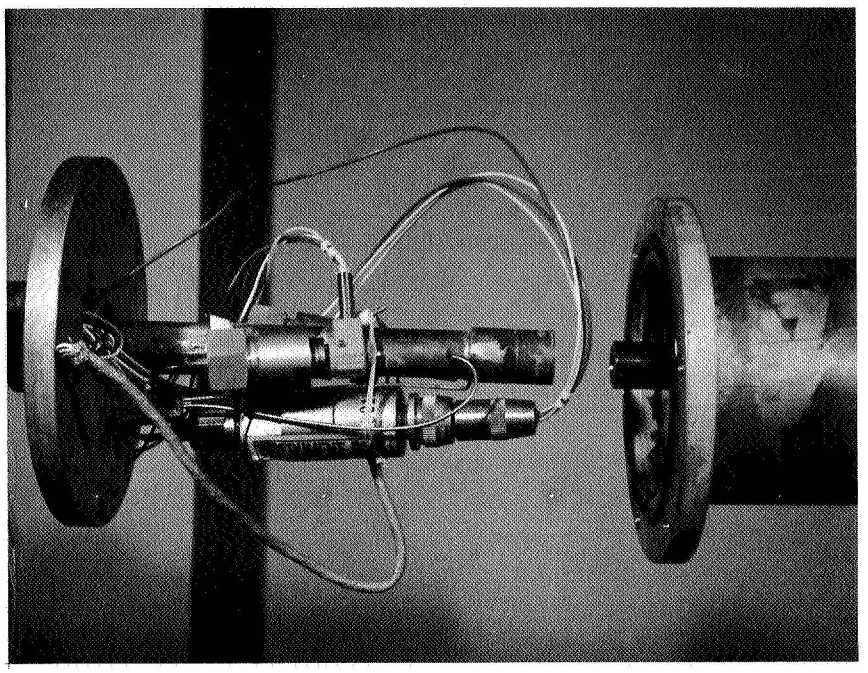


FIGURE 55 Standard Transfer Line Instrumentation Station

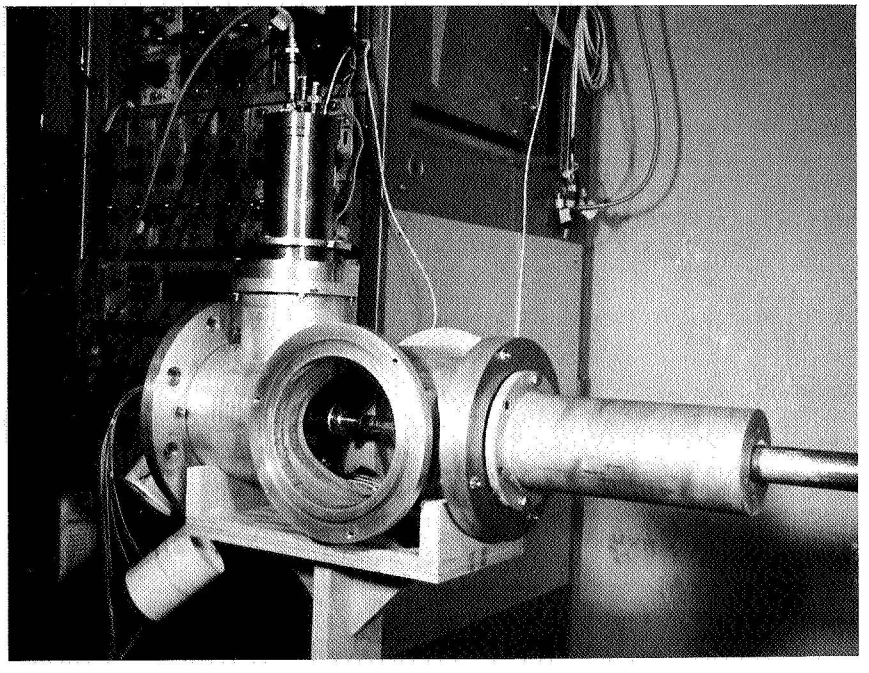


FIGURE 56 Liquid Fraction Measurement and Flow Visualization Station

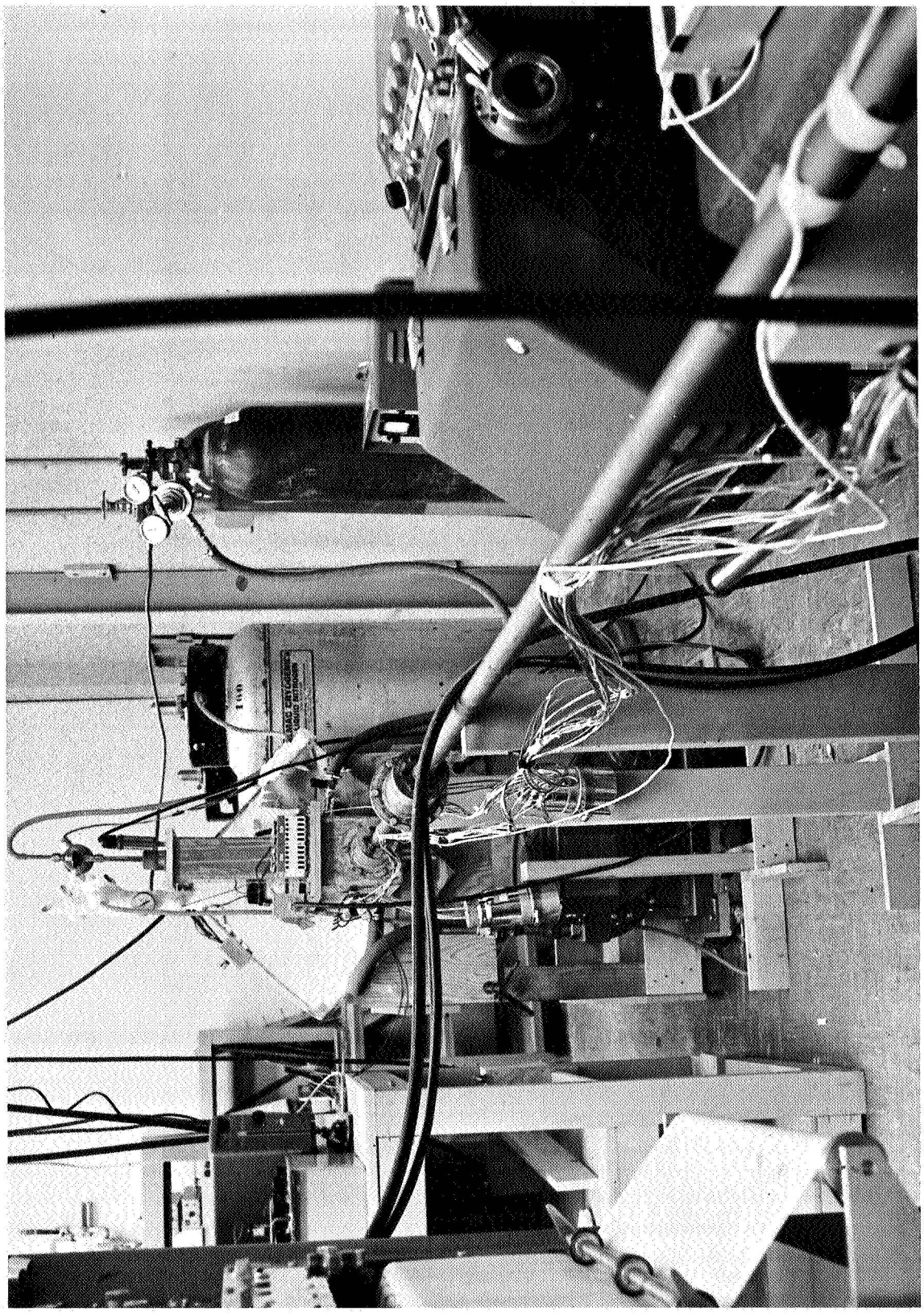


Fig. 57 View of Assembled Transfer Line

The probable uncertainty in the water calibration is less than one percent over the applicable range. The quality measurements are described in Sec.

The fluid and wall temperature thermocouples were 3 mil chromel-constantan and were referenced to an ice bath. The differential pressure transducers were referenced to the local static pressure. Both pressure and temperature sensors were connected through amplifiers to oscillograph recorders. The sensitivities of the combined pressure transducer-amplifier-recording galvanometer systems were obtained by direct pressurization of the transducers and relating the oscillograph deflection to the pressure measured by a mercury manometer. The sensitivity of each thermocouple system was obtained by relating the oscillograph deflection to the change in the cold (reference) junction temperature from ice bath to saturated LN_2, rather than using standard thermocouple tables directly.

The uncertainty in static pressure measurement is estimated to be ±3 percent of absolute pressure. The uncertainty in the differential pressure measurements is quite large because of the low sensitivities of the differential transducer systems. When the flow regime consisted of liquid droplets suspended in the vapor, the sensitivity of the differential transducers to liquid droplet dynamic pressure was good but the response was insufficient to obtain meaningful measurement of liquid droplet velocity. In the case of liquid flow, the differential transducer uncertainty was still large because the velocity for pure liquid flow was relatively low. In general, the differential pressure measurements were of little quantitative value for the above reason; however, they were of value qualitatively in indicating the

the inner line with respect to the vacuum jacket for the 28-ft line between room and liquid nitrogen temperatures.

Figure 51 shows the details of the void fraction measuring and flow visualization stations, along with the standard instrumentation station, the details of which are not shown. There are two facing 5-1/4-inch diameter ports in the tee section for viewing the flow in the approximately 4-inch length of glass tube. The dimensions for the arrangement of detector source, shields and aluminum transfer line tube are shown in section 8.3.

The locations (at room temperature) of the wall thermocouples (3 mil chromel-constantan) are shown in Figure 52, for each line segment, and for the transfer line overall.

Photographs of the LN_2 supply vessel and overall view of a portion of the line, the upstream control box, a standard instrumentation station, and the liquid fraction and visualization station, are shown in Figures 53 through 54.

8.3.1 Instrumentation

The transfer line measurements consisted of flow rate, quality, pressure and temperature. The flowrate was measured by a Fisher-Porter Model 10C1510 turbine flow meter rated for LN_2 temperatures. The meter was 1/2-inch diameter and rated for 0.15 to 10 gpm. The meter was calibrated in the LMSC flow calibration laboratory using water over the range of the meter. Although the meter was not calibrated with LN_2, Ref. 11 indicates that the difference in the volumetric flow rate between water and LN_2 is less than 2 percent.

flow regime present--i.e., sharp spikes for liquid droplets carried in vapor, etc. Furthermore, only about one-half of the differential transducers were operative during the testing, either due to failure of the transducers themselves, trouble with the amplifiers or due to large restrictions in the tubing.

The uncertainty in temperature measurement for the fluid temperature thermocouples is estimated to be ± 3°R and in wall temperatures to be ±5°R. The reason for the difference is that the recording system for the former easily allowed for determining the ice bath base line (i.e., zero signal), whereas for the latter it was difficult to establish the ice bath (zero output) base line. The actual uncertainties in the sensitivities for either were approximately the same.

8.3.2 Test Procedure

The supply vessel was filled to the upper level sensor from a 160 liter LN_2 Dewar and allowed to vent to atmosphere-pressure (with periodic topping off) for approximately one-half hour prior to test, to approach the minimum steady heat input to the vessel through the insulation. For tests where the liquid was saturated at other than atmosphere pressure, the liquid was heated with an electrical heater to above the desired vapor pressure (with periodic ventings to the desired pressure to ensure mixing of the liquid through boiling) and then vented to the desired pressure and held there for a period with the heater off. This recorded tank pressure was used to define the initial liquid subcooling. During this period, the Goddard valve was opened and LN_2 was allowed to vent slowly through the vent line (Figure 49) to prechill the portion of the line up to the solenoid. The supply pressure was

then quickly raised to the desired operating pressure using a GHe supply and regulator valve; the vent valve was closed and the main solenoid valve was opened to initiate the transfer. Except in one run with a pre-chilled line, for which the test was initiated when the line had only partially warmed up following a prior test, all runs were initiated with the line at nominal room temperature. In one test, the gate valve was maintained only partially open to determine the effect of an upstream flow restriction.

Prior to and during the transfer, the following quantities were continuously recorded: supply pressure, flow rate, static and dynamic pressures, fluid and wall temperatures, void volume fraction and in some tests, photographic coverage at the viewing section. Visual observations of the flow were made and recorded where possible, however, the action was so rapid, little could be seen except a general qualitative idea of time-wise variations in flow quality and geometry. The tests were continued in most cases until it was apparent from visual observations that the flow quality had reached a low and fairly steady value or until pressure and temperature measurements indicated complete cool-down had occurred.

8.3.3 Test Results

A summary of the nine transfer line tests conducted are presented in Table 4. All tests were conducted with liquid nitrogen. The conditions varied were: supply pressure; supply liquid subcooling with respect to supply pressure; transfer line length and transfer line initial temperature. In addition, one test was conducted with partial upstream throttling. As indicated in the "Comments", photographic coverage was made of four of these

Table 4

Summary of Small-Size Transfer Line Tests

Run Duration (sec.)	Chill-down Time (sec.)	Test No.	Date[1]	Line[2] Length (ft.)	Section Order	Supply[3] Pressure (psia)	Liquid Sat'd at (psia)	Initial Line Temp. (°R)	Control Valve	Comments
47	39	5-24-1	5-24-67	27'-10 3/4"	3, 5 1/2, 7; 11	44.5	44.5	531	Full Open	Liq. saturated near supply pres. photo coverage (good)
46	42	5-24-2	5-24-67	27'-10 3/4"	3, 5 1/2, 7; 11	43.1	39.0	537	Full Open	Liq. slightly sub-cooled w.r.t. supply pressure
31	31	5-25-1	5-25-67	27'-10 3/4"	3, 5 1/2, 7; 11	43.9	15.7	530	Full Open	Liq. sat'd near atmos. pres. (i.e. large sub-cooling) photo coverage (good) obtained in test rerun
27	27	5-23-5	5-23-67	27'-10 3/4"	3, 5 1/2, 7; 11	44.0	15.1	528	Partially Open	Effect of upstream throttling
110	62	5-23-3	5-23-67	27'-10 3/4"	3, 5 1/2, 7; 11	24.7	24.5	532	Full Open	Liq. sat'd near supply pres. photo coverage (poor)
95	70	5-23-1	5-23-67	27'-10 3/4"	3, 5 1/2, 7; 11	24.8	15.3	530	Full Open	Liq. sat'd near atmos. pres. (i.e. liq. sub-cooled) photo coverage (good) obtained in test rerun
60	54	5-23-2	5-23-67	27'-10 3/4"	3, 5 1/2, 7; 11	23.4	15.3	398	Full Open	Liq. sat'd near atmos. pres. line partially chilled initially
85	50	6-1-2	6-1-67	16'-10 3/4"	3, 5 1/2; 7	22.8	22.9	526	Full Open	Shorter line with tests run under similar conditions to I and III
64	61	6-1-1	6-1-67	16'-10 3/4"	3, 5 1/2; 7	23.1	15.0	531	Full Open	

notes: (1) Dates are not in chronological order but rather tests are listed according to operating conditions and similar to Table I of Ref. (13)
(2) Line length is measured from solenoid to end of line.
(3) Average value of supply pressure during run.

tests with the quality of all but test 5-23-3 being good. The reduced data for these nine tests is presented in graphical form in Volume VI of this report. For each of the nine tests, the following graphical data is presented as a function of time:

- o Supply pressure and supply liquid vapor pressure
- o Liquid flow rate
- o Vapor quality
- o Fluid temperature (at four locations)
- o Wall temperature at several locations along line
- o Static pressure (at five locations)

Significant data from the pitot tube (total pressure) installation were not obtained because of the unexpectedly low differential pressures recorded. These low differential pressures are attributed to the high vapor quality observed throughout the bulk of the chilldown process.

8.3.3.1 Pressure and Flow Fluctuations

Strong pressure and flow fluctuations were observed in several of these tests. In general, the degree of supply liquid subcooling accentuated both pressure and flow fluctuations. This effect is apparent in comparing the high supply pressure tests; subcoolings were approximately 0, 4, and 28 psi respectively. The fluctuations are very significant for a subcooling of 28 psi while the effect is only slightly more evident with less subcooling. Similar qualitative comparisons can be made at lower pressures between tests where $\triangle P_{sub}$ is 0 and 9.5 psi respectively, and for the shorter line between tests where $\triangle P_{sub} = 0$ and 8 psi respectively. In general the frequency is also increased with decreasing subcooling.

It is also evident that these pressure and flow fluctuations have a much higher frequency for shorter line lengths. In addition, these fluctuations also appear to persist much longer for the lower driving pressure. The effect of partially chilling the line is to somewhat alternate the fluctuations and to significantly decrease their duration; however, there appears to be better affect on the frequency.

The effect of upstream throttling with the gate valve resulted in only slight attenuation of the fluctuation; however, the presence of the nominal one-half inch turbine flow meter (with 11/32 inch i.d.) and nominal one-half inch solenoid valve (with 0.30 inch i.d. (also at the upstream end of the line) represented a significant line restriction (at least 53% for the meter and 64% for the solenoid). Additional attempts at throttling with the gate valve provided only incremental throttling effects over those due to the flowmeter and valve flow restrictions.

Significant over pressures (i.e. line pressures exceeding the supply pressure) occurred only for the 10 psig supply pressure tests. For the more highly subcooled test, the over pressure was approximately 50% for the first pressure pulse. This extended well down the line, being approximately 40% over pressure as far as 17 feet down the 28 foot line for the first pressure pulse. The over pressures were rapidly damped for successive pressure pulses, however, the pressure fluctuations persisted for a considerable time. Although these over pressures occurred in only two tests (5-23-1 and 5-23-3), there was no apparent simultaneous flow reversal as indicated by the measured flow

rate. (The meter does not differentiate between forward and reverse flow; however, for flow reversal to have occurred, the measured valve would indicate zero at reversal and this was not evident.)

In comparison for the higher pressure tests, even for a subcooling of 28 psi the peak pressure was approximately equal to the supply pressure for the shorter line the peak pressure for the first pulse was also approximately equal to the supply pressure. The degree of over pressure increases with the line flow resistance (i.e. line length, or degree of flow restriction downstream) and this result is consistent with the results of Ref. (12) on the effect of line length or downstream flow restrictions on the degree of over pressure. In the results reported in Ref. 12 for LN_2 the over pressure increased monotonically with line length for no exit flow restriction. The 25 psig supply pressure data of Ref. (12) indicates these to be negligible over pressure for a 25 foot line and this compared well with the present data. Ref. 12 does not include data for lower supply pressure to compare with the 50% over pressure observed in the 10 psig subcooled test. With exit flow restrictions, Ref. 12 indicates a minimum over pressure to occur for some intermediate line length.

The peak pressure results are summarized in Figure 58 with some of the data from Ref. 12 included for comparison.

As line chill-down proceeds the pressure and flow fluctuations subside generally before complete chill-down occurs. During the latter part of

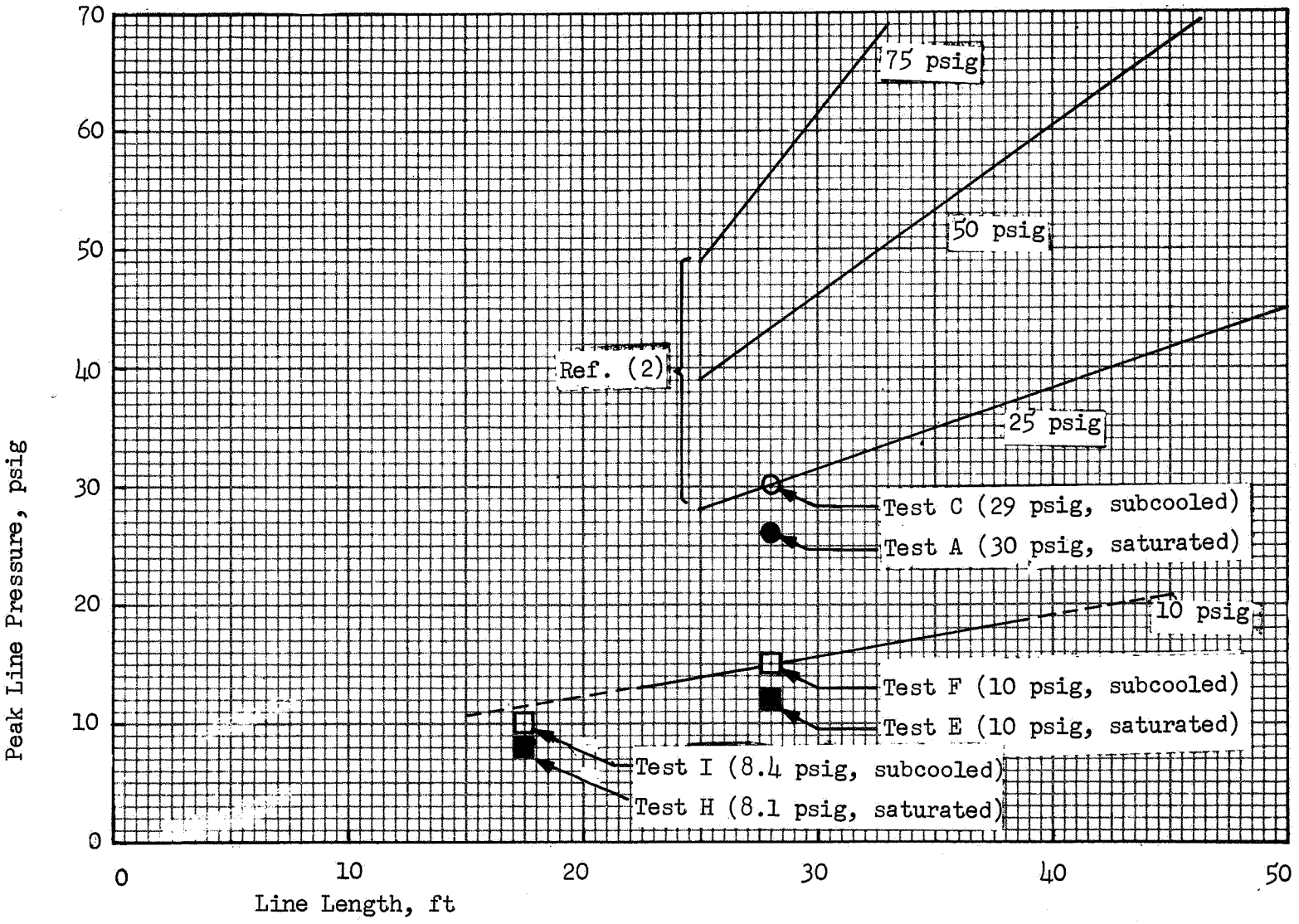


Fig. 58 Peak Line Pressures

chill-down the static pressures drop and the flow rate increases to relatively steady values once the entire line is cold. For all tests except 5-25-1 and 5-23-5 the tests were continued to beyond complete chill-down as indicated in Table 4. The line static pressure distributions near the end of each test are presented in Figs. 59 and 60 . It is seen that for both the nominal 10 and 30 psig tests 50% or more of the pressure drop occurs between the inlet and the first static pressure tap, i.e. occurs across flowmeter and solenoid valve. The static pressure tap at 108 inches (CPI) appears to give somewhat inconsistent values particularly where there was incomplete chill-down or when there was little supply liquid subcooling.

Chill-Down Time - The chill-down time as a function of line location is plotted in Figure 61, where the data for all wall thermocouples including those at the instrumentation section are included. In most cases the wall temperature data exhibit initially moderately rapid cooling (i.e., relatively high film boiling heat transfer rates for large wall super heats) then less rapid cooling as the wall super heat decreases. Finally prior to final chill-down the cooling rates are very rapid as the high heat flux of nucliate boiling occur. In some (limited) cases, the nucleate boiling portion of the curve was not apparent and this has not been explained.

It is seen from Figure 61 that in general the wall location adjacent to the instrumentation sections (closed symbols) cool most rapidly and this is attributed to the presence of the pitot tubes or the visualization section in the case of CT2. Other than these locations the cool-down distribution

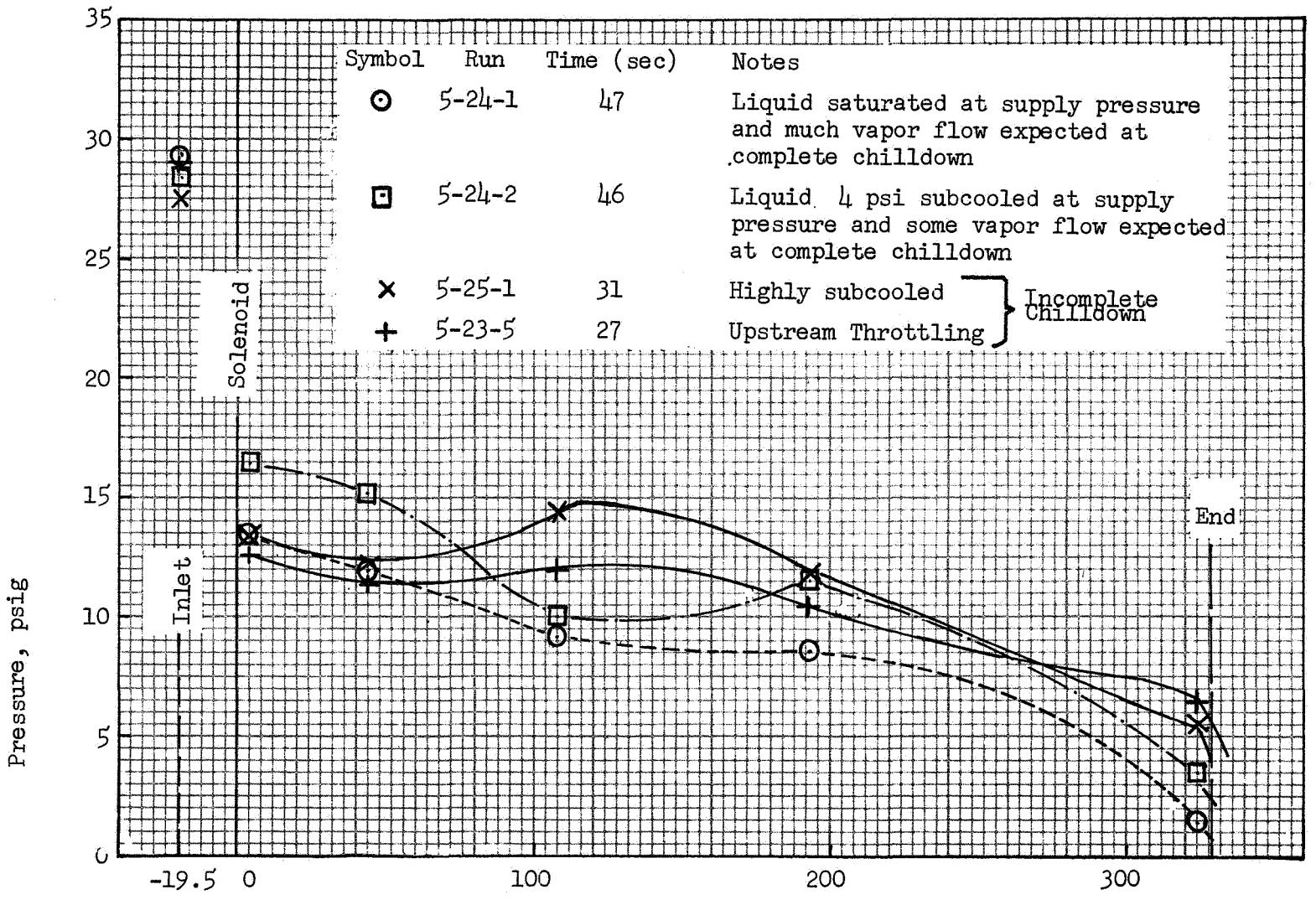


Fig. 59 Line Pressure Variation After Chilldown (Nominal 30 psig Tests)

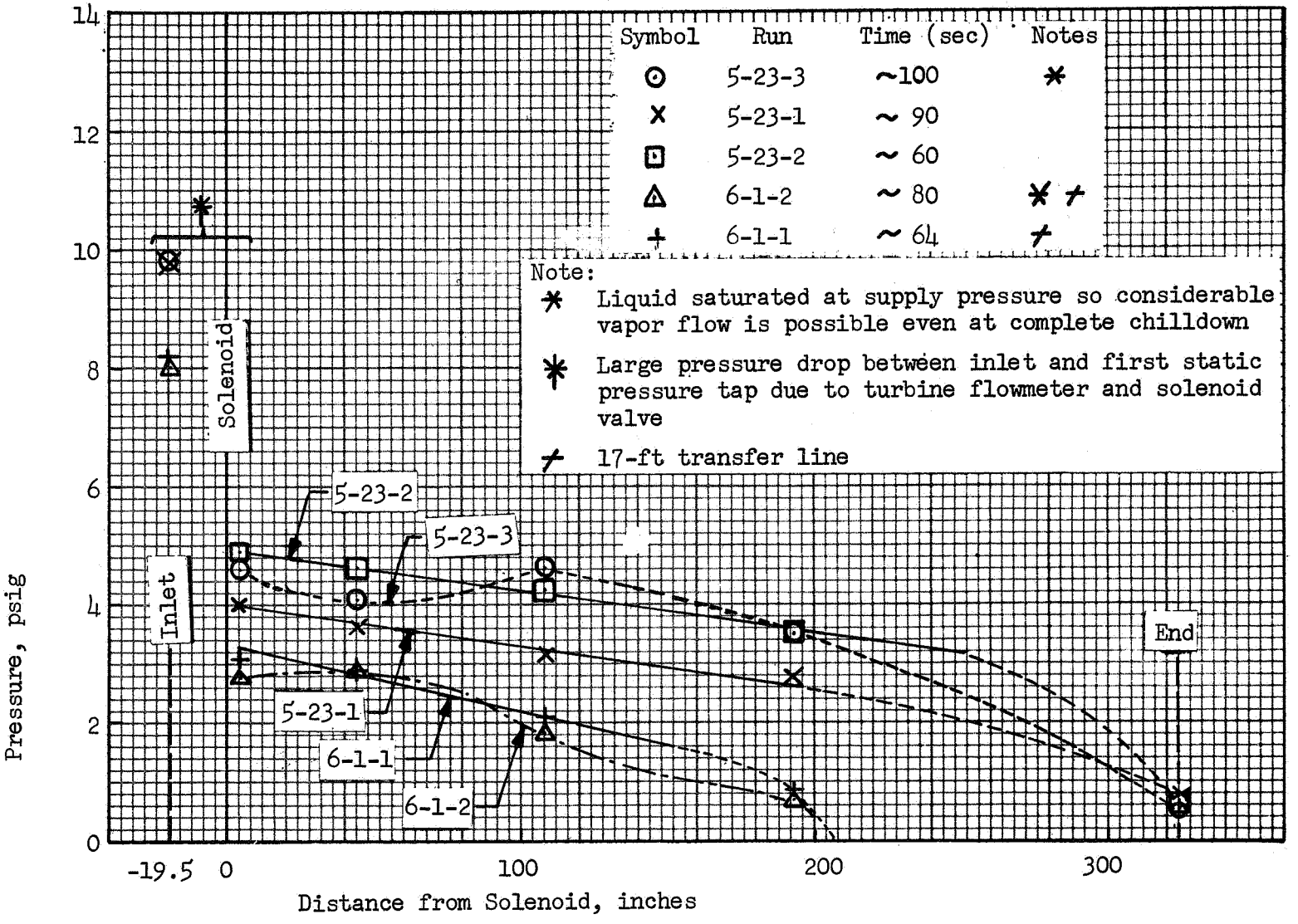


Fig. 60 Line Pressure Variation After Chilldown (Nominal 10 psig Tests)

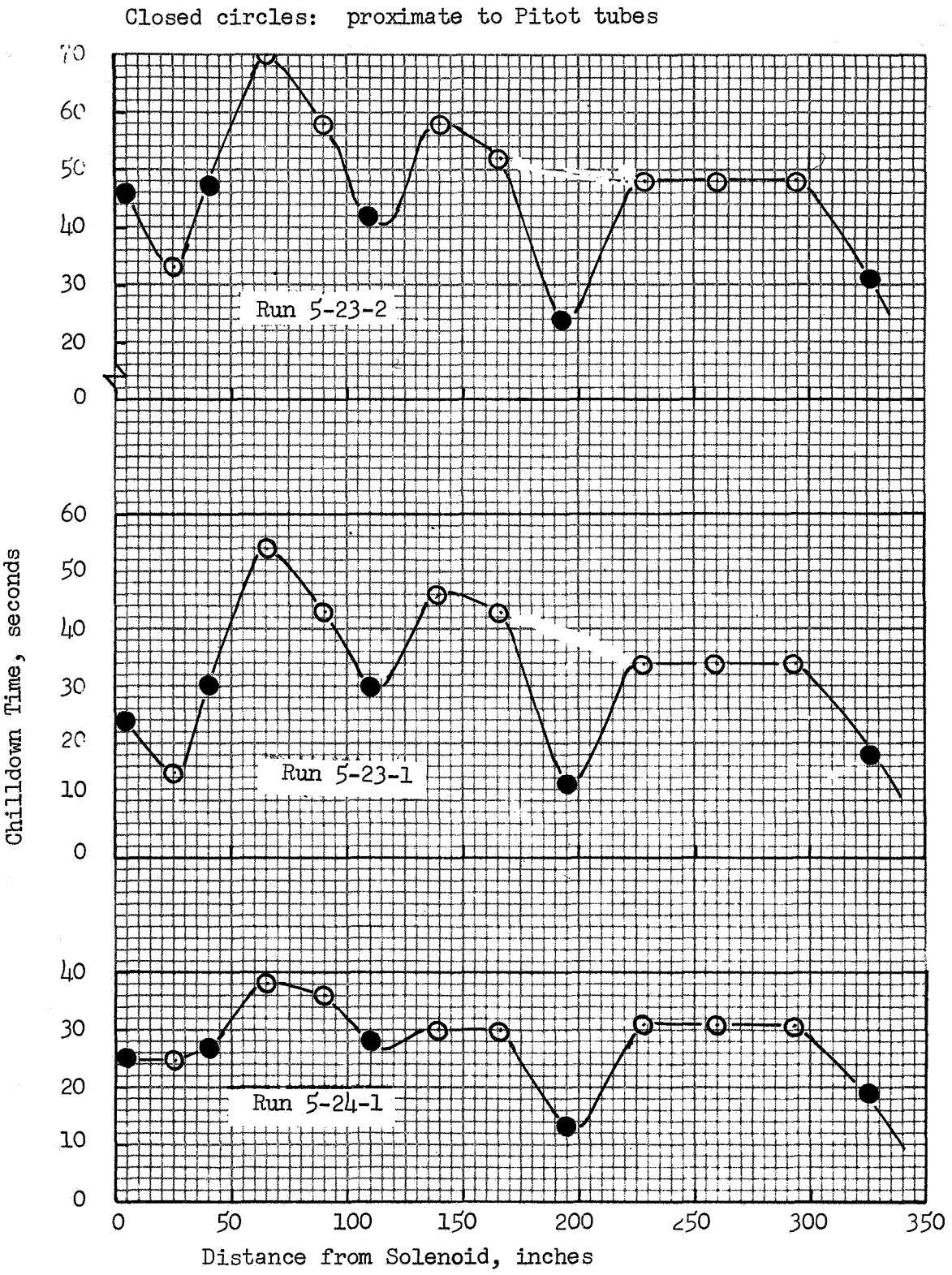


Fig. 61 Chilldown Time vs Line Location

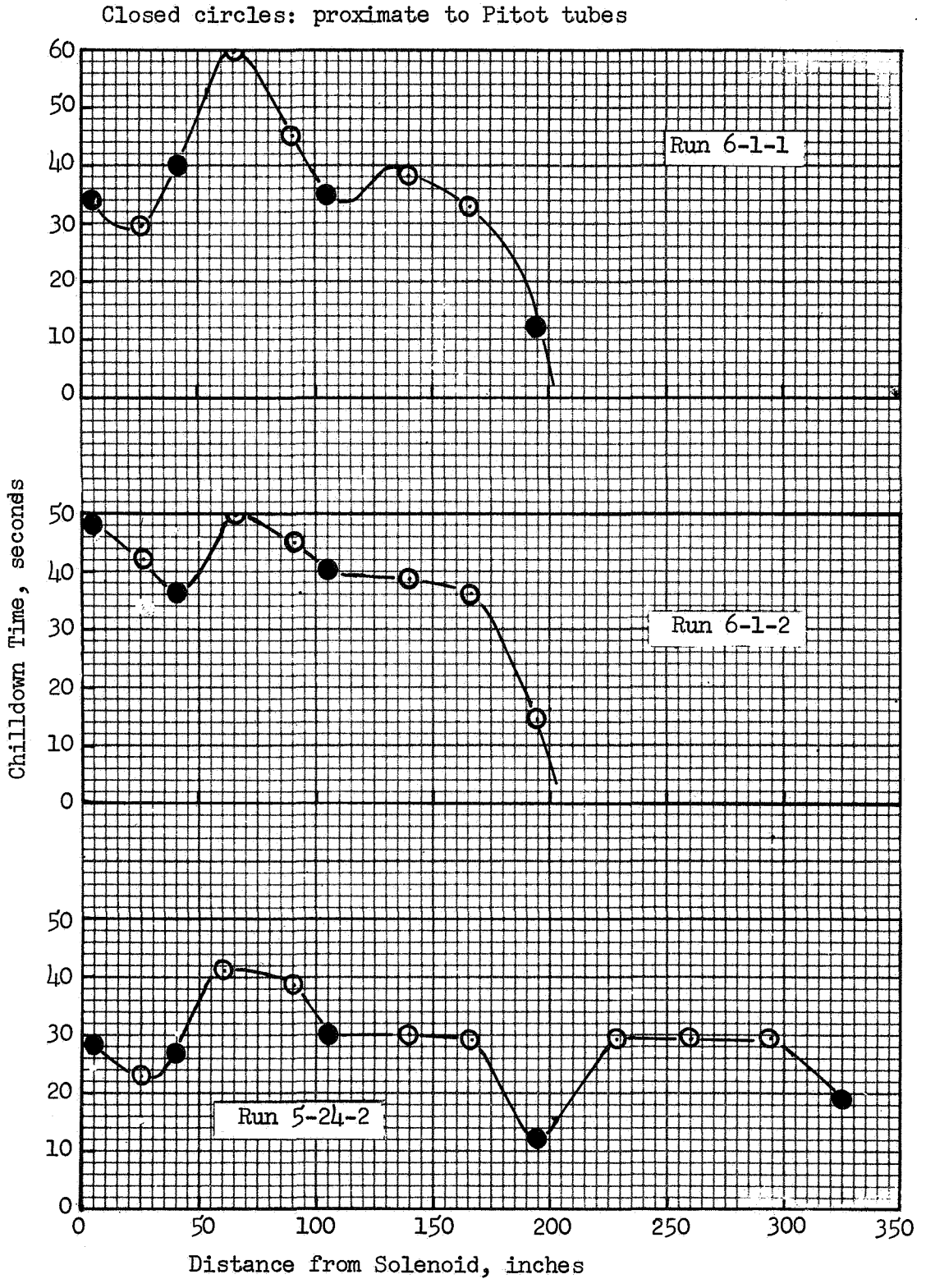


Fig. 61 Chilldown Time vs Line Location (Continued)

Closed circles: proximate to Pitot tubes

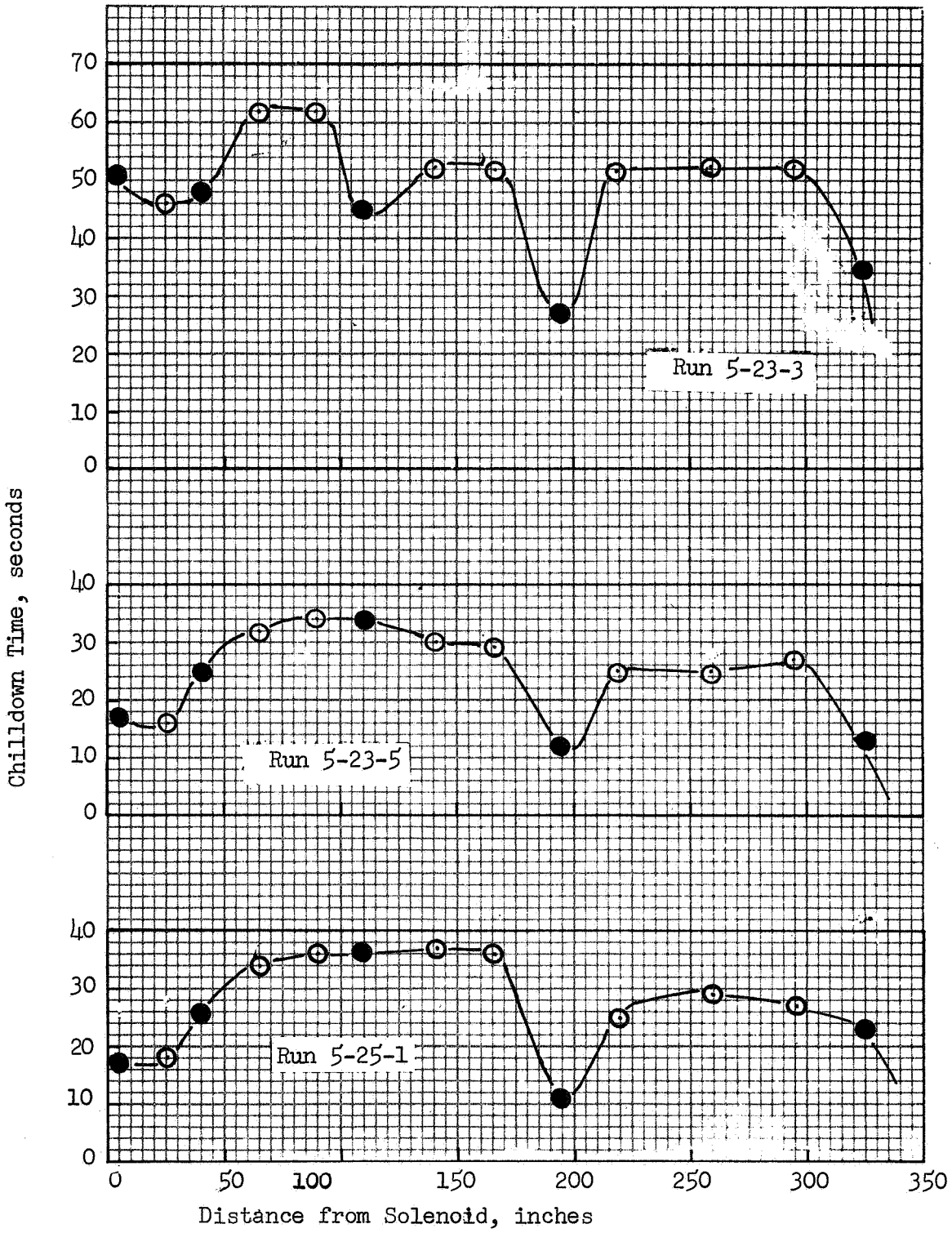


Fig. 61 Chilldown Time vs Line Location (Continued)

indicates that both upstream and downstream locations complete cool-down last. This is explained qualitatively in that the heat transfer coefficients well downstream are greatly increased by the higher fluid velocity resulting from the accelerating flow.

In a very long transfer line it would be expected that the cooldown durations would eventually increase with distance for longer lines as is reported by Ref. 13 for long transfer lines (up to 200 feet) since downstream portions of the line would be exposed to super-heated vapor during the initial part of the transfer.

Study of the photographic coverage of four tests (at nine foot downstream) indicates that two phase flow exists almost simultaneously with valve opening. The flow initially consists of dispersed liquid droplets in the vapor with some tendency for stratification (i.e. more droplets near the bottom of the horizontal line) and although reverse flow was not observed (consistent with little or no line over pressures) there were very large time wise velocity and quality fluctuations. These are most certainly associated with the rapid pressure and flow variations discussed earlier. As chill-down continues, the droplet size increases. In the latter stages an annular flow appears to develop with a liquid film on the wall and a central core of high velocity vapor containing dispersed liquid droplets. Although movies were not taken at the line exit, it appeared from visual observation that two-phase flow also occurred very early compared to the time for complete chill-down. Essentially, pure liquid was observed in the viewing section after complete

chill-down for the highly subcooled tests. This is consistent with the quality measurements from the void fraction meter.

8.3.4 Comparison of Analytical Predictions with Experimental Data

Analytical computations were performed for comparison with test data from the tests described in Sections 8.2 and 8.3. Test data on the 200 foot line were available from NBS (Ref. 16) for chill-down tests performed with both nitrogen and hydrogen. The comparison between data from these tests is presented in the next section. Only comparisons with measured wall temperature histories are presented, since no NBS data were available on the results of flowrate or quality measurements. As pointed out in Section 7, the flow phenomena occurring during chill-down are greatly affected by the length-to-diameter ratio of the line. This is reflected in the correlation of data from the tests run at LMSC on relatively short transfer lines and those run at NBS on a relatively long transfer line. The lack of data on flowrate and quality variations during chill-down of the NBS 200 foot line is not considered serious in view of the lesser importance of flowrate and pressure oscillations in the longer line.

In the comparisons presented below, the effect of flowrate and pressure oscillations on the chill-down process is marked. In spite of these effects, the computer analysis (which represents a quasi-steady approximation to the highly transient flow and heat transfer processes) provides a good approximation to the measured variations.

8.3.4.1 Chill-down of 28-foot Line

Of the seven tests performed on the 28-foot line, computer predictions were performed for six tests. In the seventh test, the flow was partially throttled at the inlet, and thus could not be simulated using the current version of the line chill-down program. A summary of the test conditions for those chill-down tests analyzed in this section was presented in Table 4. During these tests, measurements of the fluid quality were obtained with a void fraction measurement system located approximately eight feet from the inlet to the transfer line. For three of the tests, high speed movie coverage of the flow was obtained just downstream of the void fraction measurement station. As stated earlier, during all the tests, measurements of transfer line wall temperature histories were made at thirteen stations along the line; fluid temperature and static pressure measurements at five stations, and flowrate measurements at the inlet were also obtained. In addition to these measurements, total (stagnation) pressures were recorded at five stations along the line; these measurements were obtained from pitot tubes at the centerline, mid-radius and inside wall of the transfer line. However, because of a low sensitivity setting on several recorder channels, data from these measurements could not be reduced.

Because of the large number of wall temperature measurements made during tests on this line, several plots of wall temperature versus distance down the line were prepared. This was done so that thermocouples representing the average temperature profile along the line could be selected for comparison with computed wall temperature histories. Plots of measured and calculated

wall temperature profiles are shown in Figures 62 through 65 for both saturated and subcooled inlet conditions* at two driving pressures.

It will be noted from these plots that several thermocouples seem to cool down faster than their adjacent thermocouples. This is particularly noticeable in the runs at low driving pressures shown in Figures 64 and 65. In general, the measured temperatures at distances of 0.6, 2.2, 9.2, 16.2 and 27.2 feet from the inlet decrease more rapidly than at neighboring locations. This is because the wall temperature thermocouples at these locations are in areas where the flow is disturbed and the resultant increased turbulence produces higher heat transfer rates than at other locations. Near the pipe inlet the flow is unusually turbulent due to entrance effects associated with rapid acceleration of the flow from the supply tank. Also, a fluid temperature thermocouple (stretched across the pipe centerline) and pitot tubes were located just upstream of the thermcouple 0.6 feet from the inlet. Thus several sources of turbulence were present in the inlet region, contributing to higher heat transfer rates in this area. Fluid thermocouples and pitot tubes were also present just upstream of the wall thermocouples at 3.7, 9.2, 16.2, and 27.2 feet from the inlet. Additional sources of turbulence to explain the exceptionally high heat transfer rates about 16.2 feet from

---

*As noted earlier, for tests run with liquid saturated at atmospheric pressure, the liquid in these tests is referred to as subcooled liquid. In tests run with liquid saturated at the selected driving pressure, the liquid is referred to as saturated liquid.

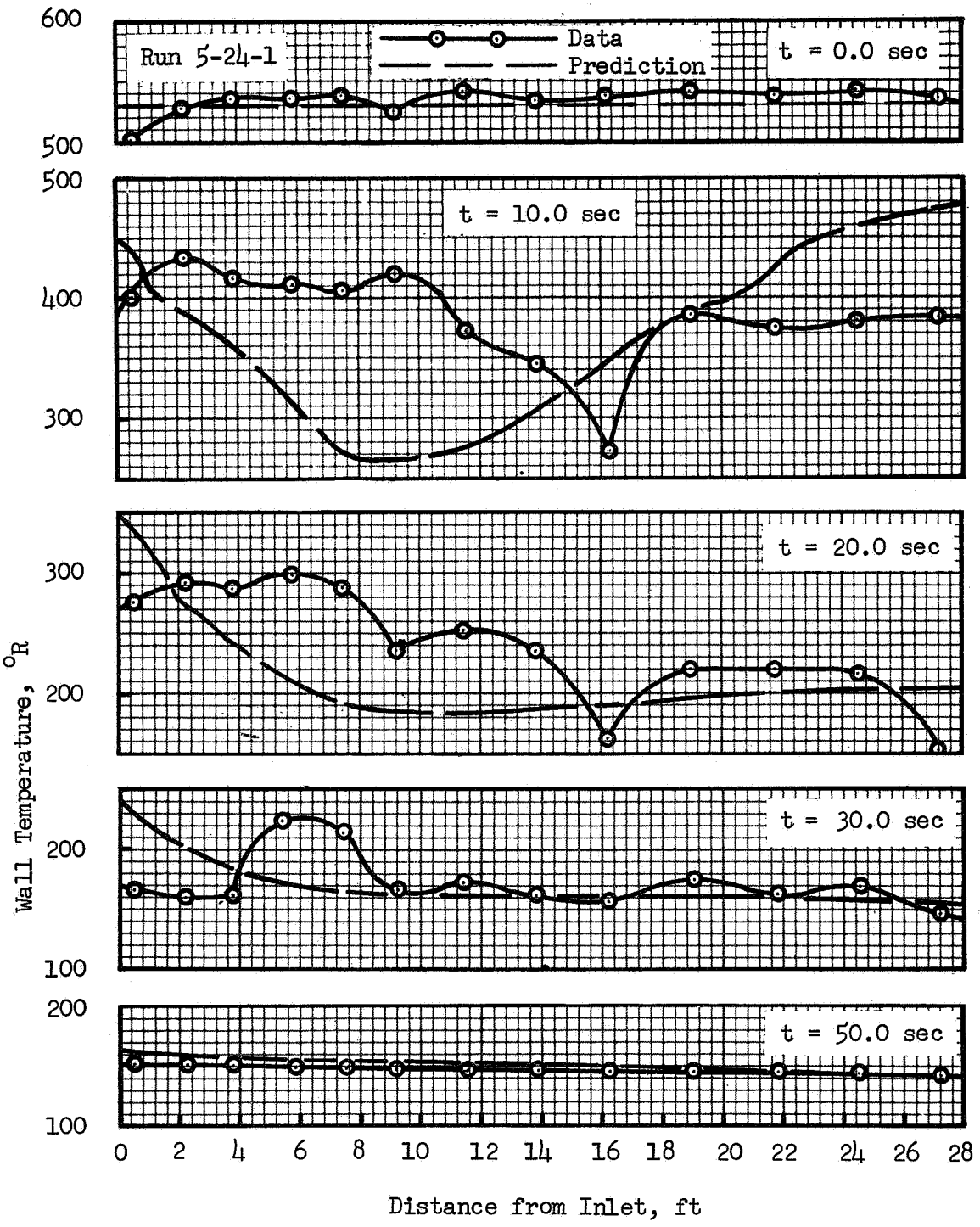


Fig. 62 Measured and Calculated Wall Temperature Profiles with Saturated Liquid Nitrogen at a Driving Pressure of 44.5 psia

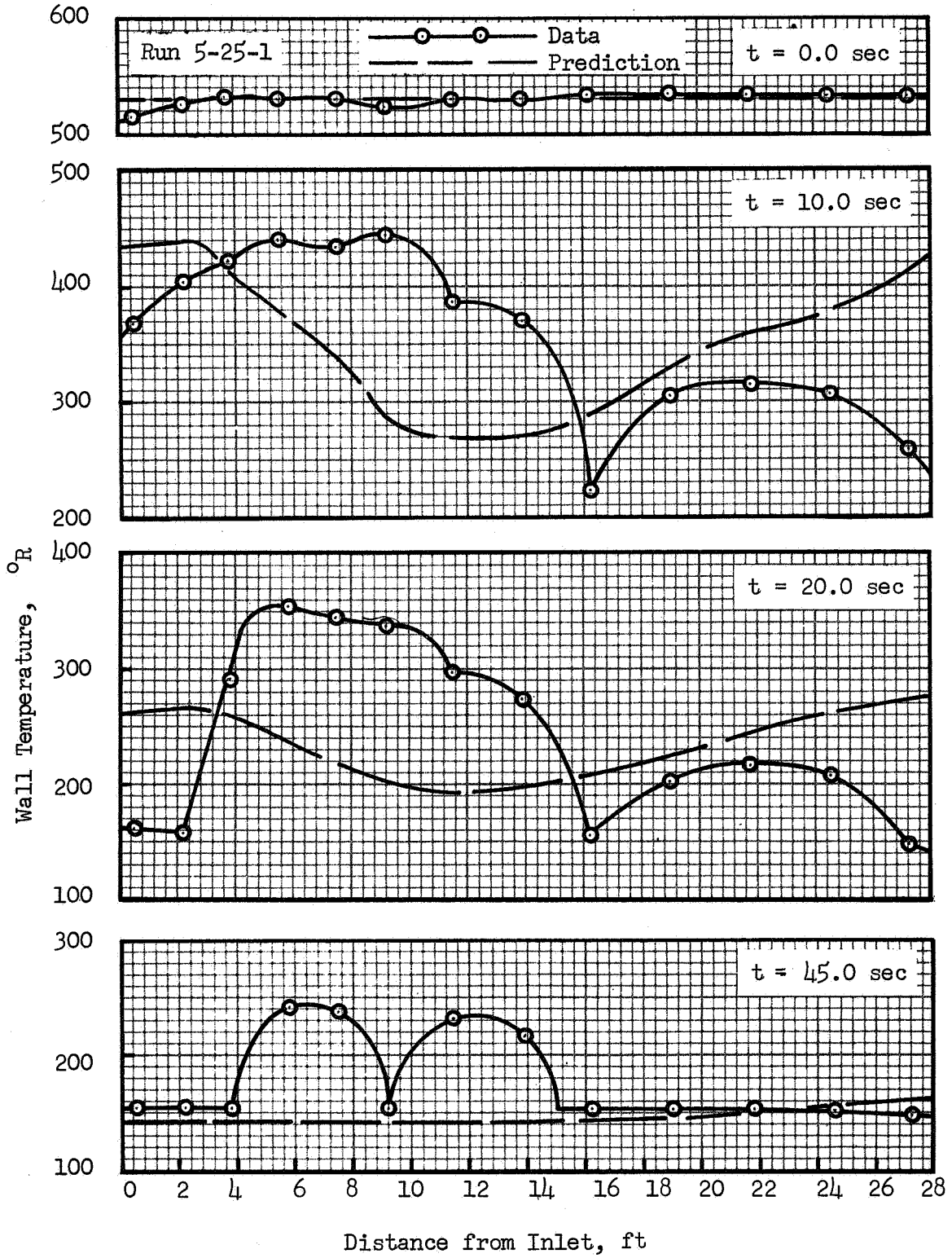


Fig. 63 Measured and Calculated Wall Temperature Profiles with Subcooled Liquid Nitrogen at a Driving Pressure of 43.9 psia

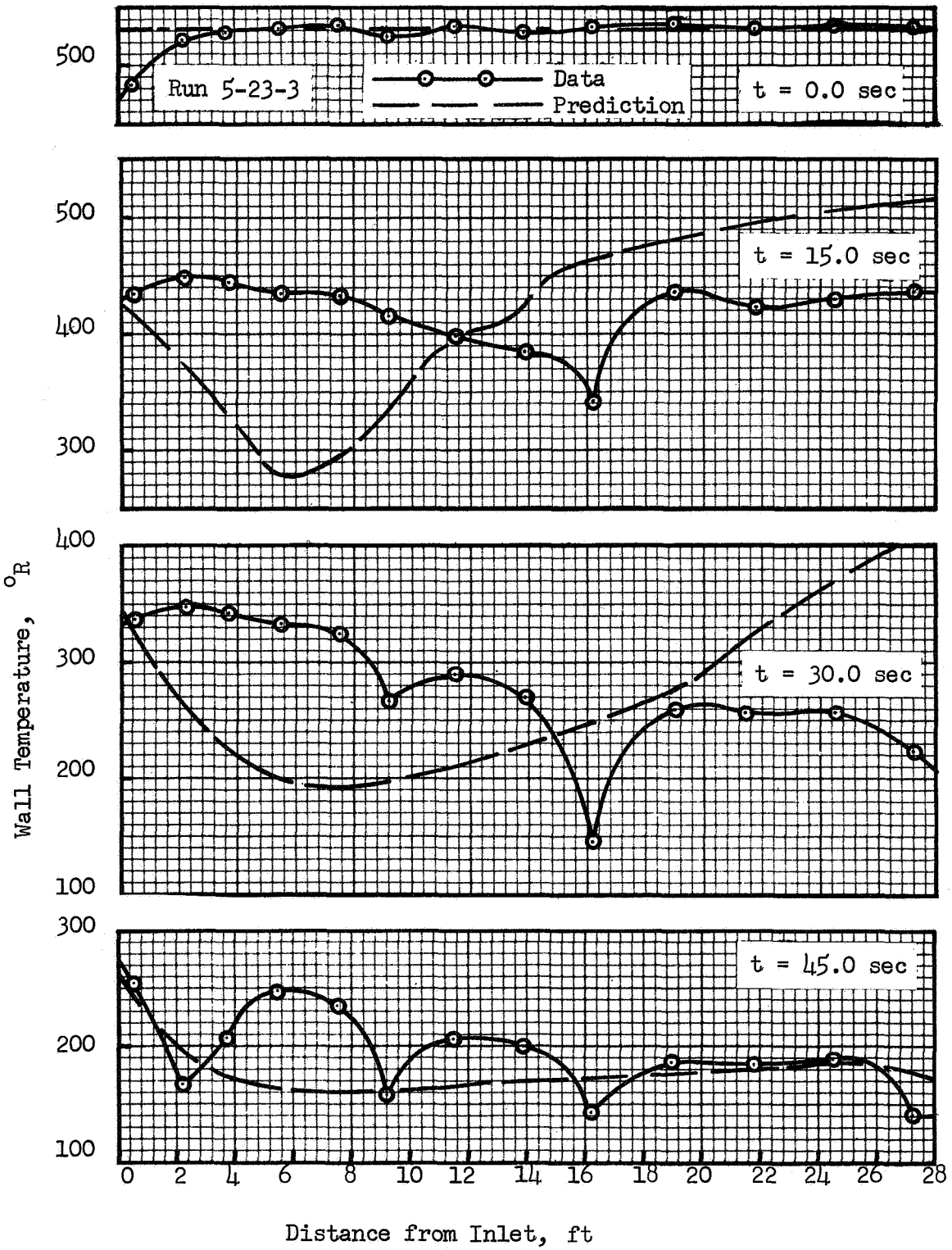


Fig. 64 - Measured and Calculated Wall Temperature Profiles with Saturated Liquid Nitrogen at a Driving Pressure of 24.7 psia

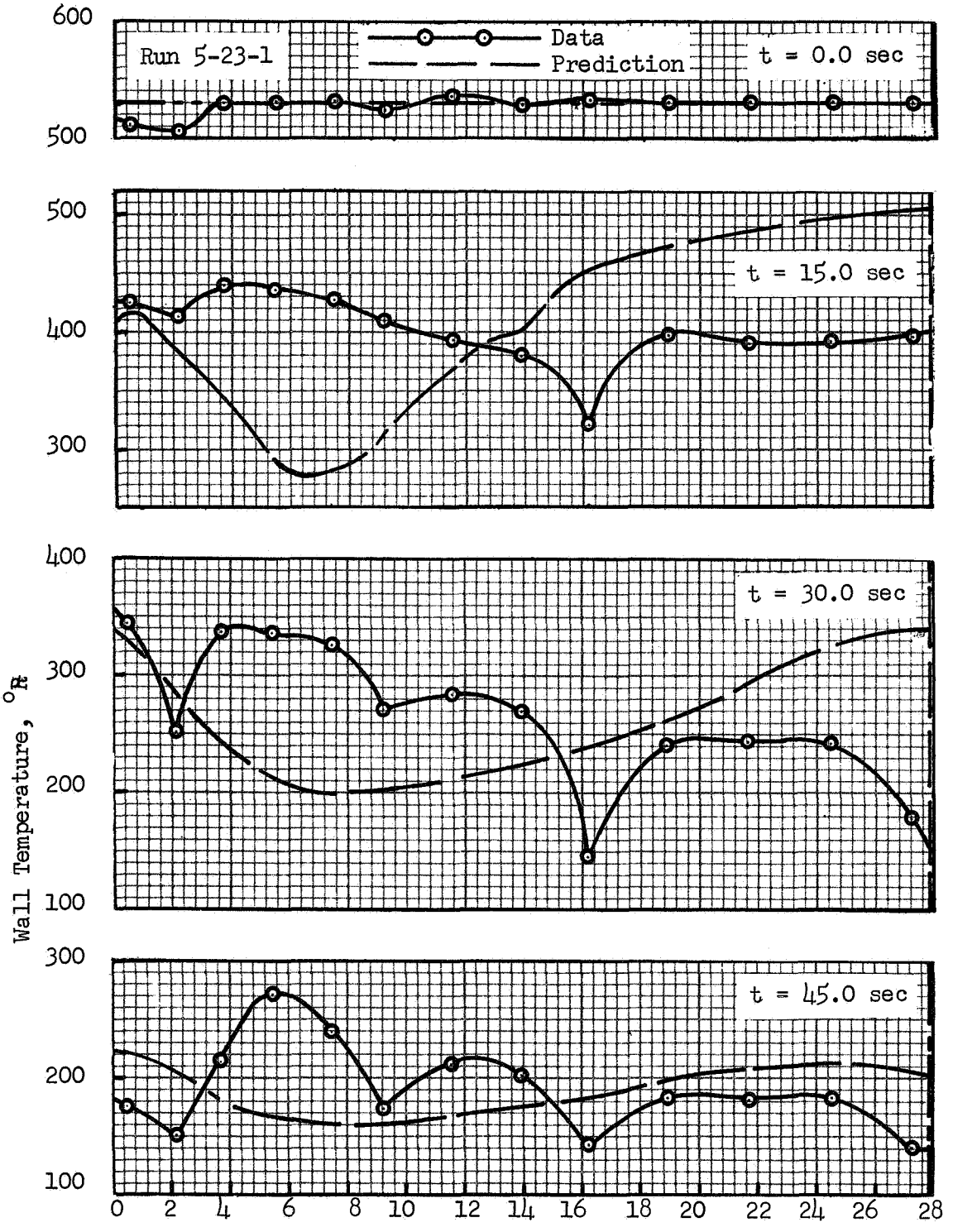


Fig. 65 Measured and Calculated Wall Temperature Profiles with Subcooled Liquid Nitrogen at a Driving Pressure of 24.8 psia

the inlet have not yet been uncovered. In selecting thermocouple data to be plotted as a function of time, those thermocouples which were deemed to represent an average spatial temperature distribution were selected. These "average" thermocouples were those located at distances of 3.7, 11.5, and 24.5 feet from the inlet.

Referring to Figure 62, it will be noted that the computed temperatures in the first half of the line are generally lower than the measured wall temperatures, especially during the early stages of chill-down. At early times, the predicted temperatures for the last half of the line are generally higher than the measured temperatures. These deviations are attributed to gross differences between the fluid mechanical model assumed in the analysis and that actually observed during the tests. As explained earlier, the computer model assumes that a column of vapor is followed by a column of two-phase fluid which is, in turn, followed by a liquid region, the whole proceeding gradually down the transfer line. This sequential progression of fluid phases is assumed to always occur in the order described. Thus, for the tests analyzed, the final lengthwise distribution of fluid regions is as shown in Table 5. It will be noted that for saturated inlet conditions the analysis predicts that the line should be virtually filled with two-phase fluid, while for subcooled inlet conditions, the line should contain a long liquid column. This result is in good agreement with experimental observations.

At early times during the chill-down process, however, the observed fluid

Table 5

Computed Fluid Phase Distribution at Chilldown

Run No.	Liquid Phase			Two-Phase Region			Vapor Phase		
	Extends From (ft)	To (ft)	Total Length (ft)	Extends From (ft)	To (ft)	Total Length (ft)	Extends From (ft)	To (ft)	Total Length (ft)
5-24-1	0.00	0.00	0.00	27.90	27.90	27.90	27.90	27.90	0.00
5-24-2	0.00	4.17	4.17	4.17	27.90	23.73	27.90	27.90	0.00
5-25-1	0.00	26.98	26.98	26.98	27.90	0.91	27.90	27.90	0.00
5-23-3	0.00	0.97	0.97	0.97	27.90	26.93	27.90	27.90	0.00
5-23-1	0.00	26.34	26.34	26.34	27.90	1.56	27.90	27.90	0.00
5-23-2	0.00	25.94	25.94	25.94	27.90	1.96	27.90	27.90	0.00

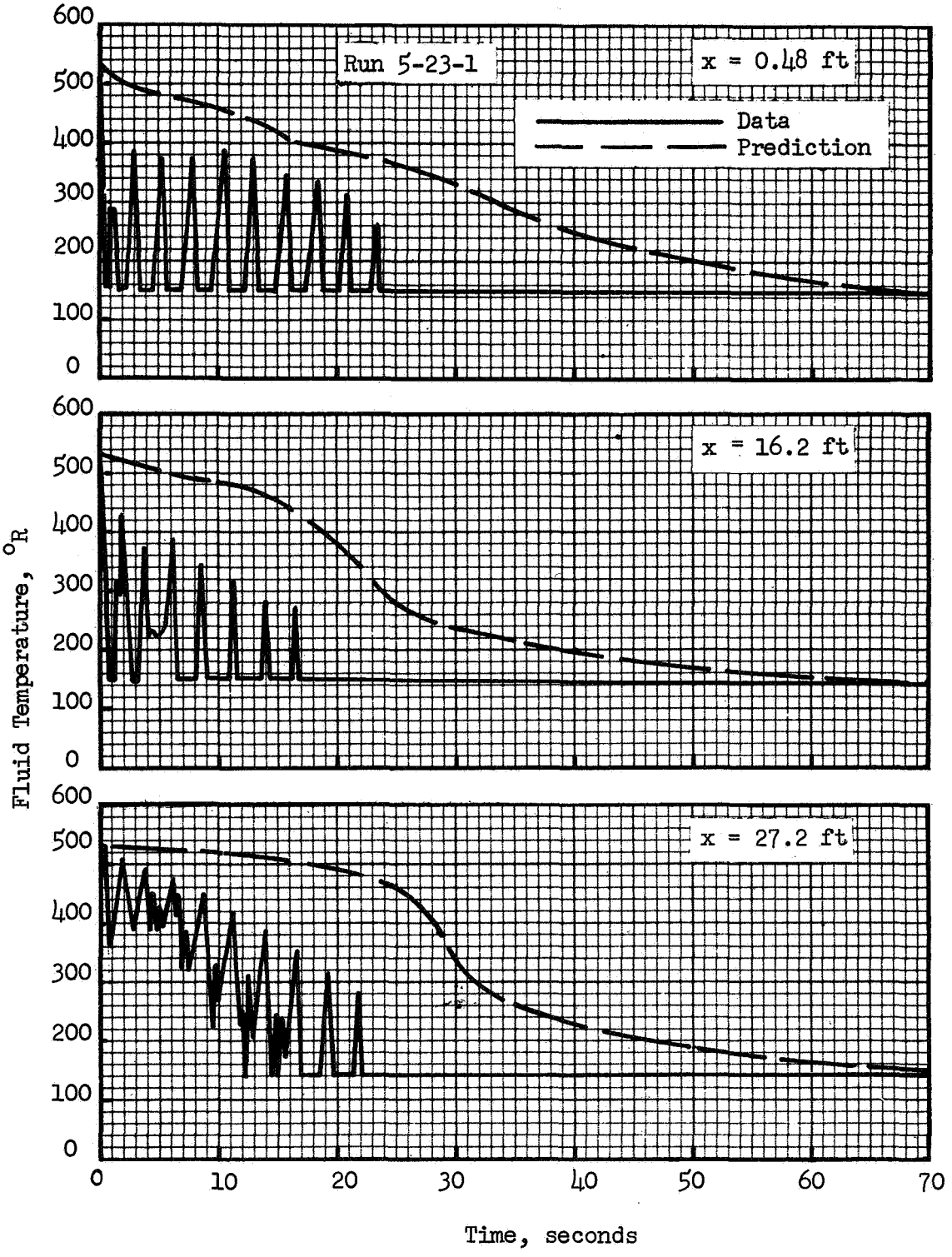


Fig. 66 Fluid Temperature History with Subcooled Liquid Nitrogen at a Driving Pressure of 24.8 psia.

distribution was very much different from that used in the analysis. Visual observations of the flow, as well as fluid temperature measurements, showed that the line was quickly filled with a two-phase mixture containing "pockets" of warm vapor. This is illustrated graphically in Fig. 66 where computed and measured fluid temperature histories are presented for the low pressure, saturated case (Run 5-23-1). The times at which the fluid thermocouples recorded the local saturation temperature are times during which the thermocouple was immersed in a two-phase mixture. At intervals, as shown in Fig.66, the thermocouples were immersed in warm vapor. These regions appear in the movies of the flow, as vapor pockets, or rarefactions, between regions filled with liquid droplets. These variations are also shown by the measured quality data plotted in Fig.67 for the same run. The observed distribution of fluid phases is clearly produced by pressure and flowrate oscillations in the transfer line during the early stages of chill-down. Apparently, during times when the flow has decelerated during a local pressure surge, a given volume of fluid absorbs heat from the wall for longer periods of time than those undergoing acceleration, causing the generation of a vapor pocket. This observation is further substantiated by a comparison between the apparent velocity of the vapor pockets and the measured surge periods. Taking Run 5-23-1 as an example, the interval between vapor pockets as indicated from the fluid temperature measurements (Fig. 66) is approximately 2.8 seconds. The measured surge period for this test was approximately 2.9 seconds. These observations also explain the mechanism for the so-called "agglomeration" of fluid regions referred to by Chi (Ref. 14). It should be noted that a larger number of vapor pockets was observed in the

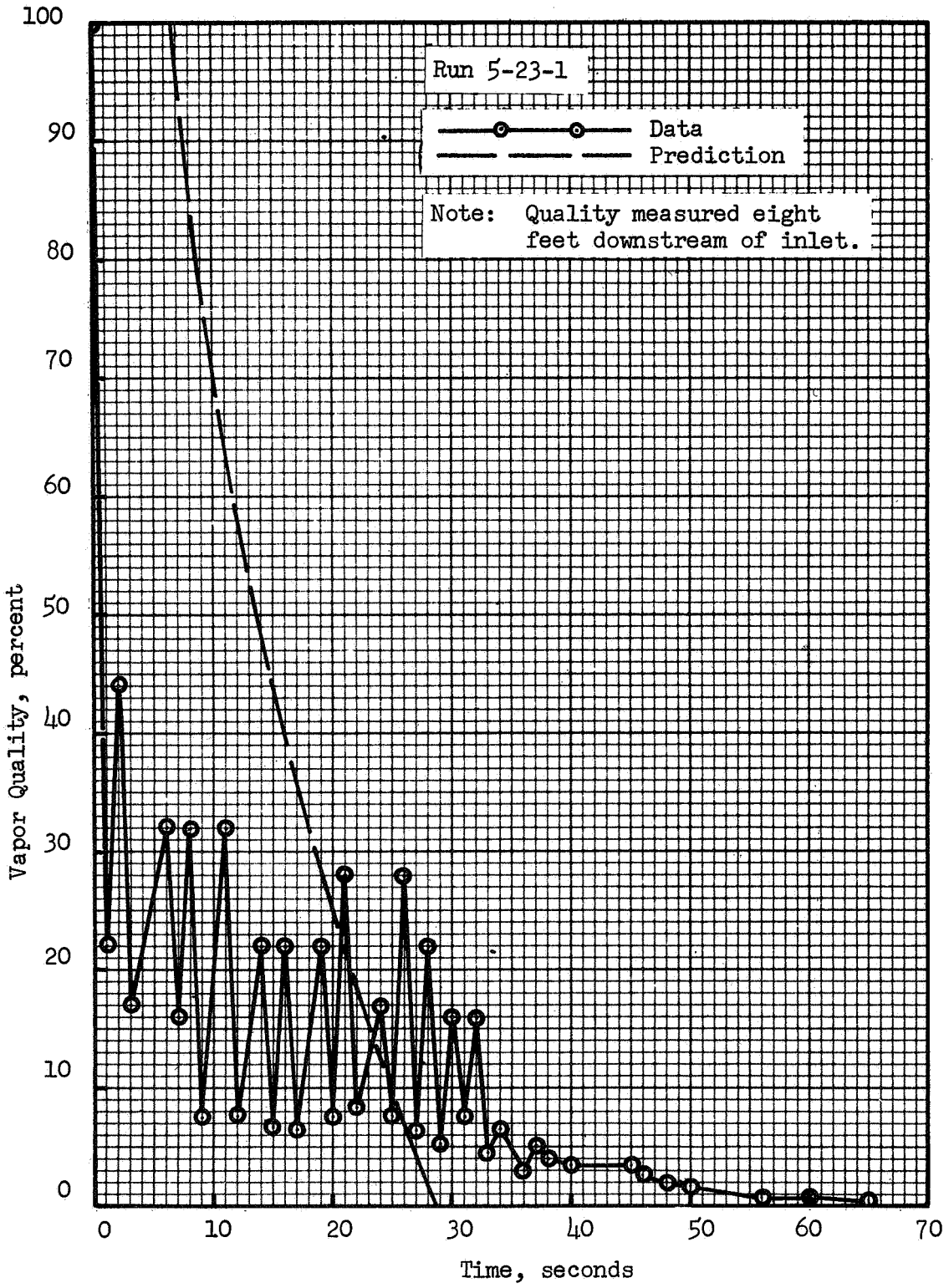


Fig. 67 Vapor Quality History with Subcooled Liquid Nitrogen at a Driving Pressure of 24.8 psia

low pressure runs; this observation agrees with the conclusions of the surging analysis, presented in Volume III of this report, wherein it was shown that surging dies out faster for lines having higher driving pressures.

As discussed above, the measured transfer line history was compared with analytical predictions at three locations along the line; that is, at distances of 2.71, 11.54 and 24.46 feet from the inlet. The results of these comparisons are shown in Figs. 68 through 73 . For the runs at the higher driving pressures (Figs. 68 , 69 and 70) the comparison is quite good. For the runs at the lower driving pressures, the predicted temperatures near the end of the line deviate from the measurements early in the chill-down process. This is again attributed to the greater effect of surging at the lower driving pressures.

8.3.5 Correlation of NBS Data for a 200 Foot Line

Due to the availability of published test data on a 200 foot long transfer line, an attempt was made to correlate the observed line temperature variation with time by using the line chill-down computer program. The test data, presented in Ref. 16, are for a vacuum-jacketed, copper transfer line, 200 feet long and 5/8 inches in inside diameter. Both nitrogen and hydrogen were used as the test fluids. At four locations along the line were located instrumentation stations at which line wall temperatures were measured. A total of nine test runs were selected for comparison with analytical predictions; the test fluid, inlet conditions and approximate chill-down time are indicated in Table 6 for these runs. Tests in which the liquid was saturated

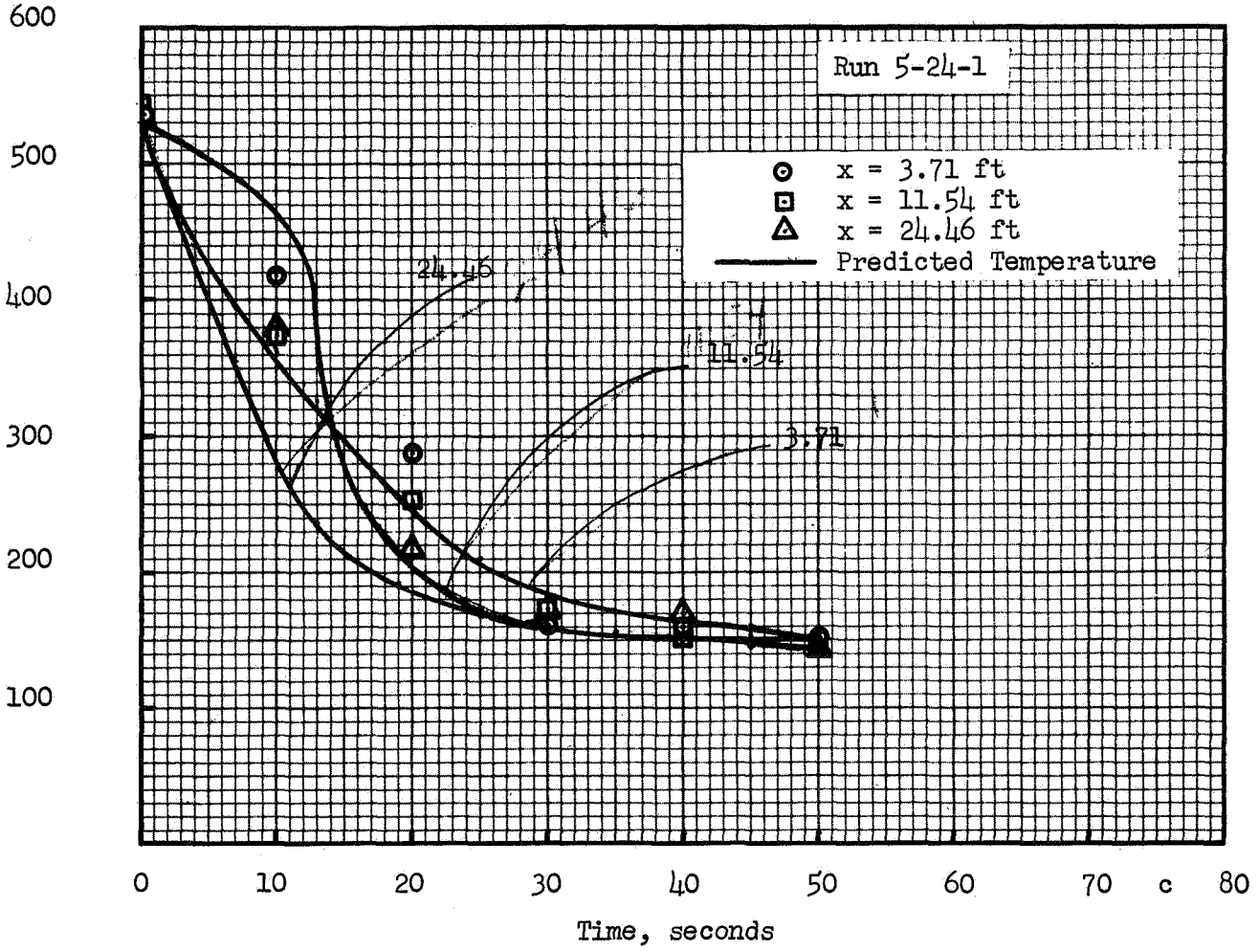


Fig. 68 - Line Temperature History with Saturated Liquid Nitrogen at a Drawing Pressure of 44.5 psia

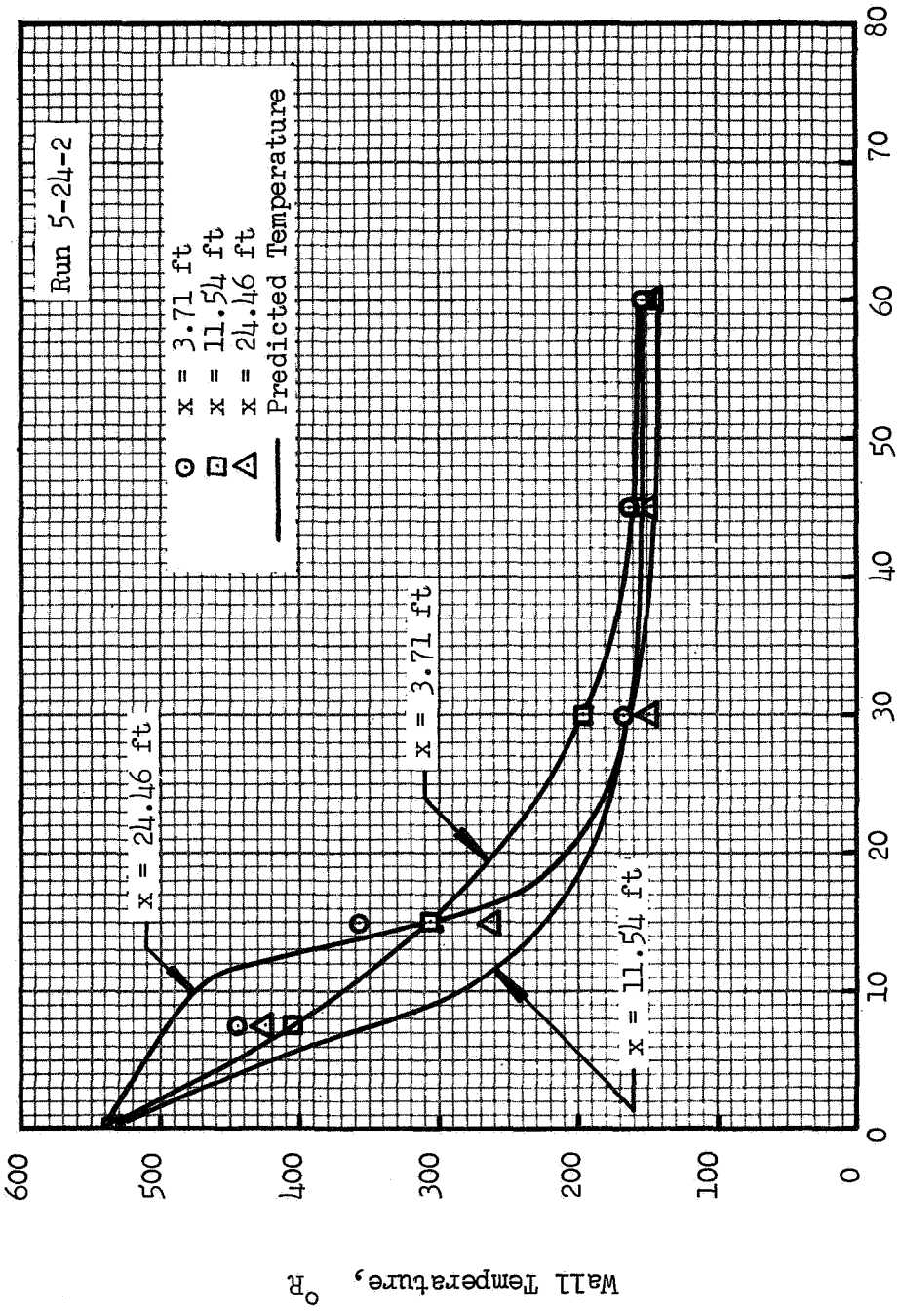


Fig. 69 Line Temperature History with Slightly Subcooled Liquid Nitrogen at a Driving Pressure of 43.1 psia

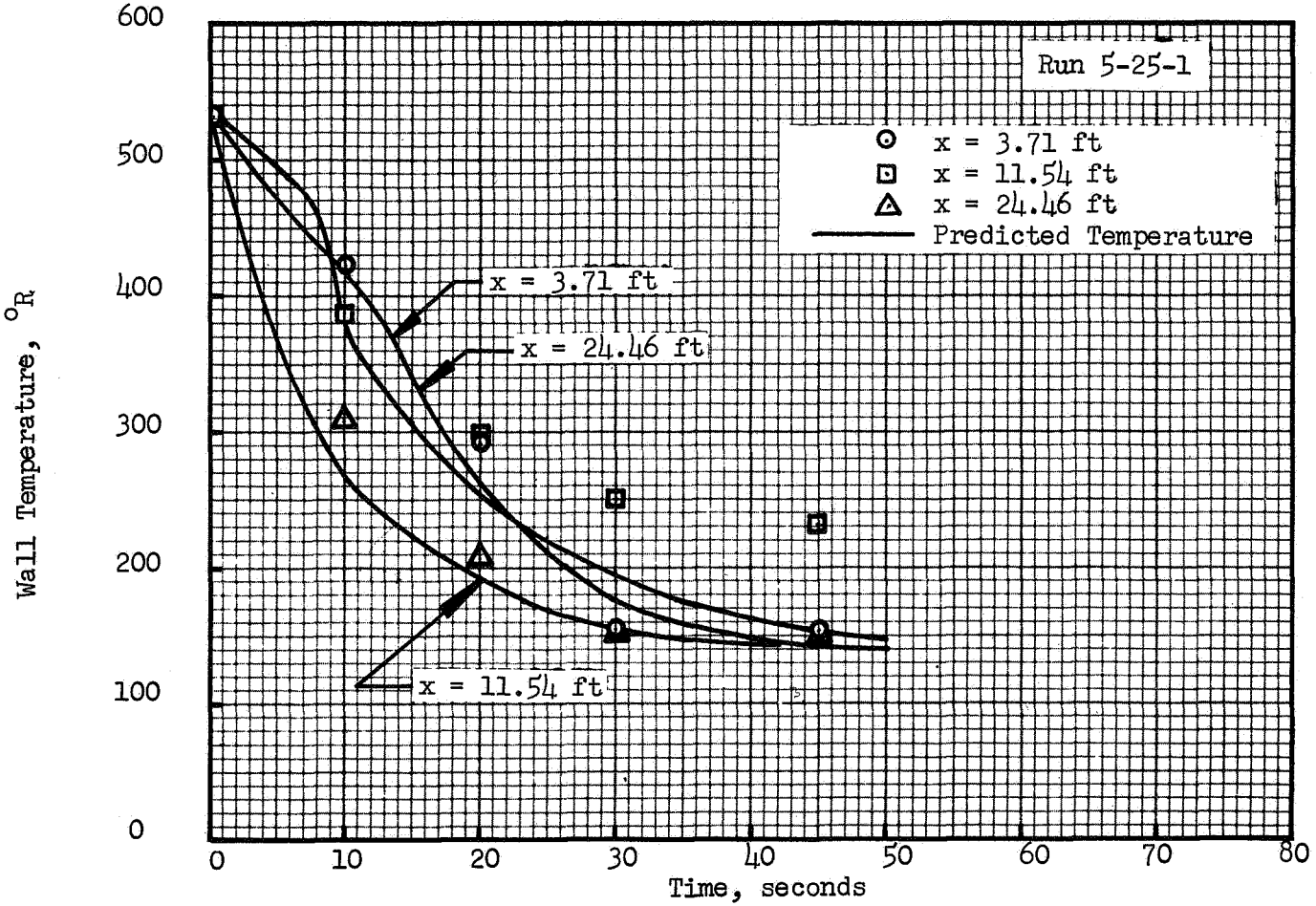


Fig. 70 Line Temperature History with Subcooled Liquid Nitrogen at a Driving Pressure of 43.9 psia

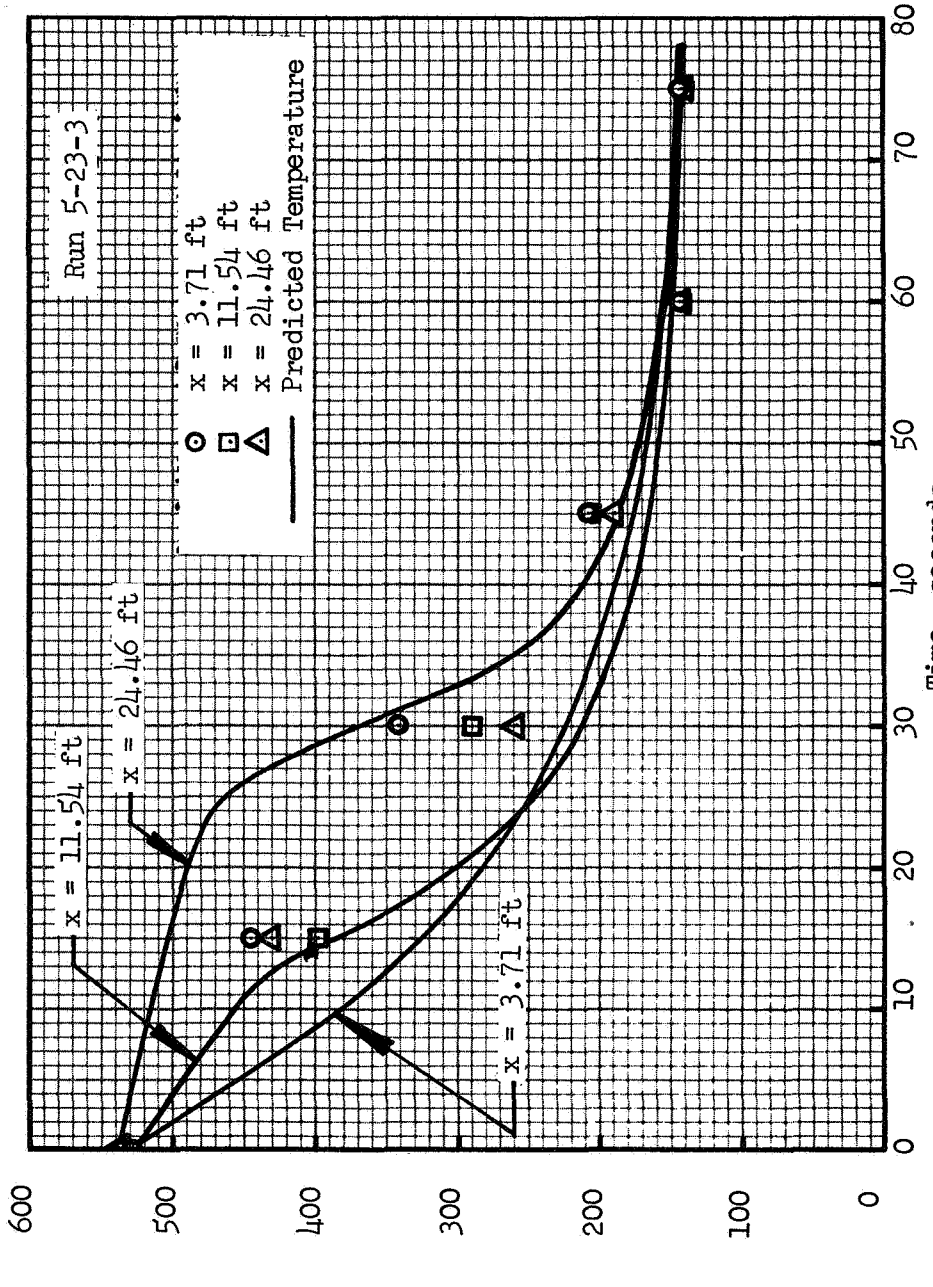


Fig. 71- Line Temperature History with Saturated Liquid Nitrogen at a Driving Pressure of 24.7 psia

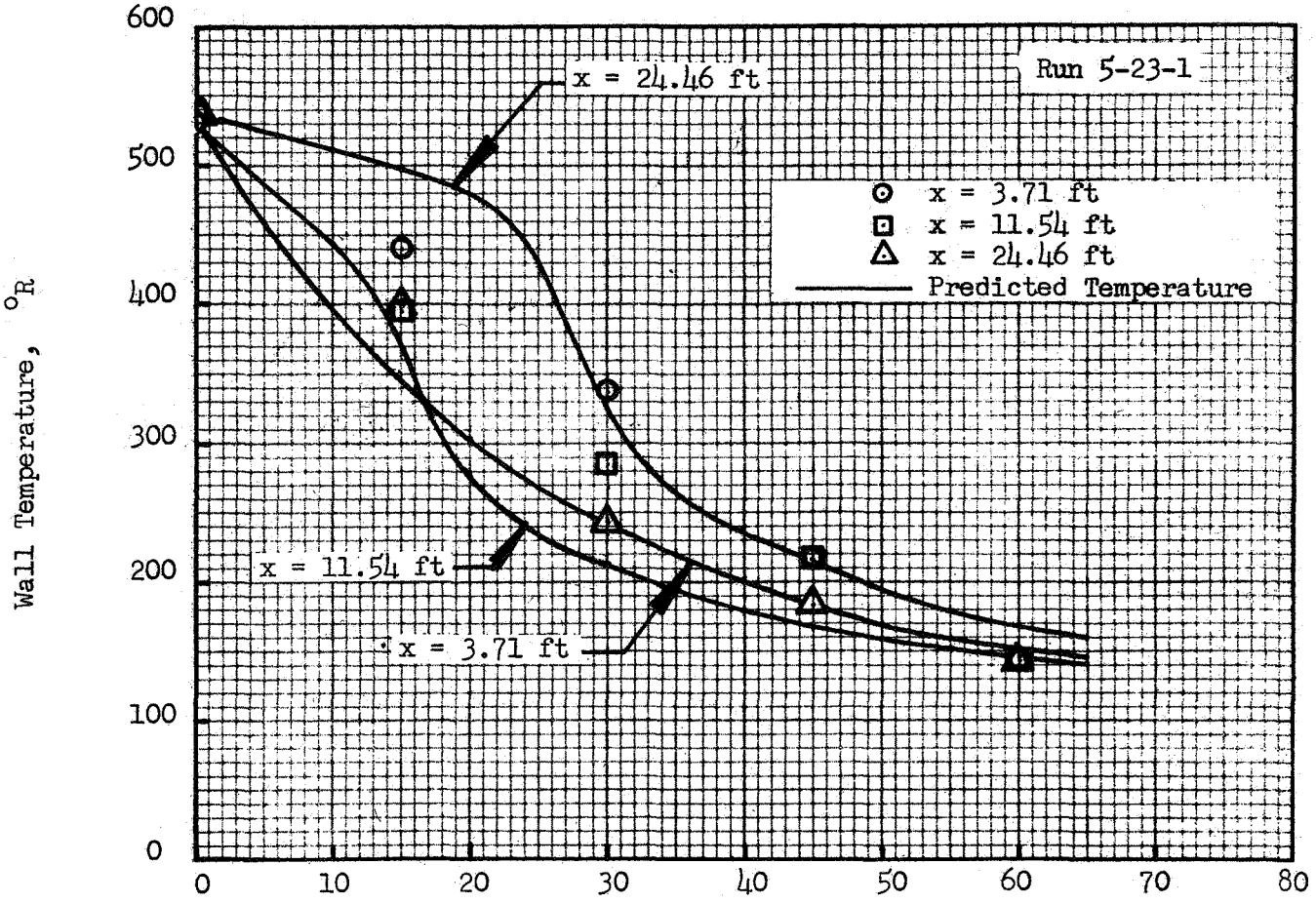


Fig. 72 Line Temperature History with Subcooled Liquid Nitrogen at a Driving Pressure of 24.8 psia

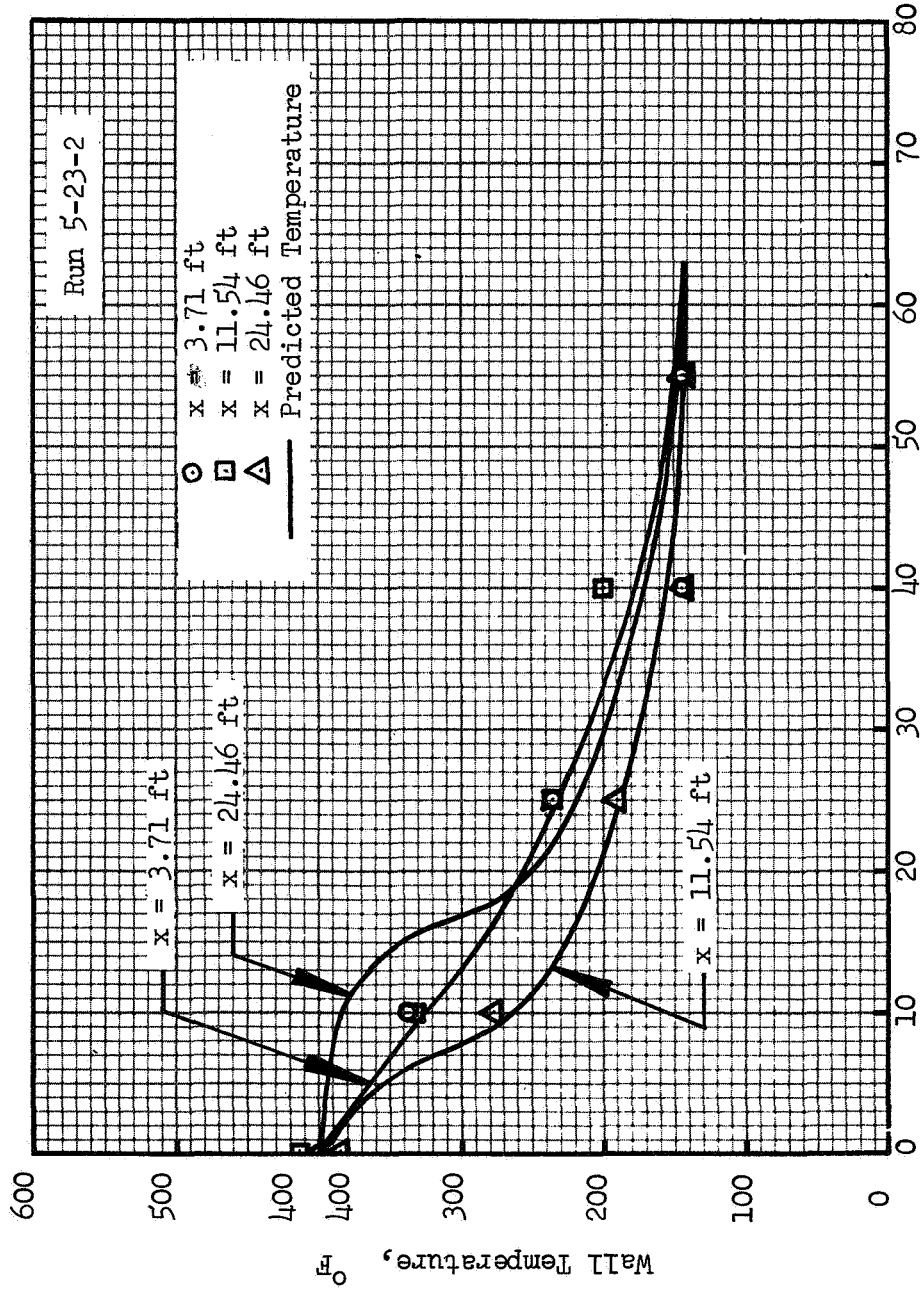


Fig. 73 Line Temperature History with Subcooled Liquid Nitrogen at a Driving Pressure of 23.4 psia

Table 6

TEST CONDITIONS FOR NBS TRANSFER LINE TESTS

Test Fluid	Inlet Pressure (atm)	Inlet Fluid Condition	Measured Chill-down Time (sec)	Computed Chill-down Time (sec)
Nitrogen	2.5	Saturated	265	280
Nitrogen	3.4	Saturated	205	200
Nitrogen	5.9	Saturated	130	122
Nitrogen	4.2	Subcooled	128	190
Nitrogen	5.9	Subcooled	85	115
Hydrogen	5.1	Saturated	68	62
Hydrogen	2.5	Subcooled	140	126
Hydrogen	5.9	Subcooled	60	56
Hydrogen	11.0	Subcooled	24	33

LOCKHEED MISSILES & SPACE COMPANY

at local atmospheric pressure (~ 12.05 psia) are indicated as having subcooled inlet fluid conditions. For tests which were run with the liquid saturated at the selected driving pressure, the liquid is referred to as saturated liquid. The data for these tests and the corresponding analytical results are shown in Figs. 74 through 82. The comparisons shown in Figs. 74 , 75 , and 76 are for saturated nitrogen at successively higher driving pressures. In general, although the shapes of the temperature-time curves near the pipe inlet are not well simulated, the agreement between the temperature-time histories for the downstream half of the line and the predicted and measured chill-down times is remarkably good. For the subcooled nitrogen data (Figs. 77 and 78), the temperature-time history near the inlet are in good agreement with the analytical prediction; however, the predicted chill-down time is about 30% greater than the measured chill-down time.

The comparison between the measured and predicted temperature histories for hydrogen are shown in Figs. 79 through 82. Here the measured and predicted chill-down times agree within ± 15% for all the runs. Furthermore, the agreement between the measured and computed temperature histories at each station along the line is surprisingly good, considering the accuracy of the measured data and the approximations made in the analysis. Indeed, there is good reason to attribute differences in the analytical and experimental results at low temperatures to inaccuracies in the measured data. As Steward points out in Ref. 16, "The crossing of temperature curves in the low temperature region in some tests is undoubtedly the result of inaccuracies in the measurement since this is where the largest errors would occur."

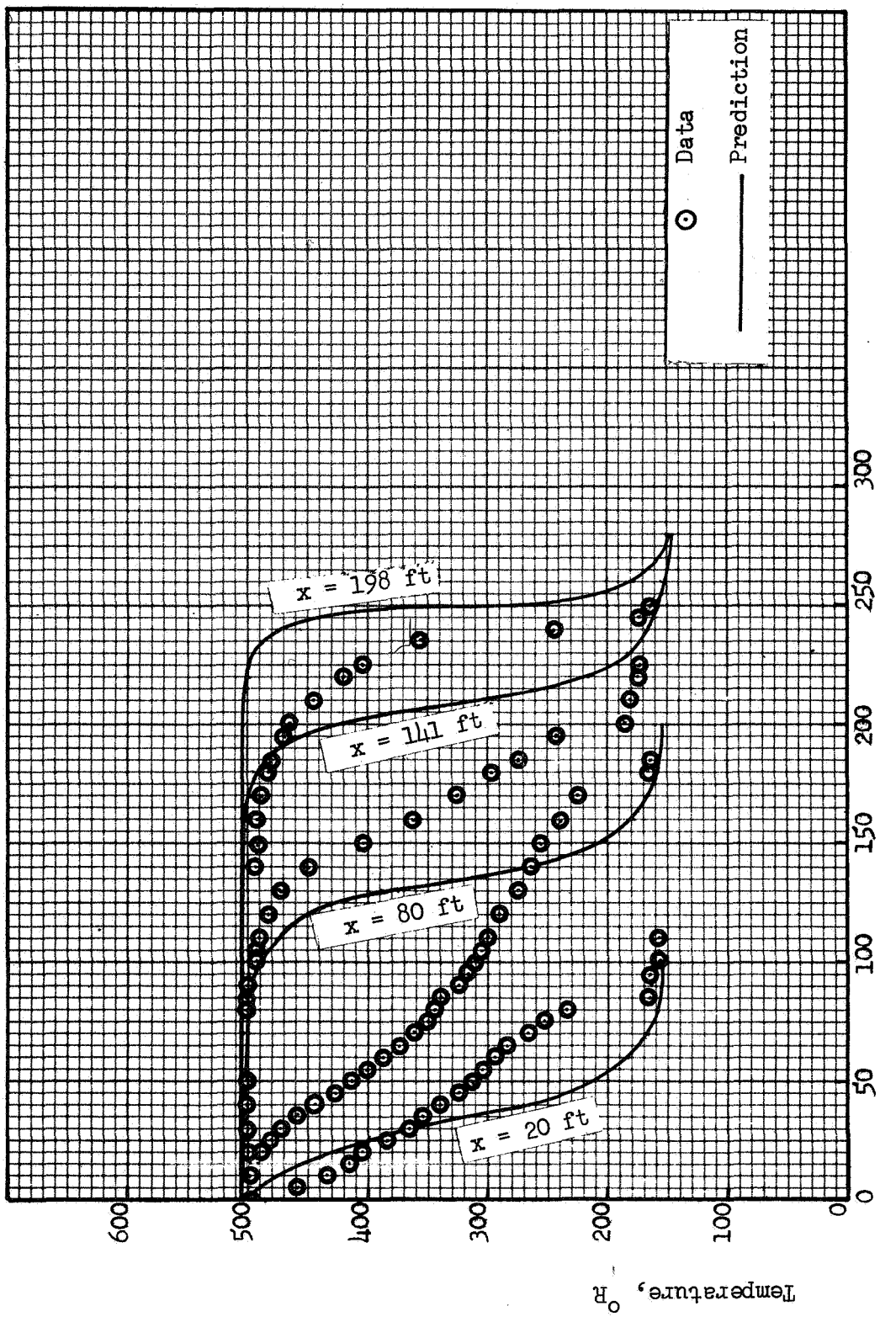


Fig. 74 Comparison Between Computed and Measured Line Temperature Histories with Saturated Liquid Nitrogen at a Driving Pressure of 2.5 atm.

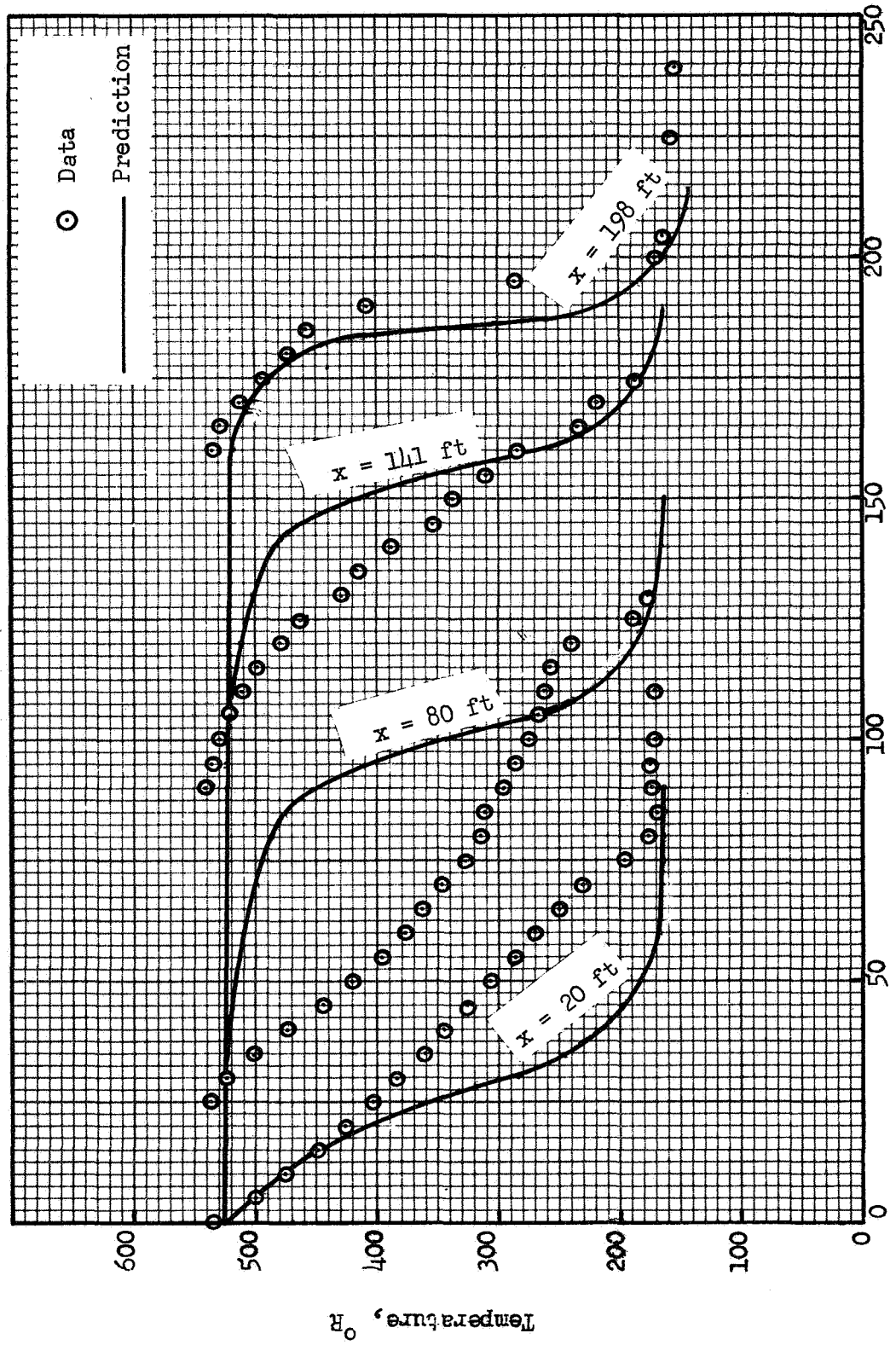


Fig. 75 Comparison Between Computed and Measured Line Temperature Histories with Saturated Liquid Nitrogen at a Driving Pressure of 3.4 atm.

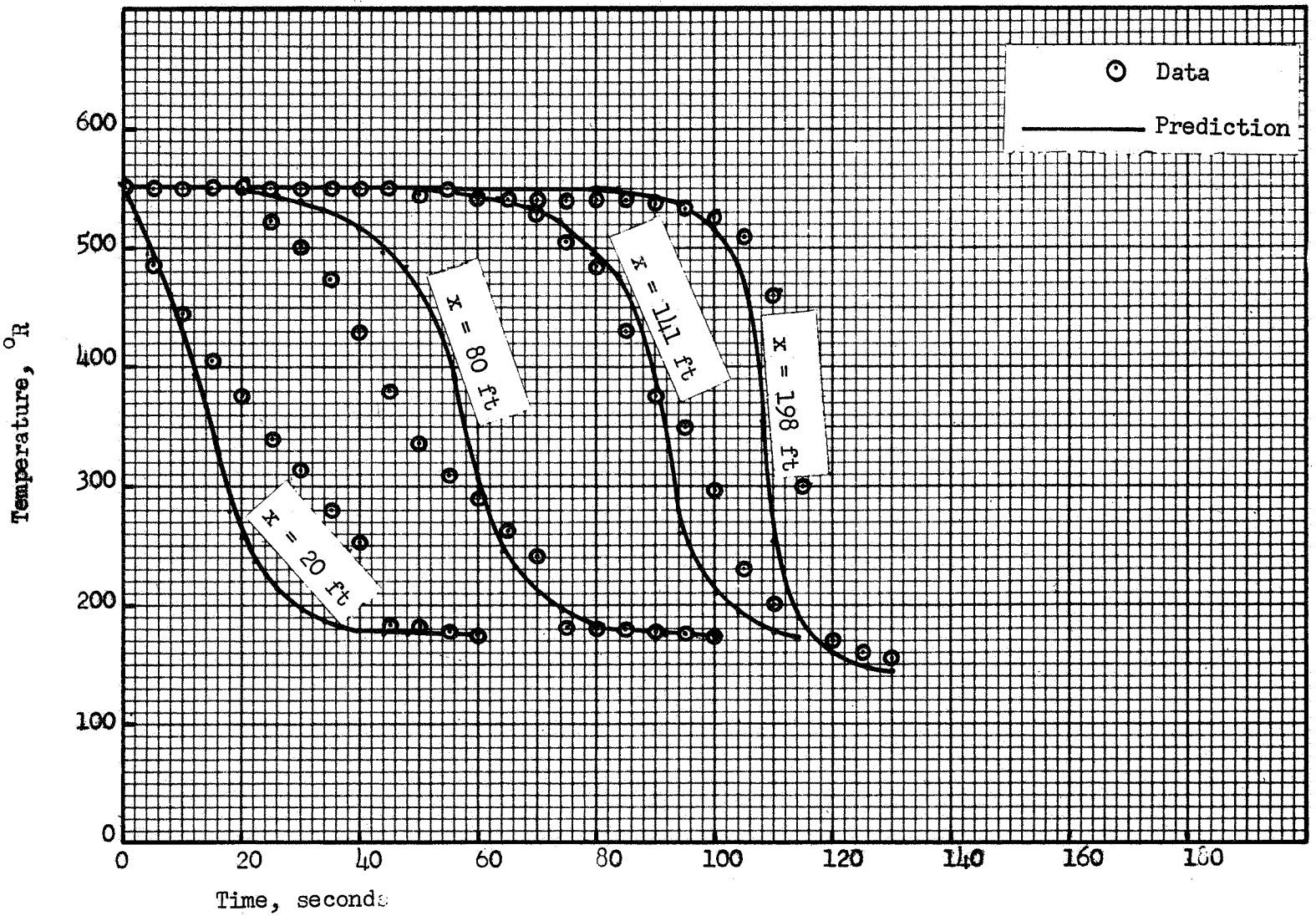


Fig.76 Comparison Between Computed and Measured Line Temperature Histories with Saturated Liquid Nitrogen at a Driving Pressure of 5.9 atm.

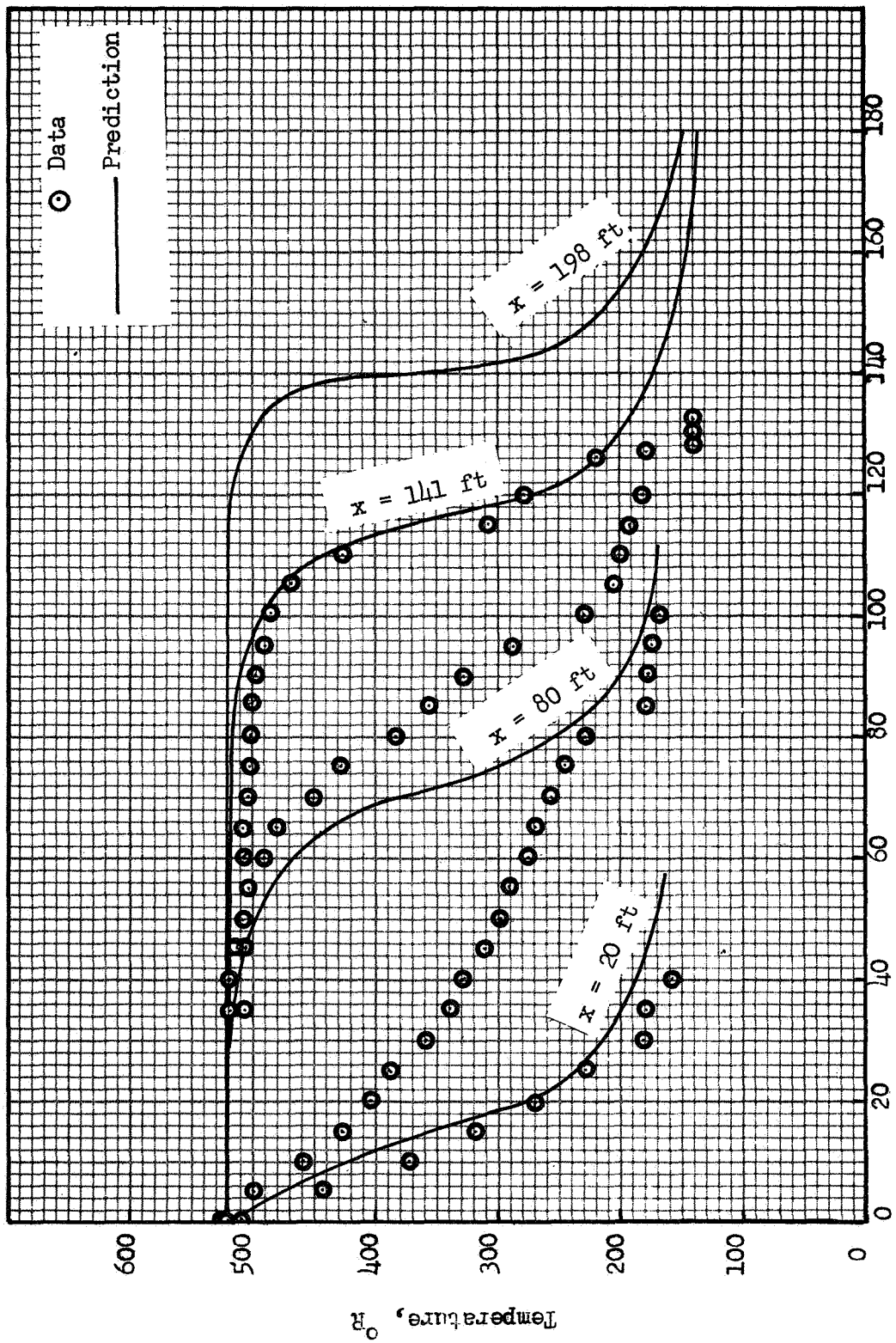


Fig. 77 - Comparison Between Computed and Measured Line Temperature Histories with Subcooled Liquid Nitrogen at a Driving Pressure of 4.2 atm.

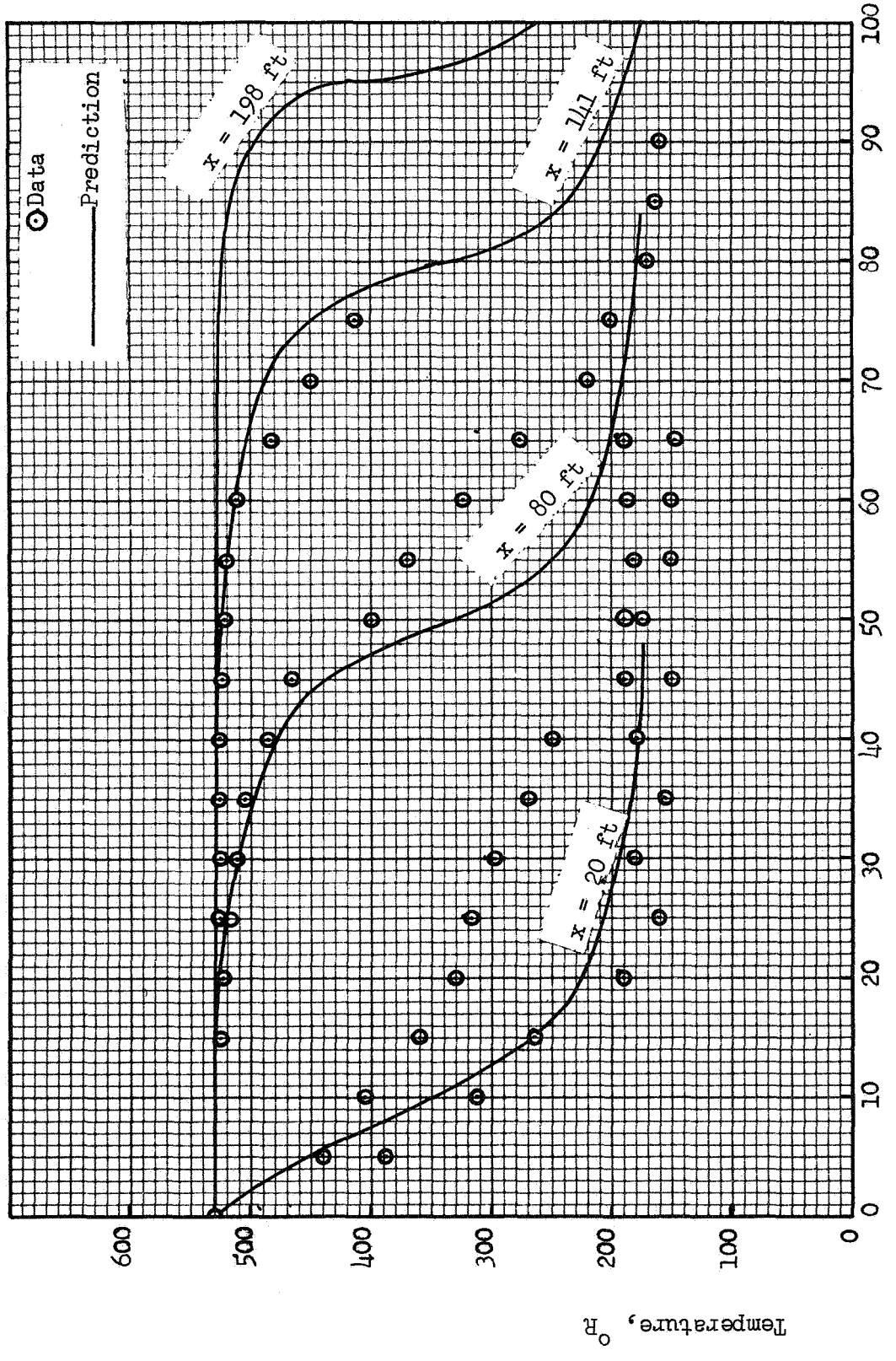


Fig.78-Comparison Between Computed and Measured Line Temperature Histories with Subcooled Liquid Nitrogen at a Driving Pressure of 5.9 atm.

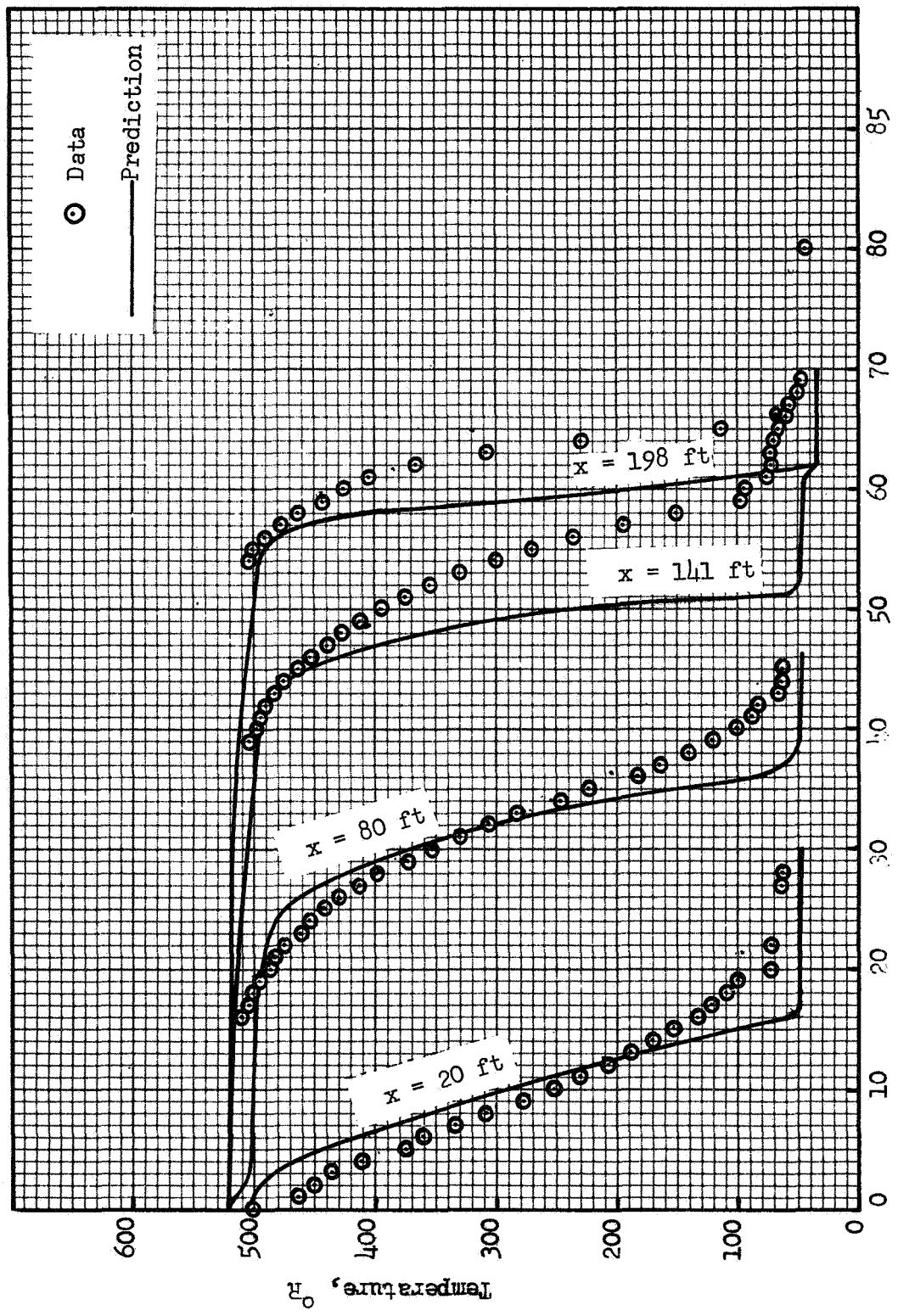


Fig.79-Comparison Between Computed and Measured Line Temperature Histories with Saturated Liquid Hydrogen at a Driving Pressure of 5.1 atm.

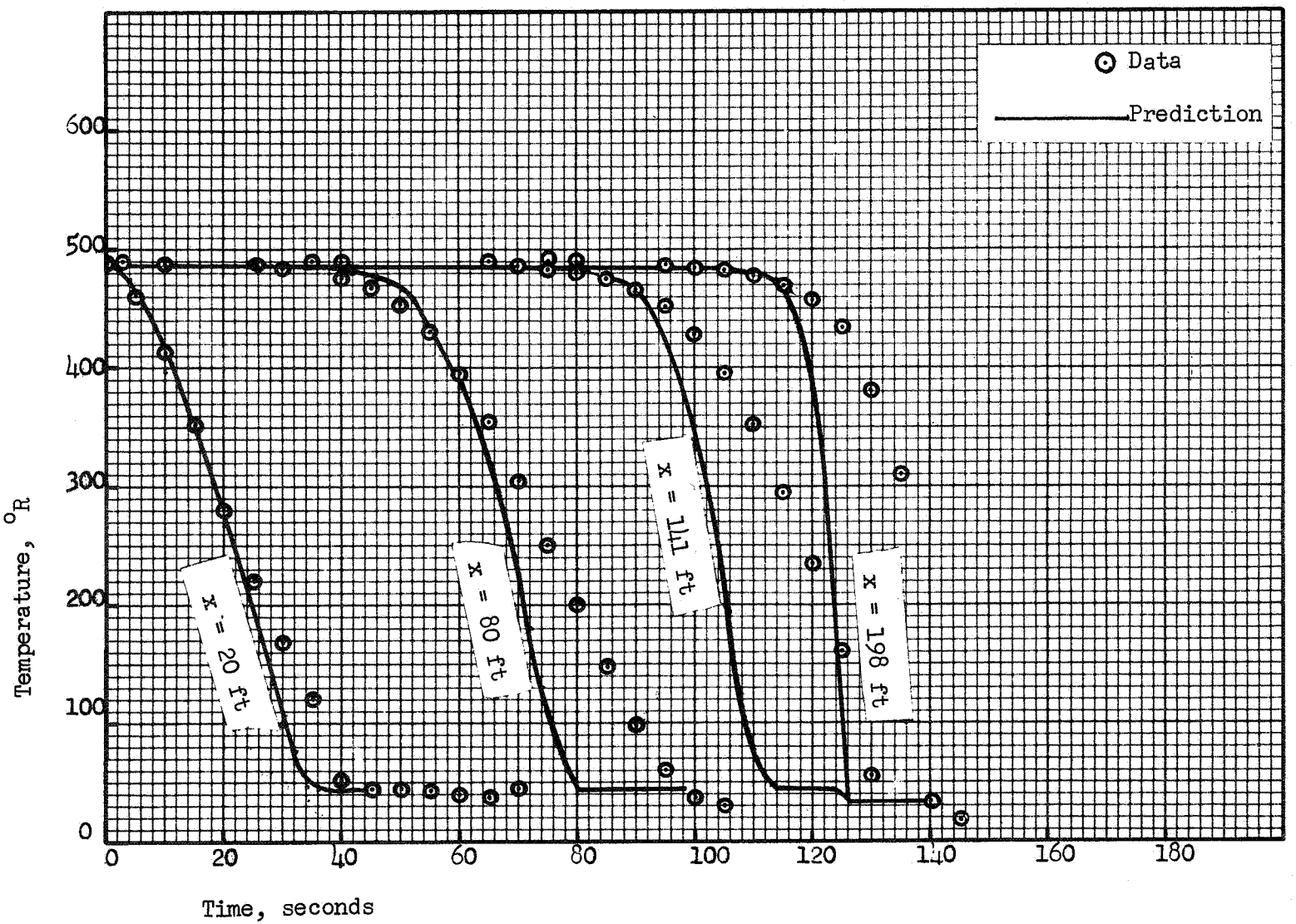


Fig. 80-Comparison Between Computed and Measured Line Temperature Histories with Subcooled Liquid Hydrogen at a Driving Pressure of 2.5 atm.

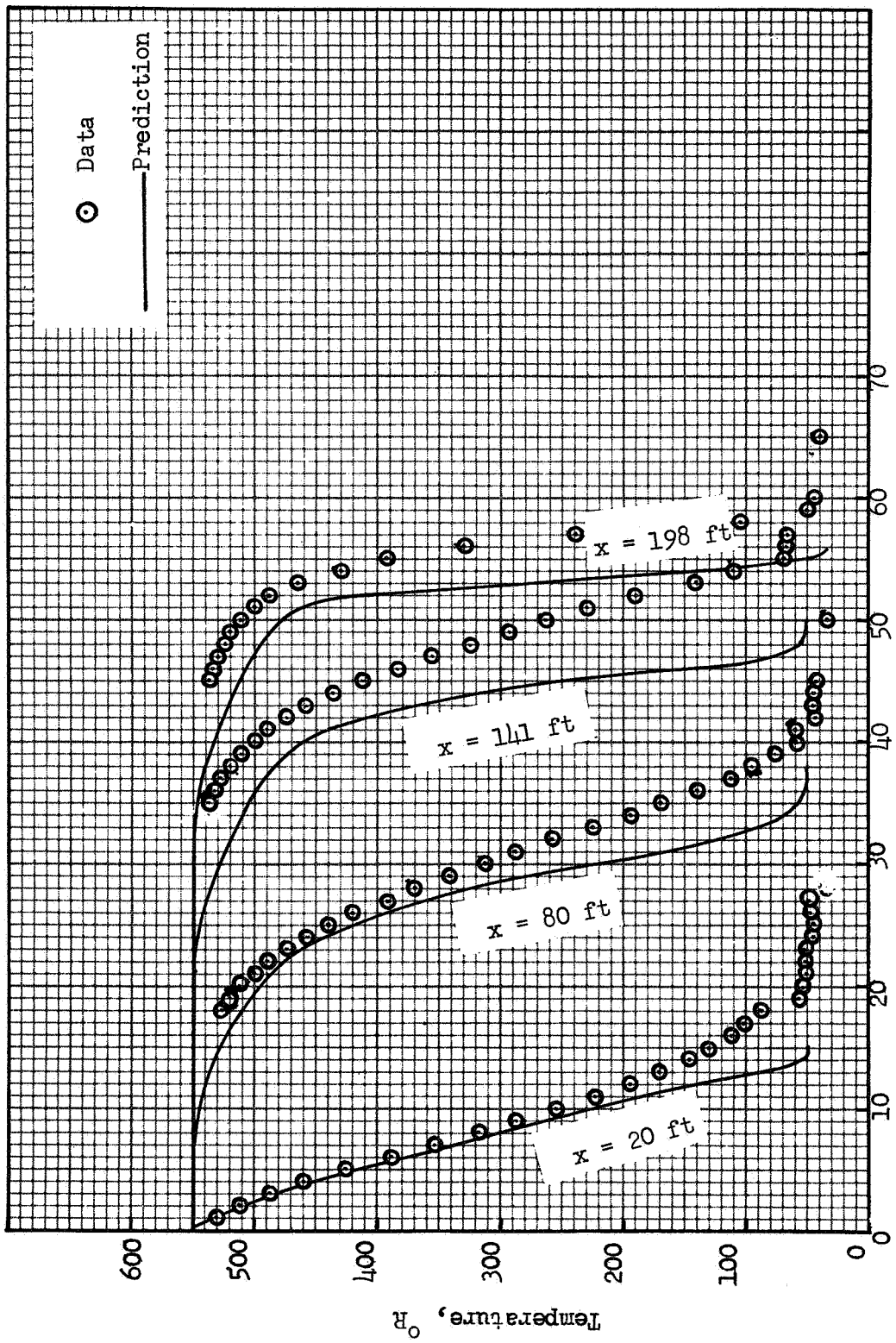


Fig. 81 Comparison Between Computed and Measured Line Temperature Histories with Subcooled Liquid Hydrogen at a Driving Pressure of 5.9 atm.

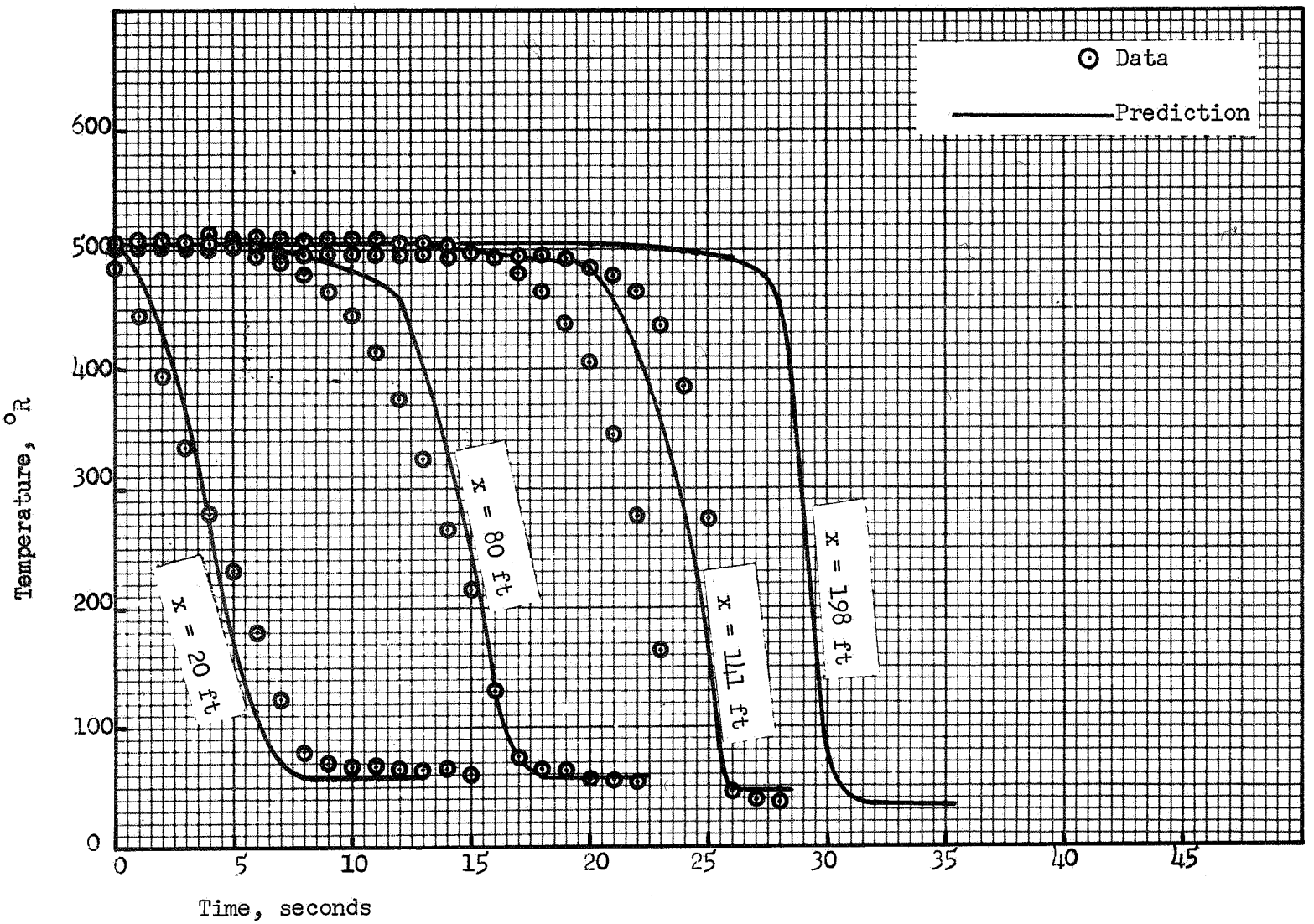


Fig. 82-Comparison Between Computed and Measured Line Temperature Histories with Subcooled Liquid Hydrogen at a Driving Pressure of 11 atm.

Altogether, the agreement between computed and measured results for this transfer line indicates that the line chill-down computer program may be used with confidence a design tool, especially for large L/D transfer lines.

Section 9

SCALING-LAW VERIFICATION AND COMPLETE SYSTEM TESTS

The objective of this series of tests is to provide data on transfer-line and tank conditions during times of transient fill which represent field conditions, and to verify the coupled transfer line-tank analytical model for this general case. A further objective of these tests is to verify experimentally the results of the scaling law analysis described in Volumes III and IV of this report.

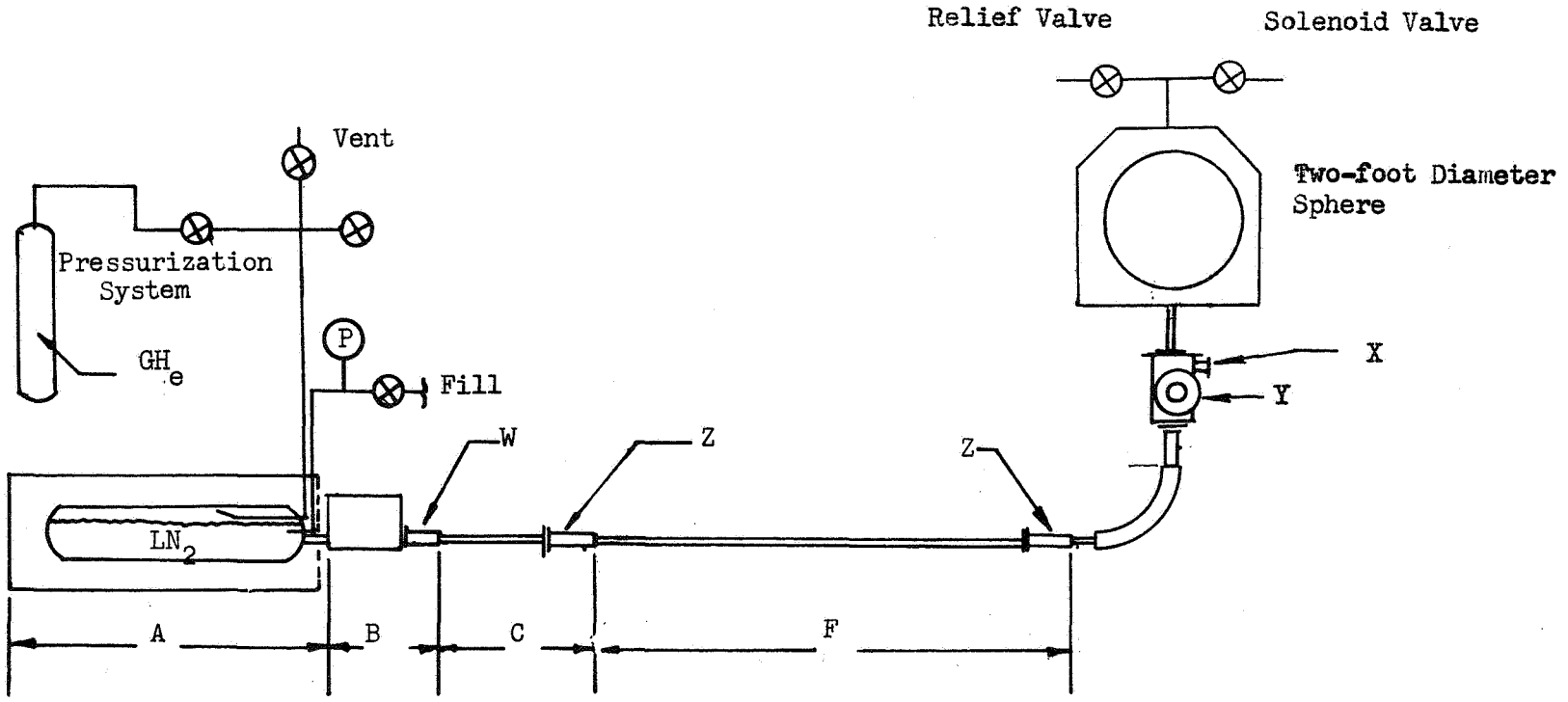
The tests performed to accomplish these objectives made use of two facilities; the coupled small-size transfer line and tank described in Section 8, and a considerably larger facility which was installed at the Lockheed Santa Cruz Test Base (SCTB). The latter facility, described in detail below, consisted of a nominal three-inch diameter, 300-foot-long transfer line coupled to a five-foot-diameter tank. The following paragraphs describe the tests which were conducted with these facilities and the correlation between the experimental data and analytical predictions.

9.1 TRANSIENT FILL TESTS WITH A COUPLED TANK AND TRANSFER LINE

The following sections describe the details of the apparatus and test procedure used in the testing of large-and small-size apparatus designed to simulate a complete propellant tank filling system.

9.1.1 Coupled Line and Tank Tests - Small-Size Apparatus.

Upon completion of the tank-fill flow phenomena tests and the transfer line flow phenomena tests, the tank (sphere) and transfer line were coupled together as shown in Figures 83. and 84., to perform limited coupled testing. A photograph showing the test sphere appears in Fig. 85. In the coupled system, the transfer line included the three and eleven-foot sections with the void fraction measuring section mounted (vertically) below the sphere as for the quasi-steady inlet flow tests. In addition to the relief valve on the sphere, a one-inch, manually operated solenoid valve was added to permit more rapid venting due to the expected high pressure rise in the sphere during the transfer. Two tests were planned: (a) an initially warm transfer line (room temperature) and (b) an initially prechilled transfer line, both with approximately 15 psig supply pressure and the sphere gas at room temperature initially. It was expected that with the relatively large thermal capacitance of the transfer line (1/16-inch wall) and the relatively small volume and low pressure capability of the sphere, that the pressure limitations might be reached prior to the appearance of significant two-phase flow at the sphere inlet; therefore, a prechilled line test was also planned. The latter test was to be conducted immediately after the warm transfer line test (during which the line would undergo complete chill-down) with only enough time between to purge the sphere with room temperature nitrogen gas. During the course of the room temperature test, the sphere structurally failed (exploded) when the ullage pressure achieved 13.5 psig. This occurred at the end of the test. It occurred because the solenoid valve was not manually opened as intended. As a result, the prechilled transfer line test was not made and further coupled testing was



A - Insulated Liquid Nitrogen Supply Tank
B - Control Box and Instrumented Upstream Area
F - Eleven-ft. standard Instrumented Transfer Line Section
W - Upstream Instrumentation Station
X - Liquid Volume Fraction Measuring Station
Y - Transparent Visualization Station
Z - Standard Instrumentation Station

Fig. 83 Complete System Test Setup - Small Size Apparatus

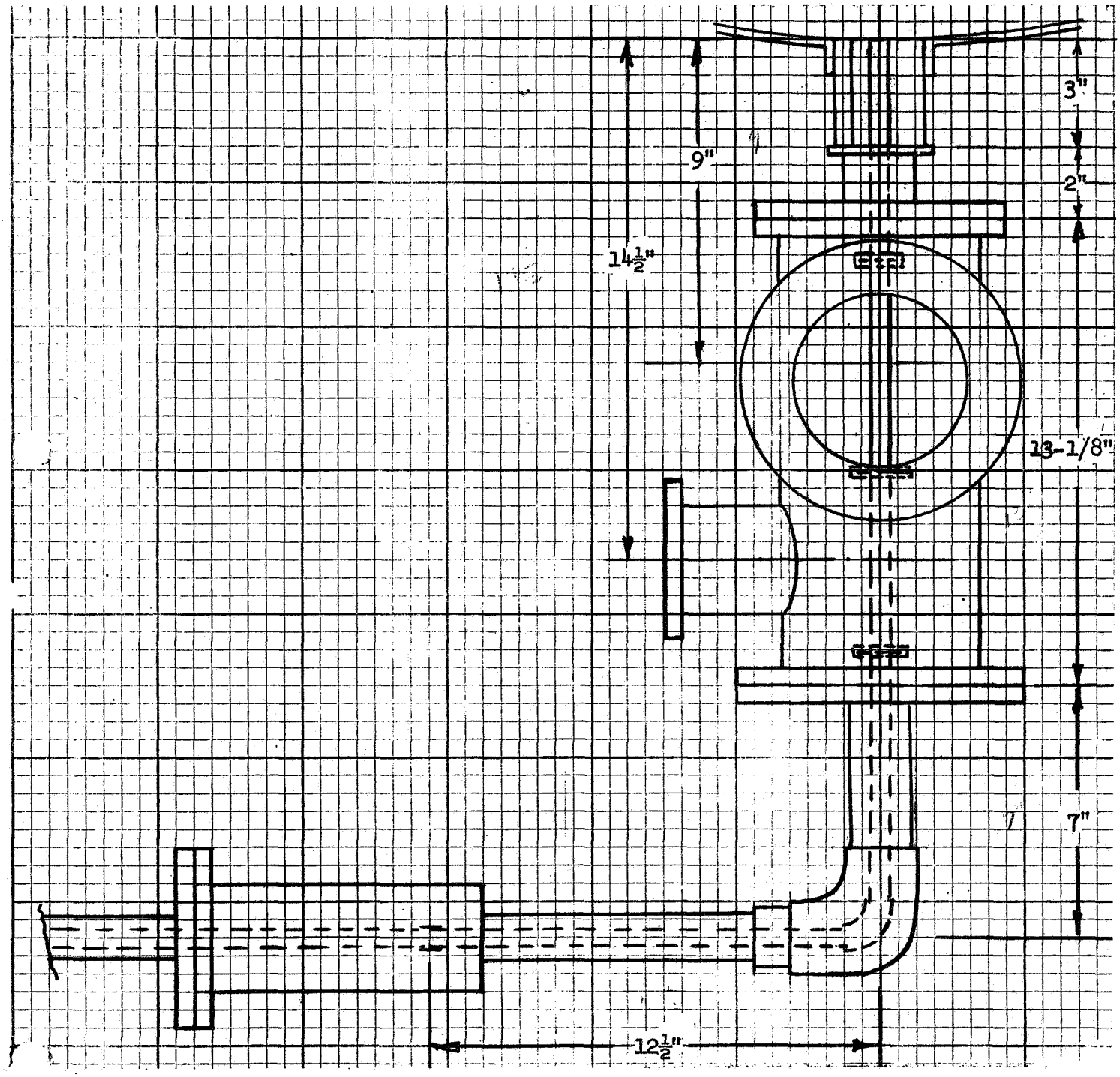


Fig. 84 Inlet Configuration for Coupled Tests

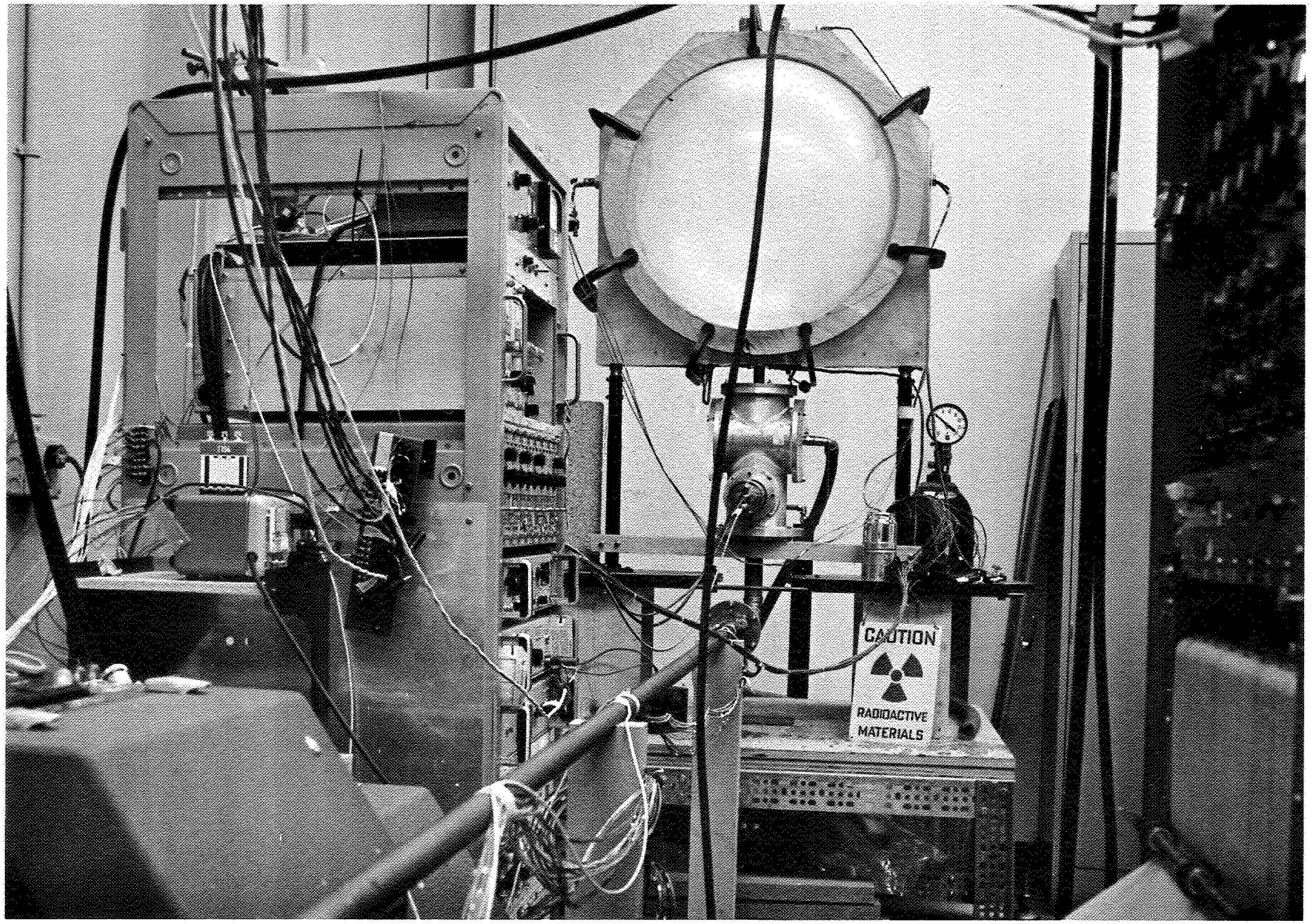


Fig. 85 Apparatus for Complete Fill System Tests - Small Size Apparatus

discontinued. The complete data for the first test were reduced and are discussed below.

The supply pressure, liquid nitrogen flow rate, receiver tank pressure and liquid nitrogen fraction near the sphere inlet are shown in Figs. 86 and 87. As indicated on the figures immediately prior to test initiation, the supply tank was vented at 0.2 psig. The test duration was approximately 5.8 seconds. The recorded tank pressure was relatively linear for the first three seconds, followed by a continually decreasing slope. This is largely attributed to the continually decreasing overall pressure drop and resulting decrease in flow rate, although the presence of two-phase flow at the inlet could contribute. Between 2.5 and 4 seconds is the only time during which the void fraction meter definitely indicated two-phase flow at the inlet (see liquid fraction curve) since it is not felt that the liquid fraction measurements are known to be better than approximately two percent. Thus at other than this time, the presence of two-phase flow is questionable even though the liquid fraction curve indicates a small ($\sim$ 1%) liquid fraction.

The transfer line static pressures, fluid temperatures and wall temperatures are presented in Figures 88, 89 and 90, respectively. The pressures in Figure 88 are seen to be similar with slightly higher peak pressures initially further upstream. There were essentially three pressure surges. The line fluid temperatures in Figure 89 located at similar locations to the static pressure in Figure, 88 , show similar temperature excursions above saturation as were evident in the previous transfer line tests. The fluid temperature increases, at approximately four seconds for all sensors, corresponds to the time in Figure 88 where the line pressure has risen to and remains approximately at the supply pressure, resulting in a reduced flow rate. Also,

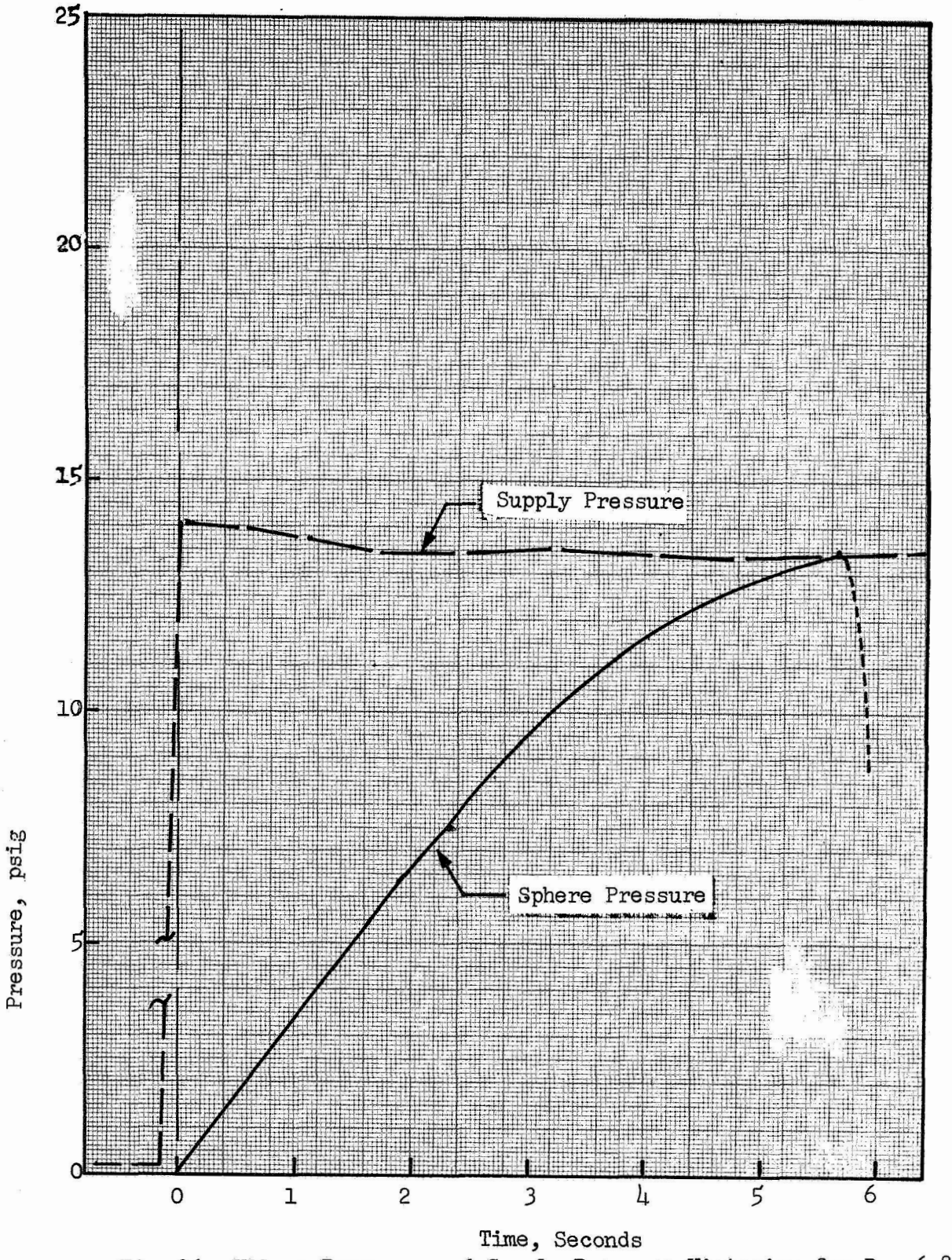


Fig. 86 Ullage Pressure and Supply Pressure Histories for Run 6-8-1

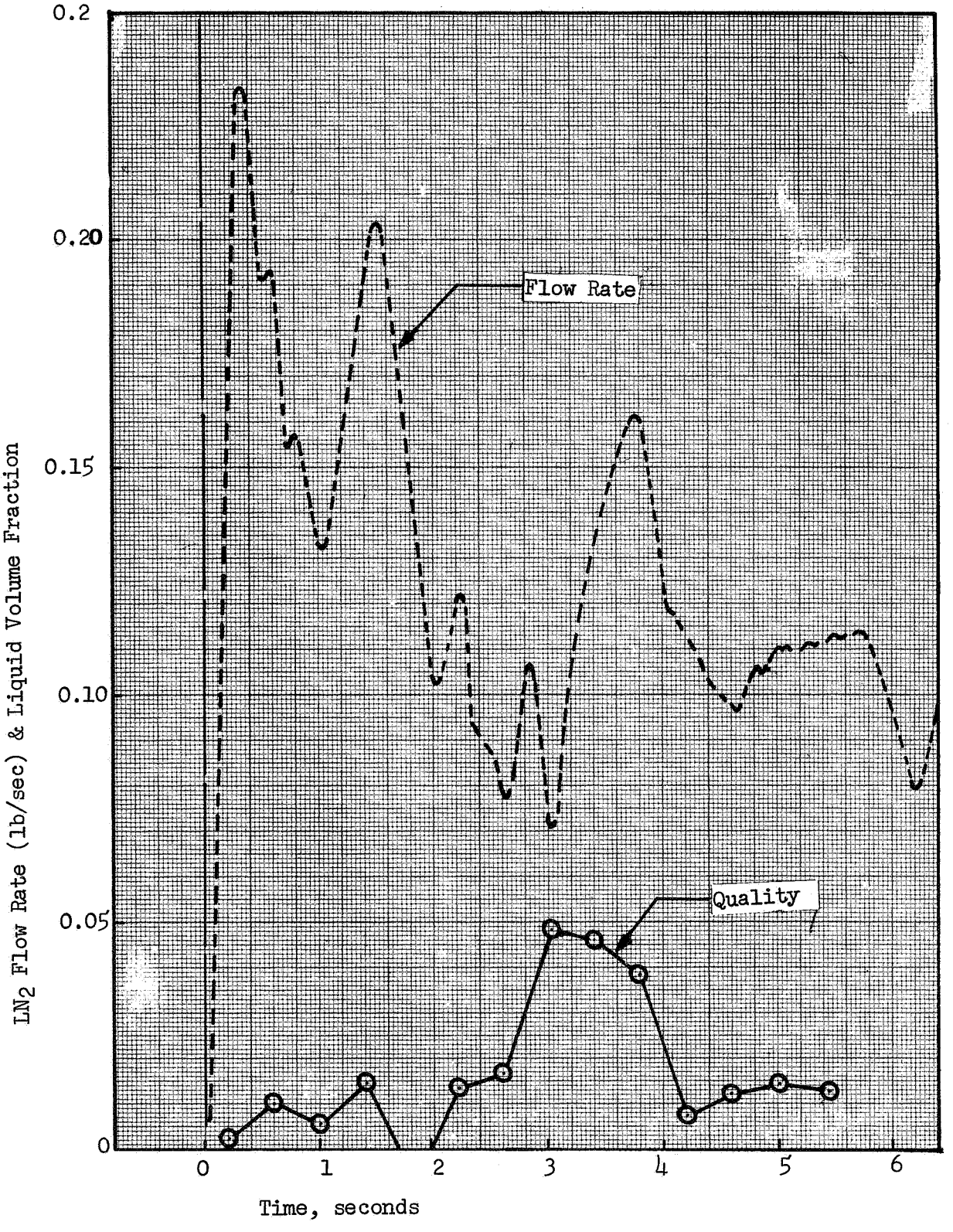


Fig. 87 Inlet Flowrate and Exit Quality Histories for Run 6-8-1

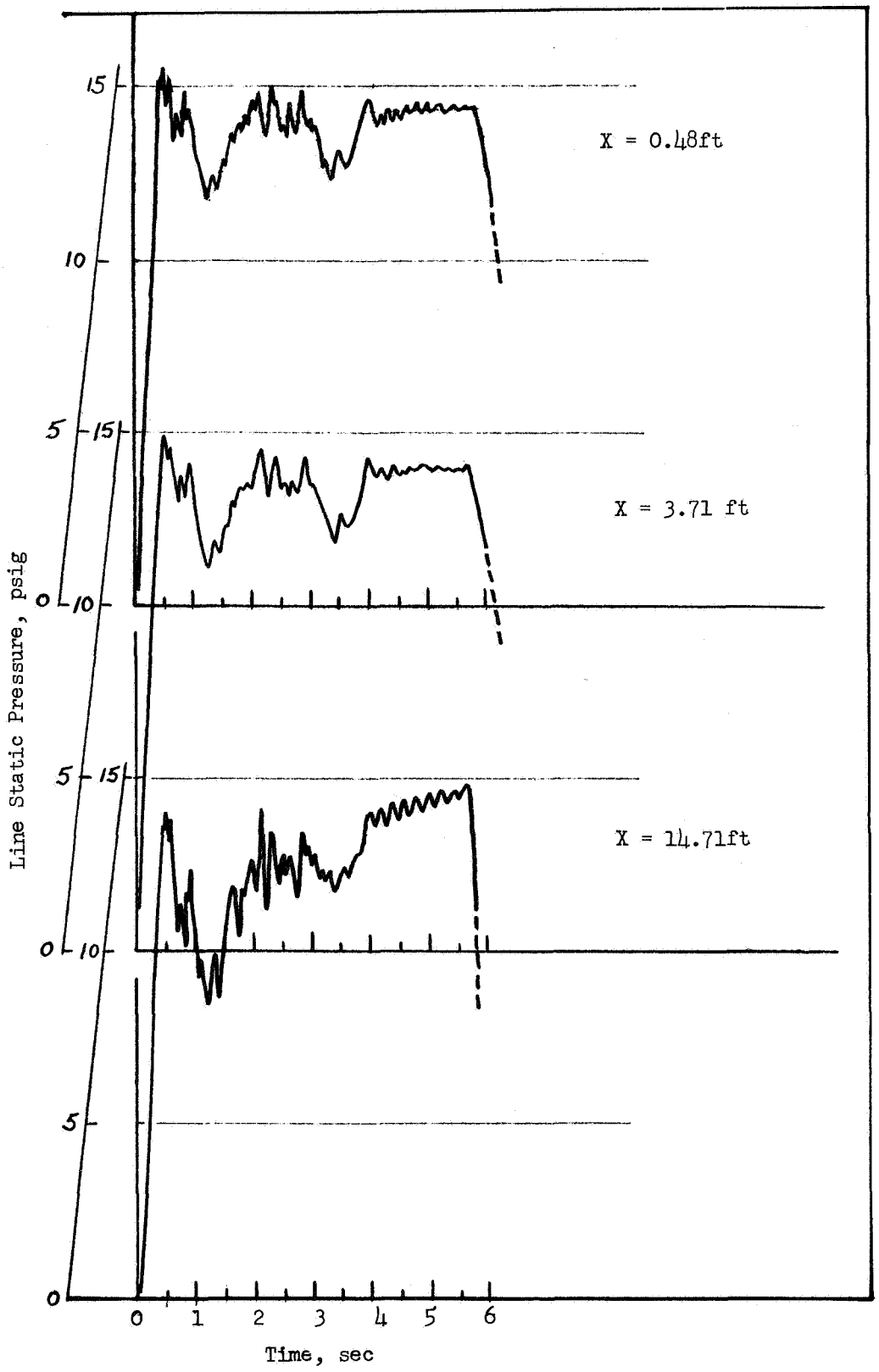


Fig. 88 **Transfer Line Static Pressures — Coupled Test 6-8-1**

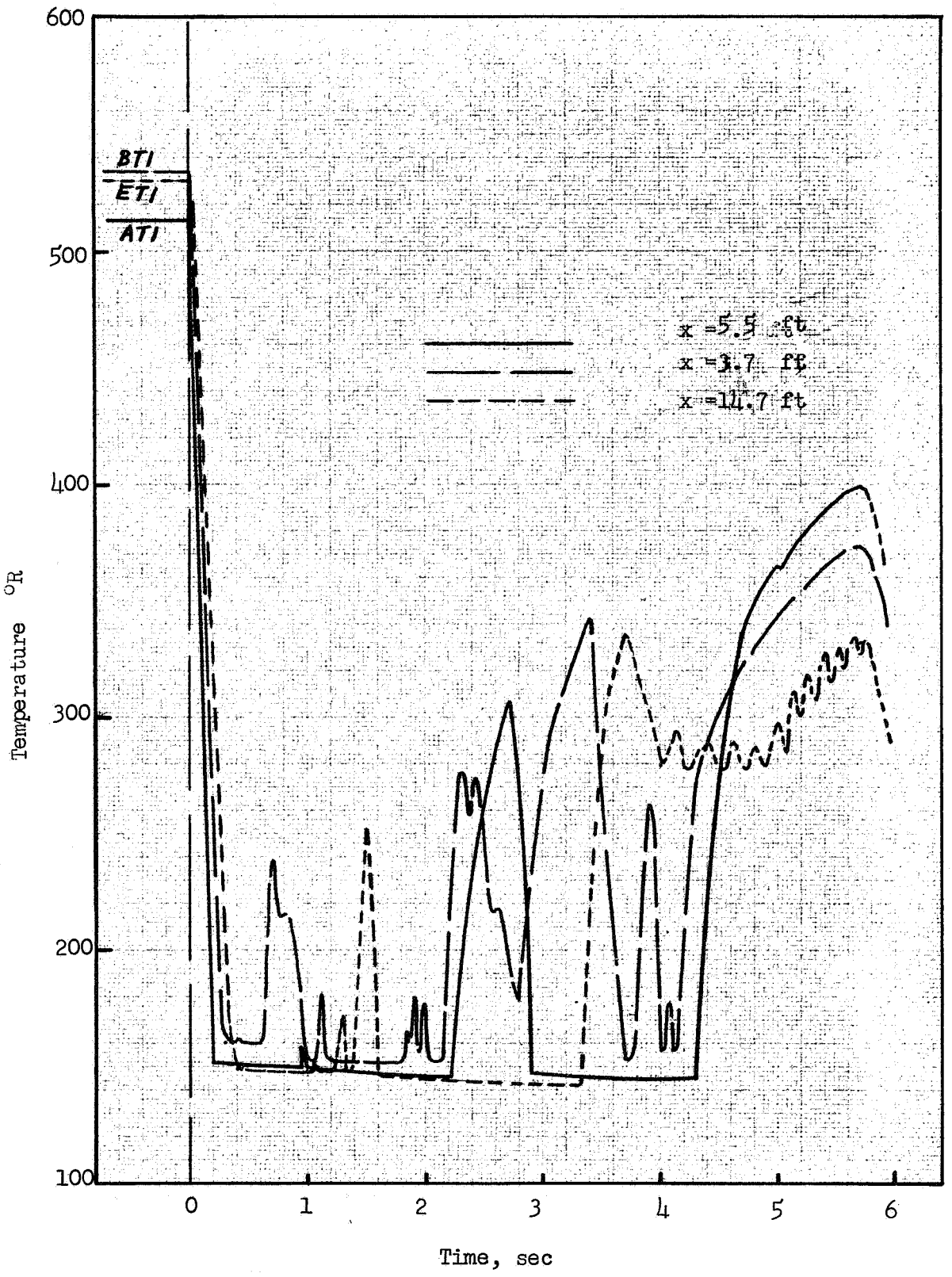


Fig. 89 Transfer Line Fluid Temperatures — Coupled Test 6-8-1

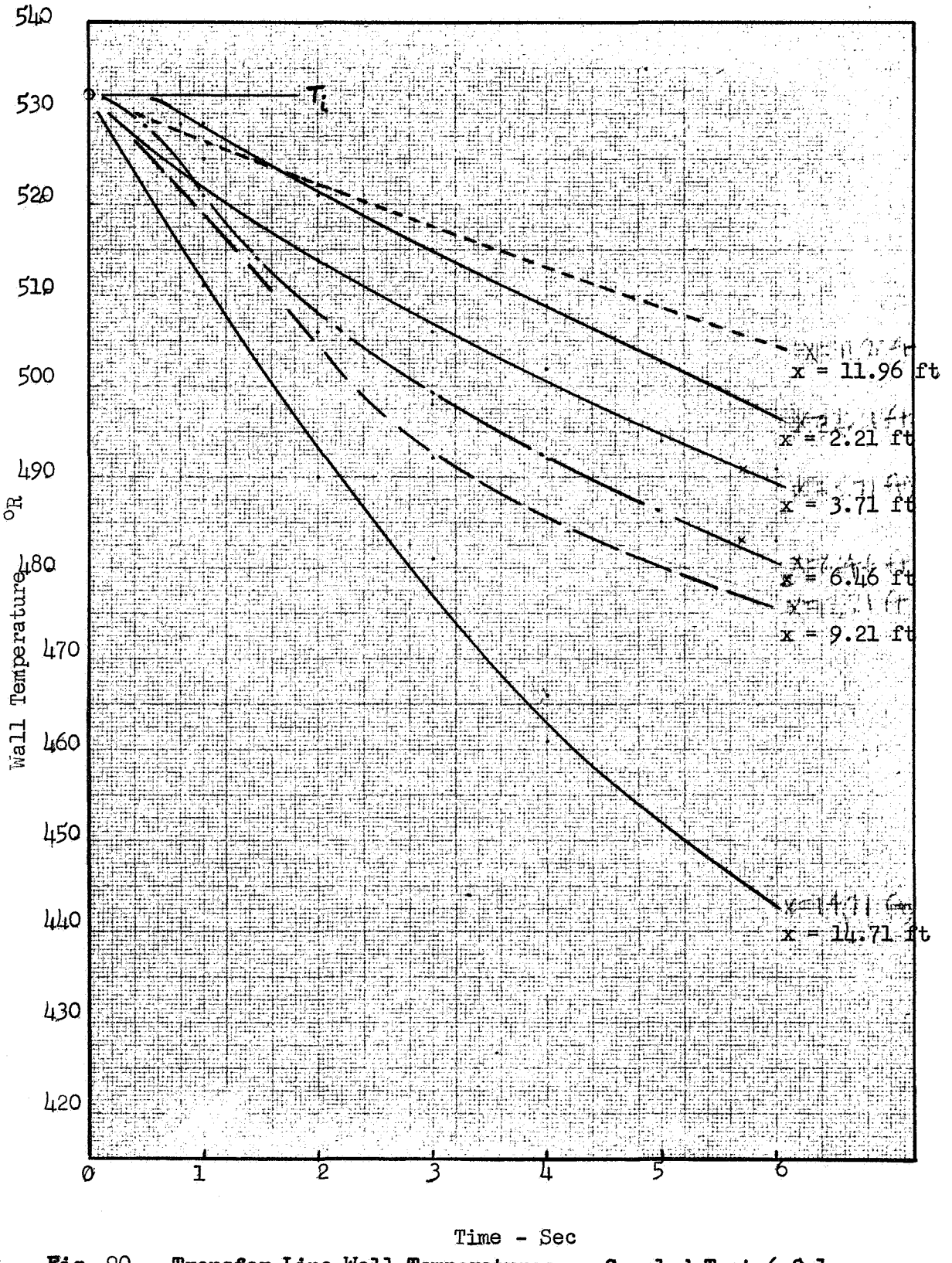


Fig. 90 Transfer Line Wall Temperatures — Coupled Test 6-8-1

superheating the gas within the line was likely. It would be expected that the flow rate would decrease to even a greater extent than is indicated in Figure 87, at this time in the test. This superheating of the gas also occurs earlier in the test although to a lesser extent. Similar observations were also made on the previous transfer line tests, indicating that superheated gas slugs periodically progress down the line during the line chilldown. The wall temperature data in Figure 90 show that the line underwent only partial chilldown during the test. The data are quite consistent with the previous transfer line tests except for wall thermocouple ET3 which appears to be high. This may be due to poor contact between the thermocouple and the wall. Although temperature sensors were not located in the elbow or vertical void fraction measuring section, it is likely that very significant chilldown occurred in the region of the elbow. The centerline and off-centerline temperatures in the receiver are presented in Figures 91 and 92 respectively. Thermocouple #1, just above the inlet, was broken during a preliminary test. These sensors show no evidence of two-phase flow at the receiver inlet, although two-phase flow was apparent in all the prior receiver tank tests. Except in the first second of the tests, the upper half of the receiver and the off-center thermocouples exhibit relatively small variations. The upper wall thermocouple (10) indicates the greatest interaction with the ullage vapor.

9.1.2 Coupled Line and Tank Tests - Large-Size Apparatus

A diagram of the apparatus installed in the test chamber at the SCTB is shown in Fig. 93 This apparatus consists of a five-foot diameter tank with a specially constructed vacuum-jacketed transfer line. This line runs between the tank

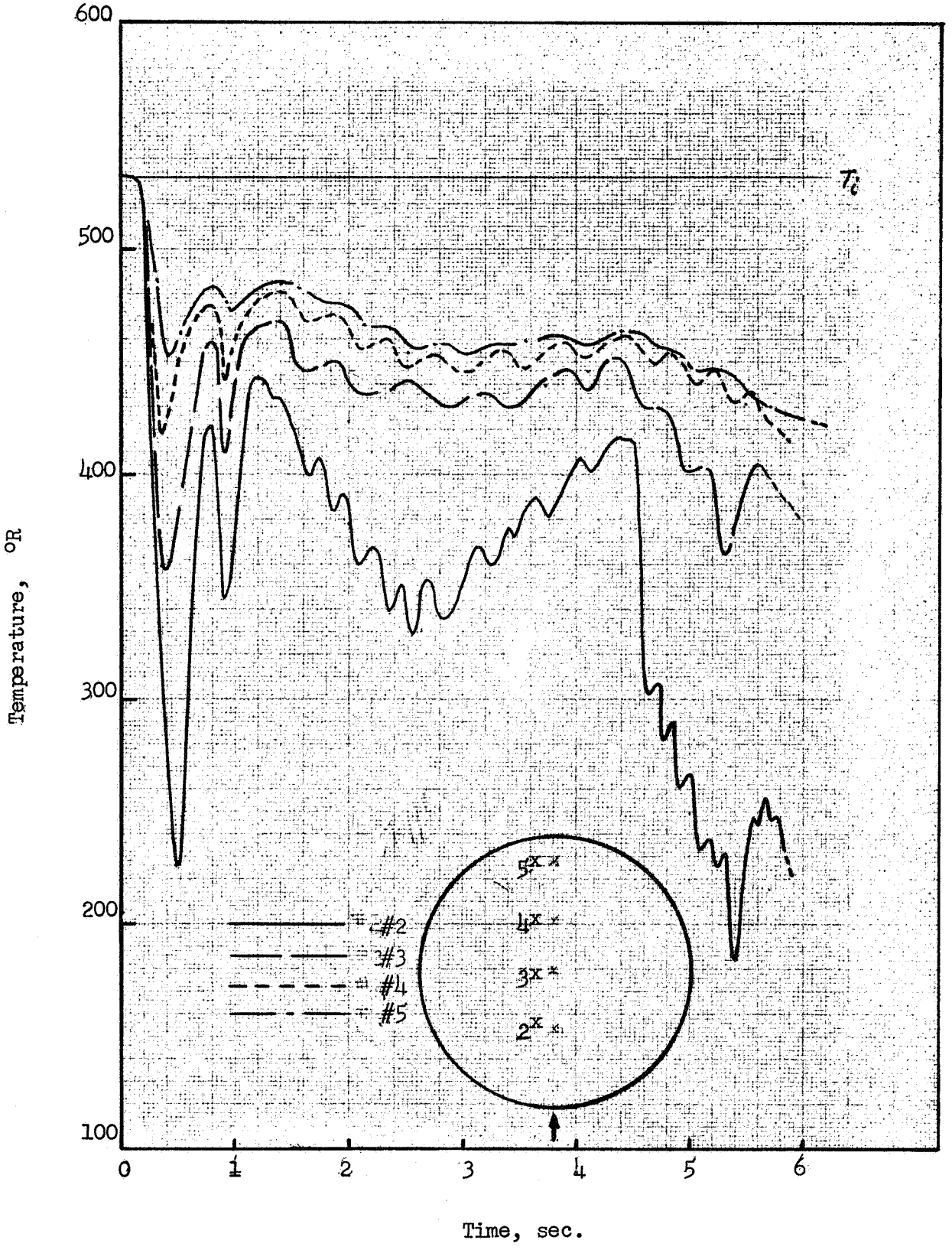


Fig. 91 Receiver Centerline Temperatures—Coupled Test 6-8-1

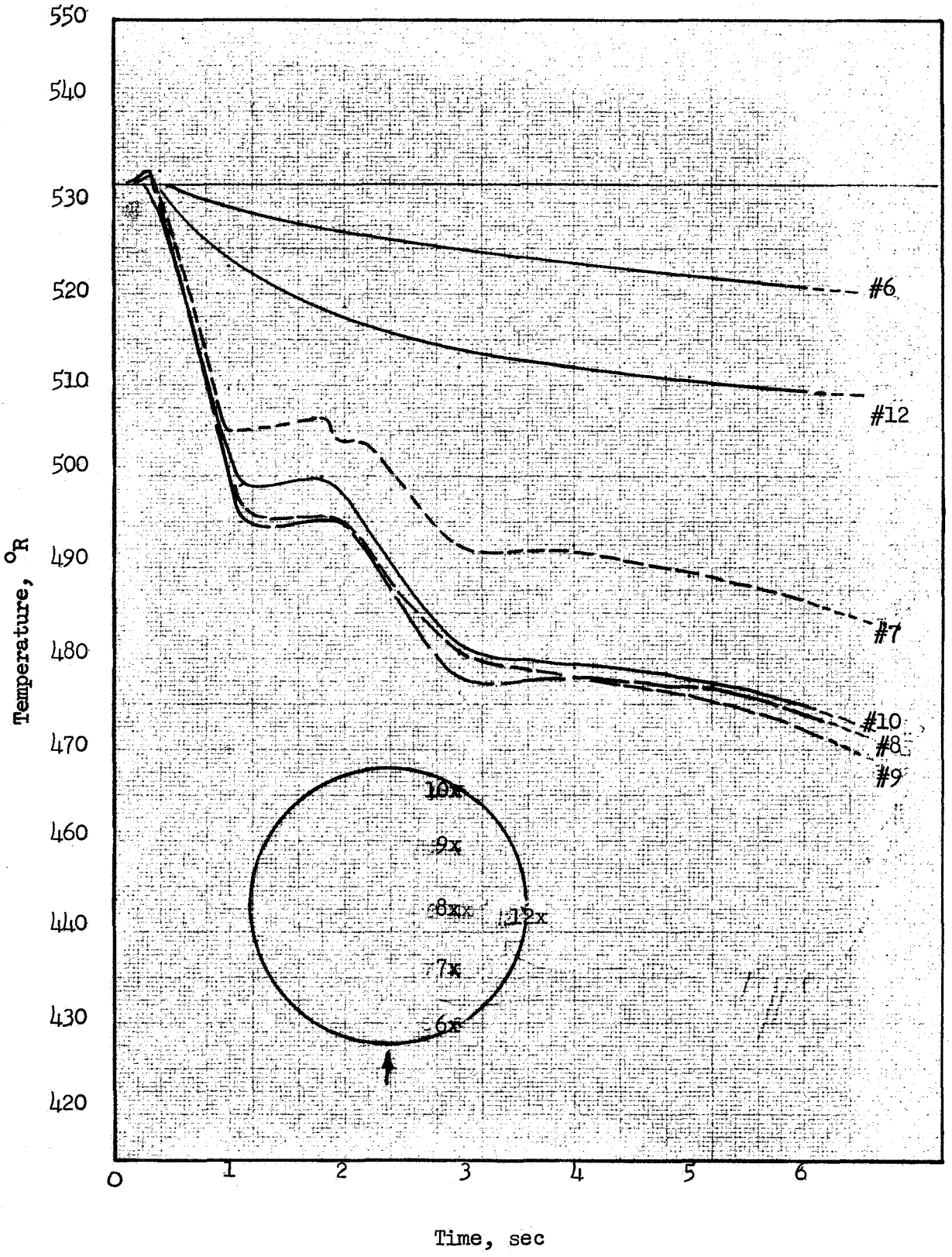


Fig. 92 Receiver Off-center and Wall Temperatures—Coupled Test 6-8-1

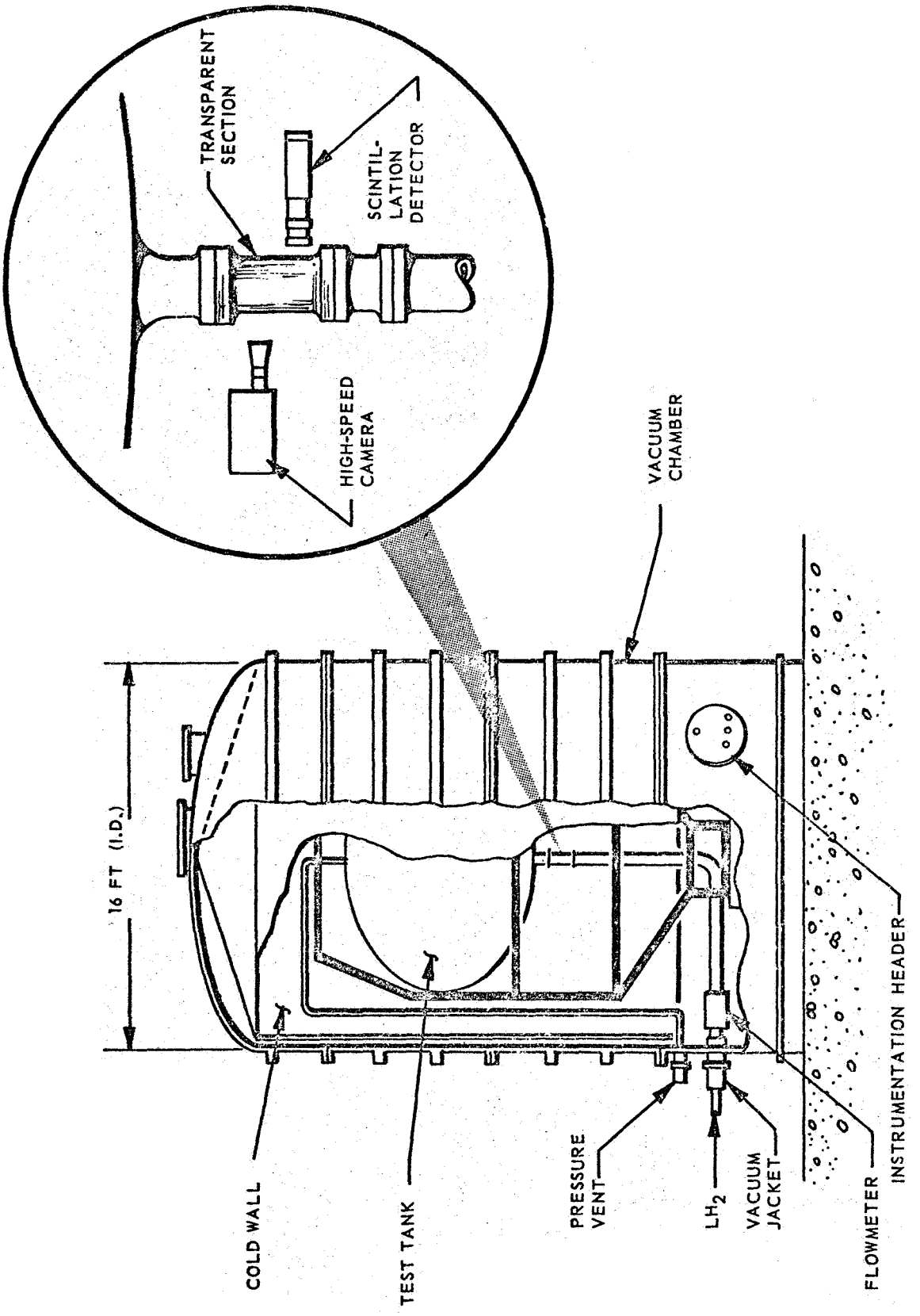


Fig. 93 Large-Scale Test Setup

and the vacuum chamber wall; a detailed drawing of the transfer line is shown in Fig. 94 and a photograph of the test tank in Fig. 95 . Although installation of the test tank in a vacuum chamber was not required for these tests, there was available a test chamber at the test base in which a great variety of instrumentation had already been installed. As indicated in Figs. 94 and 97, transfer line section installed between the chamber wall and the test tank was very heavily instrumented. Wall temperature thermocouples were located at ten stations along the line, fluid temperature thermocouples at three stations along the line, static pressure taps at six stations, and pitot tube rakes at three stations. In addition, to these pressure and temperature sensors, a transparent section (made of Pyrex glass) was installed just below the tank inlet. This section was also vacuum jacketed with a large (six-inch diameter) section of glass pipe. High-speed movies of the flow were taken through a flat glass plate mounted in a tee-section welded to the six-inch glass pipe. Below the transparent flow-visualization section the void-fraction measurement system was installed. In order to obtain the required sensitivity with this system, it was necessary to install a short, thin-walled aluminum section at the line similar to that installed in the half-inch line described earlier. The upstream end of the line was coupled to a pneumatically-actuated valve known as a Hadley valve; on the upstream side of the valve a three-inch Potter turbine-type flowmeter was installed. Upstream of the flowmeter the line was connected through a bayonet-type connection to a 280-foot long, vacuum-jacketed transfer line to a 13,000 gallon capacity storage dewar. A photograph of the line and tank installed in the test chamber is shown in Fig. 98.

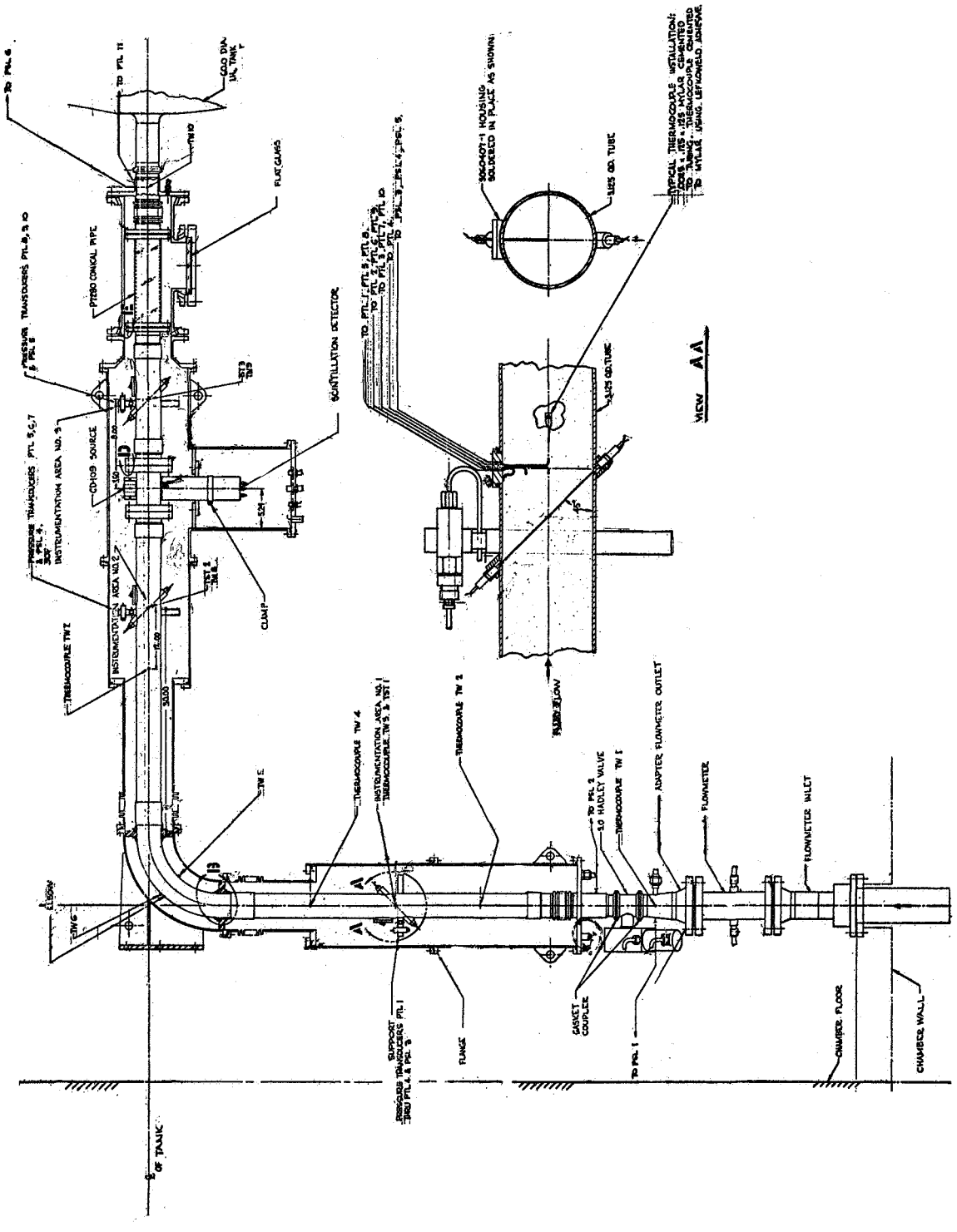


Fig. 94 Transfer Line Instrumentation - Large Size Apparatus

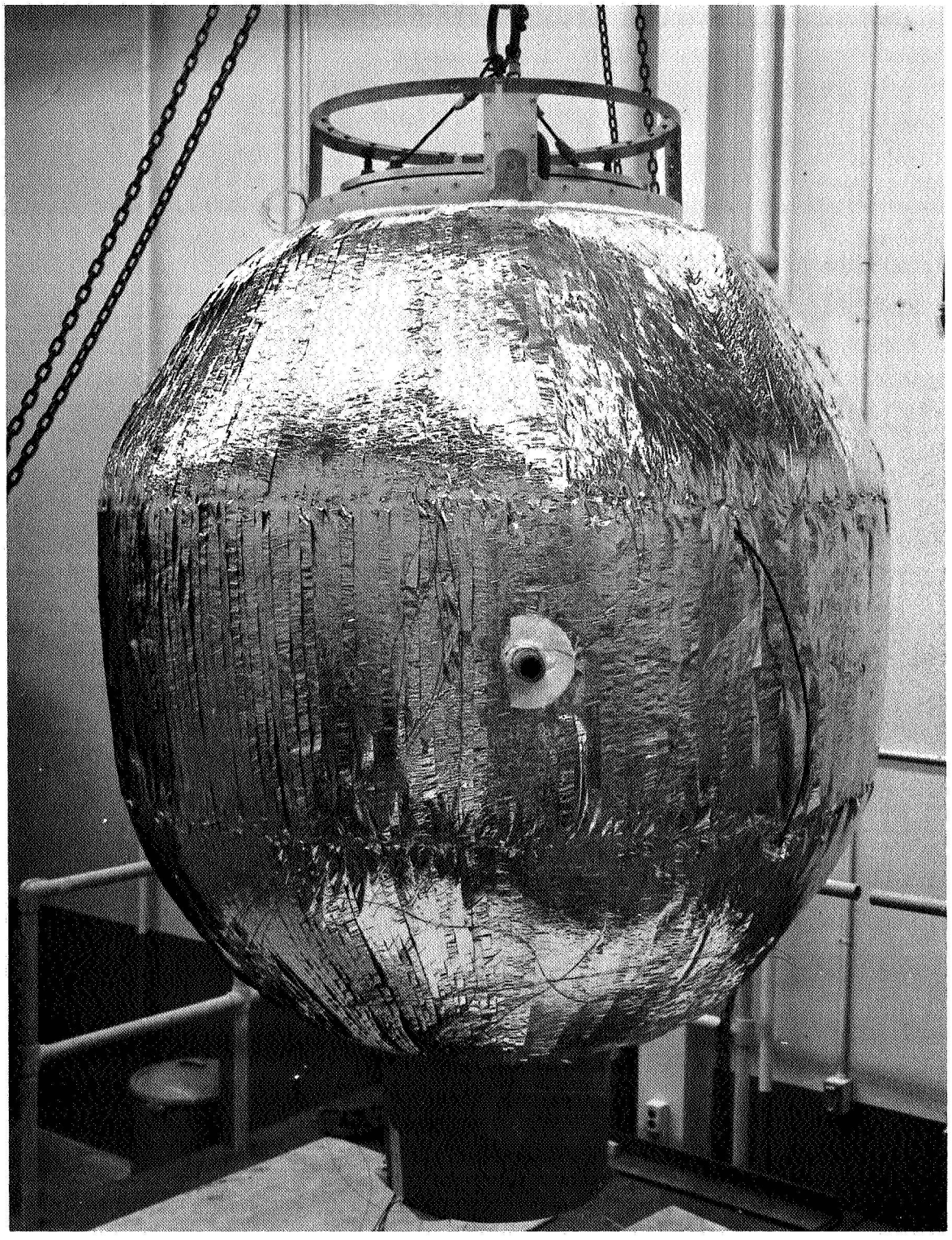


Fig. 95 Five Foot Diameter Tank Prior to Installation in Test Chamber

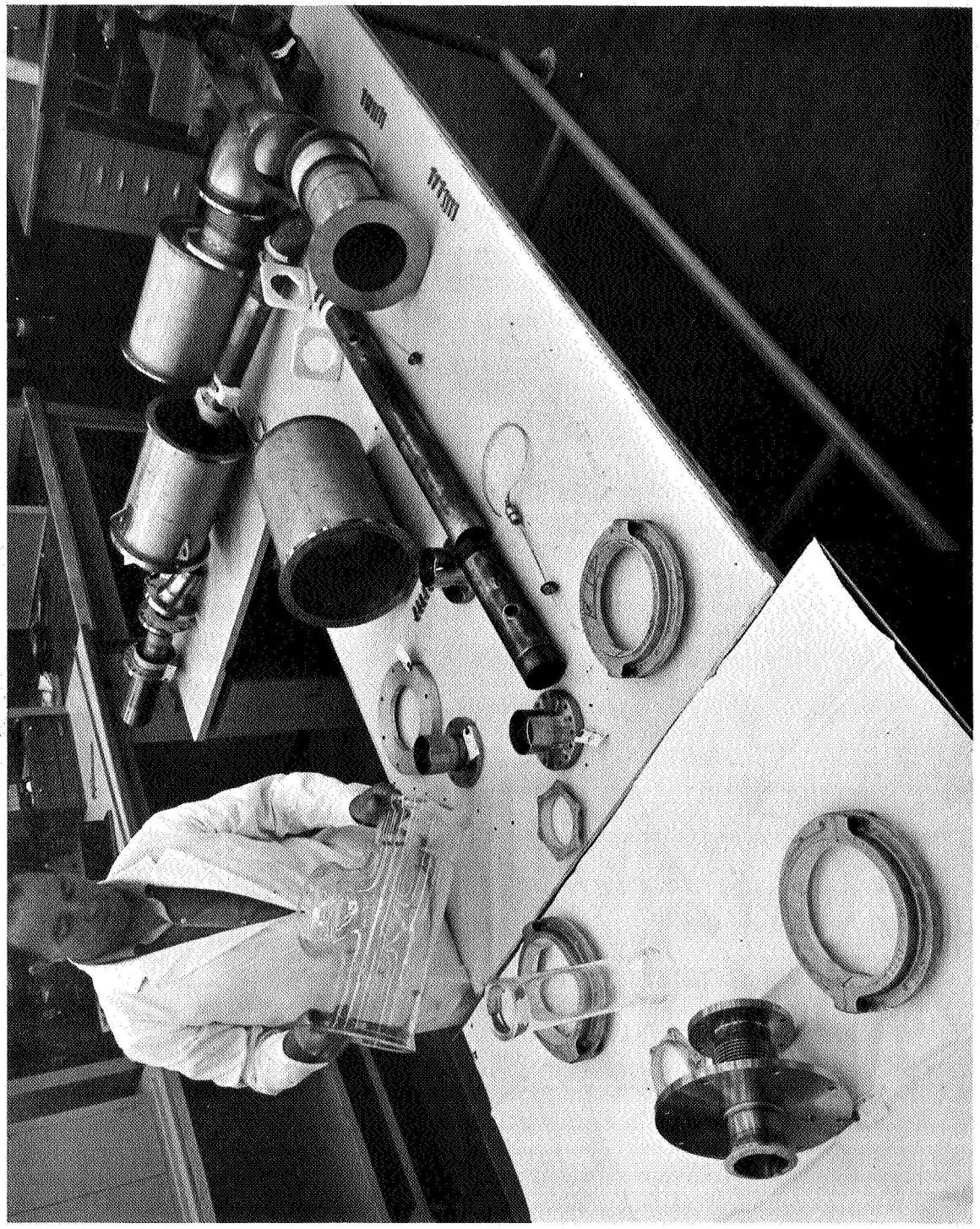


Fig. 96 - Assembly of Three-inch Transfer Line

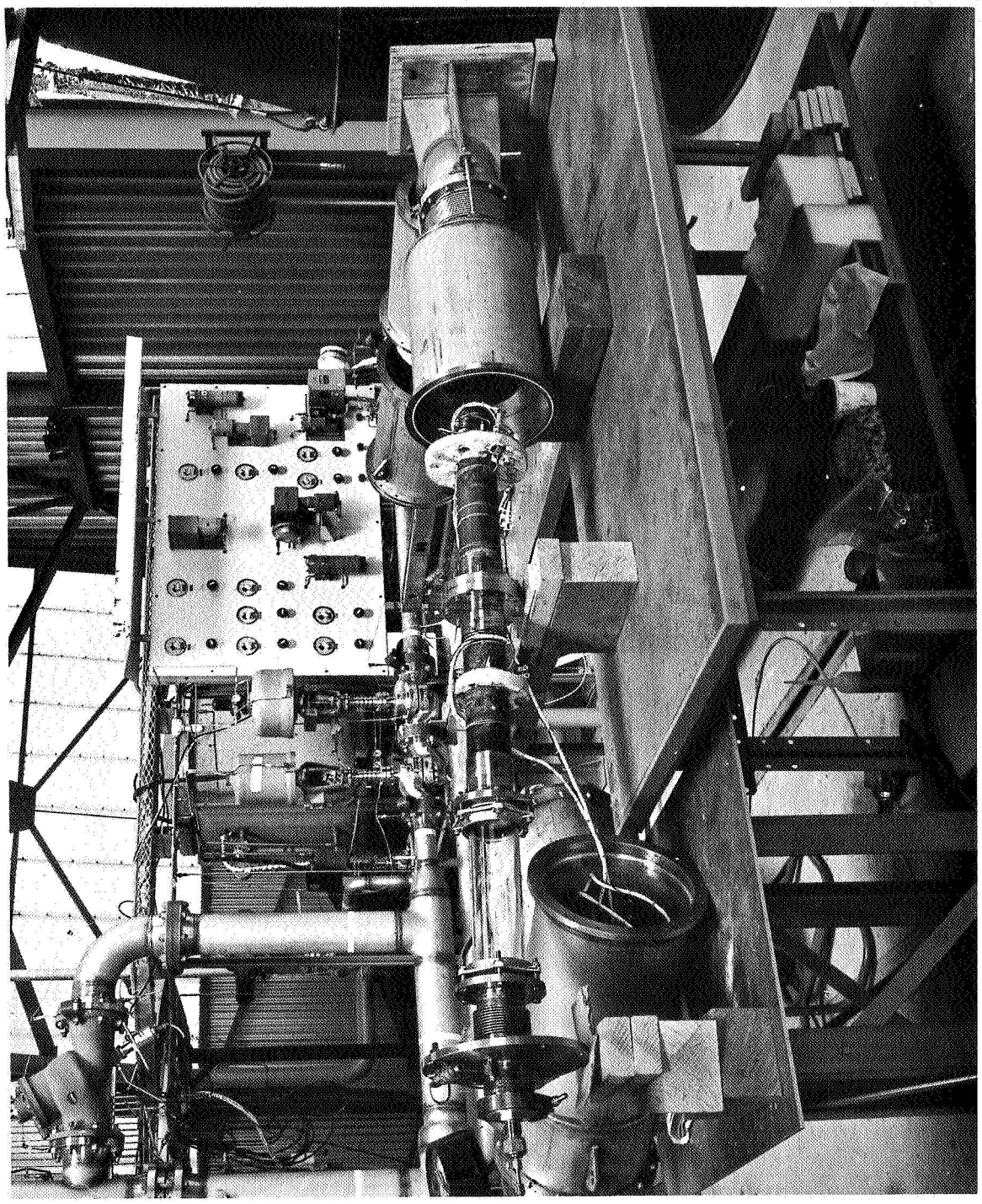


Fig. 97 - Leak Check of Three-inch Transfer Line

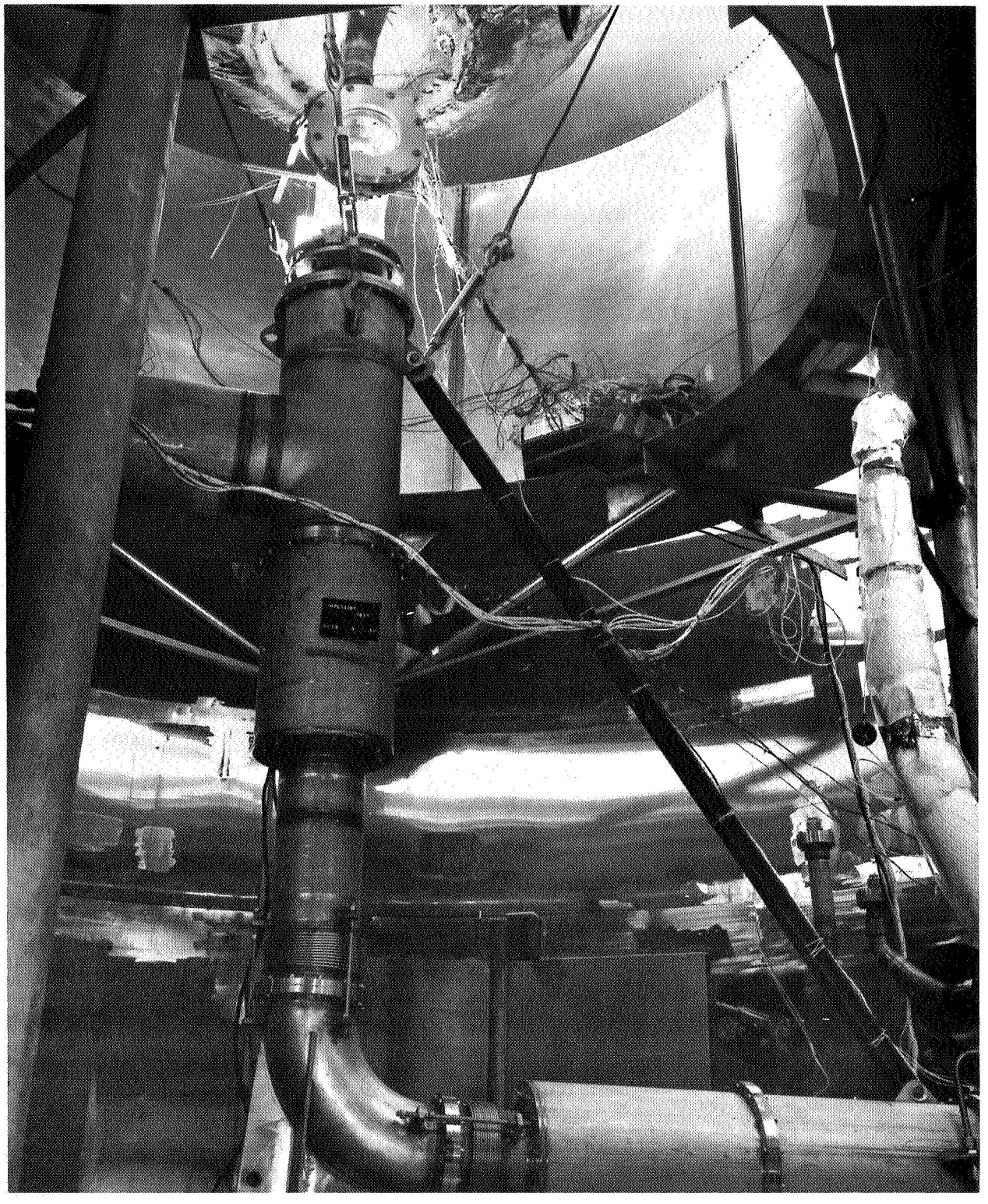


Fig. 98 - Test Apparatus for Complete Fill System Tests - Large Size Apparatus.

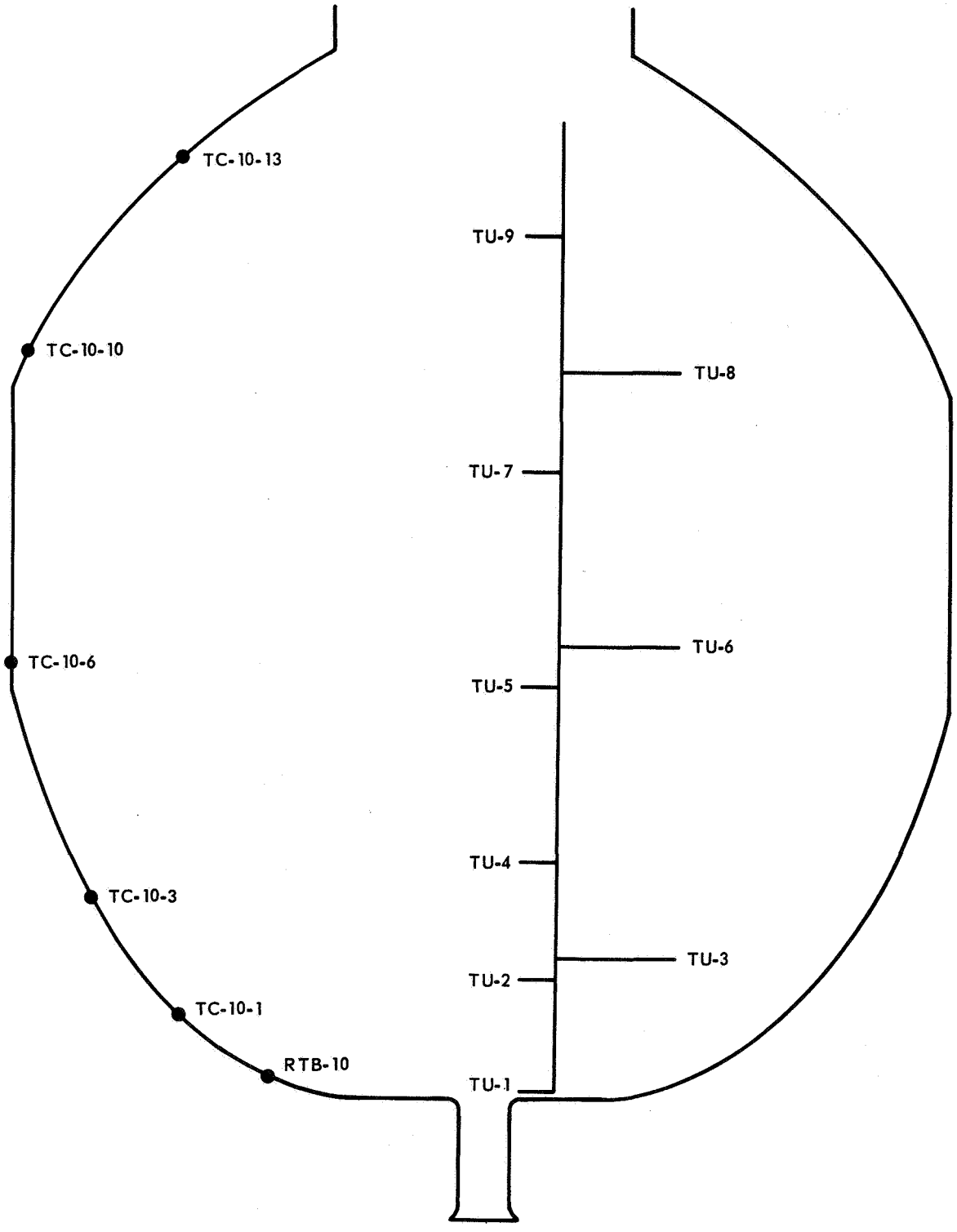


Fig. 99 Instrumentation Location-Five Foot Dia. Tank

The five-foot tank was instrumented with two ullage pressure sensors, several wall-temperature thermocouples, and an ullage temperature probe containing six thermocouples positioned along the central axis of the tank and three off-center thermocouples. The thermocouple instrumentation for this tank is shown schematically in Fig. 99 . All thermocouples used in both the tank and transfer line were chromel-constantan, except for those on the tank wall, which were copper-constantan.

A total of 27 fill tests were run, using the apparatus described above; eleven tests with nitrogen and sixteen tests with hydrogen. The complete log of all tests run is shown in Table 7 . A total of eight tests were run with a clear inlet region; i.e., with neither a baffle nor a screen over the tank inlet. These tests are described in this Section, while the test results with a baffle and screen are described in Section 10.

Each fill test began by chilling down the 280 foot line from the storage dewar to the test chamber wall by bleeding the test fluid out through the bleed port located just upstream of the Hadley valve. When there was a solid column of liquid filling this line, the test was begun by opening the Hadley valve and allowing the test fluid to flow down the instrumented section of line and into the tank. The flow length along the instrumented line was 13.9 feet, and the inside diameter of the line was 2.945 inches. During each test the transfer line wall temperature, fluid temperature, static pressure distribution, liquid volume fraction and fluid velocity were recorded.

TABLE 7

SUMMARY OF LARGE-SIZE TESTS

Run No	Test Fluid	Inlet Condition	Dewar Pressure (psia)	Initial Tank Pressure (psia)	Dewar Flow-Valve Setting (% Open)	Camera Coverage
9-8-1	LN_2	Clear	28.05	20.65	13.6	yes
9-8-2	LN_2	↓	50.0	18.8	9.3	yes
9-8-3	LN_2	↓	47.6	18.35	38.2	yes
9-8-4	LN_2	↓	33.6	21.0	9.0	yes
9-11-1	LN_2	Screen	22.2	17.4	13.2	yes
9-11-2	↓	↓	23.8	18.7	13.0	yes
9-11-3	↓	↓	23.0	16.5	13.0	yes
9-11-4	↓	↓	22.7	19.2	11.5	no
9-13-1	LH_2	Screen	24.8	16.6	15.2	no
9-13-2	↓	↓	25.2	16.55	94.5	no
9-13-3	↓	↓	26.4	16.6	95.0	no
9-14-1	↓	↓	19.7	18.0	94.0	yes
9-14-2	↓	↓	19.4	14.65	95.0	no
9-14-3	↓	↓	27.2	16.8	100.0	no *
9-14-4	↓	↓	27.9	16.8	50.3	no
9-15-1	LH_2	Baffle	34.4	18.1	29.3	yes
9-15-2	↓	↓	35.4	17.1	4.0	yes
9-15-3	↓	↓	37.5	14.35	6.0	no
9-15-4	↓	↓	46.8	14.8	1.0	yes
9-15-5	↓	↓	48.1	15.8	1.0	no
9-15-6	↓	Clear	39.8	19.2	100.0	yes
9-15-7	↓	↓	45.2	15.3	78.4	no *
9-15-8	↓	↓	50.8	14.3	4.0	yes
9-15-9	↓	↓	49.9	17.4	17.5	no *
9-20-1	LN_2	Baffle	34.9	20.3	15.0	yes
9-20-2	↓	↓	44.5	15.7	15.5	no
9-20-3	↓	↓	33.8	16.3	99.2	no *

*Film coverage camera jammed.

After the initial series of tests, it was found that the output from several of the differential pressure transducers (attached to the pitot tubes) was much lower than expected. This was later found to be due primarily to contamination and clogging of the small-diameter pitot tubes (0.020 inches inside diameter), although the transducers themselves had malfunctioned at some locations. Consequently, no attempt was made to reduce or interpret the bulk of the data from these sources.

The tank wall temperature and ullage pressure distribution, as well as the ullage pressure, were recorded during each test. As indicated in Table 7, a total of four successful tests were run with movie coverage for nitrogen as the test fluid and with no obstruction over the tank inlet. Although four similar tests were run with hydrogen, good movie data were obtained on only one test. The movie data (from which fluid velocities were obtained) were combined with the void fraction data to give fluid vapor quality at the tank inlet as a function of time, as explained in the next section.

9.2 CORRELATION OF DATA FOR COUPLED LINE AND TANK TESTS

9.2.1 Correlation of Data with Receiver Tank Analysis

Data from tests with nitrogen and hydrogen in the sixty-inch tank were obtained with a clear inlet line and with a baffle or screen over the inlet. The tests for which the data are to be compared with results from the receiver tank analysis are listed in Table 8. There are four nitrogen runs with a clear line, two with a screen and one with a baffle. There is one clear line hydrogen run and two hydrogen baffle runs. Sufficient data were not obtained during the hydrogen screen runs to obtain an analytical prediction for this case.

Data required by the analysis are initial pressure and temperatures and flow rate and quality at the inlet as functions of time. Quality is computed using the output of the void fraction meter and the properties of the fluid. The mass flow rate at the inlet is computed using the gas velocity which is obtained from the films along with the quality data. (The gas velocity is assumed to be equal to that of the droplets since only droplet velocities can be obtained from the films). Once these quantities are known, the receiver tank analysis can be used to compute the pressure and temperatures within the tank. For the clear line and screen cases a characteristic droplet diameter, D_D^* (defined as the droplet diameter at the peak of the droplet histogram) must be specified as discussed earlier.

TABLE 8

SUMMARY OF 60-INCH TANK TESTS

RUN NUMBER	FLUID	INLET CONDITION
9-8-1	Nitrogen	Clear
9-8-2	Nitrogen	Clear
9-8-3	Nitrogen	Clear
9-8-4	Nitrogen	Clear
9-11-1	Nitrogen	Screen
9-11-2	Nitrogen	Screen
9-15-1	Hydrogen	Baffle
9-15-6	Hydrogen	Clear
9-20-3	Nitrogen	Baffle
9-15-4	Hydrogen	Baffle

Pressure data for the first nitrogen clear line run are compared with analytical predictions in Fig. 100. The duration for which predictions are shown is limited by the availability of velocity data. Velocities could only be read from the films until the flow was obscured by mixing and flow reversals. As before, these results show that the characteristic droplet diameter has a large effect on the magnitude of the initial pressure drop which occurs when liquid first enters the tank. However, it has little effect on the subsequent rate of change of the pressure. Regardless of the

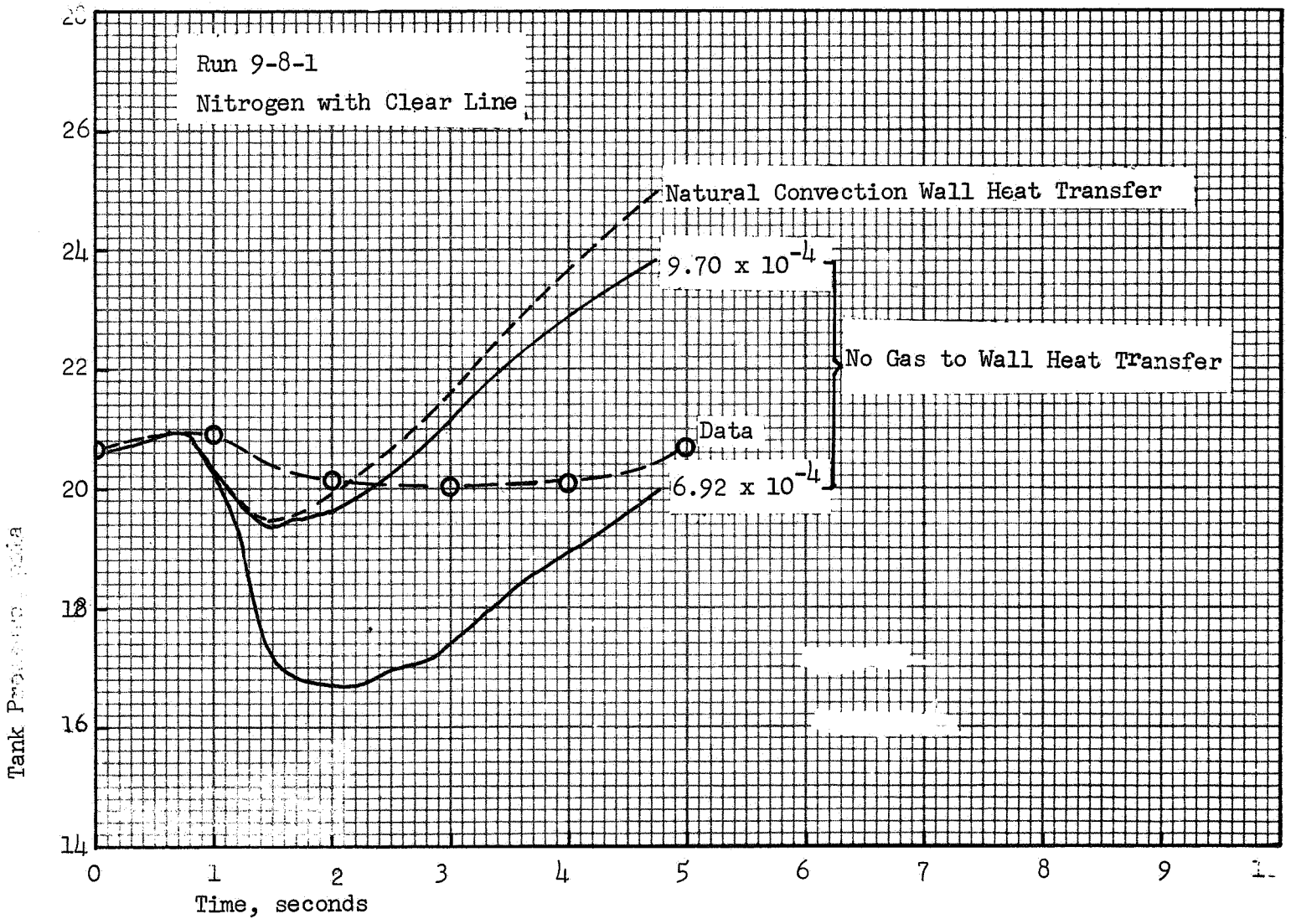


Fig. 100-Comparison of Pressure Data with Predictions

characteristic droplet diameter chosen, the computed pressure drop is much greater than the measured pressure drop. This is because the slope of the analytical curves, which is generally a function of the mass flow rate at the inlet, is much larger than that of the data for most times. It is felt that the measured mass flow rate for this run is about twice as high as the pressure data indicate it should be. It should be pointed out that it is difficult to compute accurate values for quality even when relatively good void fraction data are available. This is because a small change in vapor volume fraction translates into a large change in mass fraction since the vapor density is much less than the liquid density.

The data and predictions for run 9-8-1, however, both exhibit the same typical shape. The pressure rises slightly when the first flow, which is all gas, enters the tank.

Then, when liquid first enters the tank in the form of a droplet spray, evaporation occurs and energy is extracted from the vapor in the tank and the pressure drops. As the vapor cools, the effect of mass addition to the tank becomes dominant and the pressure again rises.

Prediction curves are shown on Fig. 1 for the cases of no heat transfer between the tank wall and the vapor and natural convection wall heat transfer. When energy addition from the tank wall is considered the pressure, of course, is higher. The effect of heat transfer from the wall to the gas becomes more significant at later times because the gas temperature decreases with time whereas the wall temperature remains relatively constant. The wall temperature

data for the clear line and screen runs, however, indicate that there was negligible gas-to-wall heat transfer; this is illustrated in Fig.101 where the wall temperature for Run 9-8-1 is shown to be unchanged for the duration of interest. The vapor in the tank was not uniformly mixed as assumed in the analysis; there probably was a warm layer of gas near the tank wall which served to insulate the wall from the cold gas and retard gas-to-wall heat transfer. For this reason, all subsequent analytical curves assume there is no heat transfer between the vapor and the tank wall.

The measured pressure history for Run 9-8-2 is compared with analytical predictions in Fig.102. Much better agreement between data and analysis is obtained for this run. It appears that the data are shifted on the time scale with respect to the analytical curves by about 0.5 seconds. Some difficulties were encountered in correlating the initial time between the Hadley valve opening, the strip charts and the movie films. During the nitrogen runs a flash bulb was used to signal the start of testing on the films. The test operator attempted to push the buttons activating the Hadley valve and the flash bulb simultaneously. This is one possible source of error. The first appearance of droplets on the films followed the first indication of liquid by the void fraction meter by about one second in most cases. It could be concluded that the first droplets, which are usually very small, could not be resolved by the film reader. The sharp drop in quality measured by the void fraction meter, once liquid starts to be detected, implies that observable droplets should be seen on the film within a small fraction of a second after the meter detects liquid. For this reason

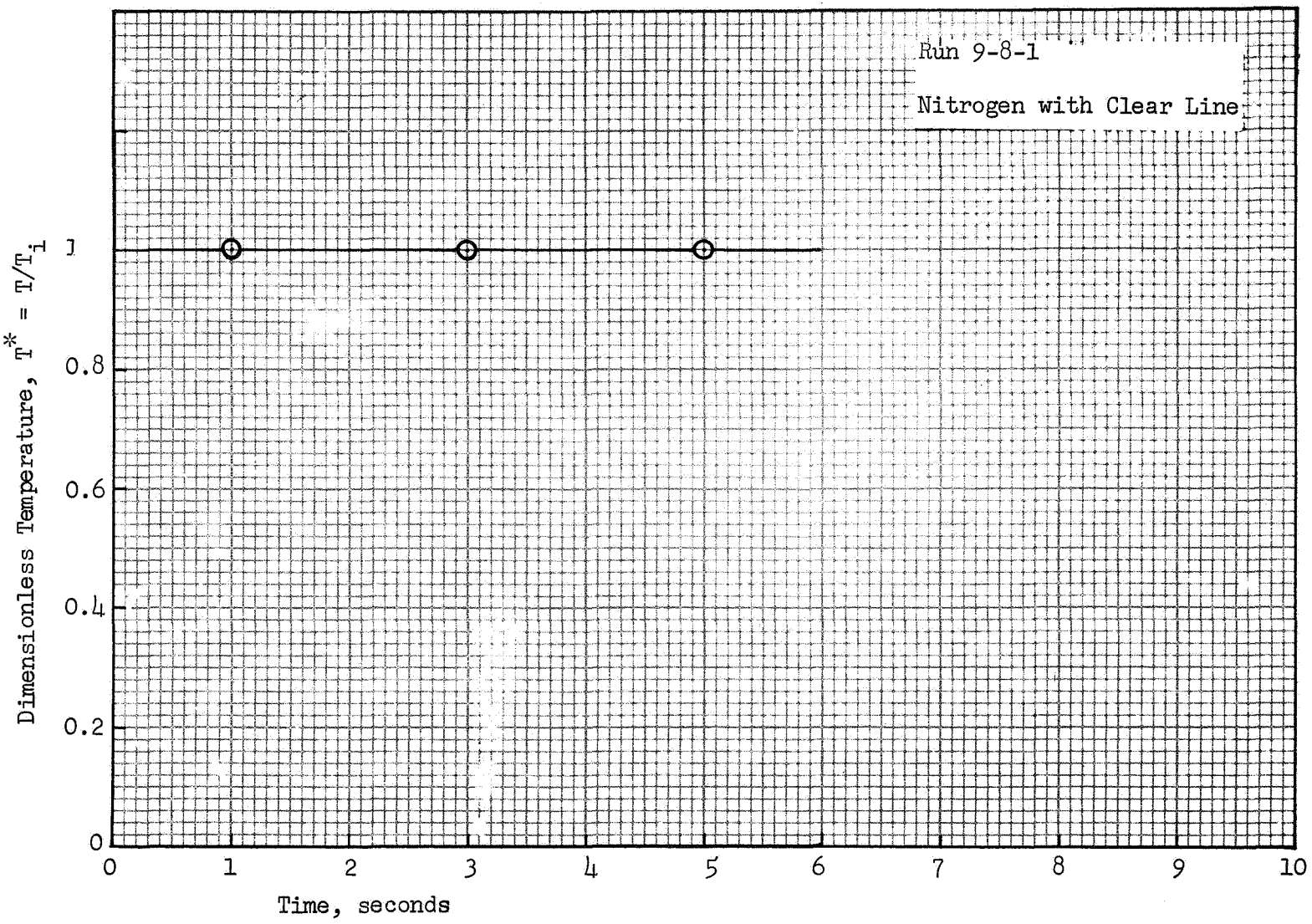


Fig.101- Tank Wall Temperature Data

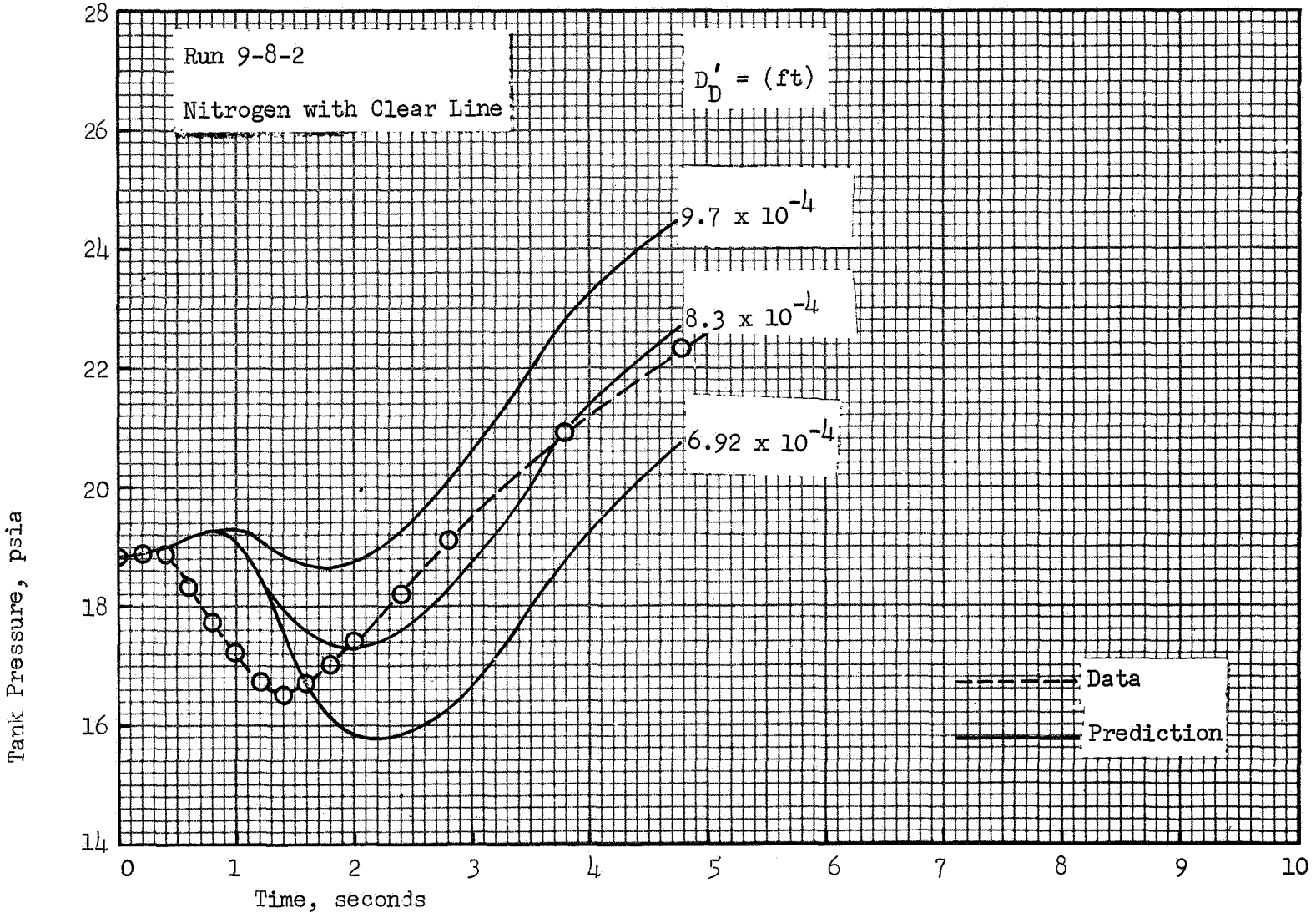


Fig. 102- Comparison of Pressure Data with Predictions

it is considered likely that the time scales for the various forms of data are not correlated with sufficient accuracy.

With this in mind a comparison of the data shown in Fig.102 with the predictions for D_D' values of 8.3 and 6.92 x 10^{-4} ft. indicates that a D_D' value somewhere between the two would give an analytical curve which nearly coincides with the data. It is of interest to compare the D_D' value which gives a good correlation of the 60-inch tank data with that which correlated the 24-inch tank data. Values for D_D' of about 1.5 or 2 x 10^{-4} ft. were used for the 24-inch tank predictions indicating that, everything else being held constant, the D_D' value is roughly proportional to tank diameter. The transfer line geometry and flow conditions also influence the droplet cloud configuration so that it is difficult to obatin an accurate prediction for D_D'.

The data for Run 9-8-3 are compared with the analytical pressure in Fig. 103. It is felt that inaccuracies in the mass flow rate input to the analysis are again the cause of the discrepancy between the data and the predicted curve.

A single prediction curve is shown on Fig.103 because smaller or larger droplet diameters produce predicted pressures for this run which are higher than this curve. This run is peculiar in that droplets are being accumulated in the vapor and on the wall (in the analysis) since the computed total rate of evaporation is less than the rate at which liquid is being added to the tank. When all the incoming liquid is being evaporated (as in most of the other cases) the analysis computes the rate of evaporation of droplets in the vapor and subtracts it from the rate at which liquid enters the tank to obtain the rate of evaporation on the wall. Under such conditions smaller droplet diameters

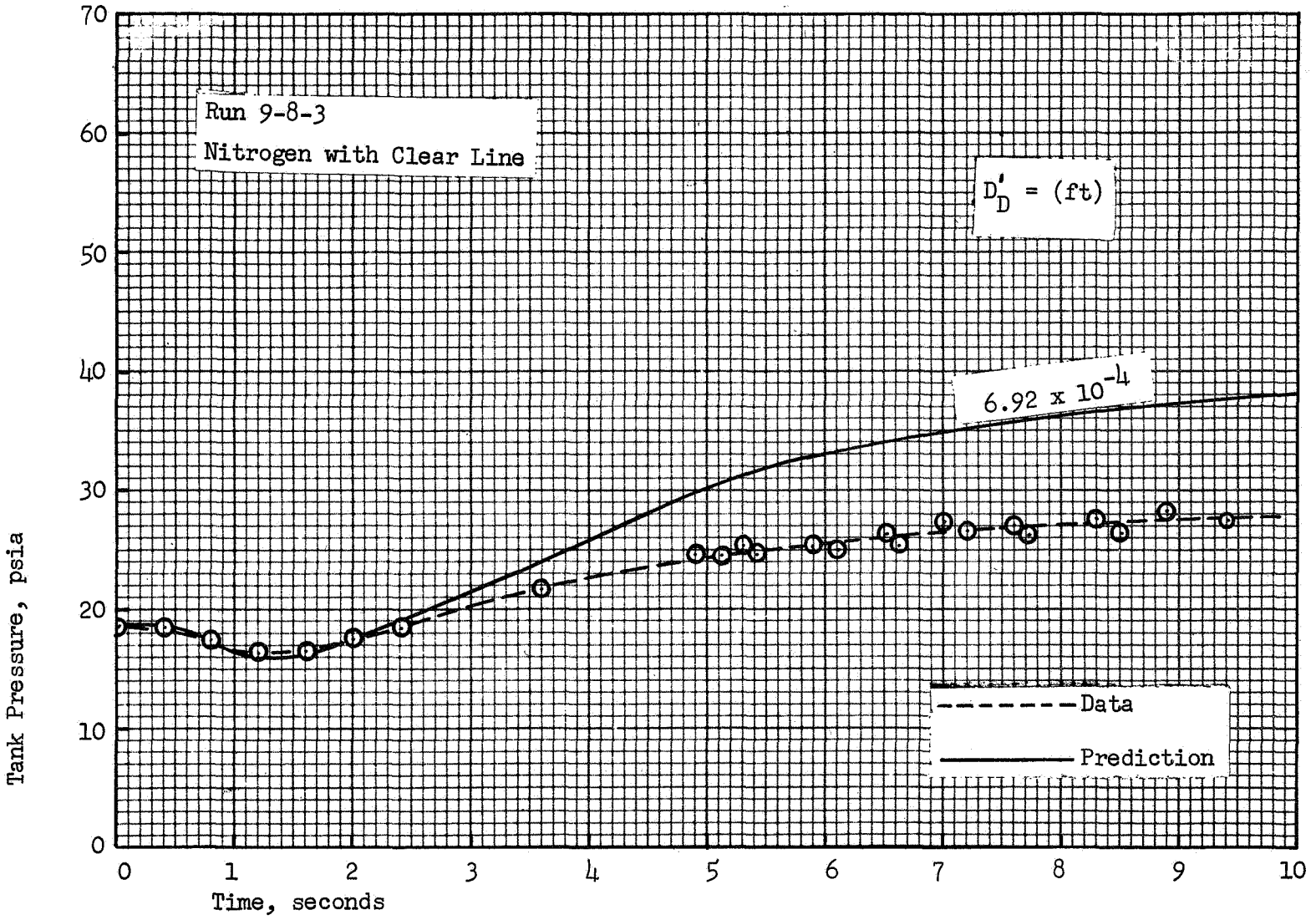


Fig.103 Comparison of Pressure Data with Prediction

always produce lower pressures since they evaporate in the vapor at a greater rate. When droplets are accumulated in the tank the rates of evaporation from the vapor and wall are computed independently. In this case the rate of evaporation from the wall increases faster with decreasing D_D' than the rate of evaporation in the vapor. Since the wall evaporation component of vapor addition to the ullage tends to cause a pressure rise the pressure will increase with decreasing D_D' .

The ullage gas temperatures measured on the centerline of the tank are compared with appropriate analytical gas temperatures in Fig. 104. The analytical jet temperature is near the saturation temperature throughout the run. A predicted value for the top region temperature is shown only for times after about 5 seconds since the jet impinges on the tank wall and there is no top region at earlier times. This figure illustrates the general agreement found between the analytical and measured temperatures.

Predictions for the last clear line nitrogen run are compared with the pressure data in Fig. 105. Droplet velocity data could only be obtained for about three seconds so the predicted pressure curves are relatively short. There is, however, good agreement with the data during this initial time for a value of D_D' somewhat greater than 8.3×10^{-4} ft. There may be some inaccuracy in the initial time correlation for this run as discussed for Run 9-8-2 since the data indicate a pressure drop about 0.5 seconds before the analytical pressure drop.

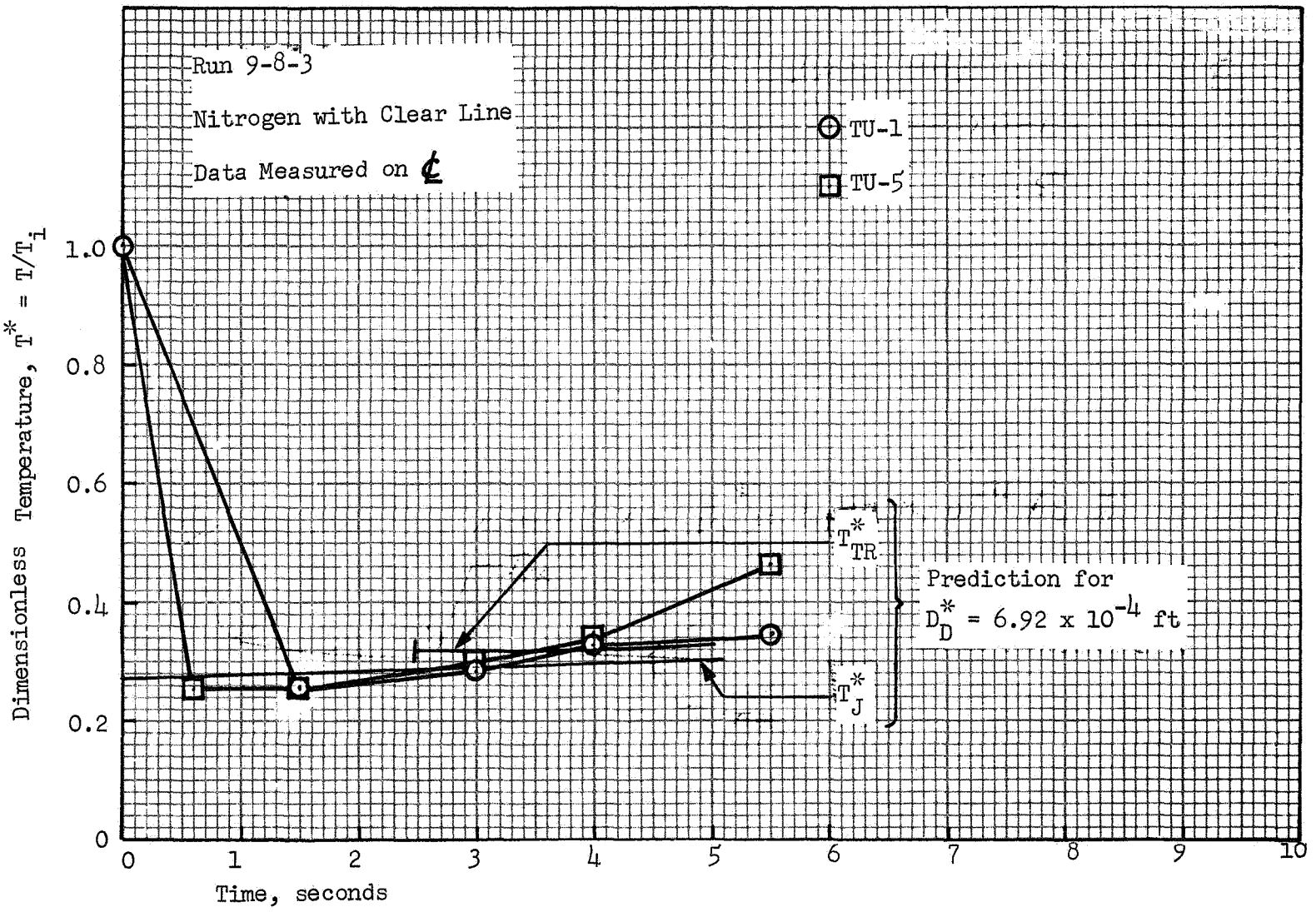


Fig.104-Comparison of Gas Temperature Data with Predictions

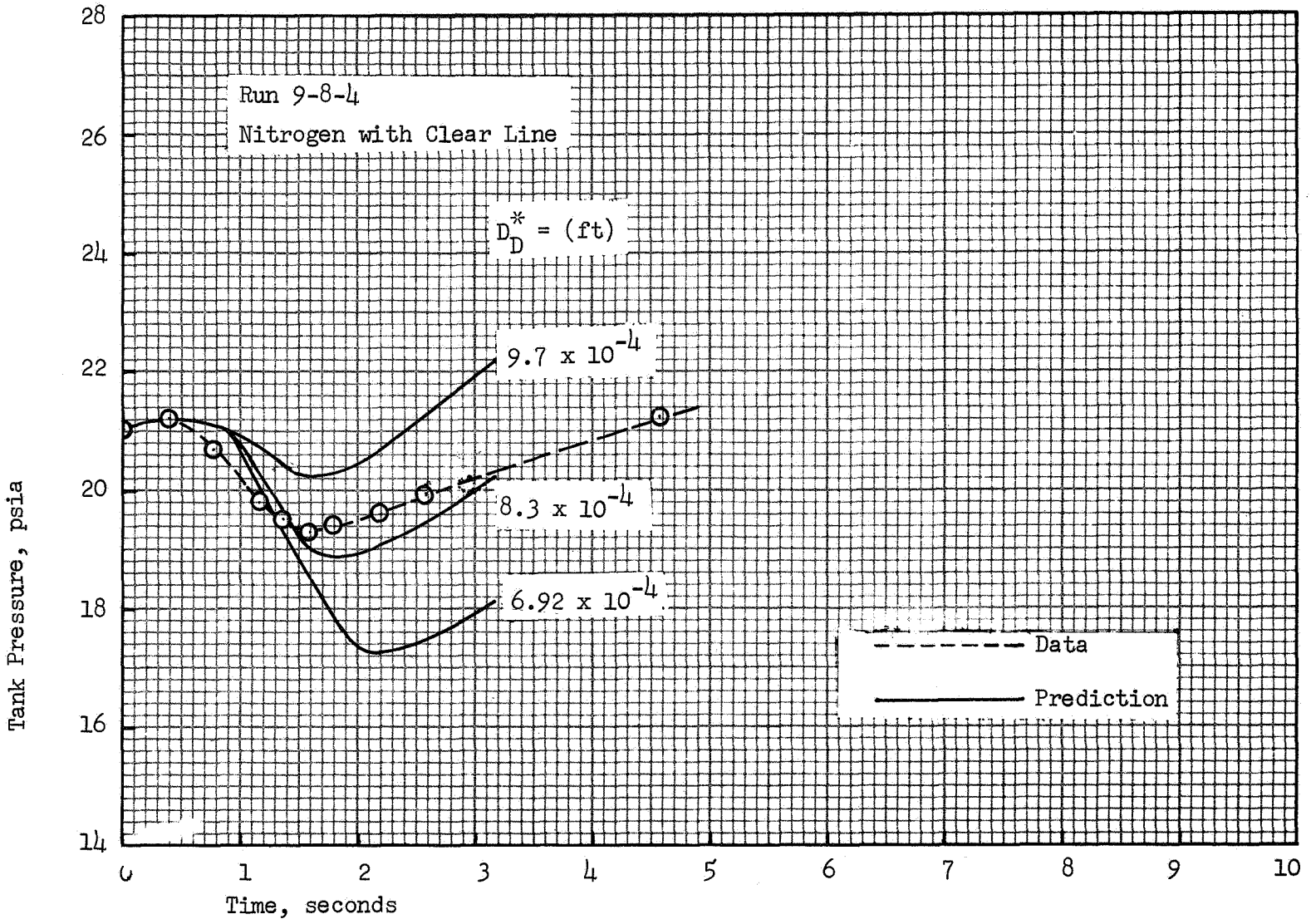


Fig. 105 - Comparison of Pressure Data with Prediction

The pressure data for a hydrogen run with a clear inlet are shown in Fig. 106. For safety seasons, a flash bulb could not be used to mark the beginning of the tests on the movie films so the droplet velocity data must be correlated with respect to time with the other data using some other means. This was done by assuming that the first observable droplets on the films occurred when liquid was first detected by the void fraction meter. This method of time correlation is subject to question since, for the nitrogen runs, it was shown that these events could be displaced in time by as much as one second.

In general the hydrogen data show sharp initial pressure rises in contrast to the nitrogen data. This implies that, in the case of hydrogen, the initial gas velocities are quite high. Since velocity data can only be obtained from the films when liquid can be observed (droplet velocities are actually measured and assumed equal to the gas velocity) there is usually no gas velocity data during the initial part of the tests. The velocity data for Run 9-15-6 are shown in Fig.107 along with three possible extrapolations for early times. These extrapolations are used to show the influence of this parameter on the predicted tank pressure in Fig.106 where the corresponding analytical pressure curves are plotted. It appears that a velocity history even higher than extrapolation number three should be used if the prediction is to agree with the data. In addition to this problem, the void fraction data for the hydrogen runs was very difficult to read and interpret. The sensitivity of the void fraction meter is reduced when hydrogen is used and the void fractions that were obtained in these tests were very close to 1.0 (all gas). The high void fractions resulted from the excessive heat

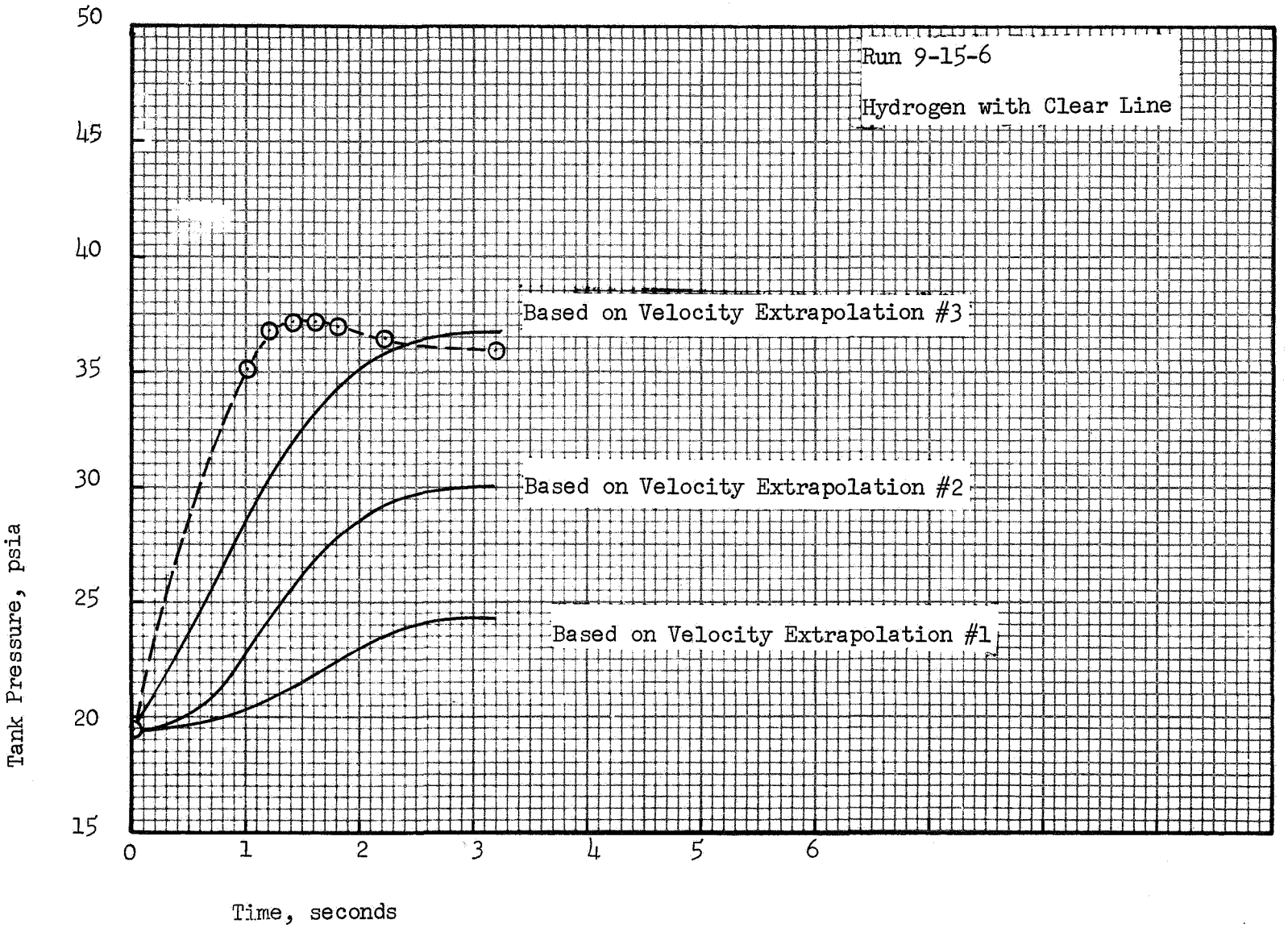


Fig. 106 -Comparison of Pressure Data with Predictions

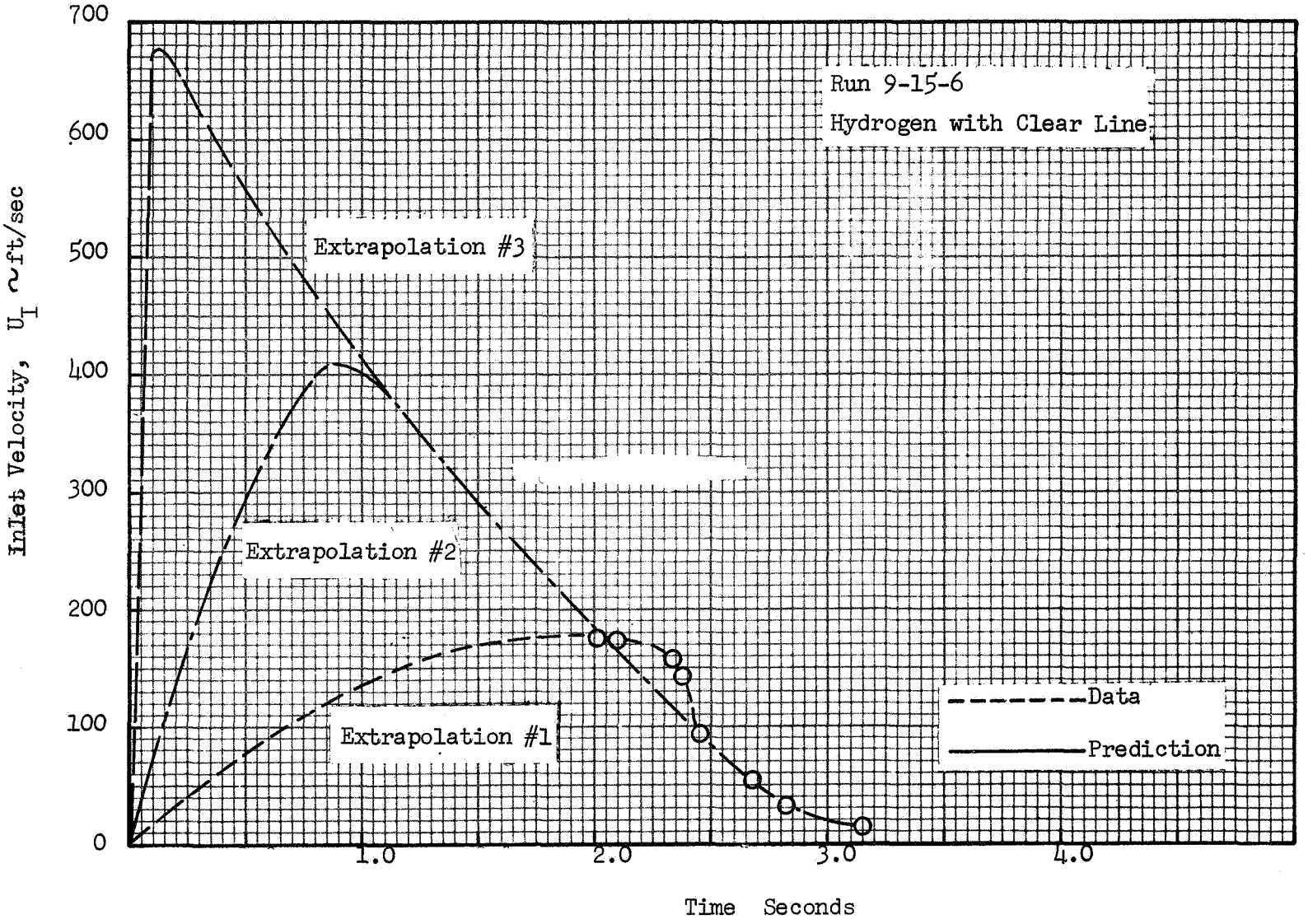


Fig. 107 - Gas Velocity Extrapolations

transfer to the hydrogen in the transfer line. These factors, combined with the magnification of error which accompanies translation of void fraction data into quality or mass fraction, make it necessary to treat the hydrogen quality data as a gross approximation.

The analysis of the hydrogen clear line data indicates that for a reasonable range of droplet diameters, all of the droplets evaporate in the ullage vapor and none survive to evaporate on the tank wall. For this reason the prediction curves in Fig. 106 are not identified with respect to droplet diameter since all reasonable diameters give the same analytical results.

9.2.2 Selection of Characteristic Droplet Diameter

Upon completion of computer analyses for the correlation of tank fill data, the value of the characteristic droplet diameter (D'_D) which would best correlate the data for each run was interpolated from the graphical comparisons of the pressure-time curves. This value of droplet diameter was denoted $(D'_D)_{optimum}$. It was then postulated that this value of D'_D was a function only of the average mass flowrate at the end of the line, the fluid properties, and the transfer in the form of a dimensionless fill rate based on the transfer line diameter. The values of optimum characteristic droplet diameter are tabulated for the nitrogen tests in Table 9. Also shown are values of the dimensionless fill rate obtained by using an average value of the mass flowrate at the tank inlet; this value is denoted by $\bar{\dot{m}}$.

As shown in Fig. 108, the optimum values of D'_D are well represented by the expression

$$D'_D = 0.0439 \left(\bar{\dot{m}}^*_L \right)^{-0.204} D_L \qquad (1)$$

where $$\bar{\dot{m}}^*_L = \frac{\bar{\dot{m}} C_\ell}{k_\ell D_L}$$

As pointed out in Section 10, the inlet screens used in these tests produced little effective reduction in droplet diameter. This is illustrated in Fig. 108 by the degree to which the four data points for the screen tests are correlated by Eq. (1).

It should be pointed out that this correlation is based only on test data for nitrogen, due to a lack of sufficient data to demonstrate a

Table 9

OPTIMUM VALUES OF CHARACTERISTIC DROPLET DIAMETER

Run No.	Inlet Condition	$(D'_D)_{optimum}$, ft	$\dot{\bar{m}}_L = \frac{\dot{\bar{m}} C_\ell}{k_\ell D_L}$ *
9- 8-2	Unobstructed	7.6×10^{-4}	3.06×10^5
9- 8-3	↓	6.9×10^{-4}	9.17×10^5
9- 8-4		8.7×10^{-4}	2.95×10^5
1-18-2		2.0×10^{-4}	1.78×10^4
3-30-1		2.77×10^{-4}	3.16×10^4
3-30-2		1.66×10^{-4}	1.68×10^4
3-30-3		1.66×10^{-4}	1.68×10^4
3-30-4		1.66×10^{-4}	1.68×10^4
3-30-5		2.77×10^{-4}	3.06×10^4
9-11-1	Screen over Inlet	8.3×10^{-4}	2.95×10^5
9-11-2	↓	6.92×10^{-4}	4.07×10^5
4- 4-4		1.38×10^{-4}	1.68×10^4
4- 4-5		1.94×10^{-4}	3.16×10^4

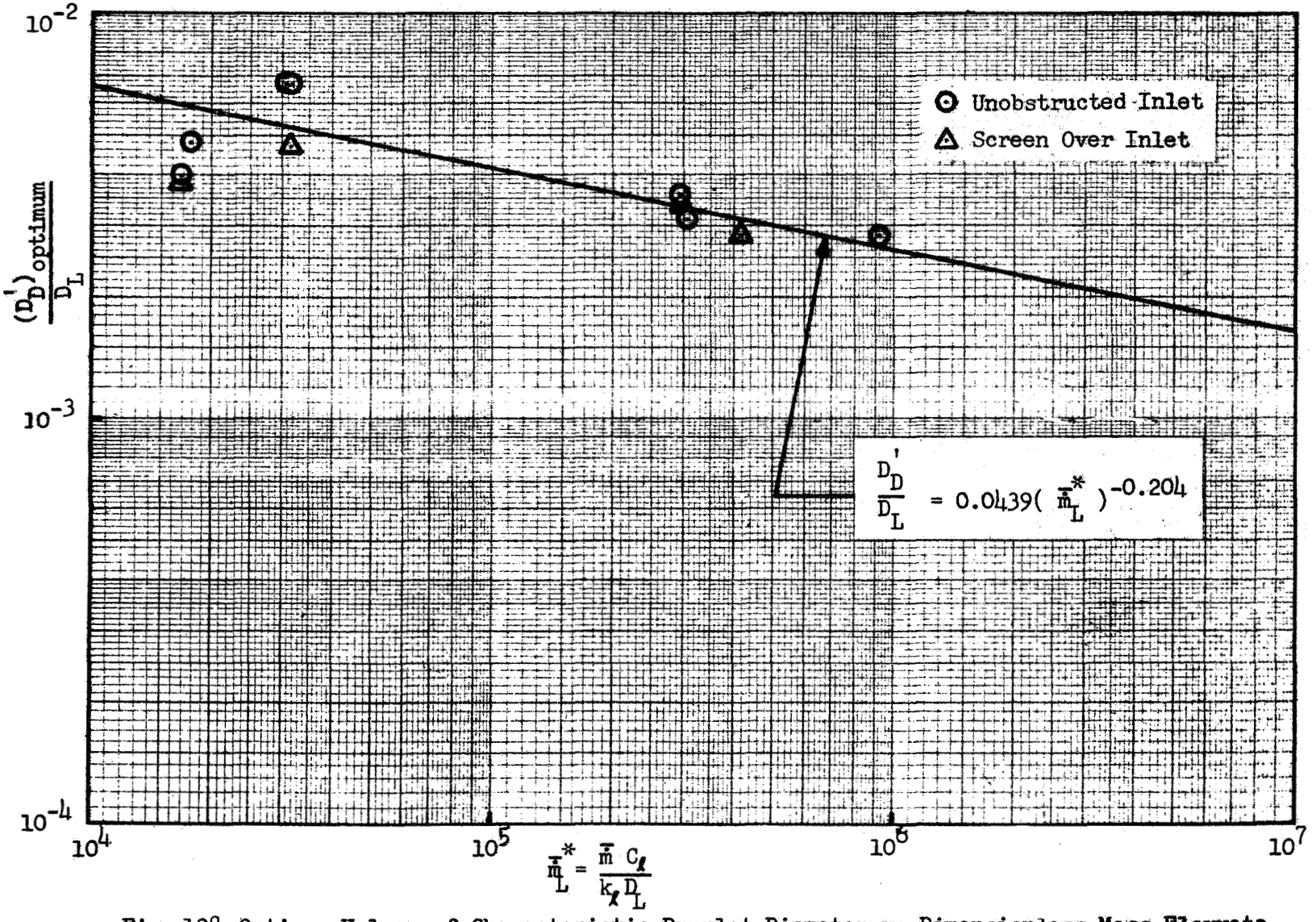


Fig. 108 Optimum Values of Characteristic Droplet Diameter vs Dimensionless Mass Flowrate

similar correlation for hydrogen. However, since fluid properties are accounted for in the calculation of the dimensionless mass flowrate, this correlation is also recommended for prediction of hydrogen droplet diameters.

In view of the close similarity between the properties of nitrogen and oxygen (Section 7), this correlation is, of course, recommended for use in the prediction of oxygen droplet diameters.

9.2.3 Correlation of Data with Complete Fill System (CFS) Computer Program

The CFS model was applied to correlate the data obtained on the coupled transfer line-tank tests using the two-foot and five-foot diameter test tanks. These correlations are described in subsequent paragraphs.

9.2.3.1 Small-Size Apparatus. The input to the CFS model required knowledge of supply pressure, initial pressure and temperature conditions in both line and tank, and all physical characteristics of the system. These data were provided and the pertinent results are presented in Figs. 109 and 110. Figure 109 shows the predicted and measured liquid volume fraction entering the tank. The analysis indicates that the liquid nitrogen vaporized in the transfer line prior to entry into the tank whereas the void fraction meter indicates some two-phase flow.

The measured liquid volume fraction corresponds to an average vapor quality of about 20% over the first two seconds of flow. This relatively high initial vapor quality accounts for the good agreement between the predicted and measured pressure response indicated in Fig. 110. After the first two seconds the measured vapor quality drops to a minimum of about 2%. This is reflected as a drop in the rate of measured pressure rise, as shown in Fig. 110.

Due to the relatively low initial liquid volume fraction (high vapor quality) these results are, in themselves, not sufficient to verify the essential feature of the CFS model, namely the proper prediction

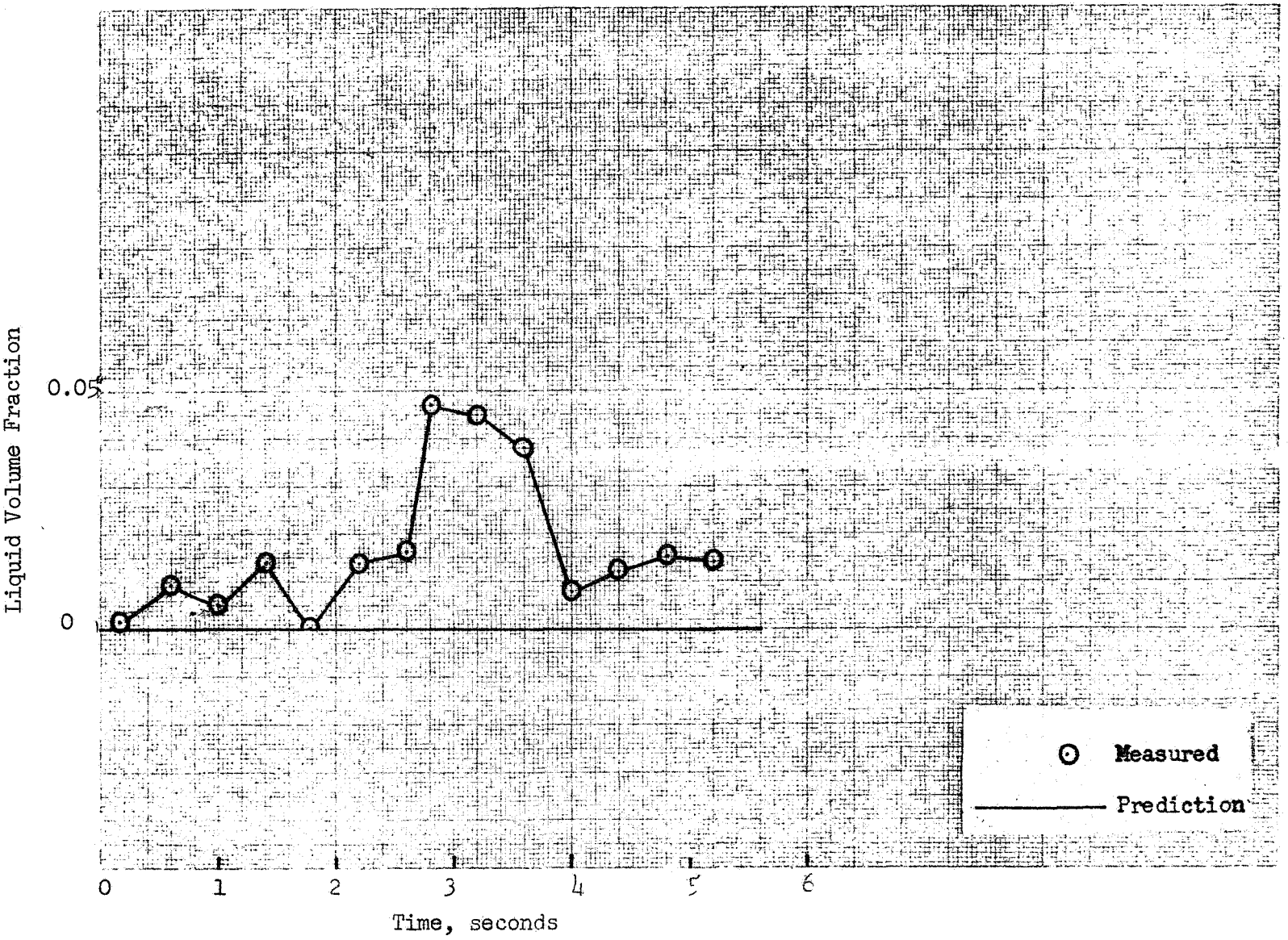


Fig. 109 Liquid Volume Fraction During Fill

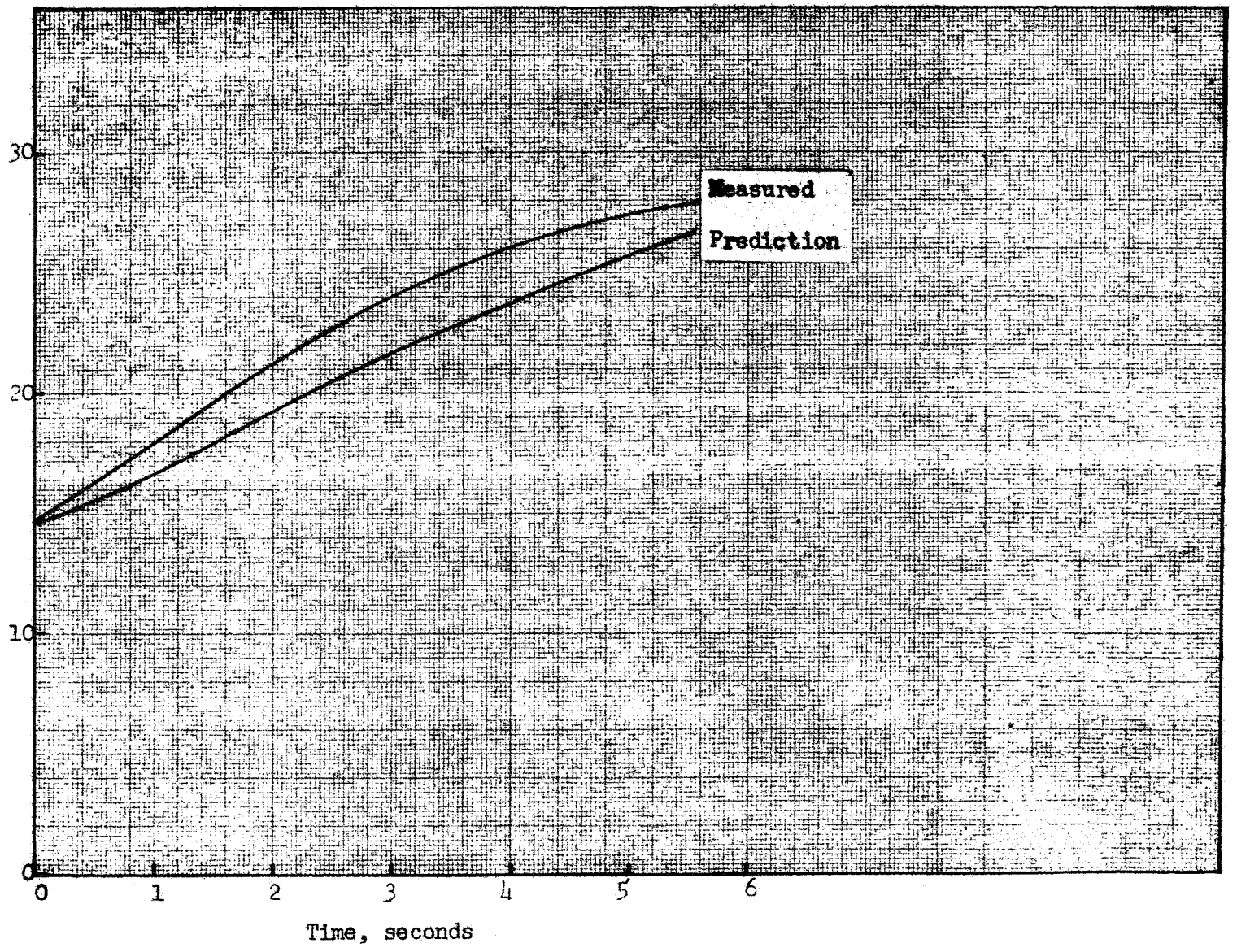


Fig. 110 - Tank Pressure History During Fill

of the interaction between incoming, two-phase fluid and the ullage vapor. This verification is presented in the following section wherein large-size test results are compared with predictions.

9.2.3.2 Large-Size Apparatus

The application of the CFS model to the prediction of phenomena occurring in the large-size test apparatus required essentially the same input data (initial and boundary conditions,etc.) as was needed for simulation of the small-size test. However, due to the large pressure drop across the turbine flowmeter and the line inlet valve(see Fig. 94) the CFS program was altered to allow tabulated values of pressure downstream of an inlet valve to read into the program. The value of this pressure drop was as large as 30 psia for some runs. In all cases, since the inlet fluid was saturated at the supply pressure, the liquid flashed across this inlet pressure drop.

Initial attempts at correlation of the test data showed that the computer model was consistently predicting higher flowrates at the tank inlet in the two-phase flow region. These results suggested that a flow limiting condition was occurring during periods of two-phase flow at the end of the transfer line. Prior to these correlation attempts, choked flow-conditions were accounted for only in the vapor region. This was because choked flow conditions may be accurately predicted in regions of single phase flow. However, prediction techniques available for estimating sonic velocities in two-phase mixtures give widely varying results depending on the flow model assumed. A review of these techniques is

given in Refs. 18 and 19.

As indicated in Ref. 19, apparently the most reliable manner of computing the two-phase sonic velocity is to use the isentropic rate of change of volume with pressure. This function was already available in the FILL program.

Therefore, the two-phase sonic velocity was computed using the relation

$$a = (g_c \gamma p v)^{1/2}$$

where

a = sonic velocity of two-phase mixture

and

$$\gamma = -\frac{v}{p}\left(\frac{dp}{dv}\right)_s$$

is the isentropic exponent relating volume change with pressure for a constant entropy process.

Modifying the computer model to provide such a flow limiting criterion in the two-phase region produced the flowrate variation shown in Fig. 111. The computations indicate that choked two-phase flow existed for a considerable time at the tank inlet.

Fig. 112 shows the accompanying predicted and measured ullage pressures

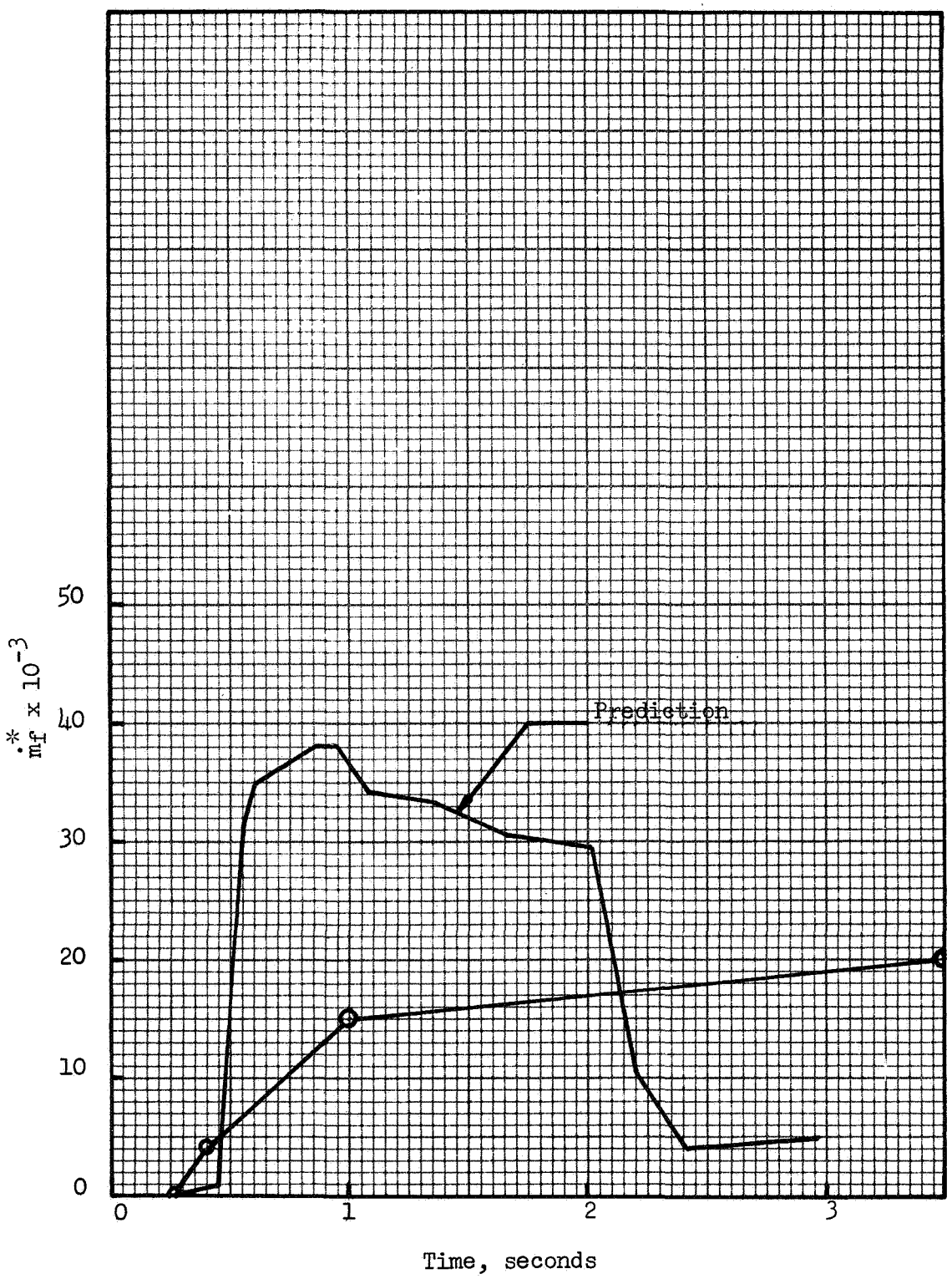


Fig. 111 Predicted and Measured Dimensionless Mass Flowrates for Run 9-8-2

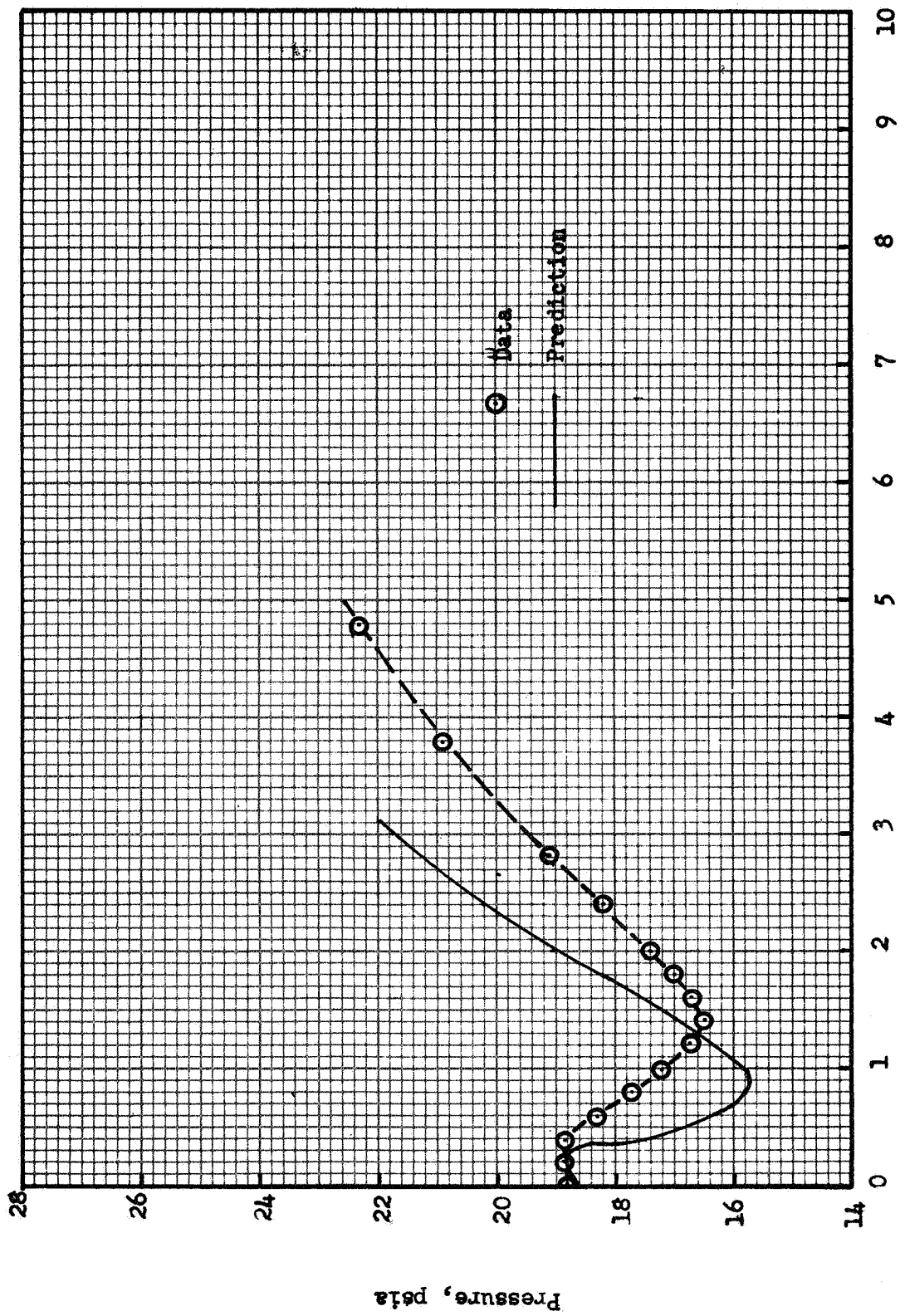


Fig. 112 - Measured and Predicted Ullage Pressure History for Run 9-8-2

for Run 9-8-2. The test fluid for this run was liquid nitrogen. The shape of predicted pressure response and the magnitude of pressure drop are in very good agreement with the measured values. The small pressure rise indicated at the beginning of the run is due to the flow of the warm gas which initially filled the line (prior to $t=0$) into the tank ahead of the inlet fluid. The pressure drop begins when two-phase fluid appears at the tank inlet. The rapid initial drop in computed pressure values occurs because the model overestimates the mass flowrate into the tank at very early times during the fill.

The predicted and measured values of ullage pressure versus time for Run 9-8-4 are shown in Fig. 113. The agreement again is very good, although the CFS model predicts that the pressure minimum occurs about 0.6 seconds too early. This is also attributed to an overestimate of the predicted mass flowrate at early times during fill. The computed rate of pressure rise after the minimum is achieved is again in fairly good agreement with measured data. This result shows that analytical estimates of heat transfer between the cooling ullage vapor and the tank wall are quite good.

Fig. 114 shows the comparison of pressure data for Run 9-11-1 (LN_2). This test run had only a 2 psig difference in pressure from the Hadley valve to the five-foot tank. This compares with a 9psig difference for Run 9-8-4.

The negative pressure condition occurs at a later time because of the lower mass flows. As before, more predicted mass of two-phase fluid enters the tank than is measured between 1 and 2 seconds, i.e., when

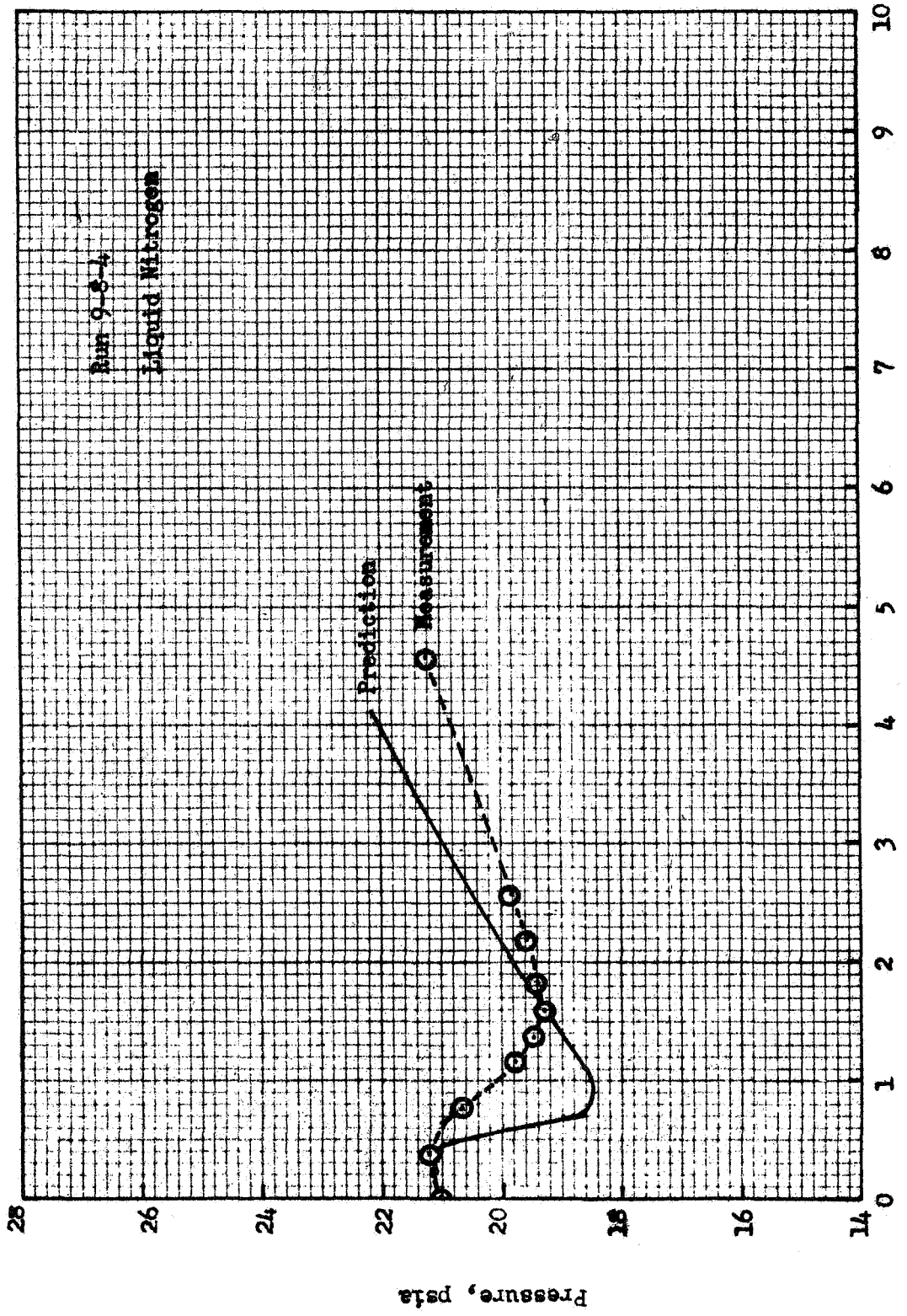


Fig. 113 Comparison of Predicted and Measured Tank Pressure -- Complete Fill System Model

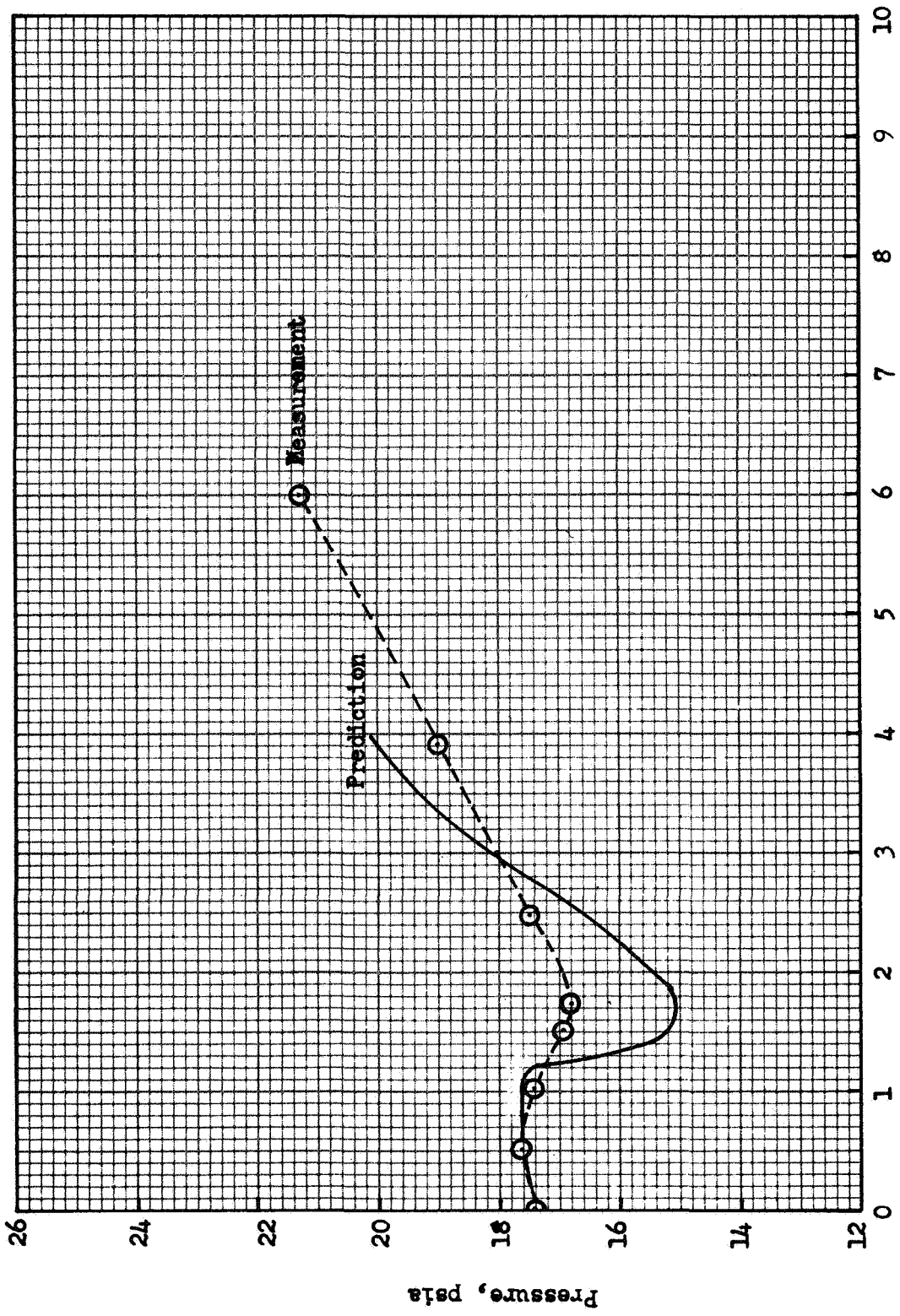


Fig. 114 -Predicted and Measured Tank Pressure for Run 9-11-1

the maximum pressure decrease is observed.

The pressure-time comparison for liquid hydrogen Run 9-15-6 is shown in Fig. 115. This run is representative of those made with LH_2 wherein the combination of the high inlet pressure drop and high initial rates of heat transfer to the fluid produced all vapor, or high-quality vapor, flowing into the tank during the first few seconds of fill. As a result no decreases in pressure below the initial tank pressure were observed.

It is felt that the simulation of implosion conditions achieved with LN_2 provides a very comprehensive check on the CFS model predictions. Nevertheless, the degree of agreement between the measured and predicted pressure response with LH_2 provides an important verification of the model for this fluid. These results contribute to the conclusion that, unless a transfer line is chilled down completely to the tank inlet, the occurrence of an implosion condition during fill with LH_2 is unlikely.

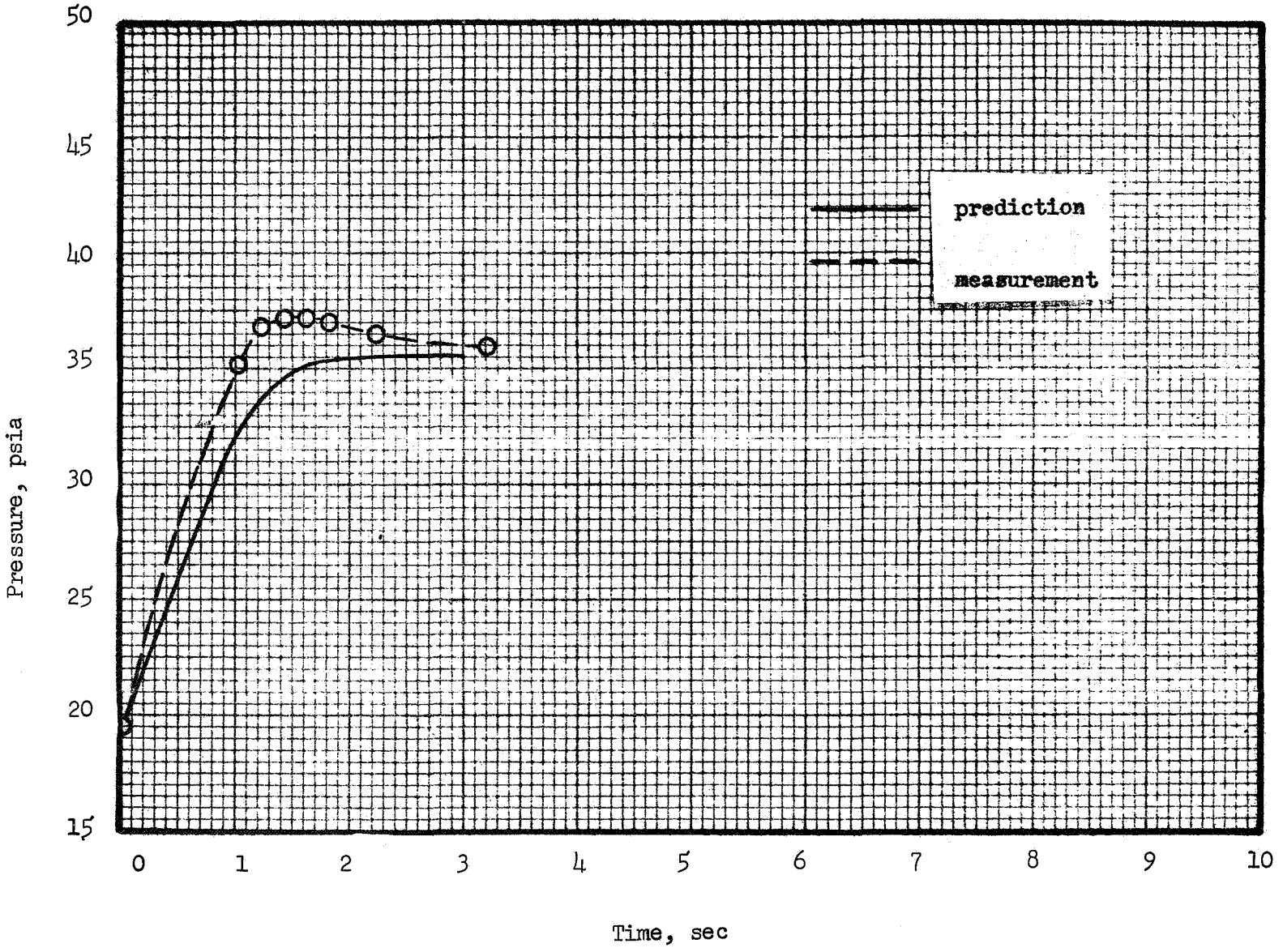


Fig. 115 Comparison of the Predicted & Measured Tank Pressures - Run 9-15-6

Section 10

IMPLOSION PREVENTION TECHNIQUES

During the course of conducting the quasi-steady flow tests in the two-foot diameter tank, the inlet flow conditions were varied considerably as described in Section 8. However, at no time during testing was an implosion condition or even a negative pressure derivative achieved. Careful analysis of the measured pressure and temperature data and comparison with the Tank Fill Model predictions provided a high degree of confidence in defining the basic cause of the negative pressure gradient. The Tank Fill analyses clearly showed that, when liquid first enters the tank in the form of a droplet spray, evaporation occurs and energy is extracted from the vapor in the tank and the pressure drops. As the ullage vapor cools, the effect of mass addition to the tank becomes dominant and the pressure rises. Thus, an increase in the rate of droplet evaporation and/or heat exchange with the ullage vapor produces a larger initial pressure drop.

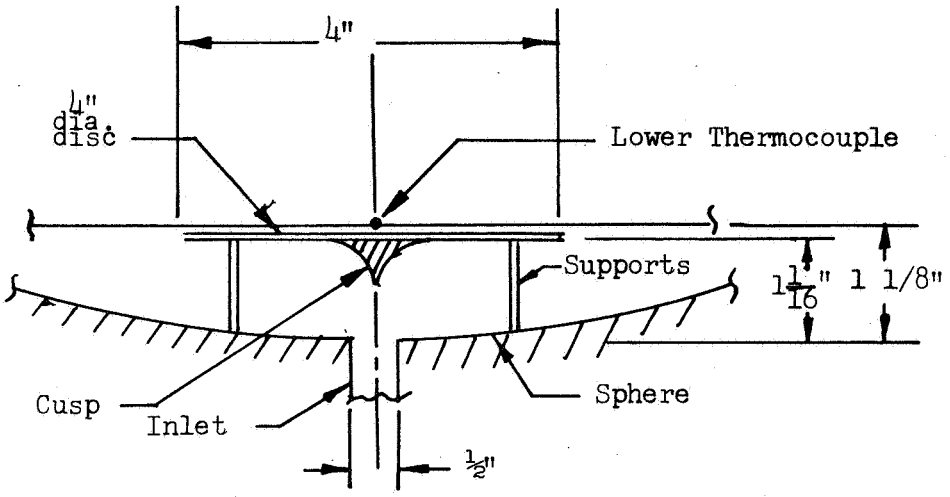
In order to demonstrate this effect more clearly, a simple method for increasing the rate of droplet evaporation and heat exchange with the ullage vapor was devised; namely, the use of a screen placed in the post-inlet region of the tank. Conversely, by suppressing the interaction between the incoming droplet spray and the ullage vapor by means of a baffle placed over the inlet, a greater rate of pressure rise than is observed in an unbaffled tank was expected to occur.

Both devices were tested on the two-foot diameter and five-foot diameter test tanks. The results and accompanying data correlation are presented below.

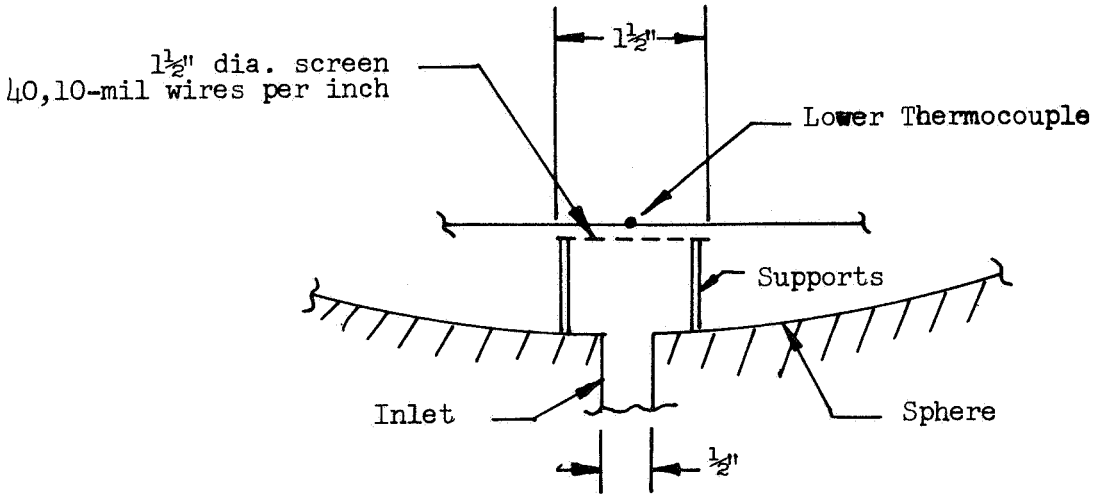
10.1 Two-foot Diameter Tank Tests

The screen used on the two-foot-diameter tests is shown in Figs. 116 and Fig. 117(a) The screen was made of copper, and was 1 ½-inch diameter with 10 mil wires and 40 wires/inch, i.e., 15 mil square mesh and approximately 36% open. It was mounted horizontally 1 1/16-inch above and concentric with the inlet. The baffle was configured as shown in Figs. 116 and 117(b) was used. This baffle consisted of a thin four-inch diameter phenolic disc with a cusp approximately one-half inch high by one-half inch radius at the base. This baffle was mounted horizontally with the cusp down, concentric with the tank inlet and 1 1/16-inch above the inlet, i.e., 1/16-inch below the lowest thermocouple. Both the screen and the baffle were mounted on three screws for support. To have "clean" tests for comparison, the test conditions for Runs 3-30-1, 2 were chosen, and each of these two test conditions were repeated for the screen and the baffle. A summary of the test conditions is presented in Table 40 . Both photographic and duplicate runs were made. The photographic coverage consisted of the overall sphere coverage (500 fps) and the closeup coverage of the post inlet flow (1250 fps) which for these tests showed a field of view of approximately eight inches high by ten inches wide at the bottom of the sphere.

All of the measured data for both screen and baffle tests appears in Volume VI of this report. Comparisons of pressure response for the "clean", screen, and baffle tests are shown in Figures 118 and 119 for similar high and low flow rate for each post inlet configuration.



BAFFLE



SCREEN

Fig. 116 Sketches of Anti-Implosion Baffle and Anti-Vortex Screen

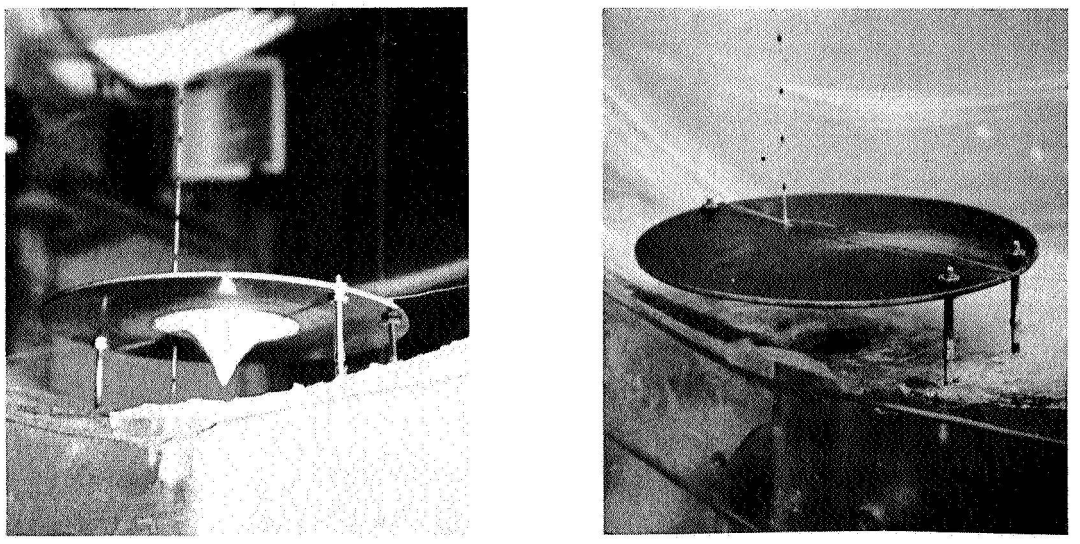


FIGURE 117a Views of Anti-Implosion Baffle Mounted in Two-foot Tank

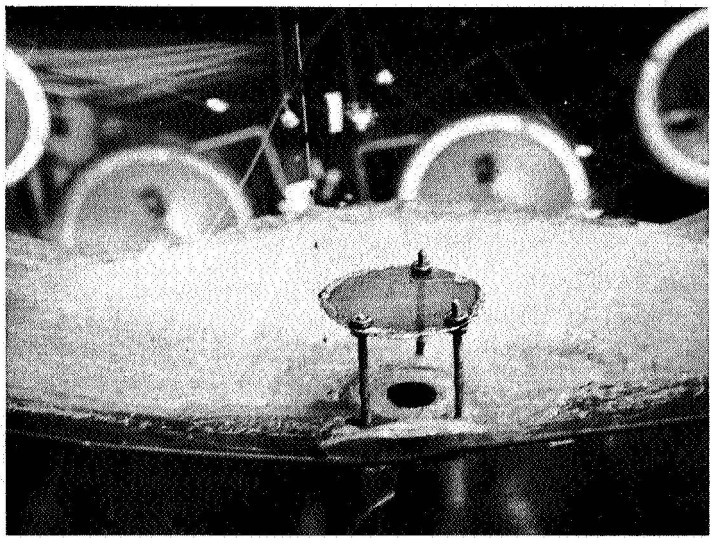


FIGURE 117b View of Anti-Vortex Screen Mounted in Two-foot Tank

Table 10

Summary of Small-Scale Tank Fill Tests

With Baffle and Screen

Test No.	Fill Duration (Sec)	Initial Flowrate[1] (lbm/sec)	Final Flowrate[1] (lbm/sec)	Initial Pressure (psia)	Final Pressure (psia)	REMARKS
4-4-1	7.5	0.0351	0.0310	14.70	19.94	Implosion Suppression baffle over tank inlet, $(F_\ell)_{max}$ = 0.100[3]
4-4-3	7.5	0.0672	0.0578	14.70	20.70	Implosion Suppression baffle over tank inlet, $(F_\ell)_{max}$ = 0.210[3]
4-4-4	10.0	0.0351	0.0309	14.70	18.90	Screen over tank inlet, $(F_\ell)_{max}$ = 0.114[3] Pressure drop 0.12 psi below ambient
4-4-5	9.0	0.0672	0.0584	14.70	20.14	Screen over tank inlet, $(F_\ell)_{max}$ = 0.265[3] Pressure drop 0.12 psi below ambient

Notes: (1) Flowmeter Data
(3) F_ℓ = Liquid Volume Fraction

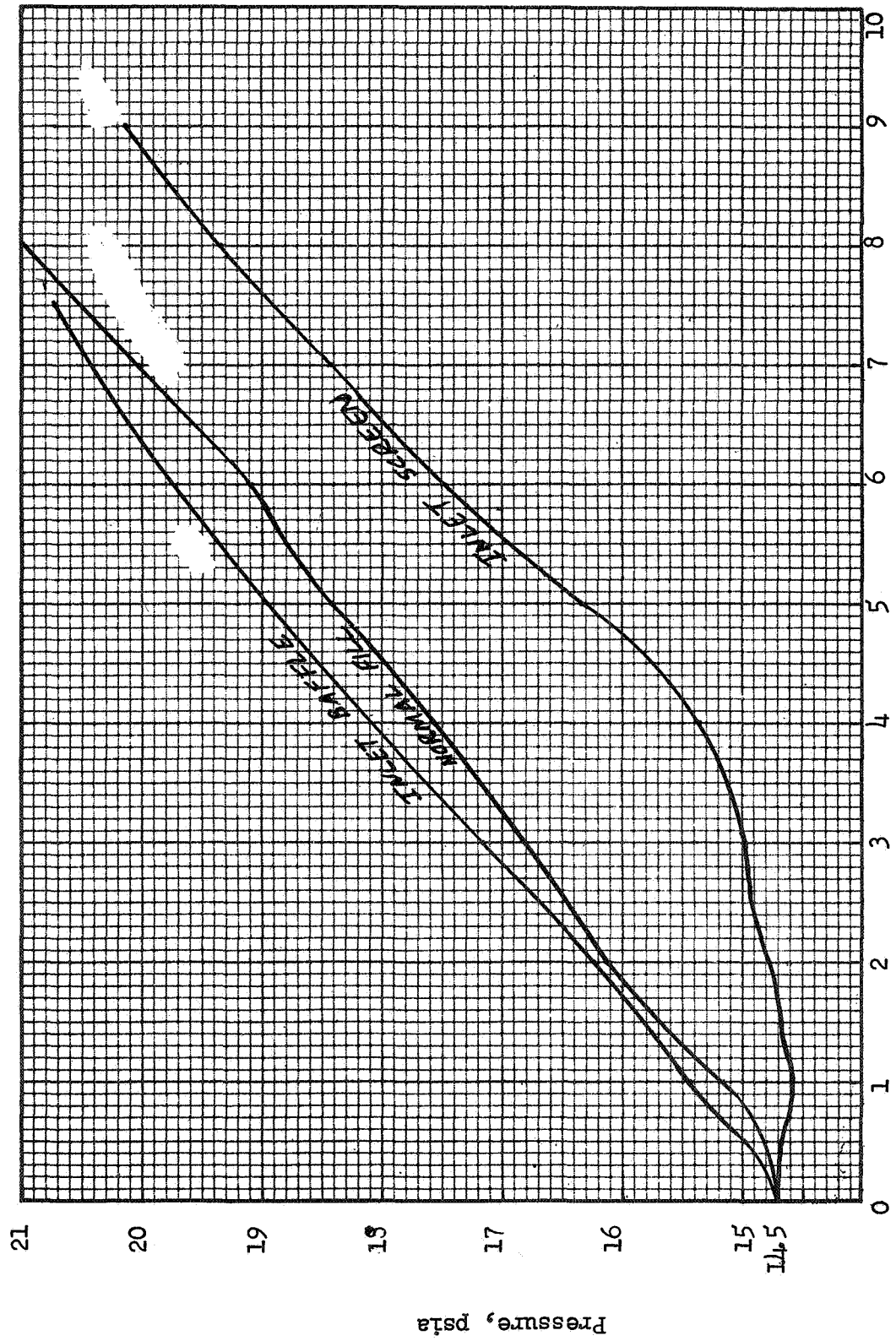


Fig. 118 Comparison of Measured Pressure Response With High Inlet Flowrates

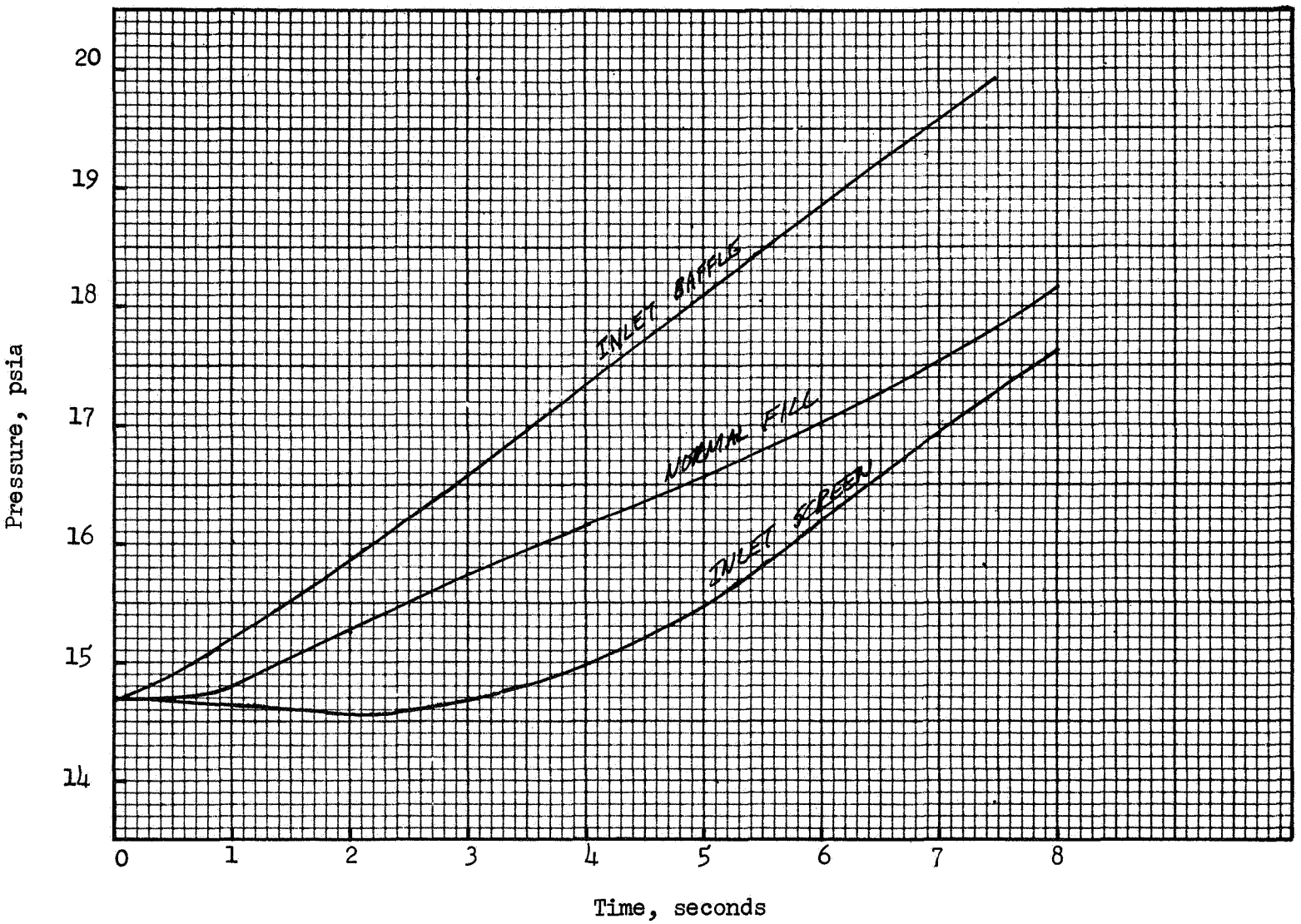


Fig. 119 Comparison of Measured Pressure Responses With Low Inlet Flowrates

The effect of the screen is most apparent by observing the pressure response. A pressure drop of approximately 0.1 psi was measured and, further for approximately 3 seconds (or 1/3 of the test) the pressure was essentially constant. The gas temperature was found to be reduced significantly more than in previous corresponding tests, indicating the larger absorption of energy from the gas in vaporizing the liquid droplets. The motion pictures showed that whereas the thickening of the two-phase jet for the "clean" vessel was minor in traversing the vessel, the presence of the screen caused the jet to expand into a plume of at least 30 degrees internal angle with very fine droplets, the result being extreme interaction of the liquid droplets with the warm gas.

The effect of the baffle on diverting the plume is obvious from the small temperature variation in the gas and the rather large effect on the lower wall thermocouple (No. 6), as shown in Fig. 120. The photographs indicated that the plume is diverted symmetrically as it flows out along the wall. The flow initially reaches almost the mid-height of the vessel, then quickly recedes, thereafter only reaching six to eight inches along the wall.

When comparing the pressure data of Figures 118 and 119, it is apparent that use of screen did the intended task. Further, the steeper slope of the pressure-time curve for both high and low flow rates indicates that use of this simple anti-implosion device also did its intended task. As a result, both configurations were evaluated further in the sixty-inch diameter tank tests.

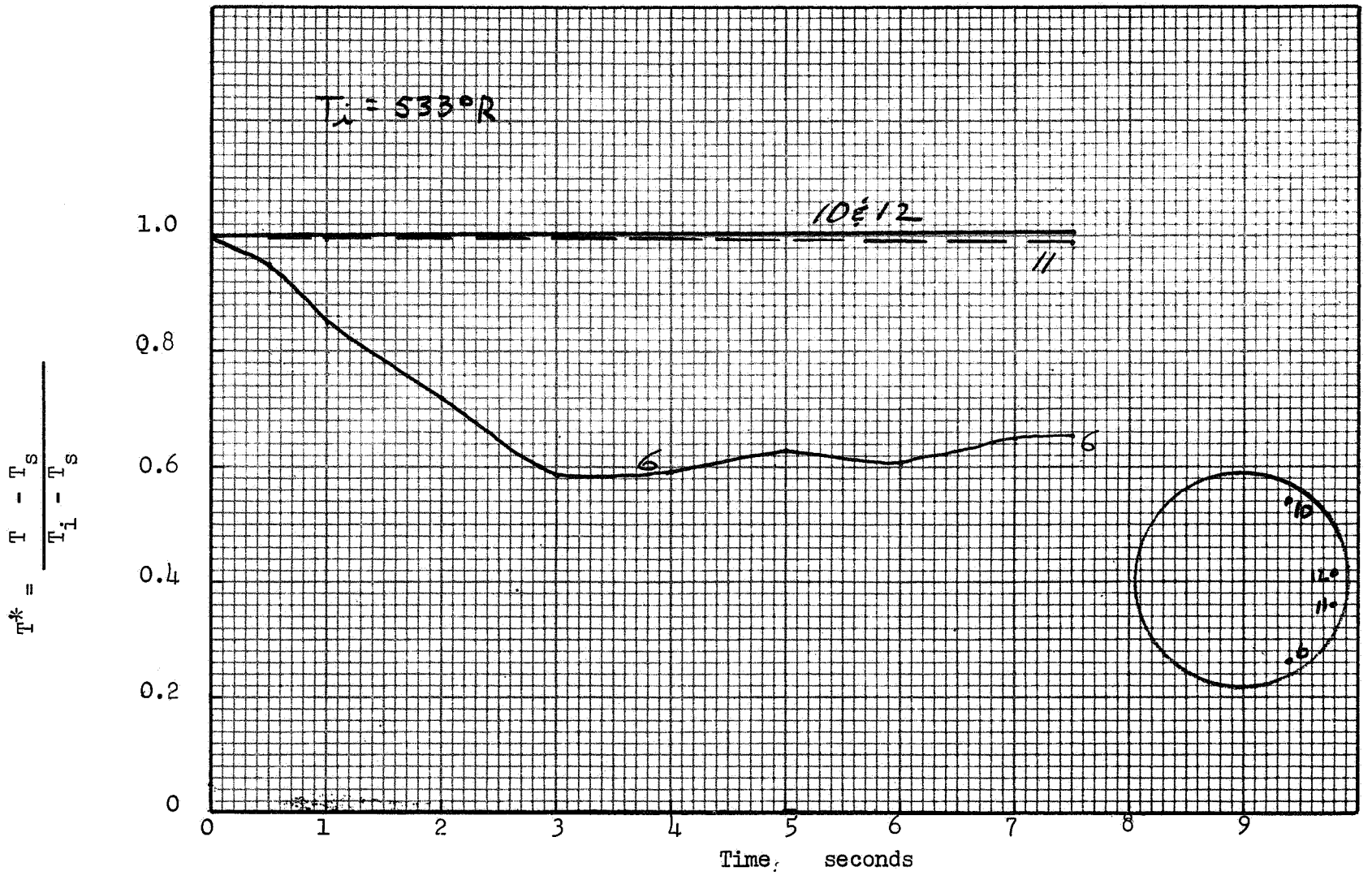


Fig. 120 Tank Wall Temperatures for Baffle Test, Run 4-4-67

10.2 Test Data Correlation

Using simple refinements in the basic Tank Fill Model analysis, predictions were made of ullage pressures and temperatures for comparison with test data for each configuration.

10.2.1 Screen Tests

The screen was expected to atomize the incoming liquid stream. Therefore, it was expected that the conditions in the screen tests could be simulated in analysis by specifying relatively small values for the characteristic drop diameter. As shown in Figs. 121 and 122 , the values of this diameter which closely match the measured data are slightly smaller than those without the screen. Thus, the importance of this parameter as defined on the analysis was confirmed in the test. It can be seen that the measured pressure-data show a nearly flat slope with a small negative gradient early in the test run. As indicated in the analysis results shown in Fig.121 larger negative pressure gradients are expected if smaller droplet diameters were attained. Careful observation of the pre-inlet films showed that much liquid was vaporized and effectively atomized in the line prior to encountering the screen. The same phenomenon was observed for the "clean" tank runs. The effect of the screen is noticeable in this test, however, it does its intended job of further reducing the size of the incoming droplets. A more dramatic effect of the screen would result if slugs of liquid rather than pre-atomized droplets impinged on the screen. Numerous attempts were made to encounter the former condition although none were successful.

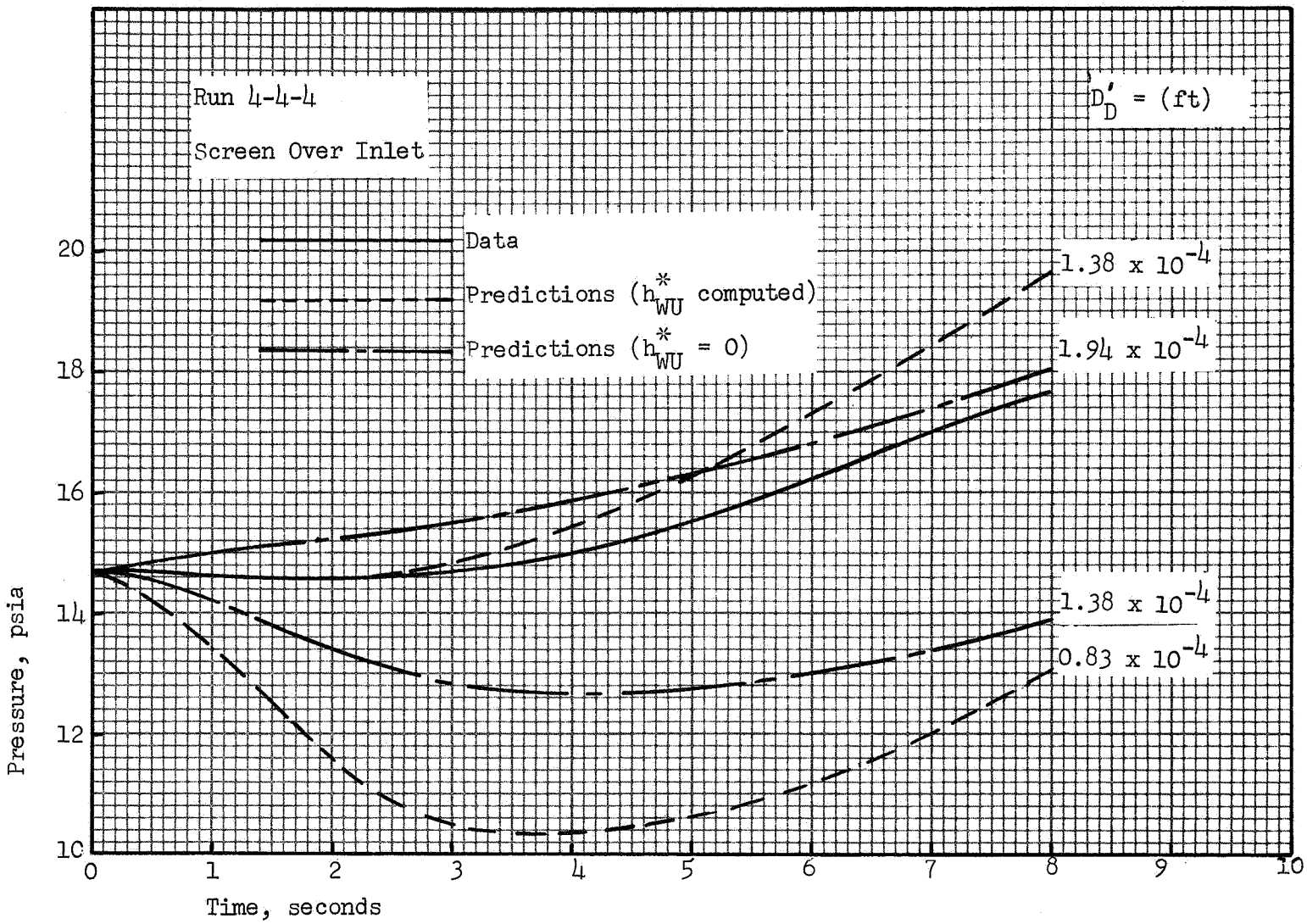


Fig. 121 Comparison of Pressure Data with Predictions --- Two-ft Transparent Tank

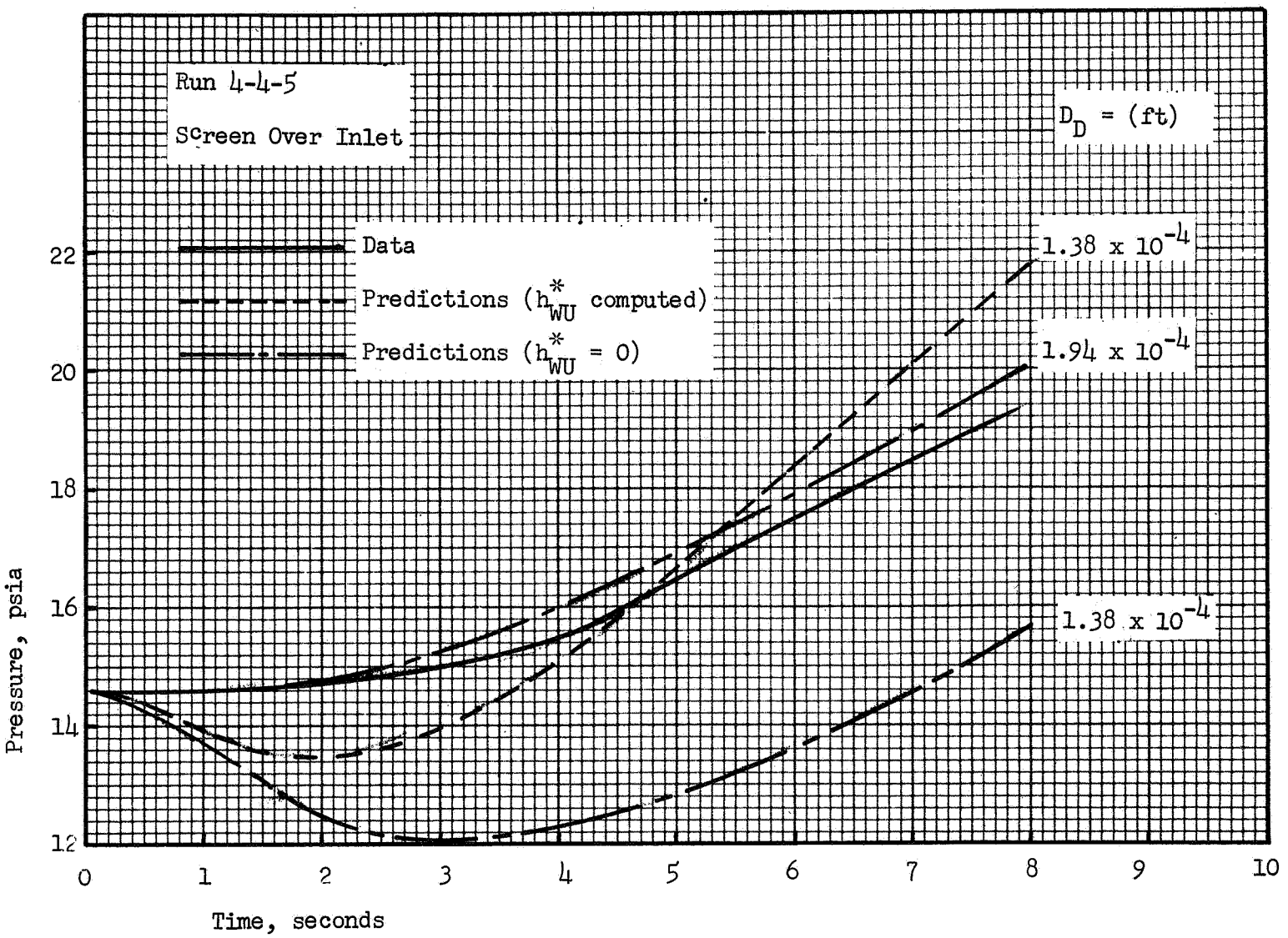


Fig. 122 Comparison of Pressure Data with Predictions --- Two-ft Transparent Tank

The effect of heat transfer between the tank wall and the vapor is also shown again in Figs. 121 and 122 . The data for Run 4-4-4 (Fig. 121) are bracketed by the two predictions with $D_D' = 1.38 \times 10^{-4}$ ft. It appears that a close simulation of the data could be obtained if a smaller value for h_{WU}^* were specified with this value of D_D'. The data for Run 4-4-5 (Fig. 122), however, appear to agree best with the zero-heat-transfer predicted. Almost exact agreement with the data could be obtained if a value of D_D' somewhat less than 1.94×10^{-4} were used. Again, it is emphasized that the relative effect of heat transfer from the wall to the vapor will decrease for larger tanks.

The temperature data obtained during Run 4-4-5 are compared with the predictions in Figs. 123 , 124 , and 125 . The "top" vapor region temperature, T_{TR}^*, and the jet temperature T_J^* agree quite well with the data (Fig. 123). As previously explained, T_{TR}^* predictions are shown only when the jet does not impinge on the top of the tank. The point at which the analytically described jet begins to drop away from the tank wall (4 seconds) agrees well with the observed temperature rise at thermocouple number 5.

Fig. 124 shows the average temperature in the "bottom" vapor region compared with the off-centerline data. As before, the predicted value is lower than the measured values because the "bottom" region includes some of the cold gas in the jet mixing region. Except for thermocouple number 6, the tank wall data agree well with T_{WU}^* (Fig. 125). Most of the droplets which evaporate from the tank wall probably do so near the bottom of the tank, thereby reducing the wall temperature in this region. In the model analysis, this

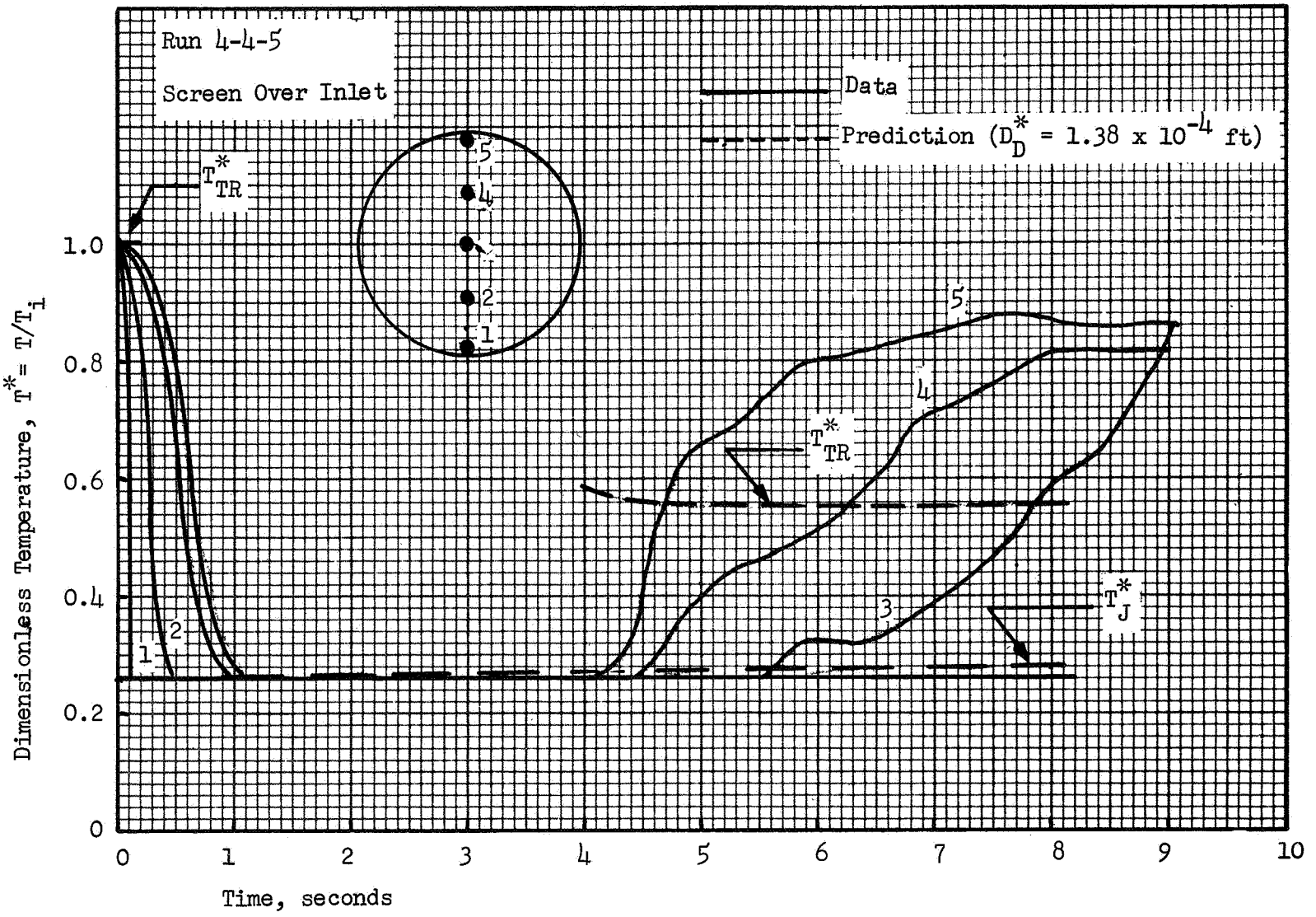


Fig. 123 Comparison of Temperature Data with Predictions --- Two-ft Transparent Tank

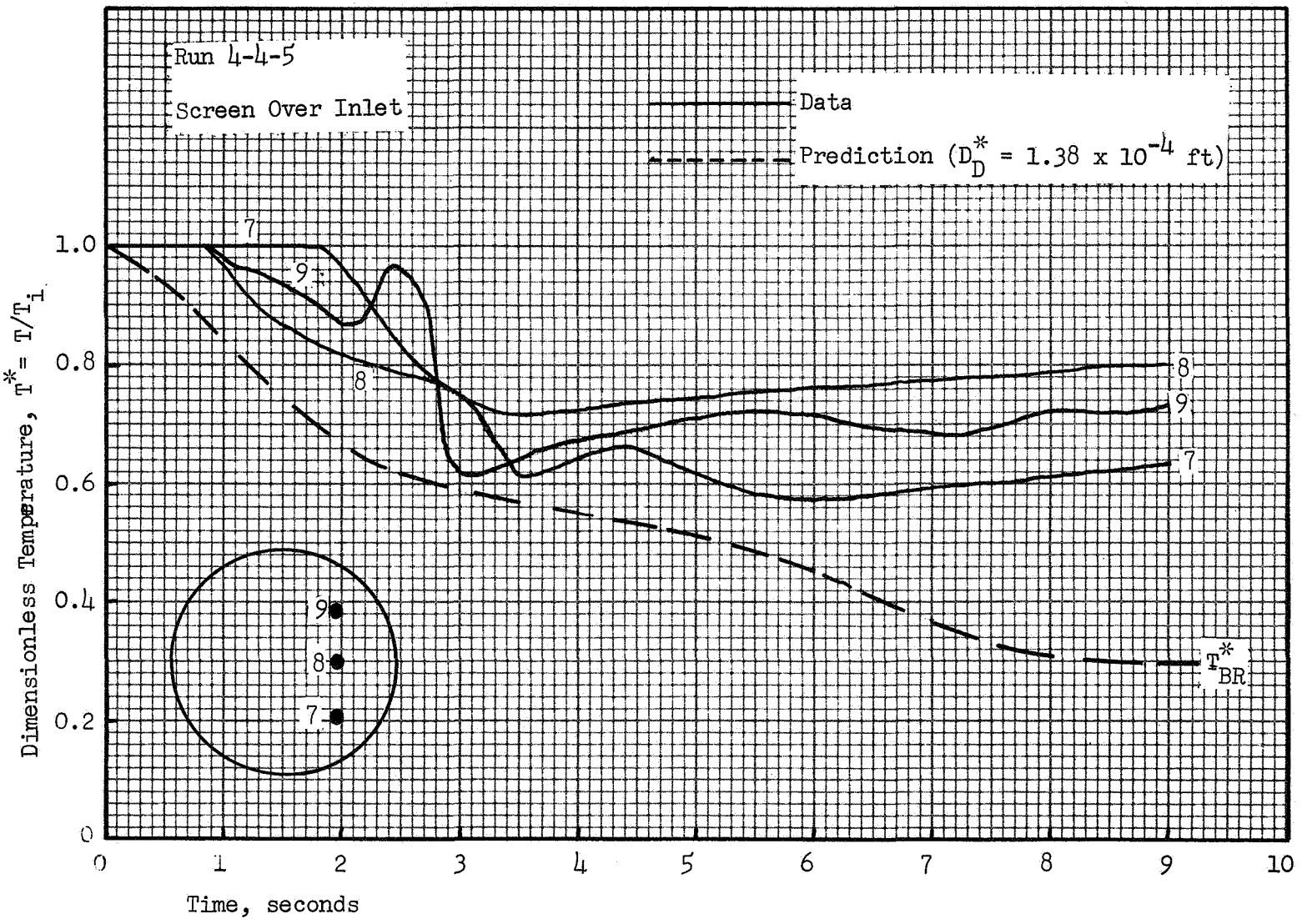


Fig. 124 Comparison of Temperature Data with Predictions --- Two-ft Transparent Tank

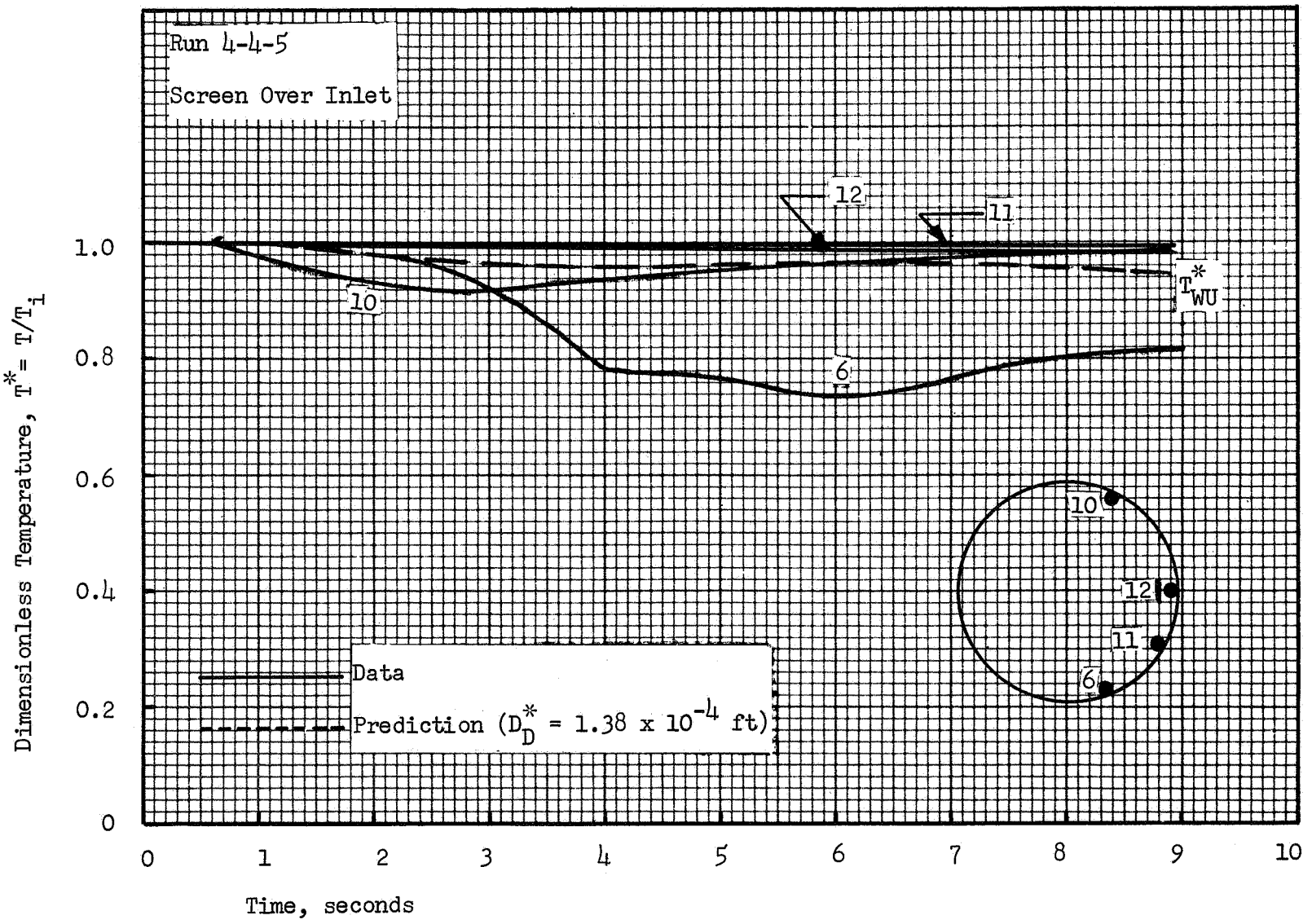


Fig. 125 Comparison of Temperature Data with Predictions --- Two-ft Transparent Tank

energy is removed from the wall uniformly over the inside surface; therefore, the resulting change in T^*_{WU} is relatively small.

10.2.2 Baffle Tests

Where there is a baffle in the post-inlet region, the incoming liquid is directed along the tank wall and there is no jet. To simulate this situation a single vapor region analysis is used and several assumptions are made concerning the distribution of the liquid on the tank wall. Based on the wall temperature measurements, it was estimated that the liquid rises along the tank wall to a height of one-fourth the tank diameter. It is also assumed that the mass of liquid in the tank is small enough such that $A^*_S \approx A^*_{WL}$. A film boiling heat transfer coefficient of 25 Btu/ft^2 hr°R was used for h_{WL} (the coefficient between the wall and the liquid on the wall). A value of 0.2 Btu/ft^{2}hr°R was used for the heat transfer coefficient between the vapor and the liquid-vapor interface, h_{US}. The value used for h_{US} has a small effect on the pressure for this baffled condition because most of the evaporation occurs at the wall. For this reason the value used was an estimate of a reasonable value and no attempt was made to develop an auxiliary analysis for h_{US}. Fluid velocity values could not be read from the post-inlet films when there was a baffle or screen over the inlet. To obtain predictions for these runs the computed flow rates (based on measured velocities) from equivalent runs without inlet obstructions were used. The runs were considered equivalent, for this purpose, when the metered flow rates were very close to being the same.

Predicted pressure histories are compared with the data for the two baffle runs in Figs. 126 and 127 . The predicted pressure for Run 4-4-1 (Fig. 126) agrees very well with the data. The prediction for Run 4-4-3 (Fig. 127) has a slope which is greater than that of the data initially but falls off to a smaller slope at later times. This behavior of the prediction can be traced to the specification of a value for A^*_{WL} which is too large. In the analytical model when the computed rate of evaporation (at the wall and at the liquid-vapor interface) is greater than the rate at which liquid is being added to the tank, the rate of evaporation is set equal to the rate of addition of liquid. This situation was found to exist in the analysis during most of Run 4-4-1, but for only the first two seconds of Run 4-4-3, where there was a higher rate of liquid addition. Therefore, for Run 4-4-1, the predicted rates of evaporation and the corresponding pressure rise are limited by the fill rate. A rate of evaporation which is too high is predicted at first for Run 4-4-3, thereby over-cooling the tank wall and giving a rate of evaporation (reflected in the pressure rise) which is too low at later times. This is further illustrated by the predicted tank wall temperature which is shown in Fig. 128 . The behavior of thermocouple number six implies that initially the liquid splashed up the wall in this region. The splashing subsided after approximately three seconds. The measured vapor temperatures are compared with the predicted values in Fig. 129 . Most of the temperature change in the vapor occurs near the bottom where the cold gas generated at the tank wall is added. The cold gas is buoyantly stable in the bottom of the tank and tends to inhibit mixing.

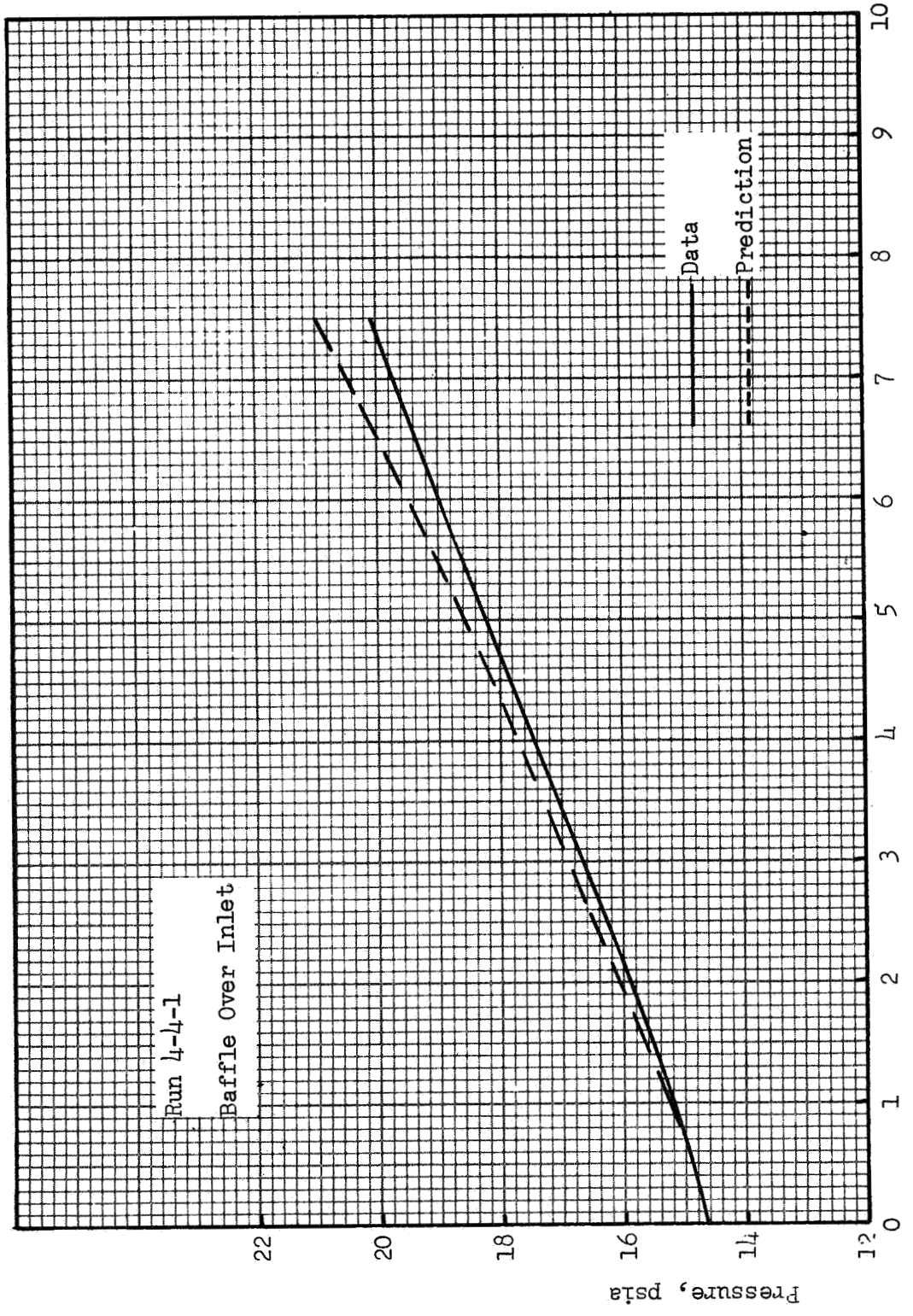


Fig.126 Comparison of Pressure Data with Predictions --- Two-ft Transparent Tank

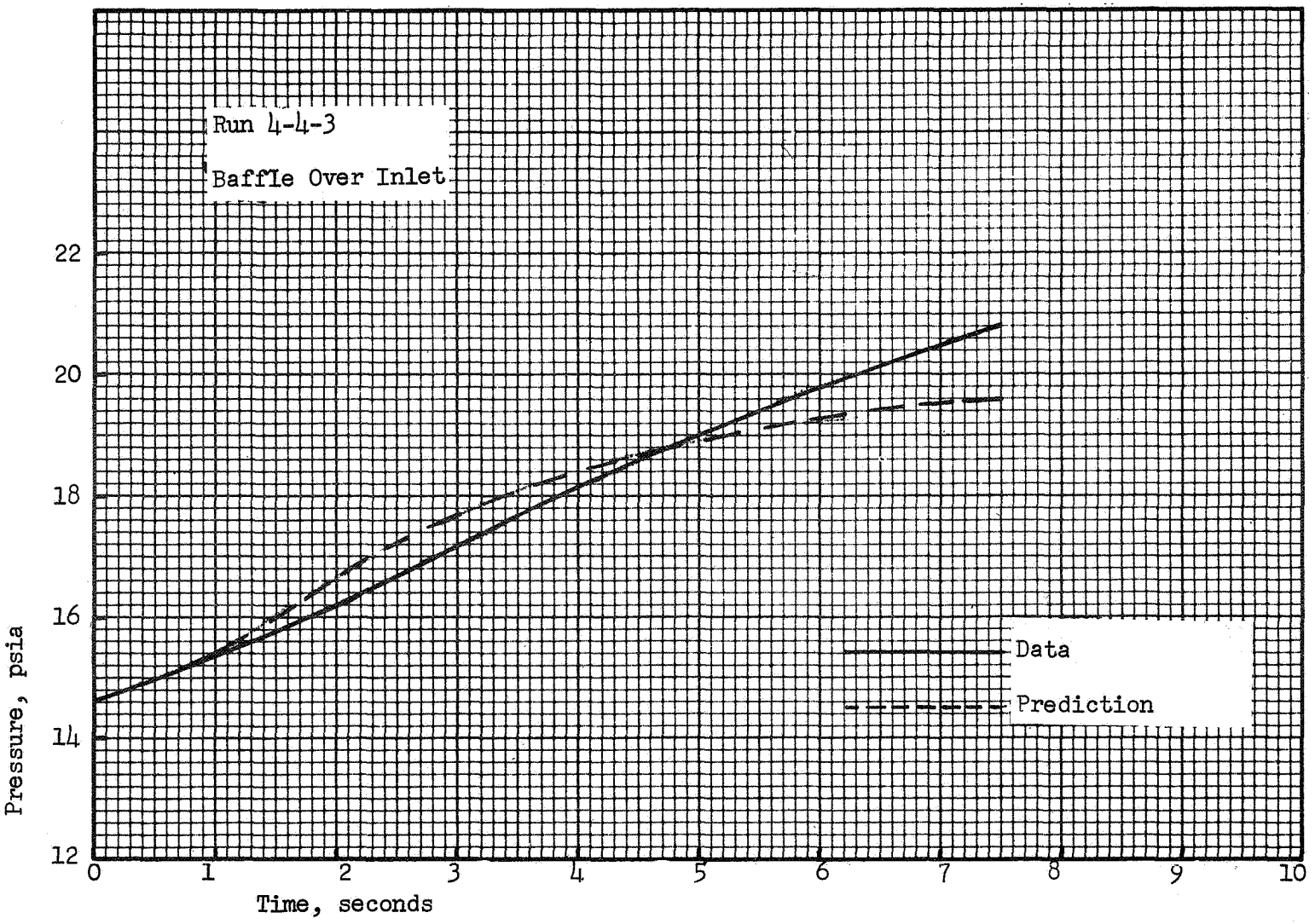


Fig. 127 Comparison of Pressure Data with Predictions --- Two-ft Transparent Tank

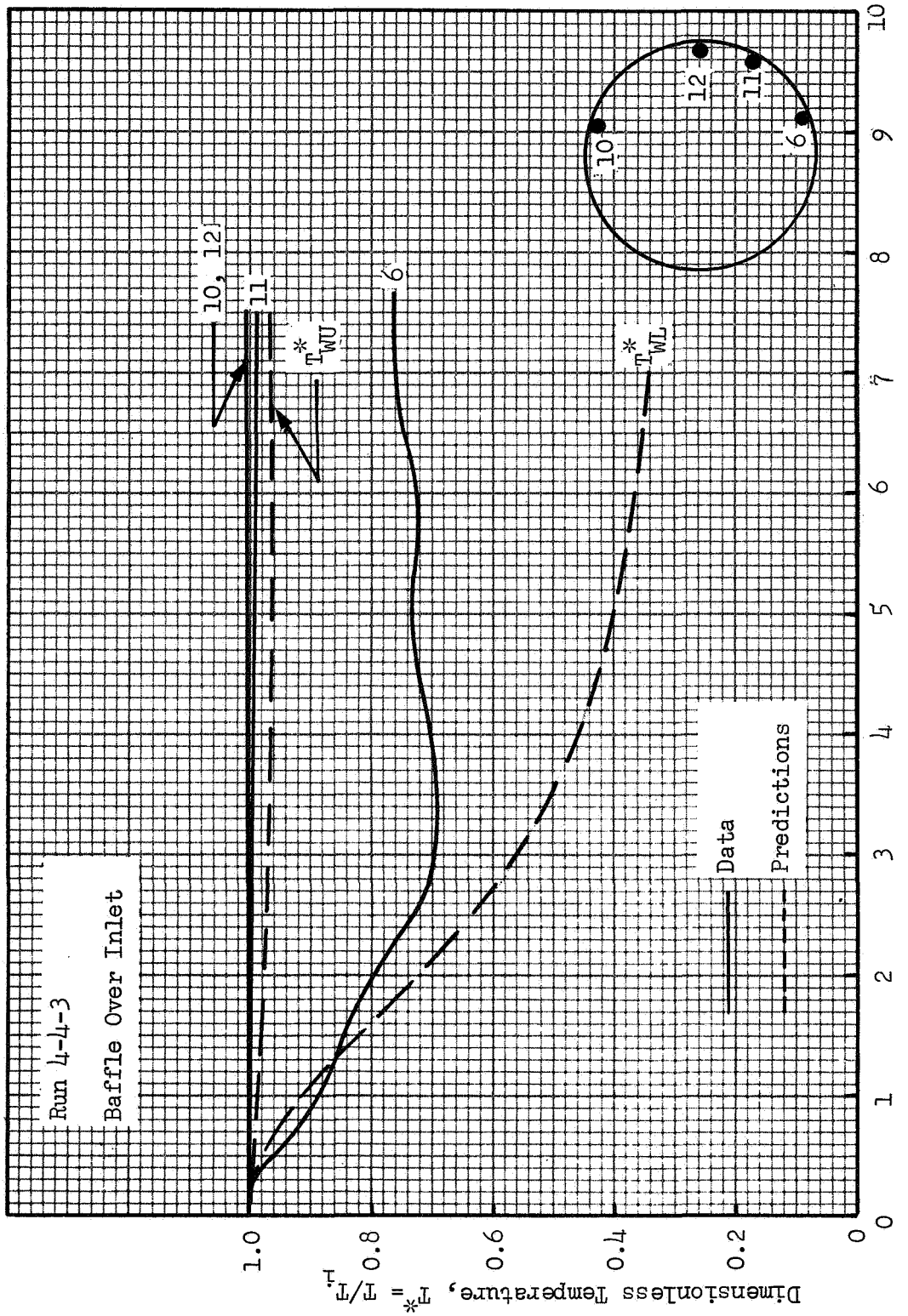


Fig.128-Comparison of Temperature Data with Predictions --- Two-ft Transparent Tank

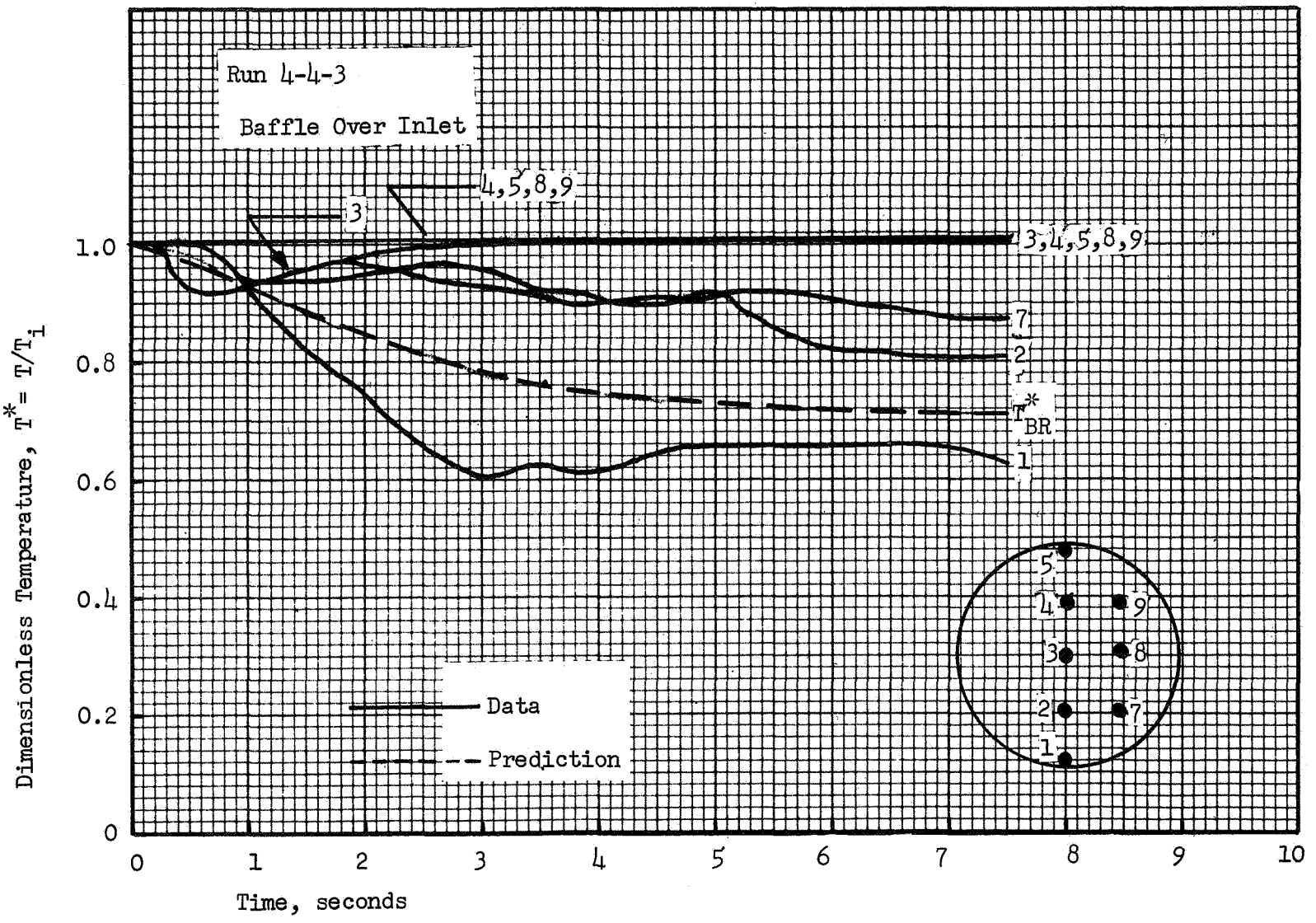


Fig. 29-Comparison of Temperature Data with Predictions --- Two-ft Transparent Tank

A high level of confidence in the Tank Fill Model analysis was achieved in performing the data correlation for the screen and baffle configurations. The correlation confirmed the importance to tank pressure of the energy transfer between incoming liquid and initial ullage gas. Proper application of the Model analysis defined the manner in which a negative tank pressure gradient could be achieved in test. Further, use of the Model defined a technique to alleviate this potential problem. Application of the Model to test data obtained on larger tanks with similar screen and baffle configurations was the next logical step in verifying the Tank Fill Model.

10.3 FIVE-FOOT-DIAMETER TANK TESTS

A screen and a baffle were designed and fabricated for further testing in LH_2 and LN_2 in the Lockheed five-foot diameter test tank. The overall dimensions of both the screen and baffle were scaled geometrically from those used in the two-foot-diameter tank tests. The basis of this scaling was the tank diameter; thus all pertinent dimensions relating to the small-size baffle and screen were multiplied by a factor of 2.5 to obtain the large-size designs. In addition, a cruciform section was added to the base of the screen. This particular configuration was added to simulate a combined drain fine inlet screen and vortex suppressor design presently used on the LO_2 tank of the S-IC. A drawing of the screen-cruciform and baffle, showing their location in the five-foot tank, is presented in Fig 130 . All materials used were aluminum, with the aluminum screen having a wire diameter of 0.01 inches and a wire spacing of 18 wires per inch.

The assembled screen-cruciform configuration installed on the instrument probe of the five-foot-diameter tank is shown in Fig 131. The baffle appears in Fig 132 . A full size view of the baffle configuration together with the entire instrumentation probe tank manhole assembly is shown in Fig 133.

A total of nineteen tests were conducted with these devices using the liquids hydrogen and nitrogen as the test fluids. The complete list of all tests conducted in this five-foot tank appears in Table 7 (Section 8).

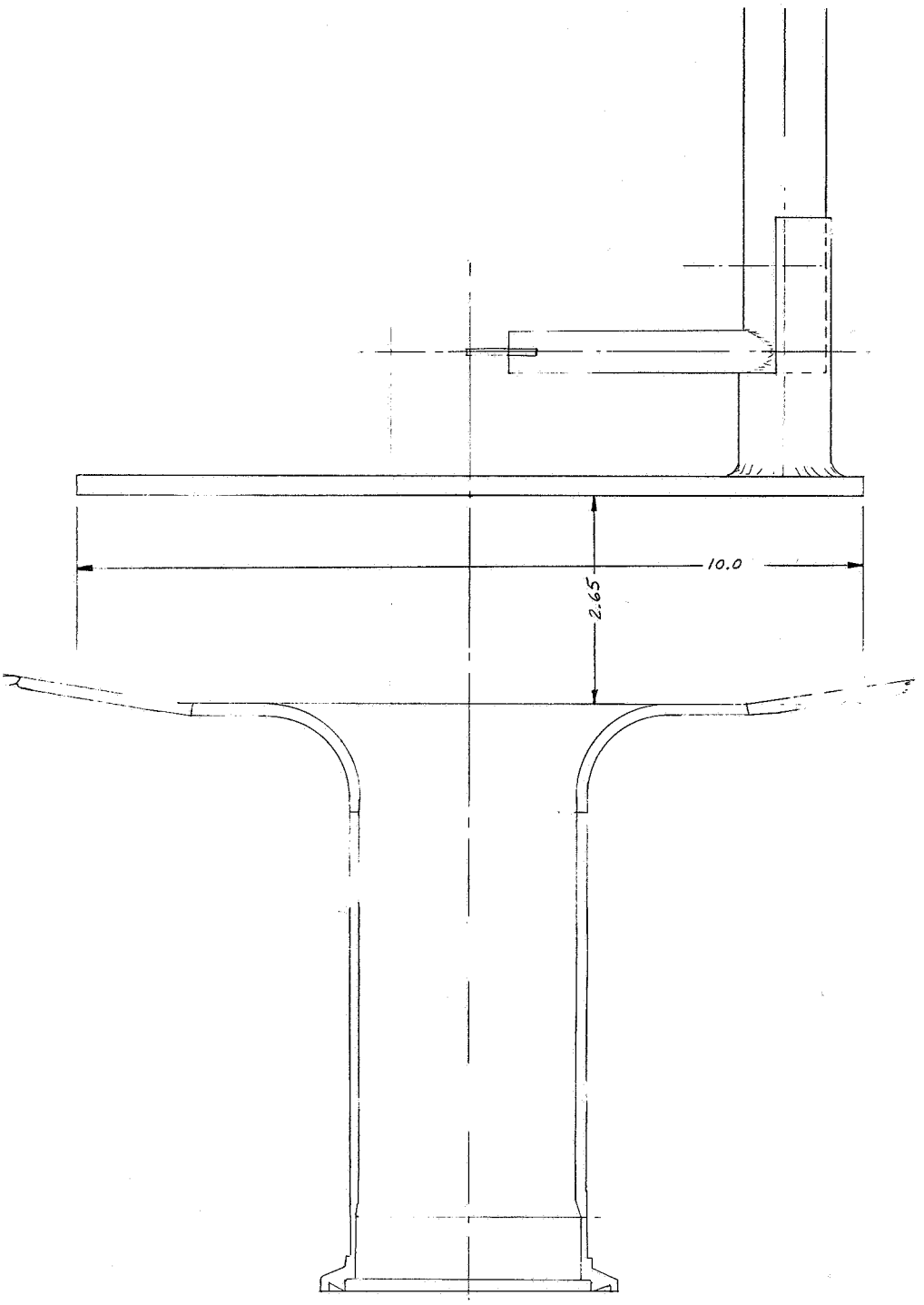


Fig. 130 Large Size Baffle Installation

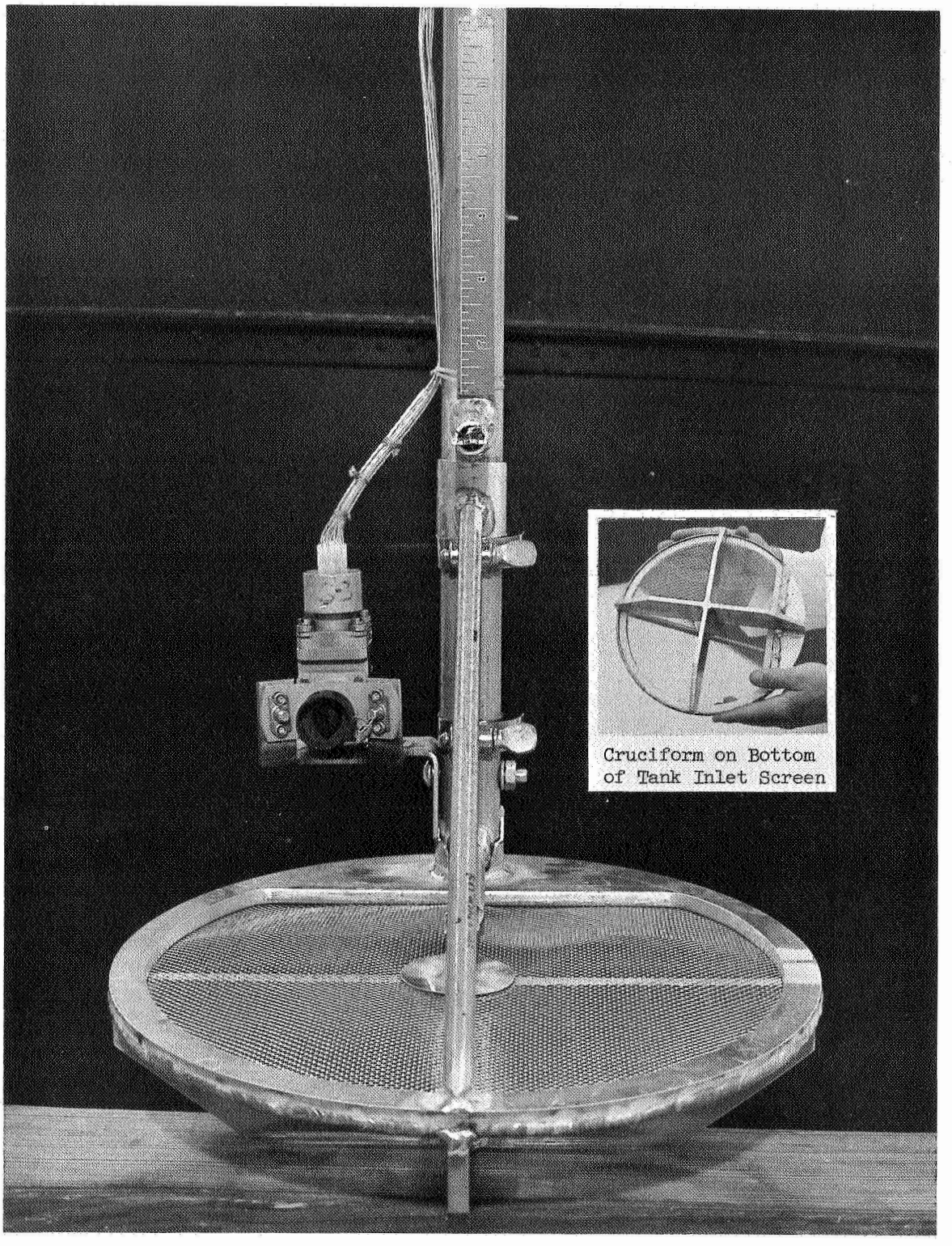


Fig. 131 Inlet Screen Attached to Instrument Probe

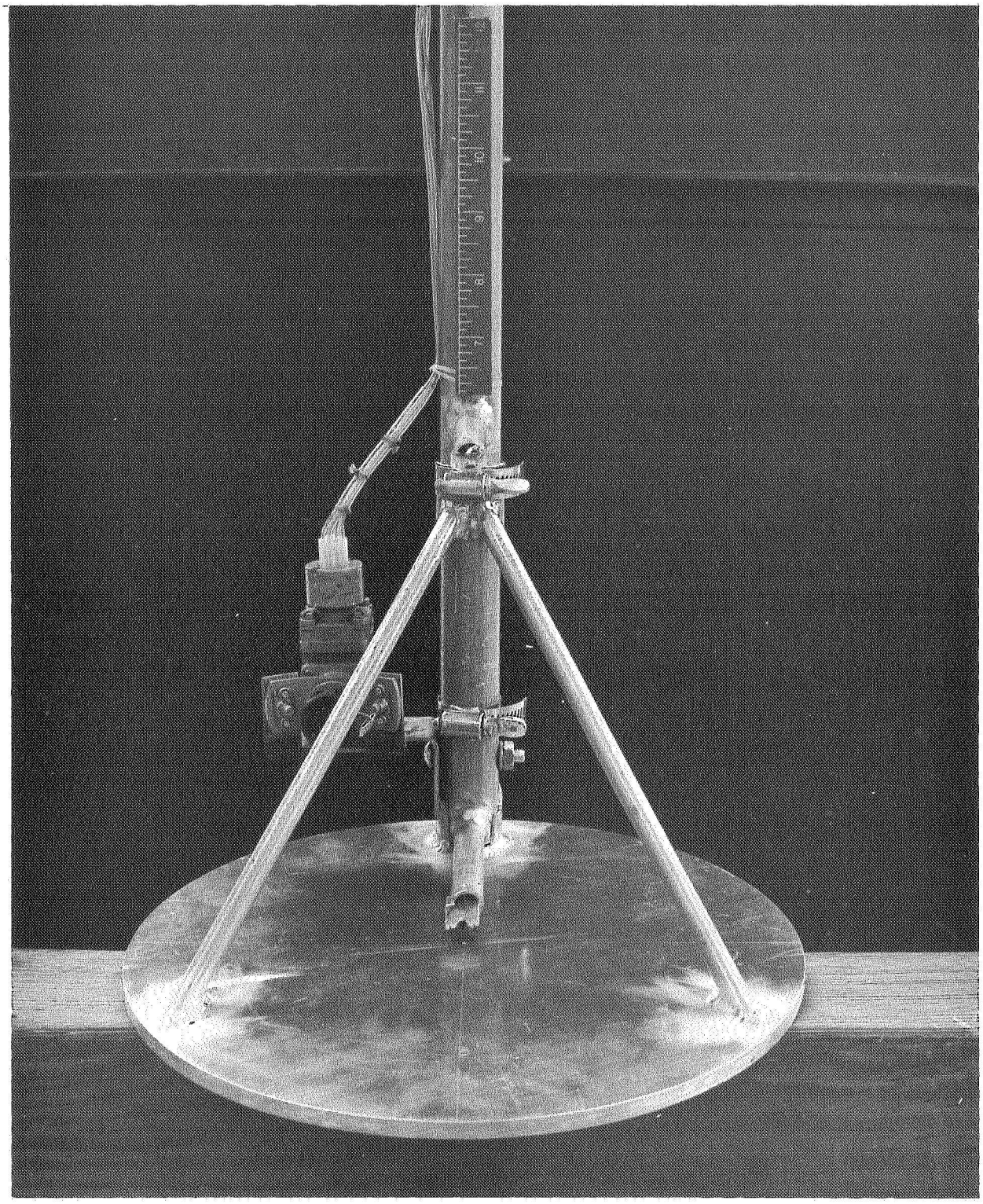


Fig. 132 Inlet Baffle Attached to Instrument Probe

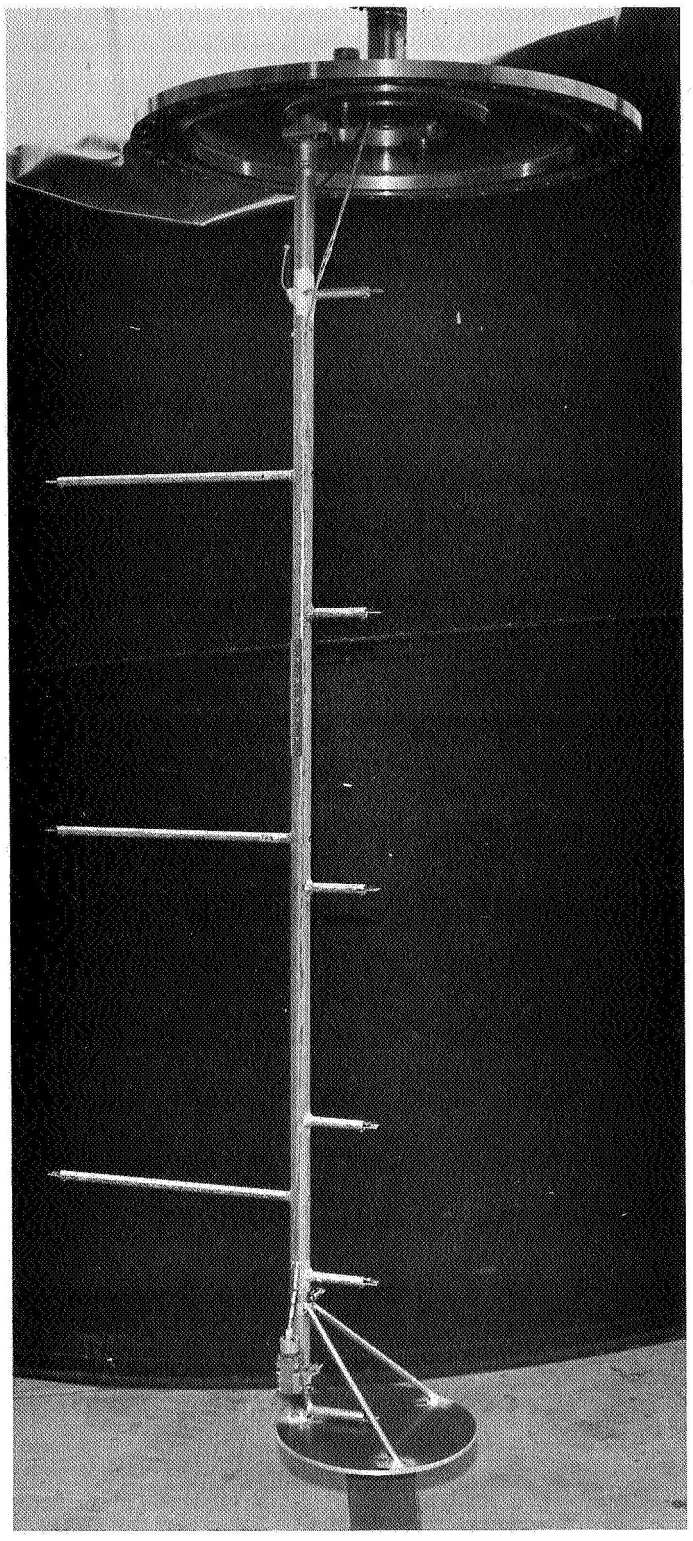


Fig. 133 Instrument Probe Mounted on Tank Manhole Cover

10.4 TEST DATA CORRELATION

10.4.1 Liquid Nitrogen Tests

Results of applying the Tank Fill Model analysis to predict the measured ullage pressure data for nitrogen tests, 9-11-1 and 2, using the Screen-cruciform are presented in Figs 134 & 135. It was found that use of a smaller droplet diameter, than applied in "clean" tank analysis, provides a better correlation of the data. The effect of the screen is evident whereas it is felt that use of the cruciform did not noticeably affect the droplet diameter.

Ullage gas temperatures, measured both on and off the tank centerline, are compared with analytical values in Figs 136 & 137 for run 9-11-1. Agreement is especially impressive in Fig 137, where the off-centerline temperatures are shown. Again, the analytical top region temperature is only shown when the analysis predicts that a top region exists.

It is felt that the best agreement between data and the analysis was obtained for the nitrogen screen tests. This implies that the resulting droplet cloud in these tests was very similar to that assumed in the analytical model, after it passes through the screen.

The pressure history for fill with nitrogen with the baffle over the post-inlet region is shown in Fig 138. The baffle directs the incoming flow against the tank wall, so there is no centerline jet in this case. In the analysis, it is assumed that the incoming liquid spreads along the tank wall with evaporation occurring at the wall by the mechanism of film boiling.

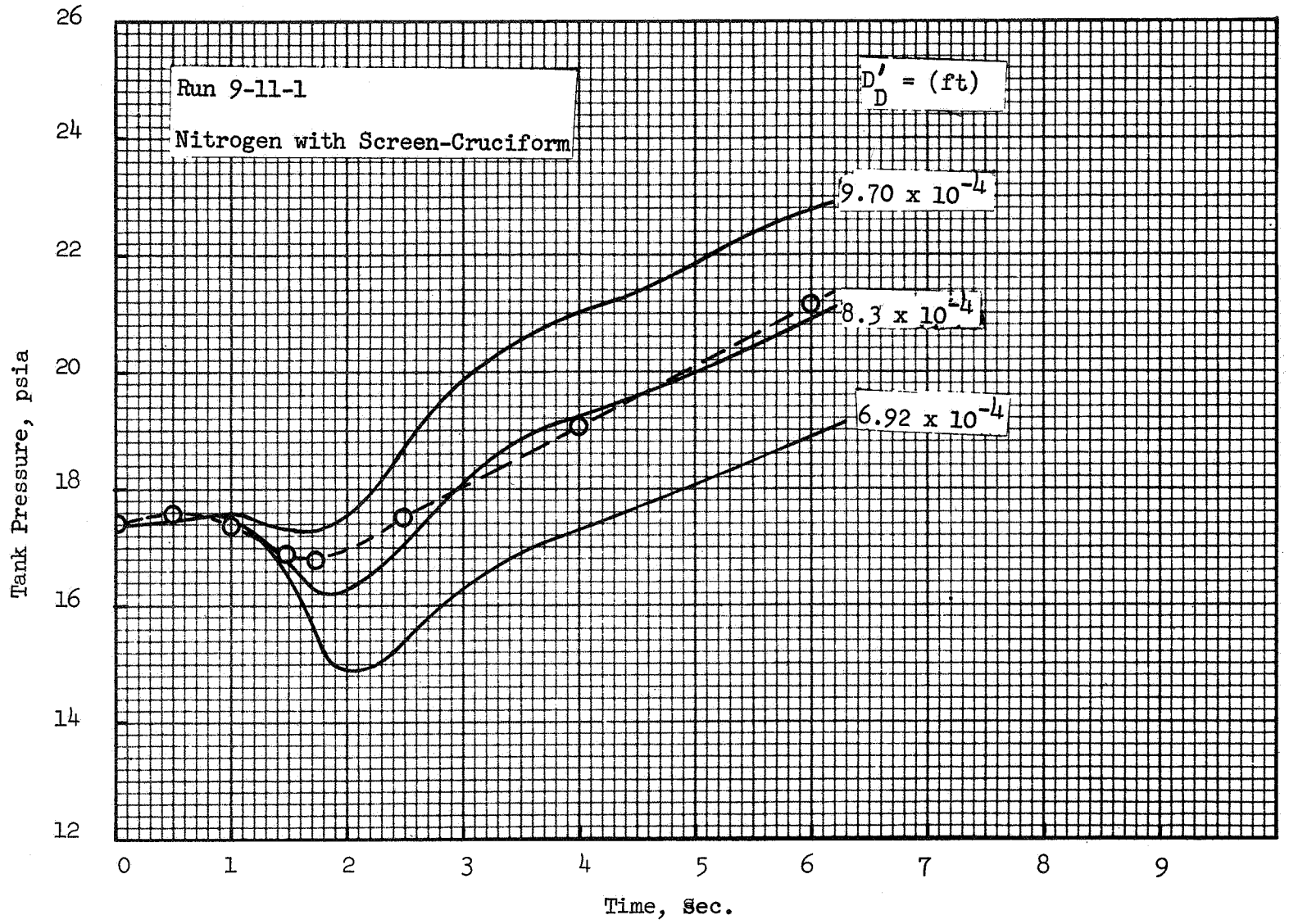


Fig. 134 Comparison of Pressure Data With Predictions for Run 9-11-1

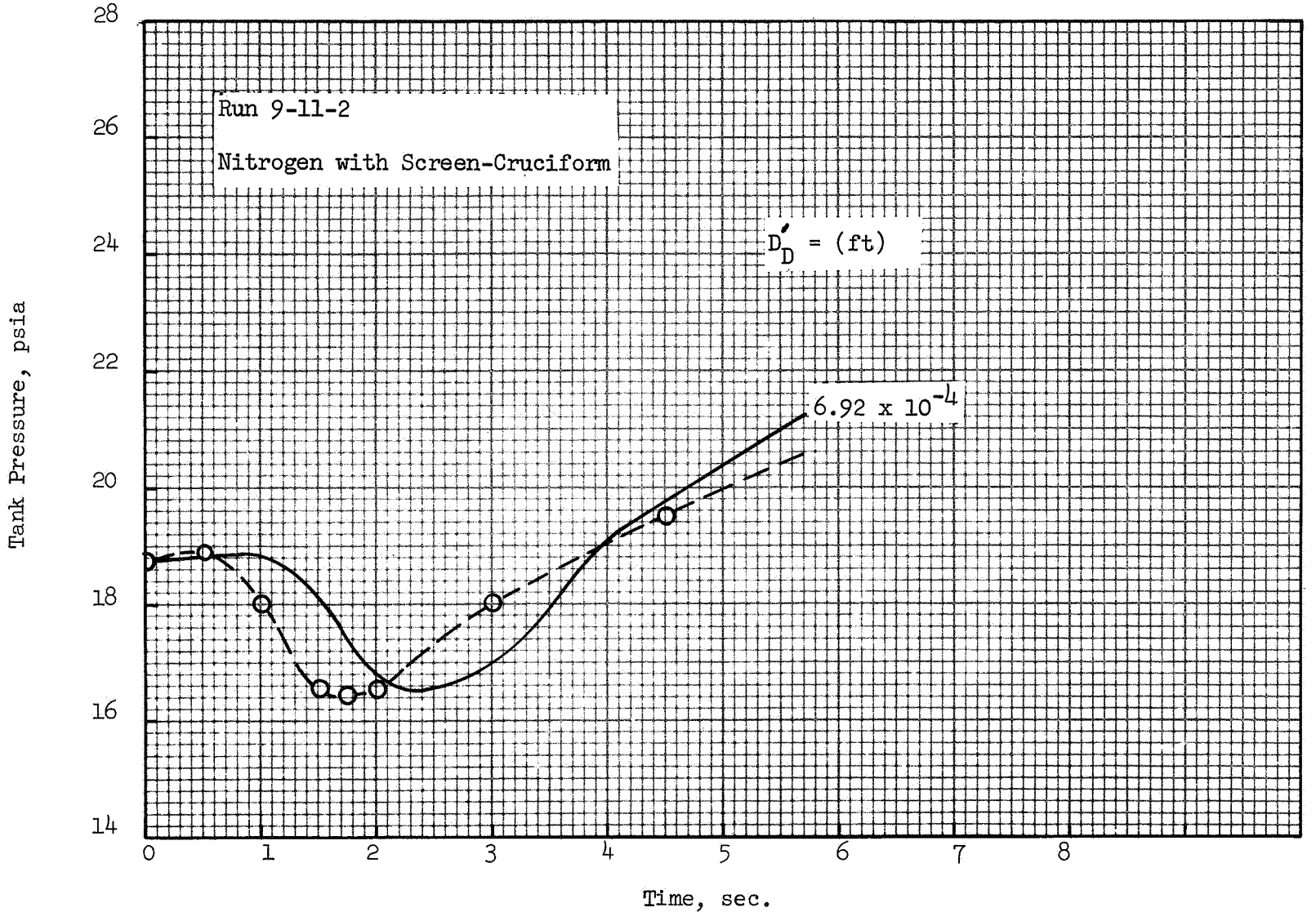


Fig.135 - Comparison of Pressure Data With Prediction for Run 9-11-2

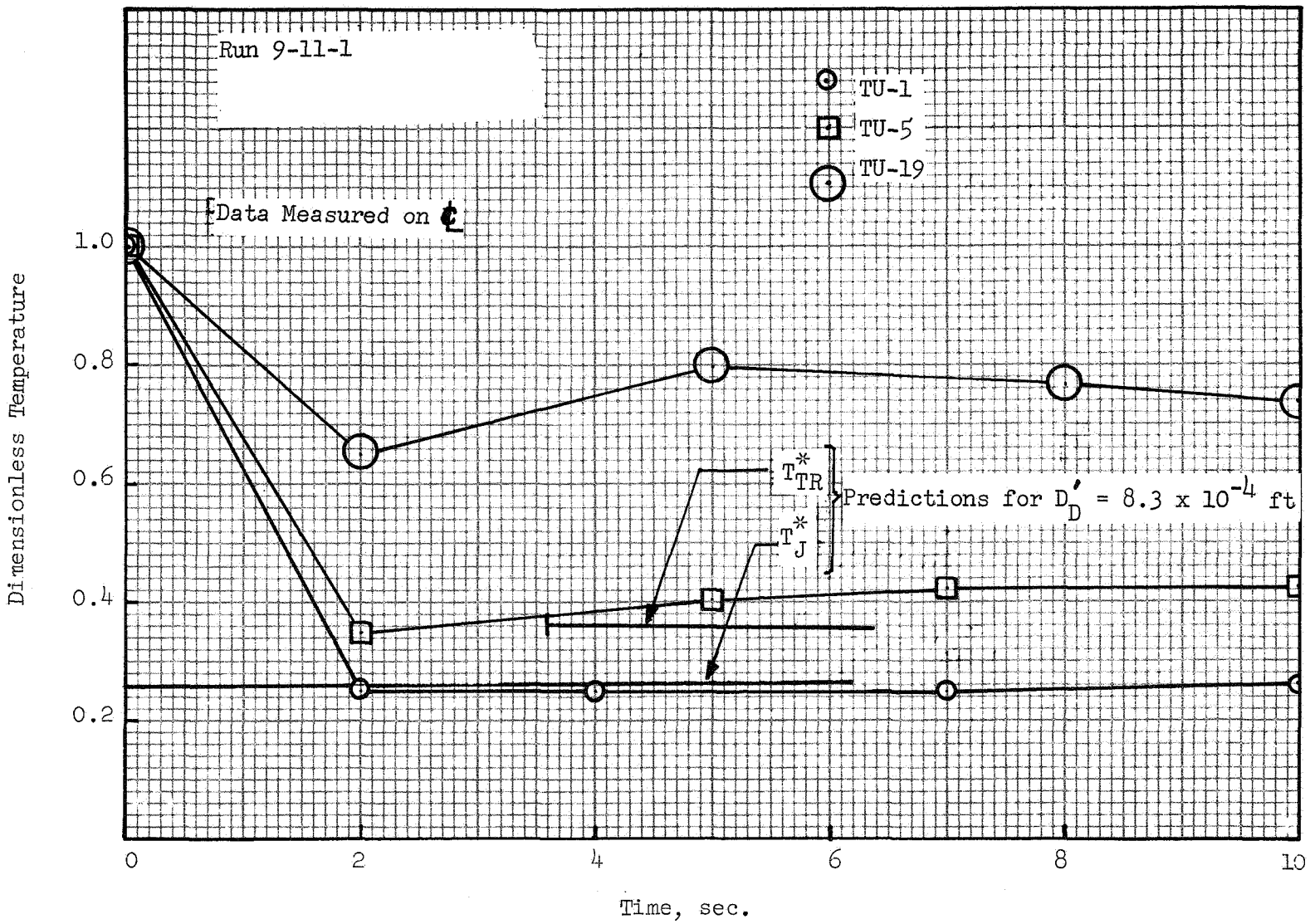


Fig. 136 Comparison of Gas Temperature Data With Predictions For Run 9-11-1

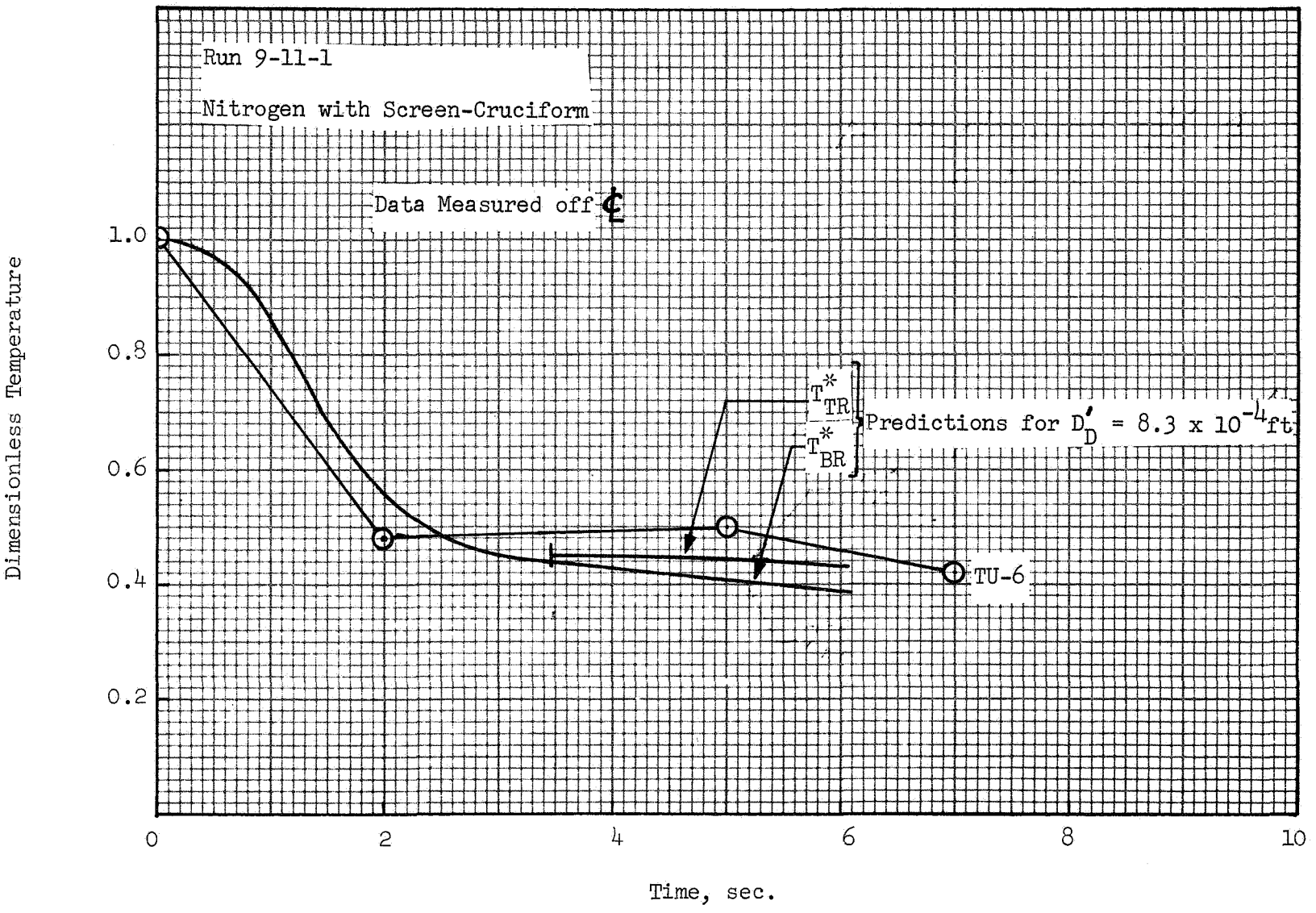


Fig.137-Comparison of Gas Temperature Data With Predictions For Run 9-11-1

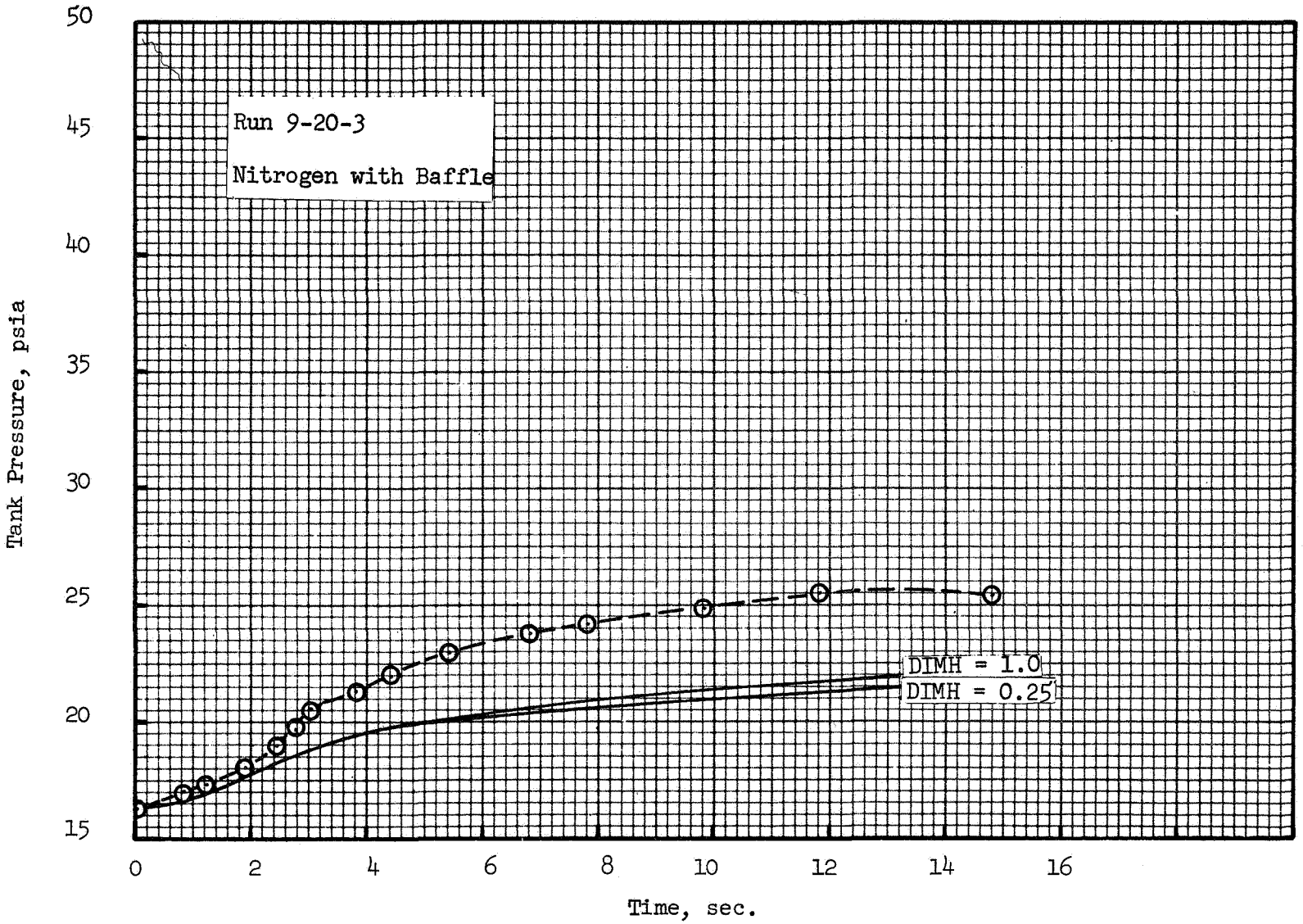


Fig.138-Comparison of Pressure Data With Predictions for Run 9-20-3

Evaporation also occurs at the liquid-tank vapor interface. Although this latter contribution to mass transfer is usually much smaller than that from boiling at the wall, it is included in the Model analysis. For the nitrogen run, the film boiling heat transfer coefficient used was 25.2 Btu/hr ft^2 ^oR and the ullage vapor-interface coefficient was taken as 0.2 Btu/hr ft^2 ^oR . As pointed out earlier the numerical value of this coefficient has a small effect in tank pressure response. The boiling coefficient can be input as a function of the wall-liquid temperature difference if desired. The manner in which the liquid spreads along the wall must also be specified for the wetted-wall model. For the purposes of this study arbitrary values for the dimensionless liquid height (DIMH) were chosen and assumed constant throughout each run. A value could be computed assuming dissipation of the incoming velocity head at the top of the liquid on the wall. The prediction curves for the tank pressure shown in Fig 138 are for liquid spreading over the entire wall (DIMH=1.0) and spreading to a height of 0.25 times the tank diameter. It is clear that this parameter is not significant in this case. This occurs because the amount of liquid being evaporated at the tank wall is small compared with the rate that mass is being added to the tank. As a result, an increase in this rate of evaporation by a factor of 3 (increasing DIMH from 0.25 to 1.0) has a very small effect on the tank pressure.

Thorough evaluation of the test data was made to determine the unsatisfactory comparison between predicted and measured pressure data for this run. Careful reevaluation was made of the analysis within the Model which describes liquid evaporation. It was found that even major changes in the analysis could not

bring the predicted and measured data into close agreement. For the first four seconds, all of the entering liquid evaporates (in the analysis) from the wall producing the maximum possible pressure rise over this time period. Fig 138 data clearly show a divergence of the curves. The conclusion reached is that the flow rate and/or quality data must be wrong for this run, at least at early times. For this run, liquid was first observed on the films at 0.835 seconds after the flash bulb was recorded. The void fraction meter registered liquid at 3.57 seconds after the first tank pressure rise was observed. In all other runs, liquid was indicated on the void fraction meter before it was observed on the films as would be expected. For this reason the quality and/or velocity data for this run are of doubtful accuracy and the corresponding pressure prediction must be regarded in this light. It should be noted, however, that when liquid begins to collect on the tank wall the slope of the pressure predictions agrees well with that of the data thereby supporting the validity of the wetted wall analysis used in the Tank Fill Model.

10.4.2 Liquid Hydrogen Tests

Analysis was made of the test data for liquid hydrogen using the Tank Fill Model. The pressure data comparison for hydrogen run 9-15-1 in which a baffle was used appears in Fig 139. For hydrogen baffle analysis a film boiling heat transfer coefficient of 64.5 Btu/hr ft^2 ^oF is used and, as with the nitrogen, an interfacial coefficient of 0.2 Btu/hr ft^2 ^oF is assumed. To better understand differences between measured and predicted pressure data the effect of the choice of gas velocity extrapolation at early times was investigated. The two extreme extrapolations used are shown in Fig 140.

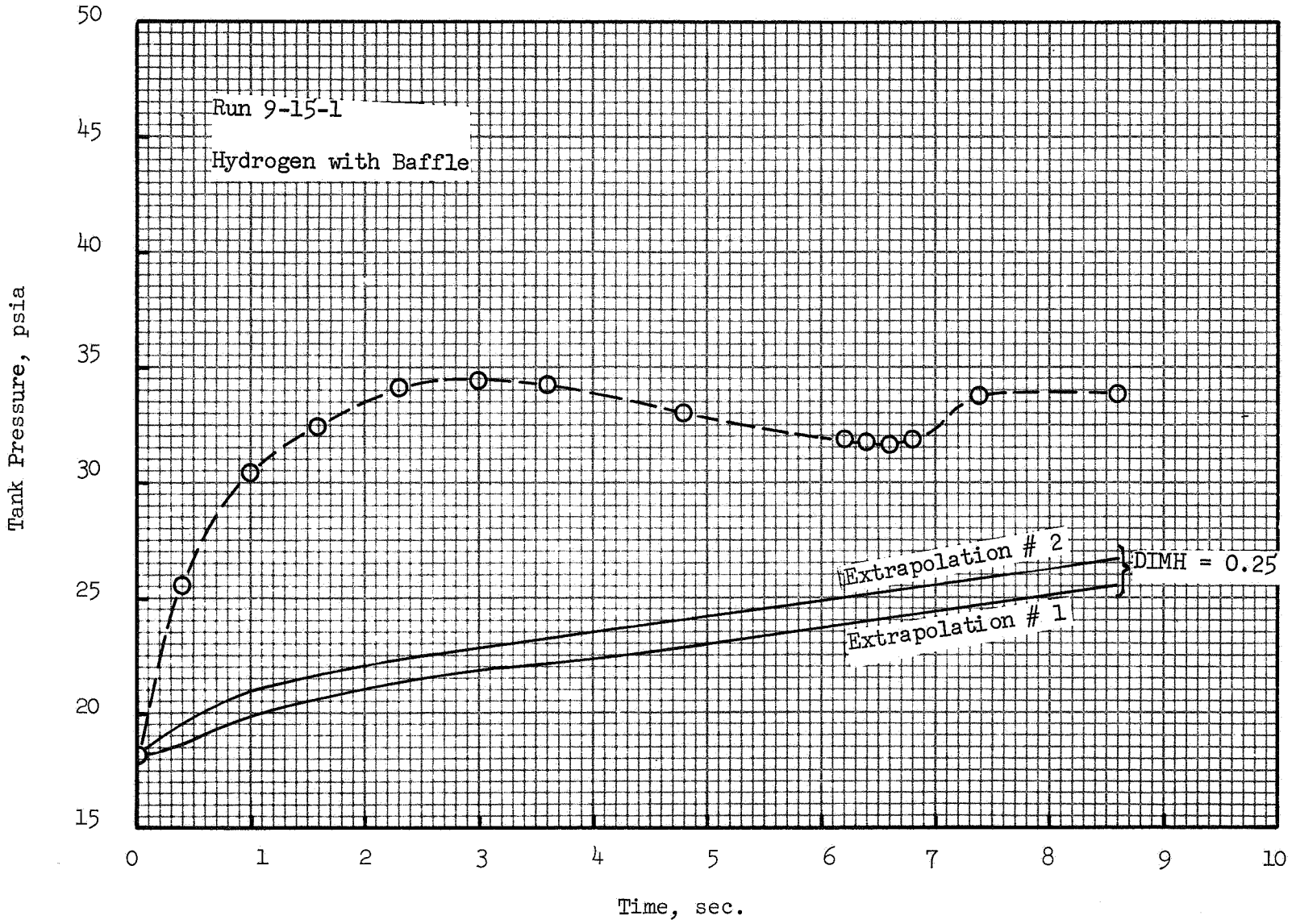


Fig.139-Comparison of Pressure Data with Predictions for Run 9-15-1

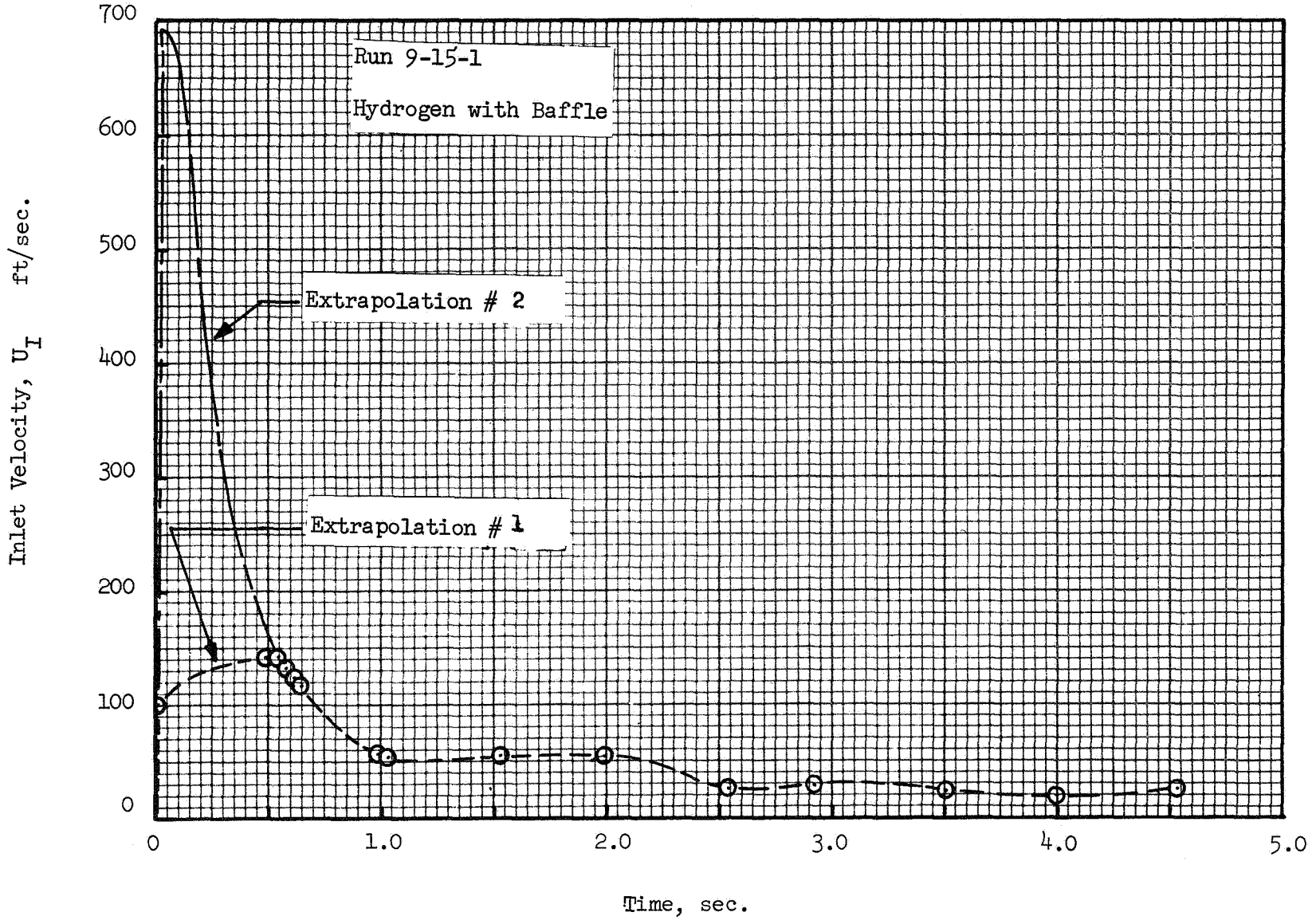


Fig. 140 Gas Velocity Extrapolations For Run 9-15-1

In this case an extrapolation of the velocity data to high initial values does not yield a prediction which, when applied in analysis, approaches the data. For this run the void fraction meter indicated liquid (with the interpretation of the data which was used) at approximately the same time that the first pressure rise was observed. When this quality history is input to the analysis a low pressure rise is predicted because the ullage vapor was found to be excessively cooled by the evaporating liquid. This is further illustrated in Fig 141, where the ullage gas temperatures measured on the tank centerline are compared with the predicted gas temperature.

Pressure data from another hydrogen baffle run (9-15-4) are shown in Fig 142. Again the prediction using a reasonable velocity extrapolation, cannot match the sharp initial pressure rise which was observed. However, the measured pressure level is attained and exceeded by the prediction at later times in this instance. In the analysis all of the incoming liquid is evaporated until approximately four seconds and thereafter liquid begins to accumulate on the tank wall. In reality these must be more mass entering the tank initially that indicated by the interpretation of the void fraction and film data as used in the analysis. At later times it is possible that the assumed value for DIMH is too large. Also, the resulting computed rate of evaporation at the wall could be too large as indicated by the slope of the predicted curve. The value of DIMH is much more significant for this run than for run 9-15-1 because the rate of evaporation at the tank wall is of the same magnitude as the rate of mass addition to the tank.

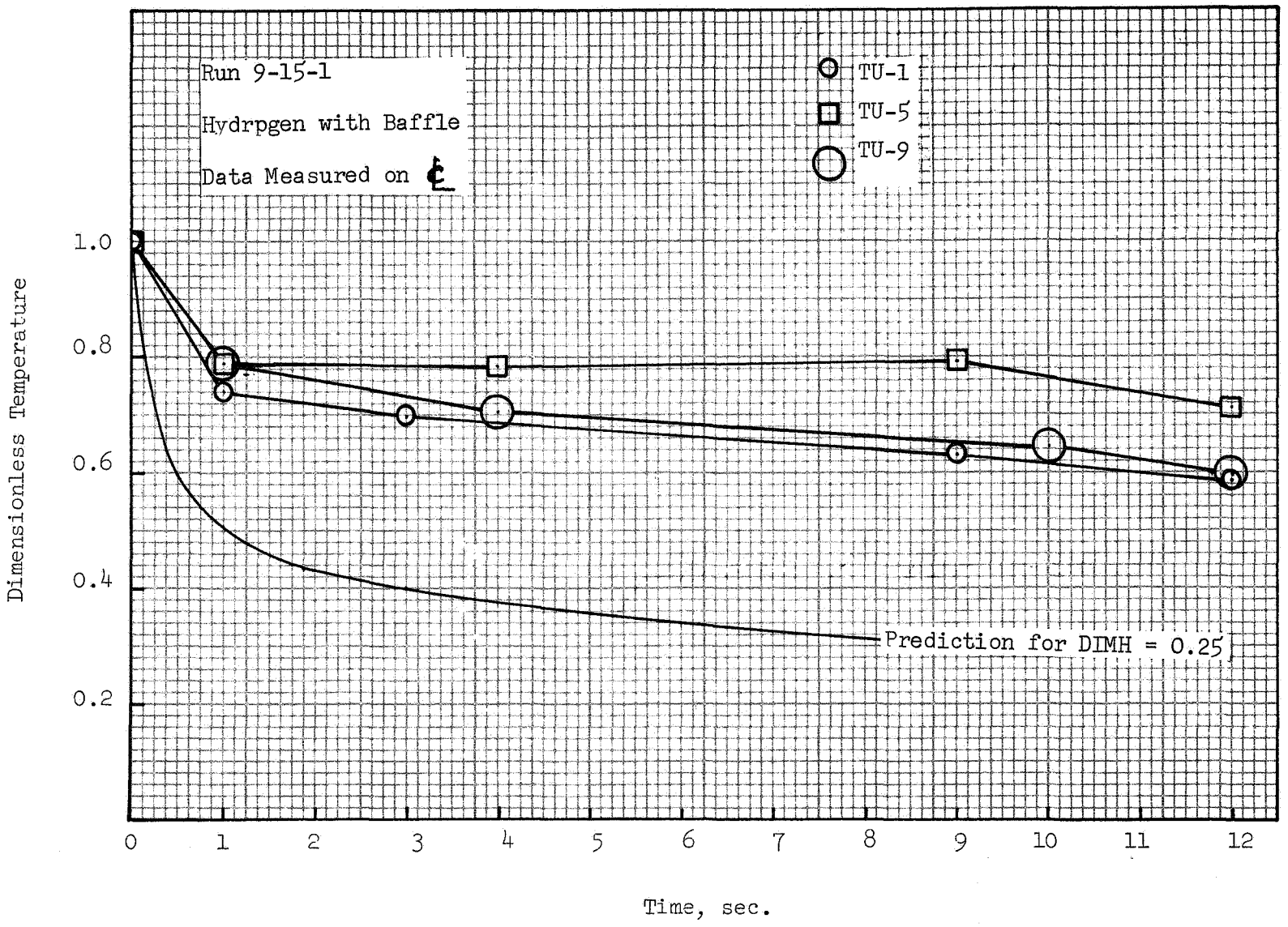


Fig.141-Comparison of Gas Temperature Data With Prediction For Run 9-15-1

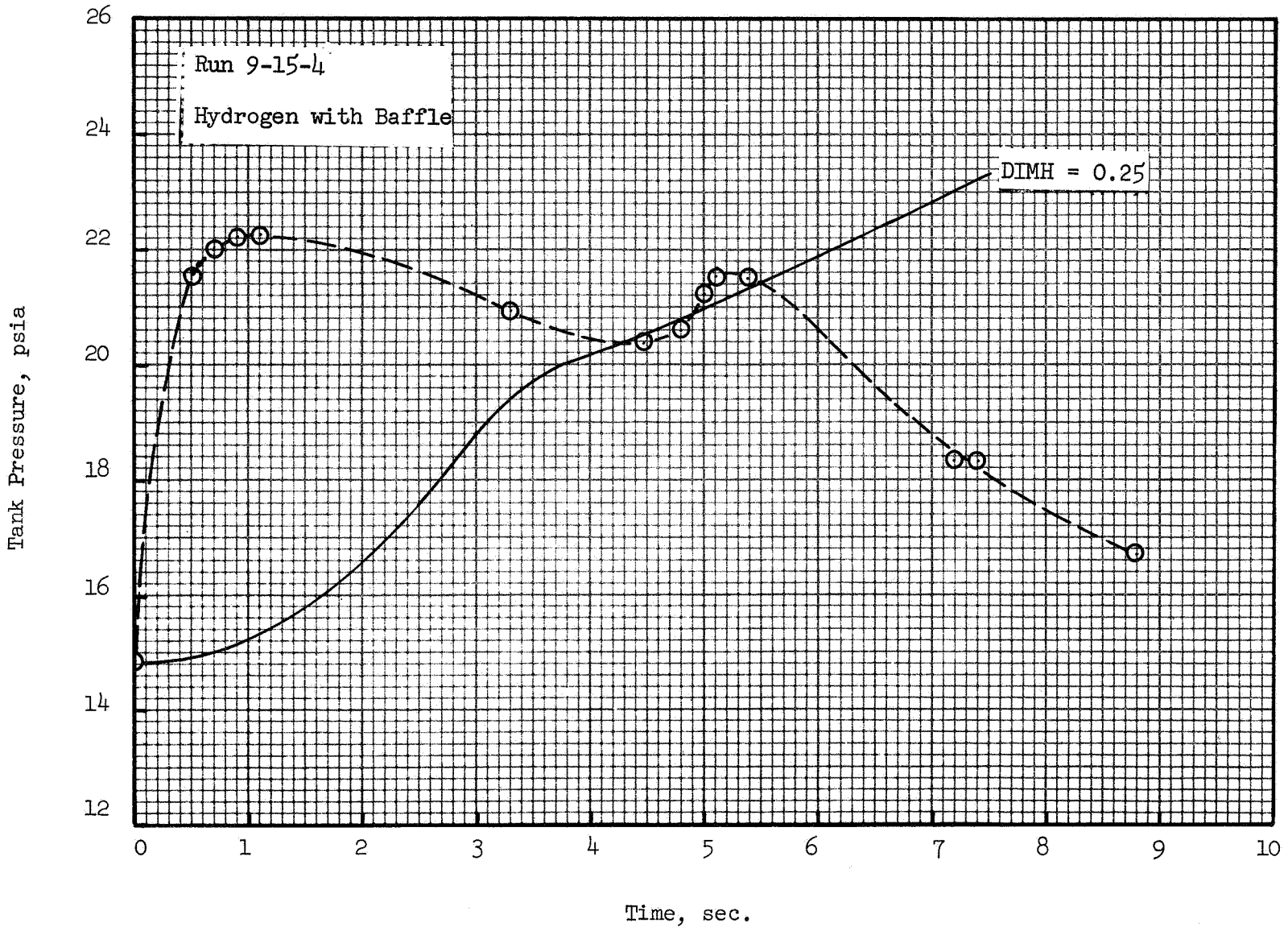


Fig.142 Comparison of Pressure Data With Prediction For Run 9-15-4

Section 11

CONCLUSIONS

The following sections contain a compilation of the major conclusions which have been reached as a result of the analytical and experimental studies described in the preceding sections. For convenience, these conclusions are presented under four headings, covering the work relating to transfer line flow, tank fill thermodynamics, complete fill system thermodynamics and implosion prevention.

11.1 TRANSFER LINE THERMODYNAMICS

An analytical technique has been developed which allows the prediction of the pipe wall temperature variation and the flowing fluid state during chilldown of a cryogenic transfer line. This technique has been very successful in estimating chilldown times for relatively long transfer lines. Both the analytical and experimental results indicate that, as the length-to-diameter ratio of the transfer line is decreased, the effects of surging dominate the fluid flow and heat transfer. The analytical model used for chilldown predictions does not account for these surges. Experimental studies have indicated that, for the "short" lines tested, high frequency surging can readily produce a form of two-phase flow known as slug flow. Modeling the fluid pressure drop and heat transfer for such a flow would be a very complex and demanding task.

Thus, while the existing analytical model is satisfactory for application to "long" lines (lines having an L/D ratio greater than 3800 for liquid hydrogen and 475 for nitrogen or oxygen), increasingly larger discrepancies are to be expected between observed and predicted chilldown times as the line length is decreased.

An analytical method of predicting the magnitude and frequency of flowrate oscillations during the initial stages of chilldown has been developed; agreement between predicted and measured values of the frequency and magnitude of these oscillations was generally between ± 10% of the measured values.

11.2 TANK FILL THERMODYNAMICS

An analytical technique has been developed which provides predictions of transient pressure and temperature variations in a tank being filled with a fluid of known thermo-and hydrodynamic properties. This analysis technique is not restricted to any given fluid or tank material or configuration, fill line orientation or gravity level. It has been used successfully to predict pressure and temperature variations in a tank being filled with a cryogenic fluid for tanks having an unobstructed inlet, or a baffled or screened inlet. Comparisons between prediction and test data have shown that these variations on a characteristic dimension of the liquid particles, or droplets, entering the tank. For tests performed during this study, the fluid initially entering the tank was generally in the form of a two-phase spray, with liquid as the dispersed, droplet phase. Prior to attempts at test data correlation, neither an analytical nor an emperical method of predicting the characteristic droplet diameter was available. As a result of comparisons between analytical predictions and test data an emperical method of specifying the characteristic droplet diameter was obtained.

By specifying the correct value for the characteristic droplet diameter, agreement between measured and predicted tank pressures during fill within ± 0.15 psia were obtained in fill tests with nitrogen. Corresponding values of ullage vapor temperatures were predicted within about ±5% of the absolute values of

the measured temperatures.

11.3 COMPLETE FILL SYSTEM THERMODYNAMICS

By coupling the transfer line and tank-fill analysis, an analytical technique has been developed which combines the capabilities of the two single techniques, the resulting computer program is capable of simulating the operation of a complete fill system. Comparisons with test data from four complete system tests were made; agreement between predictions and test data was quite good. During three of the four runs for which correlations were attempted, an implosion condition (drop in tank pressure below its initial value) was observed. The predicted pressure variation for these tests was generally within 1 psi of the measured values.

The complete fill system computer program, like the tank-fill program, may be used for fill from varying orientations and at any gravity level.

11.4 IMPLOSION PREVENTION TECHNIQUES

Both the analytical and the experimental work performed during this study have contributed toward an understanding of the mechanisms leading to an implosion, or a sudden drop in pressure, during tank fill with a cryogenic fluid. It was found that when a cryogenic liquid first enters the tank in the form of a droplet spray the droplets evaporate, extracting energy from the (relatively warm) ullage vapor. As a result the pressure and temperature of the ullage vapor becomes dominant and the pressure begins to rise. Consequently, any means of promoting energy interchange between the incoming, cryogenic fluid and the ullage vapor will tend to produce a drop in ullage pressure. Conversely, any means of reducing energy interchange between the entering fluid and the ullage

vapor (as with a solid baffle covering the tank inlet) will reduce the possibility of an implosion.

SECTION 12

REFERENCES

1. Massachusetts Institute of Technology, "Notes for Special Summer Program in Two-Phase Gas-Liquid Flow," by P. Griffith and S. W. Gouse, Jr., 27 July 1964.

2. Argonne National Laboratory, "Two-Phase (Gas-Liquid) Systems: Heat Transfer and Hydraulics, An Annotated Bibliography," by R. R. Kepple and T. V. Tung, ANL-6734, Argonne, Illinois, July 1963.

3. Massachusetts Institute of Technology, "An Index to the Two-Phase Gas-Liquid Flow Literature, Part 1," by S. W. Gouse, Jr., Report No. MIT-DME-8734-1, May 1963.

4. O. Baker, "Design of Pipe Lines for Simultaneous Flow of Oil and Gas," Oil and Gas J., 26 July 1954.

5. M. G. Hubbard and A. E. Dukler, "The Characterization of Flow Regimes for Horizontal Two-Phase Flow," Proceedings of the 1966 Heat Transfer and Fluid Mechanics Institute, Stanford, California, Stanford University Press, 22-24 June 1966.

6. E. S. Kordyban, "A Flow Model for Two-Phase Slug Flow in Horizontal Tubes," J. Basic Eng., December 1961, pp. 613-618.

7. S. W. Gouse, Jr., and C. Hwang, "Visual Study of Two-Phase, One-Component Flow in a Vertical Tube with Heat Transfer," ASME Paper No. 63-WA-165.

8. W. R. Zahn, "A Visual Study of Two-Phase Flow While Evaporating in Horizontal Tubes," ASME Paper No. 63-WA-166, 17 November 1963.

9. J. C. Bronson, et al., "Problems in Cool-Down of Cryogenic Systems," Adv. in Cry. Eng., Vol. 7, K. D. Timmerhaus, ed., New York, Plenum Press, 1962, p. 198.

10. P. Griffith and G. Wallis, "Two-Phase Slug Flow," J. Heat Transfer, August 1962, p. 307-320.

11. W. J. Alspach and T. M. Flynn, "Considerations When Using Turbine Type Flow Meters in Cryogenic Service," Advance in Cryogenic Engineering Vol. 10 pp. 246, 1964.

12. NBS Report No. 9268 - 24th P.R. to NASA on Cryogenic R&D for Period Ending 12-31-66.

13. "Cool-down Times for Simple Cryogenic Pipetimes," W. G. Steward, R. V. Smith, J. A. Brennan, NBS Cryogenics Division, Boulder, Colorado.

14. J. H. Chi and A. M. Vetere, "Two-Phase Flow During the Transient Boiling of Hydrogen and Determination of Non-Equilibrium Vapor Fractions," Advances in Cryogenic Engineering, Vol. 9, p. 243, 1963.

15. J. W. H. Chi, "Cool-down Temperatures and Cool-Down Time During Mist Flow," Advances in Cryogenic Engineering, Vol. 10, p. 330, 1964.

16. National Bureau of Standards, Boulder Laboratories, "An Experimental Report on Cool-down of Cryogenic Transfer Lines," by J. A. Brennan, et. al., NBS Report No. 9264, Boulder, Colorado, 7 November 1966.

17. Steward, W. G., Smith, R. V. and Brenna, J. A., "Cool-down Time for Simple Cryogenic Pipelines," to be published.

18. R.V. Smith, "Some Idealized Solutions for Choking, Two-Phase Flow of Hydrogen, Nitrogen, and Oxygen," Advances in Cryogenic Engineering, vol. 8, Plenum Press, New York, 1963, pp. 563-573.

19. S.W. Gouse, Jr., and G.A. Brown, "A Survey of the Velocity of Sound in Two-Phase Mixtures," A.S.M.E. Paper 64-WA/FE-35, October 1964.

Appendix A

CALIBRATION OF LIQUID VOLUME FRACTION METER

The volume fraction measuring system is illustrated in the block diagram of Figure A-1. It consists of a scintillation detector (and preamplified), a pulse height analyzer (scaler-timer); a high voltage power supply and a Cd.109 X-ray source (8 mc). In addition, a digital-to-analog converter and oscillograph recorder are used to convert the scaler digital droplet to a DC output and record the signal. The Cd.109 radioactive source was chosen because a weak X-ray (22 Kev) was determined to give good resolution for the present application.

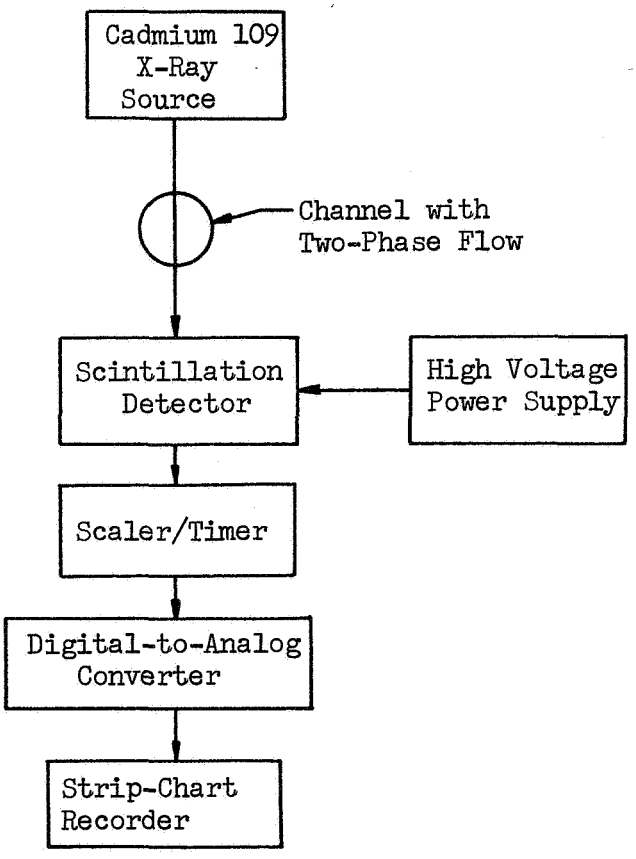


Fig. A-1 Schematic Diagram of Liquid Volume Fraction Measuring System

Although the volume fraction meter is a very useful device, it measures "instantaneous" volume (or mass) fraction, not quality. Furthermore, the fluid flow geometry affects the results of the meter calibration. Quality can only be determined if the slip ratio is determined independently. Two methods of calibration of the meter for use with LN_2 were considered: (a) use of an analog non-cryogenic liquid and non-condensible vapor combination, and (b) use of an analog solid-gas combination. The former was chosen since it was felt the true flow geometry could be best simulated. From a calculation of the absorption cross sections for 22 Kev X-rays, it was found that a methanol (CH_3OH) - ethanol (C_2H_5OH) mixture would simulate LN_2 absorption cross section: i.e.,

$$(\mu' \rho)_{LN_2} = 0.372 \text{ cm}^{-1}$$

$$(\mu' \rho)_{meth.} = 0.398 \text{ cm}^{-1}$$

$$(\mu' \rho)_{eth} = 0.359 \text{ cm}^{-1}$$

where μ' is the mass absorption coefficient (tabulated in Ref. 5 for different molecules and as a function of X-ray energy), ρ the fluid density in the equation $I=I_o e^{-\mu' \rho x}$, and x is length.

The arrangement of the scintillation detector, Cd-109 source, lead collimation, and 1/2-inch diam tube is shown in Figure A-2. These components are mounted in the tee section which is used in the transfer line and sphere tests.

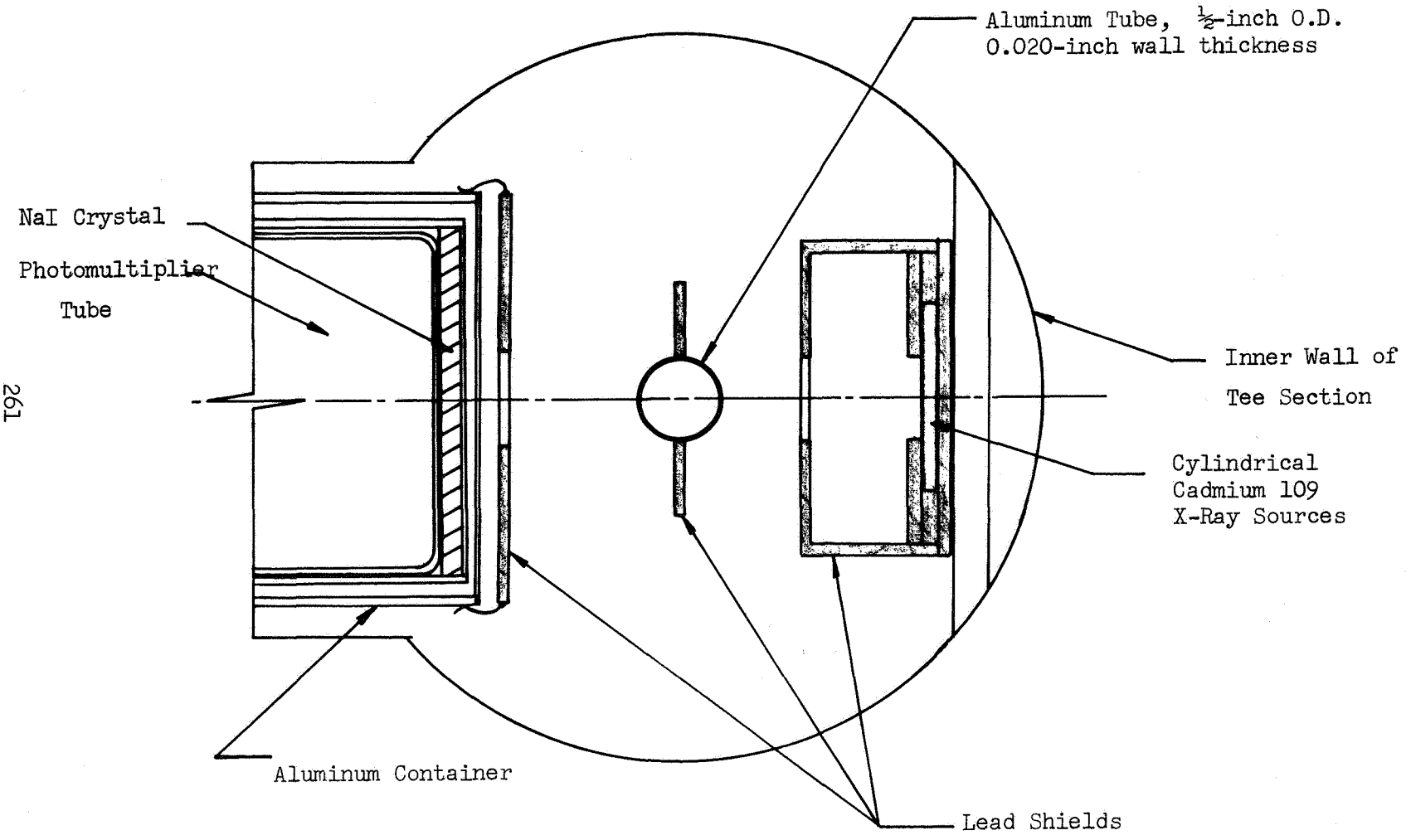


FIGURE A-2 Arrangement of Detector, Source Tube and Shielding.

To ensure a high sensitivity, a relatively thin-walled aluminum tube, 1/2-inch O.D. by 20 mil wall and 4-13/16 inches long, is used, since aluminum has a relatively low absorption cross section. It was necessary to mount the scintillation detector in the tee in an aluminum can with a 10 mil aluminum window to prevent large deflections of the beryllium window on the detector due to pressure differences inside and outside the detector.

Preliminary tests were made to establish the operating high voltage, the scaler window width and the Cd-109 spectrum. With the scaler in integral mode (counts all pulse above E_{min}) the count rate was determined as a function of E_{min} (window voltage lower level) and E_H (phototube high voltage). The results shown in Figure A-3 indicate that most of the pulses (i.e., the 22 Kev-photo peak) occur in the range $1.0 < E_{min} < 2.0$ volts and for $E_H \approx 1200$ volts. A high voltage value of E_H = 1190 volts was selected. Next, the source spectrum was run using E_H = 1190 volts for both 100% ethanol and 0% ethanol (air) to determine if there was a significant spectrum shift over the extreme liquid fraction range. These spectra, shown in Figure A-4 are seen to be very similar. The 22 Kev-photopeak occurs at E_W = 1.0 volts and the 88 Kev peak at E_W = 3.9 volts. The scaler multiplication factor at E_H = 1190 volts is therefore approximately 22 Kev/volt. Since it is desired to use only the 22 Kev radiation, the window settings for subsequent calibration and test were selected to be E_{min} = 0.25 volts (window lower bound) and E_{max} = 1.80 volts (window upper bound). Since these occur at low points on the spectrum, errors are minimized due to small inaccuracies in their settings. The scaler settings to be used are:

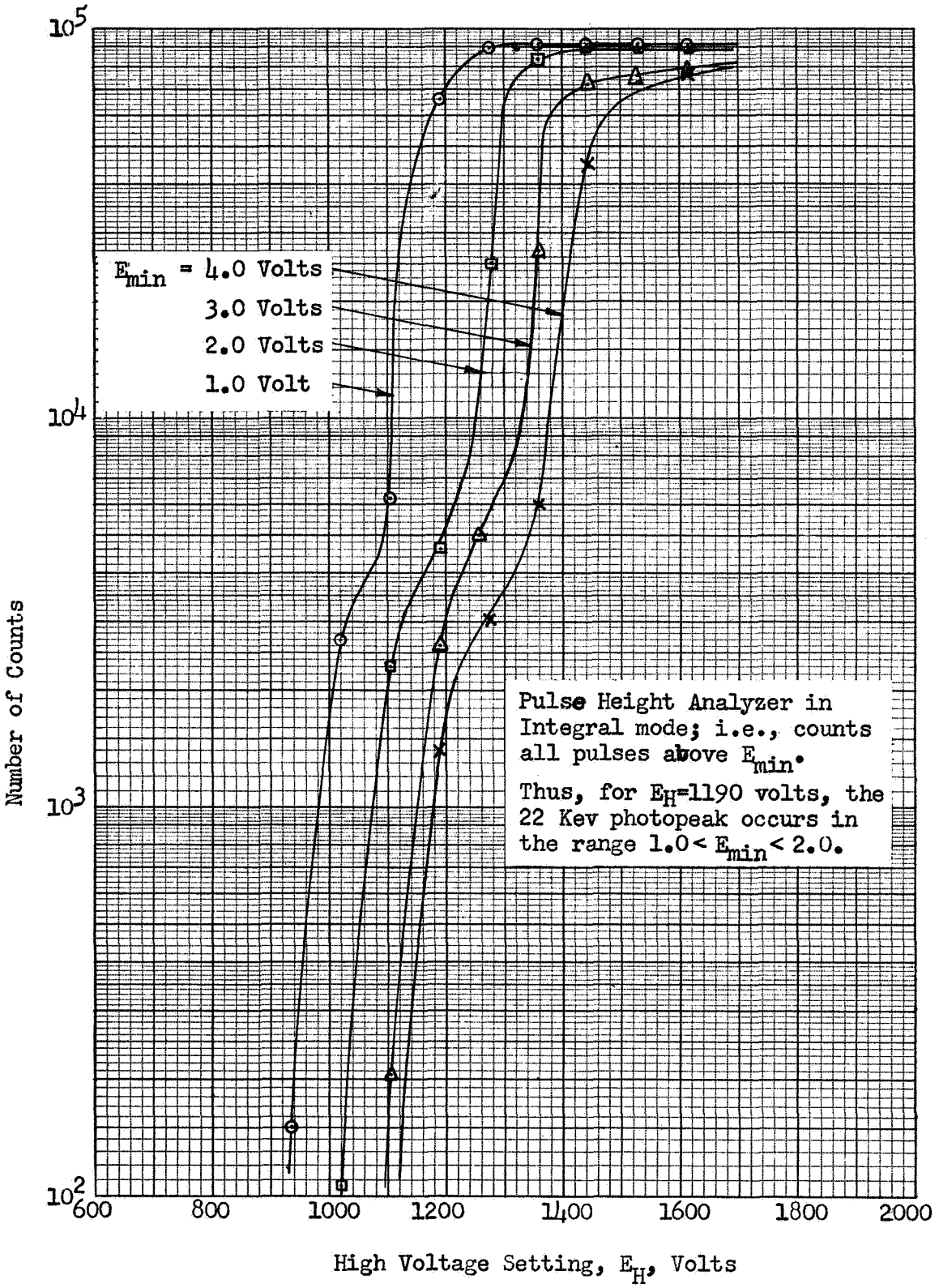


FIGURE A-3. Relationship Between Cadmium 109 Activity and High Voltage Setting

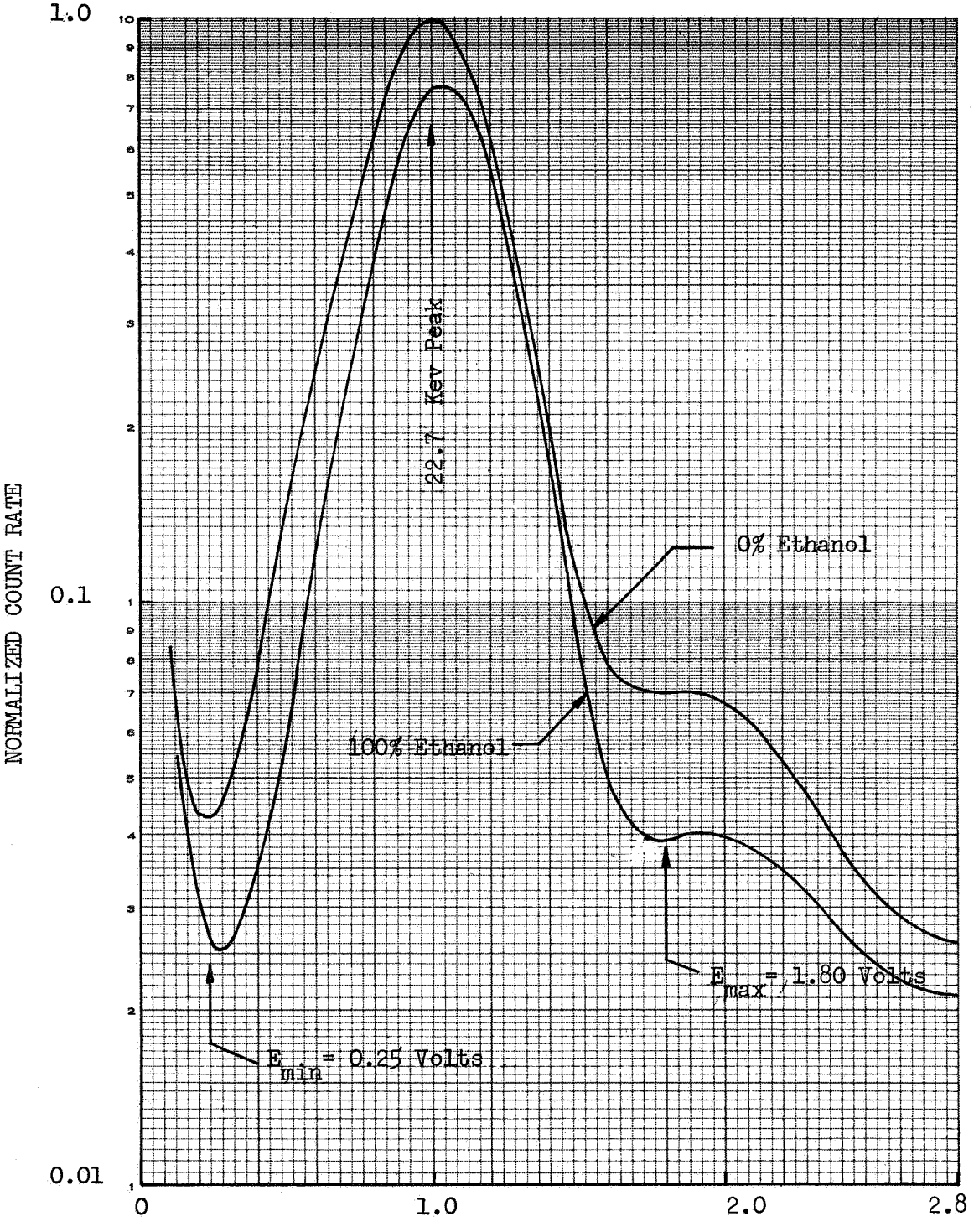


FIGURE A-4(a) Cadmium 109 Spectrum with Ethanol

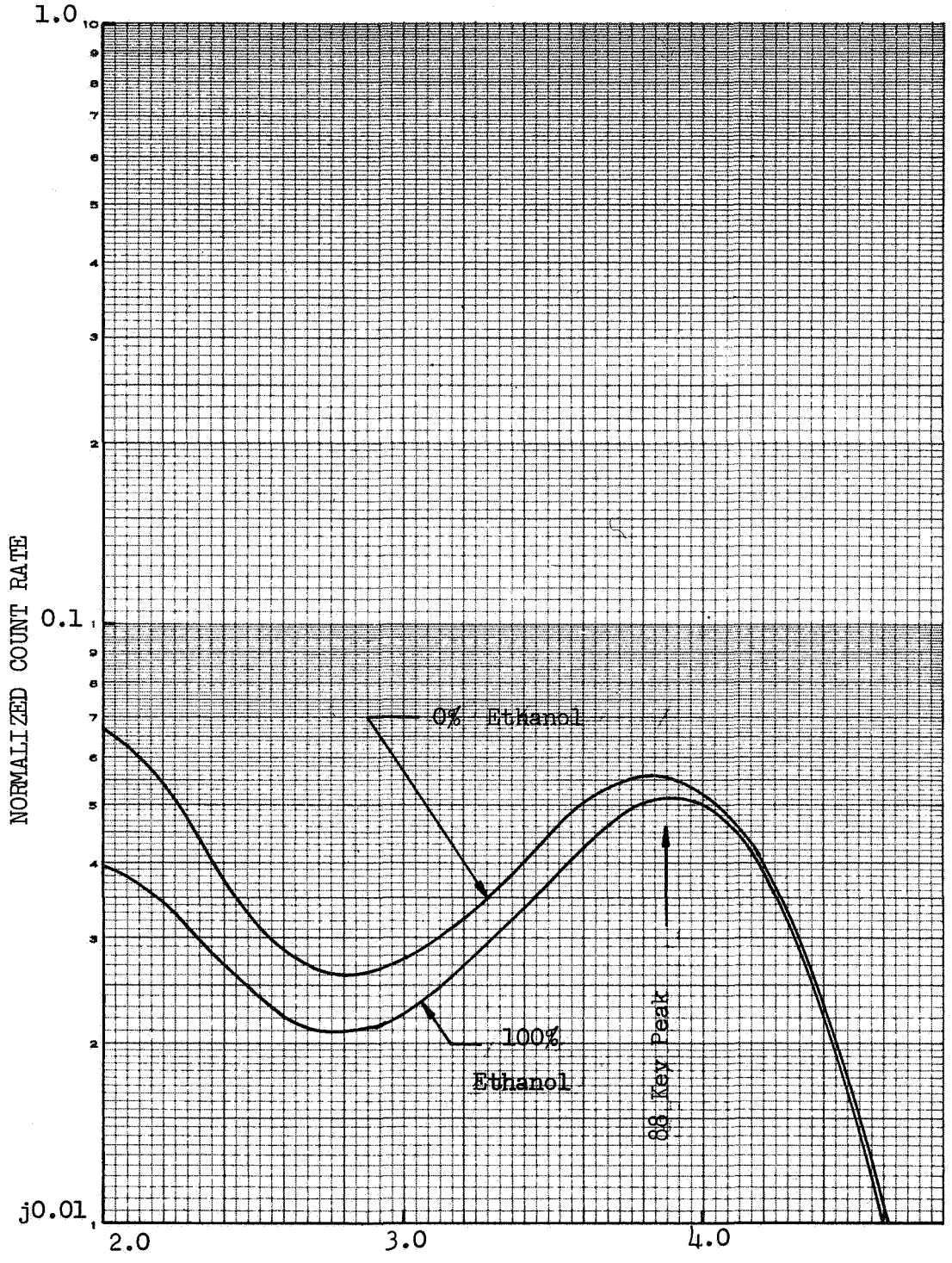


FIGURE A-4(b) Cadmium 109 Spectrum with Ethanol

E_H = 1190 volts (high voltage)

X 100 gain (preamplifier)

E_{min} = 0.25 volts (lower window bound)

E_{max} = 1.80 volts (upper window bound)

It is desirable to operate at as high a count rate as possible; however, the resolution of pulses begins to drop off significantly above 100,000 cts/sec. The lead shielding around the aluminum tube was selected as shown in Fig. A-3 to give a maximum count rate (i.e., for no liquid) of approximately 175,000 cts/sec. Since actual calibration is being performed, the loss of some pulses will not affect the accuracy of the measurement and a high count rate is desirable. The end points for LN_2 have been run and were:

0% LN_2 - 174.35 Kcts/sec

100% LN_2 - 129.57 Kcts/sec

The all liquid condition for both methanol and ethanol were:

100% methanol - 127.66 Kcts/sec

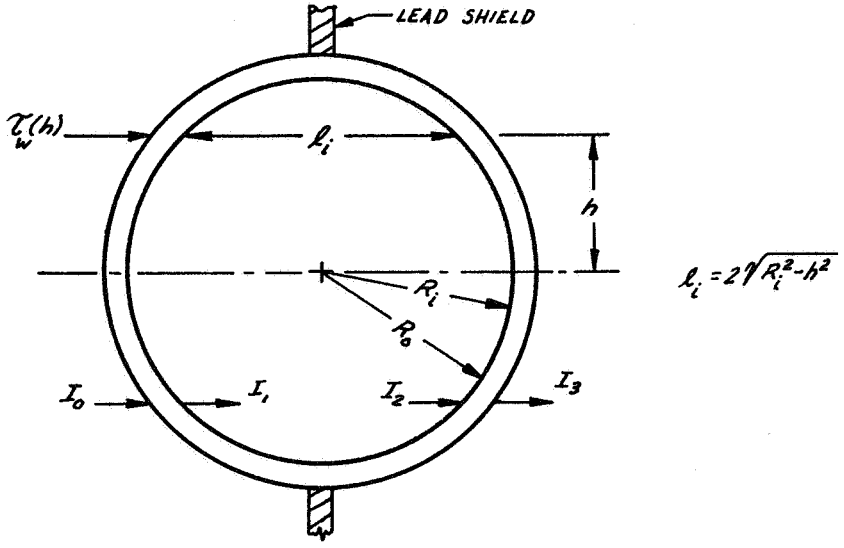
100% ethanol - 129.29 Kcts/sec

Since the latter simulates LN_2 within 1/2% of the difference in count rate between the all gas (GN_2) and all liquid (LN_2) cases ethanol was used as the calibration fluid to simulate LN_2.

The calibration technique consisted of passing measured quantities of GN_2 and ethanol (liquid) in a thoroughly mixed condition through the volume fraction measuring station. The calibration therefore represents the

homogeneous two-phase flow distribution. The system is sketched in Figure and shown photographically in Figure A-6.The ethanol and GN_2 flow rates are measured by the turbine flow meter and calibrated rotometers respectively. The two fluids are thoroughly mixed in the mixing section to ensure equal liquid and gas velocity as the mixture passes downward through the measuring station. Since there is little evaporation or gas absorption, the volume fraction of each phase can be computed from the measured flow rates, assuming equality of liquid and gas velocities. It was found that at the extreme of volume fraction and primarily for low liquid fractions, it was difficult to maintain a thoroughly mixed condition. However, over the major portion of the range from 0 to 100% liquid, the technique was successful. The results are presented in FigureA-7 where some deviation is seen for low liquid fractions.

In addition to this experimental calibration, the functional relation between transmitted radiation flux (count rate) and liquid volume fraction was computed for the circular tube and fluid, assuming a plane X-ray flux initially. For the geometry shown in the following sketch:



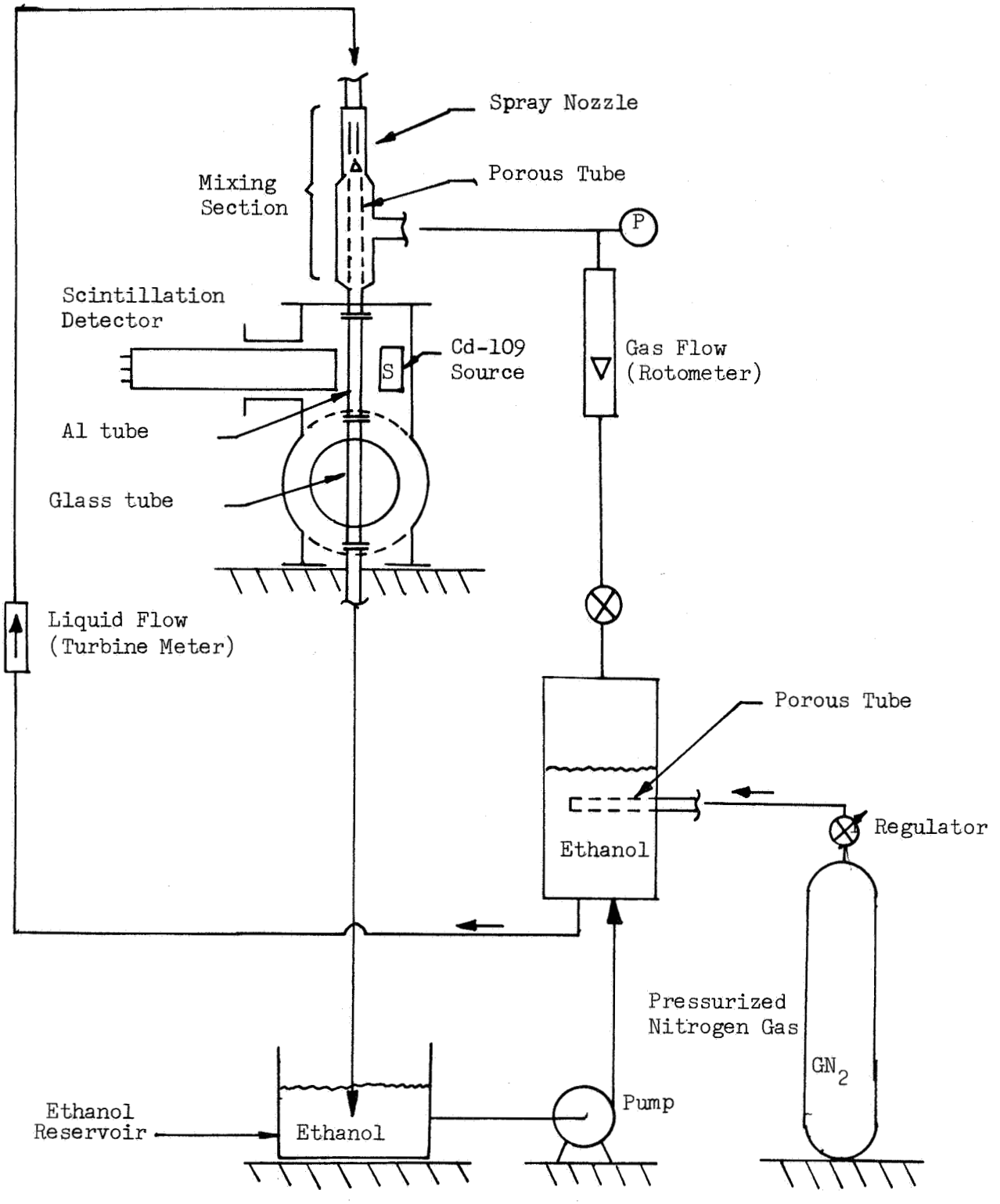


FIGURE A-5 Schematic Diagram of Calibration Apparatus for Liquid Fraction Measurement System

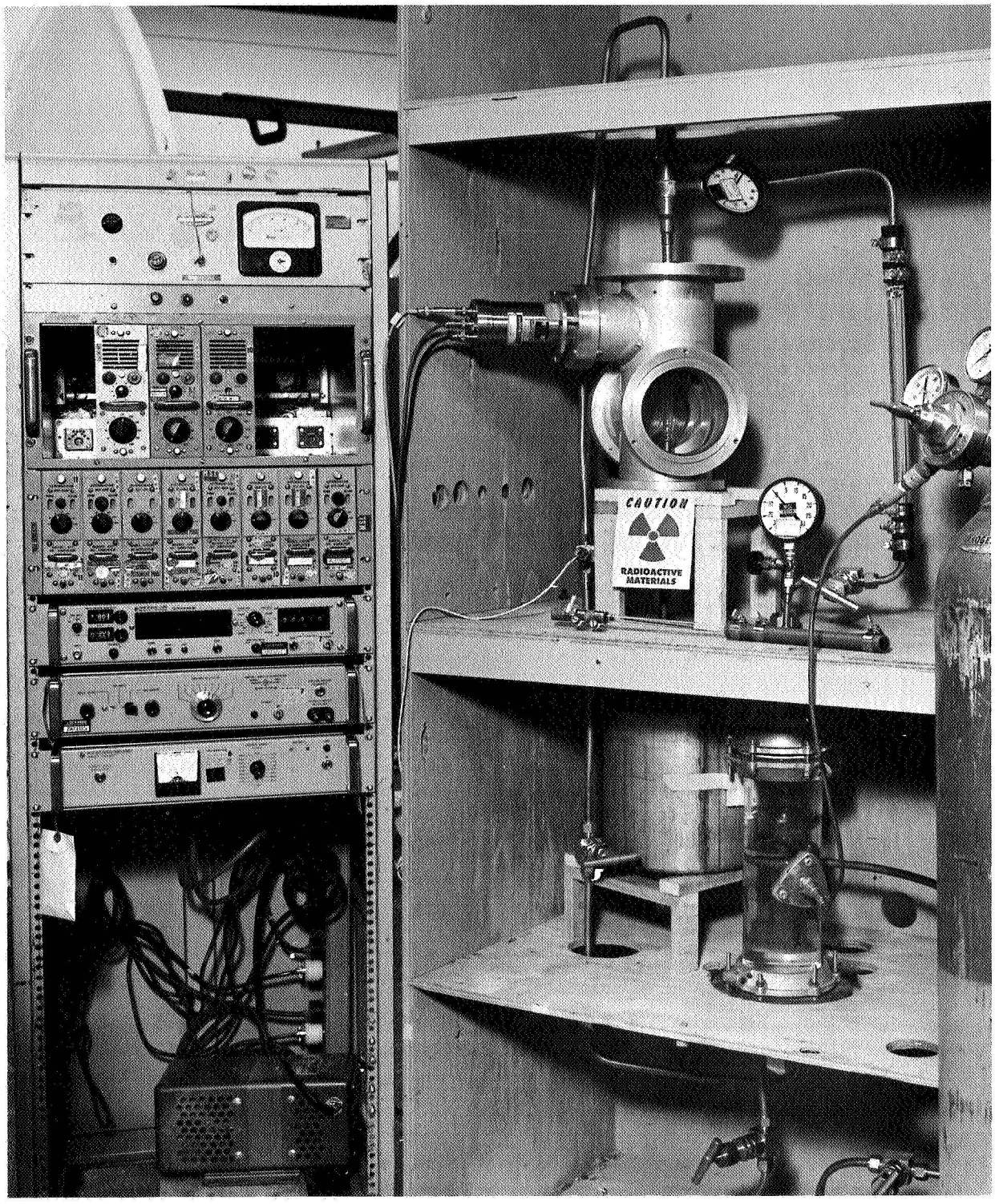


FIG. A-6 Liquid Volume Fraction Meter Calibration Apparatus

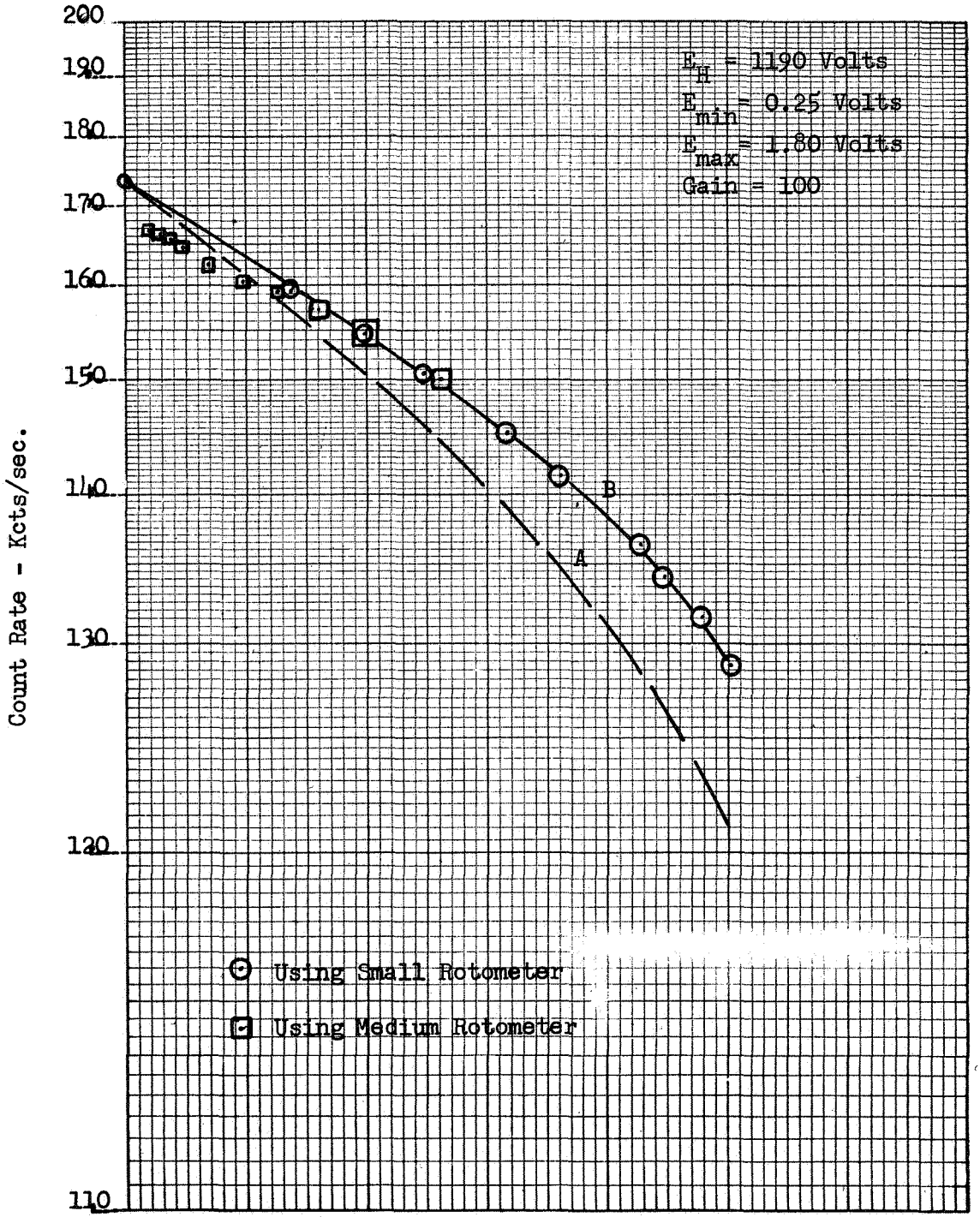


Fig. A-7 Calibration of Volume Fraction Measurement System

The relations between the fluxes I_0, I_1, I_2 and I_3 as a function of h and mean liquid volume fraction F_L are:

$$I_1(h) = I_o\, e^{-\mu_A' \rho_A \tau_w(h)}$$

$$I_2(h) = I_1\, e^{-\mu_L' \rho_L F_L \ell_i(h)}$$

$$= I_o\, e^{-\mu_A' \rho_A \tau_w(h)}\, e^{-\mu_L' \rho_L F_L \ell_i(h)}$$

and similarly:

$$I_3(h) = I_o\, e^{-\left[2\mu_A' \rho_A \tau_w(h) + \mu_L' \rho_L F_L \ell_i(h)\right]}$$

where the subscripts A and L refer to aluminum and the liquid, respectively. Eq. A-1 was integrated numerically over $-R_o \le h \le R_o$; for the geometry of interest R_0 = 0.50 inch and $\tau_w(o)$ = 0.020 inch and for aluminum property values of ρ_A = 2.82 g/cm^3 and μ_A' = 2.44 cm^2/gm, and ethanol property values of ρ_L = 0.794 and μ_L' = 0.462 cm^2/gm. The results are shown on Figure A-7as curve A normalized to the 0% liquid-count rate. The curve shows 5% deviation from the calibration data at 100% liquid, and it is not expected that the calculation should be exact because the portion of the X-ray spectrum used is from approximately 5.4 to 39 Kev and a mean mass absorption coefficient corresponding to 22 Kev X-ray was used. The end points for the calibration are known to be accurate. The shape of the curve is of primary importance, and since it is very similar in shape to the calibration data (except for low F_L), confidence in the calibration data is greatly increased. Curve (B) will be the established calibration curve and it is replotted in dimensionless form in Figure A-8.

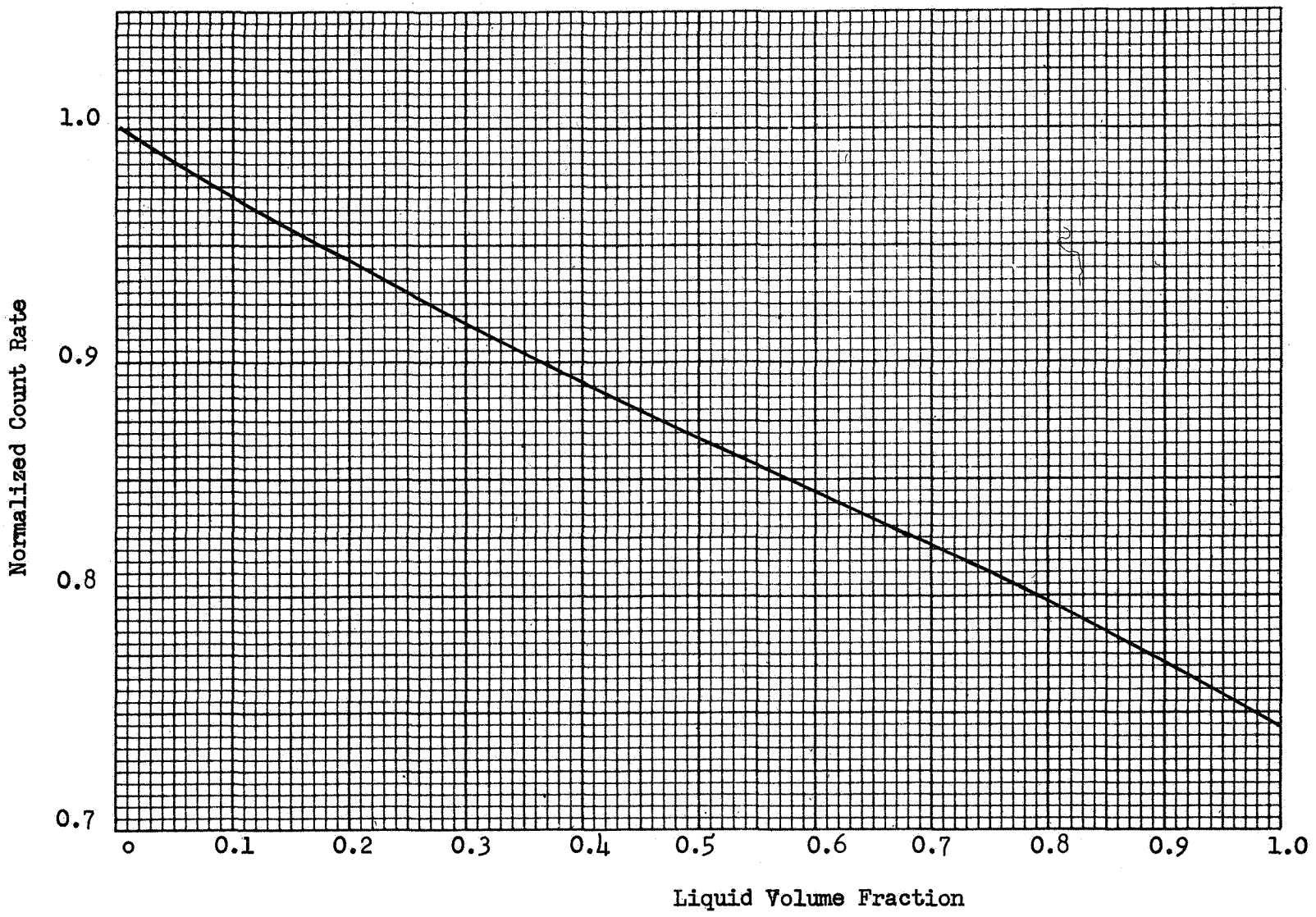


FIGURE A-8 Normalized Calibration Curve for Volume Fraction Measuring System

Appendix B

LITERATURE SURVEY AND PRELIMINARY CALCULATIONS

B.1 LITERATURE SURVEY

The objective of this task is to collect in a central location the results of work previously performed in the following areas:

- Line Chilldown Analysis
- Receiver Tank Thermodynamics
- Transfer of Cryogenic Fluids
- Receiver Tank Implosion
- Two-Phase Flow in Cryogenic Fluids
- Experimental Studies of Transfer Line and Receiver Tank Behavior During Cryogenic Liquid Transfer

Virtually all of the literature reviewed has pertained to the problem of transfer line chilldown or such related phenomena as the characterization of two-phase flow geometry and quality measurement. Because of the extremely large number of references available on the subjects (over ten thousand on two-phase-gas-liquid flow alone), the review was restricted to only the most recent, pertinent references and those of a bibliographical nature. Three of the most notable of the latter are included in this report as References 1, 2, and 3.

Abstracts of the pertinent references, many of which have been used extensively in the transfer line analysis, have been reviewed by individuals working on specific tasks.

B.2 PRELIMINARY CALCULATIONS

The objective of preliminary hand calculations of transfer line and receiver tank conditions was to provide an estimate of the boundaries of parameters which should be varied during initial flow phenomena tests, and to give some insight into the magnitude of changes in mass and energy transfer required to produce significant eff cts on receiver-tank internal pressure and inlet flow geometry. These estimates have been directed primarily toward two areas which are expected to strongly influence planning and execution of the flow phenomena tests:

1. The flow pattern occurring in two-phase fluid flow in the transfer line
2. The gross thermodynamic phenomena affecting transient pressure changes within the receiver tank during fill

B.2.1 Two-Phase Flow Maps

Researchers have recognized several two-phase flow patterns; in an attempt to analyze two-phase flow phenomena, they have categorized these patterns on the basis of empirical observations. These classification attempts have been made because, owing to the complex nature of the two-phase flow phenomenon, there are presently no analytical models applicable over the entire range of two-phase flow flow geometries. If the flow pattern is known, the appropriate analytical model can be chosen; and, subsequently, pressure drops and heat-transfer coefficients can be determined.

The number of distinct two-phase flow patterns is somewhat arbitrarily determined and varies from observer to observer. Because of the asymmetric direction of the gravity vector, generally more flow patterns are distinguishable for horizontal two-phase flow than for vertical flow. Alves (Ref. 4) has described these flow patterns as follows:

1. Bubble Flow. Flow in which bubbles of gas move along the upper part of the pipe at approximately the same velocity as the liquid. This type is similar to froth flow, in which the entire pipe is filled with a froth similar to an emulsion

2. Plug Flow. Flow in which alternate plugs of liquid and gas move along the upper part of the pipe

3. Stratified Flow. Flow in which the liquid flows along the bottom of the pipe and the gas flows above, over a smooth liquid-gas interface

4. Wavy Flow. Flow which is similar to stratified flow except that the gas moves at a higher velocity and the interface is disturbed by waves traveling in the direction of flow

5. Slug Flow. Flow in which a wave is picked up periodically by the more rapidly moving gas to form a frothy slug which passes through the pipe at a much greater velocity than the average liquid velocity

6. Annular Flow. Flow in which the liquid forms in a film around the inside wall of the pipe and the gas flows at a high velocity as a central core

7. Spray Flow. Flow in which most or nearly all of the liquid is entrained as spray by the gas. This has also been called dispersed flow.

Geometries typical of these types of flow are illustrated in Fig B-1.

In an attempt to define the various flow patterns in terms of flow properties, a variety of flow geometry maps have been devised. Most of the experimental data with which these correlation attempts have been conducted were gathered under adiabatic or isothermal two-component conditions in which the ratio of gas to liquid mass flow along the pipe remains constant.

Figs. B-2,B-3 and B-4 illustrate four of the proposed correlations. The symbols symbols used on these plots are identified in Table B-1.

Of these flow maps, the one which has received the most attention is the Baker correlation (Fig B-2).An advantage of this map is that the correlation parameters include physical properties of the fluid, thus making the correlation more specifically applicable to a particular flow.

The Baker correlation is based on data obtained from the adiabatic flow of a two-component water-air mixture flowing at atmospheric pressure in a pipe. The various lines on the map indicate general regions of transition rather than distinct flow boundaries. Data for two-component adiabatic flow, obtained from Ref. 4 and 5, have been plotted on Fig. B-2.

The data obtained from Ref. 4 are a compilation of the work of three independent investigators, Alves, Gazley, and Kosterin.

The parameters used in Baker's correlation are defined as

$$\lambda = \left[\left(\frac{\rho_g}{7.5 \times 10^{-2}}\right)\left(\frac{\rho_\ell}{62.3}\right)\right]^{1/2} \qquad \Psi = \frac{73}{\sigma_s}\left[\mu_\ell \left(\frac{62.3}{\rho_\ell}\right)^2\right]^{1/3}$$

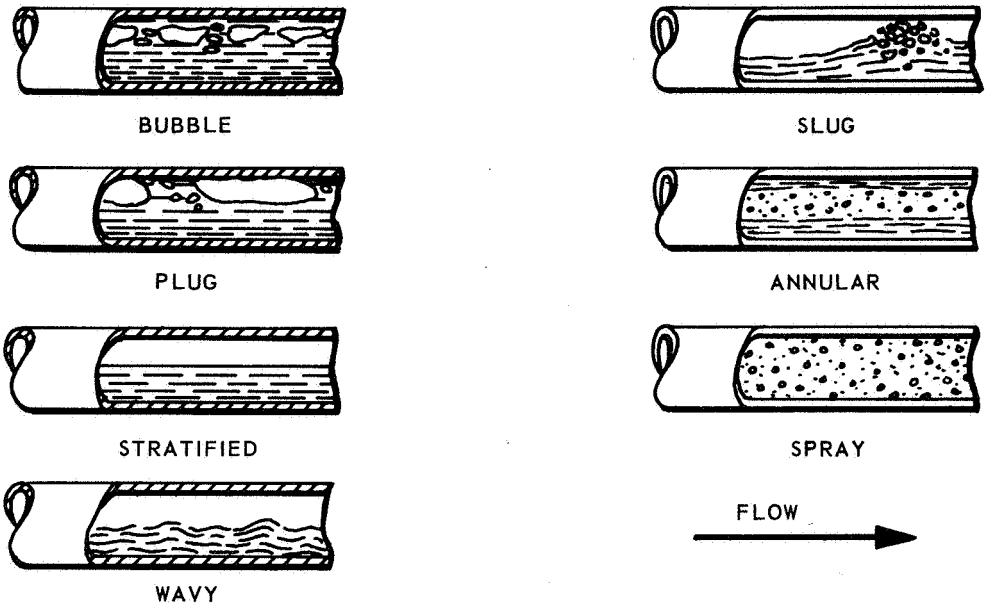


Fig. B-1 Flow Patterns

Table B-1

SYMBOL IDENTIFICATION (FLOW GEOMETRY MAPS)

⊙	WAVY	▽	SPRAY ANNULAR
●	SLUG-WAVY	▼	SPRAY
▲	WAVY-ANNULAR	×	SLUG
△	SEMI-WAVY-ANNULAR	+	BUBBLE
⊡	ANNULAR	⊕	STRATIFIED
■	SEMI-ANNULAR	⊞	PLUG

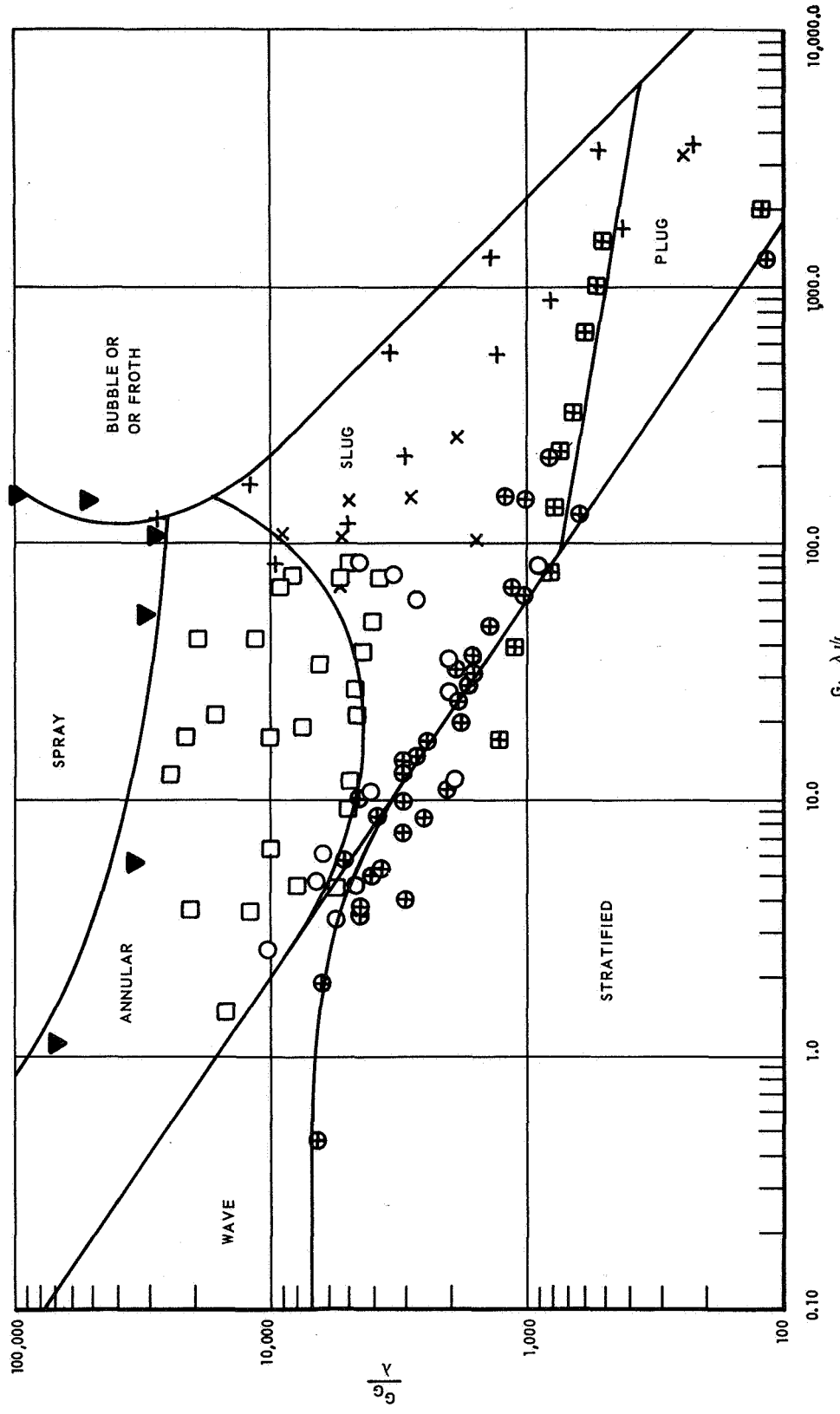


Fig.B-2 Baker Correlation With Adiabatic Data

where ρ_g and ρ_ℓ are the gas and liquid densities, μ is liquid viscosity, and σ_s is liquid surface tension.

As indicated, there is excellent correlation between the data and the Baker flow map. Kordyban (Ref. 6) has extended Baker's correlation to single-component adiabatic two-phase flow in the plug-flow region. The flow correlation reported has confirmed the basic similarity of one- and two-component adiabatic two-phase flows and has verified the applicability of the correlations originally developed for two-component flows.

Relatively few attempts have been made to extend Baker's correlation to diabatic evaporating two-phase flow. Efforts in this report to extend the diabatic correlation have been hampered by a lack of visual-observation data. Some data for diabatic single-component evaporating flow have been obtained from Refs. 7 and 8; these have been plotted in Fig B-3.This graph reveals that the flow correlation holds true only for annular flow, even though numerous flow geometries were observed. Bronson (Ref. 9) has indicated that it is permissible to apply the Baker correlation to the diabatic flow of liquid hydrogen. However, no data were presented to substantiate his claims.

The lack of correlation between diabatic data and an adiabatic flow map is not surprising. For the case of diabatic evaporating flow, both heat flux and heating length affect the flow pattern; the result is that the flow is much more complicated than in the adiabatic case. A major effect of heat addition is the generation of large amounts of vapor, with resulting acceleration forces on the flow. Since the vapor volume of the fluid is increasing, the flow patterns and transitions can be expected to differ from those of an adiabatic flow. This

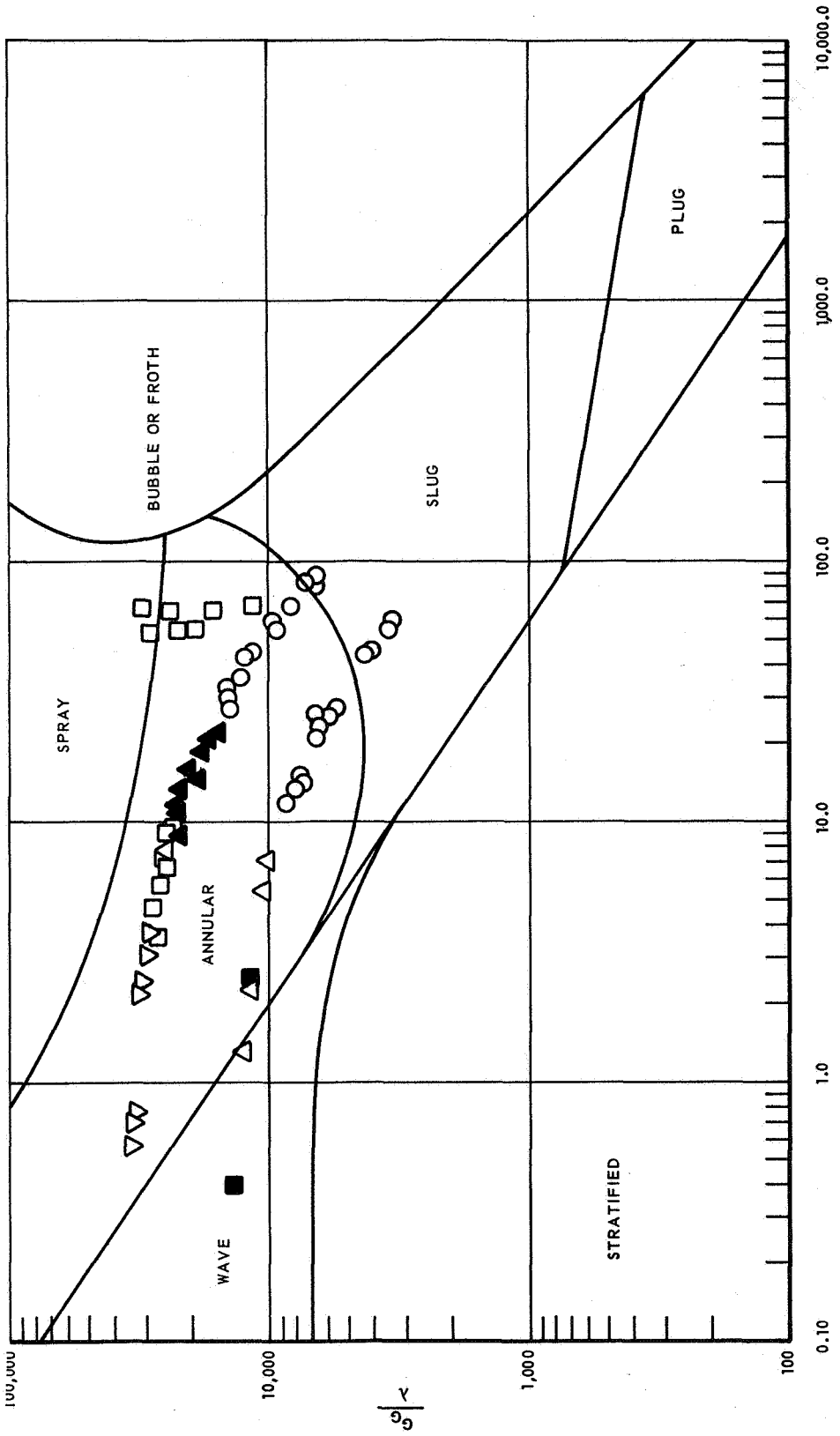


Fig. B-3Baker Correlation With Diabatic Data

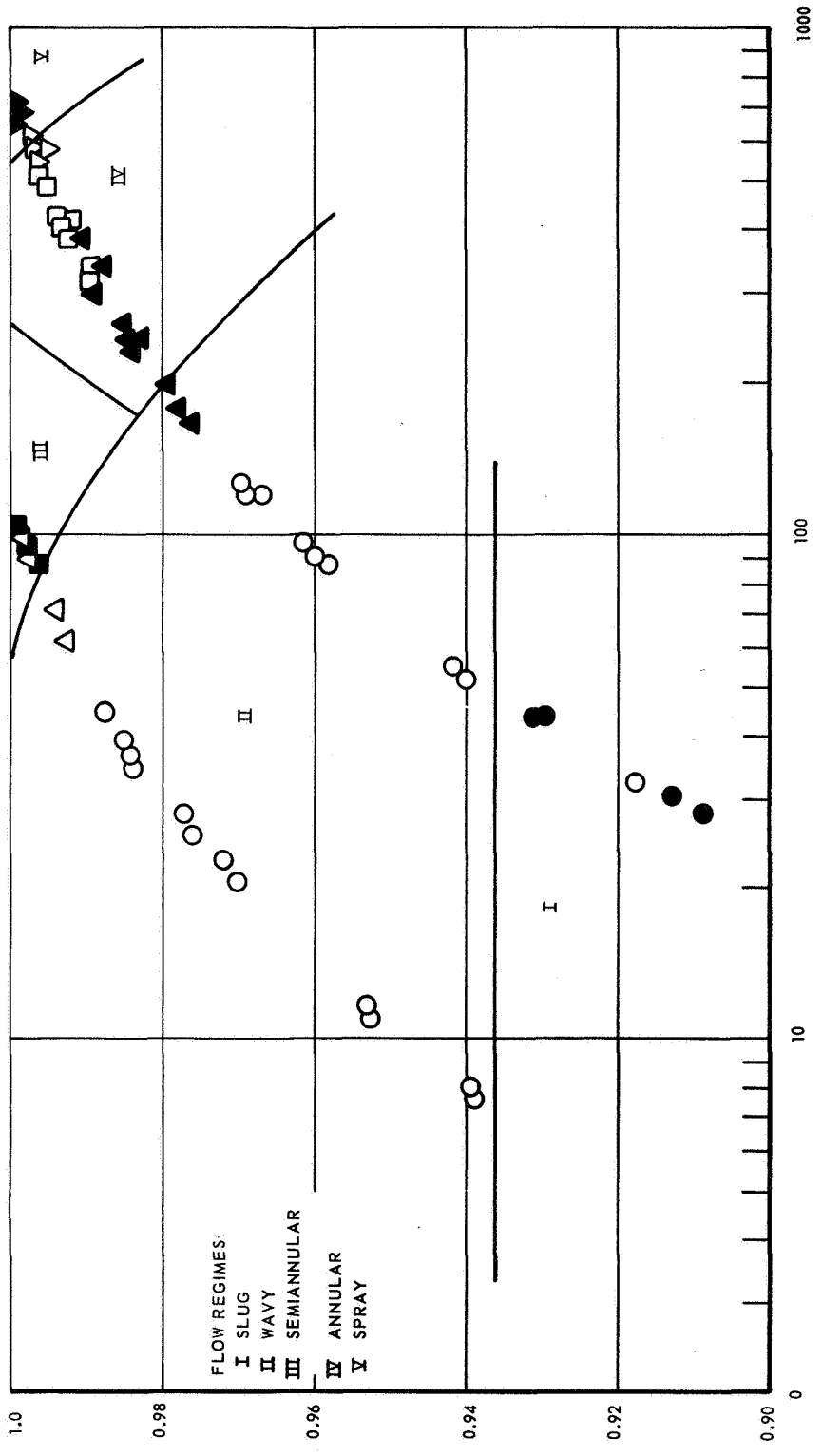


Fig. B-4 Flow Map for Diabatic Two-Phase Flow

vapor acceleration is thought to be the controlling factor in the formation of single-component diabatic two-phase flow patterns.

To account for vapor generation in diabatic flow, a flow map (Fig B-4) based on the parameters of volume flow fraction and Froude number has been developed in Refs. 8 and 10. It was felt that these two parameters would take into account the effects of flow acceleration. These parameters are nondimensional and therefore have the advantage of more general applicability than Baker's parameters.

B.2.2 Estimate of Tank Pressure Response

Using the results of the tank fill analysis (described in Section 4 along with appropriate simplifying assumptions, a simplified set of equations were obtained which can be solved by hand to yield an approximation to the tank pressure response during fill. The simplified model is based on the following assumptions:

- Liquid which enters the tank is saturated and vaporized instantaneously, the temperature of the vapor then being raised instantaneously to that of the bulk of the ullage vapor.
- The quality history at the inlet is given by $X = e^{-at^*}$, where the term a represents a dimensionless constant.
- There is no venting.
- There is no heat transfer between the tank wall and the ullage vapor.
- The dimensionless fill rate is constant.

With these assumptions, the dimensionless pressure response may be calculated from Eq. (1)*:

$$\frac{dp^*}{dt^*} = \frac{\dot{m}_\ell^*}{\left(1 - \frac{R}{C_{p_v}}\right)} \left\{ \frac{1}{\frac{1}{T_i^*} - \frac{R}{C_\ell \Delta} \ln\left(\frac{R T_i p^*}{p_i v_\ell}\right)} - \frac{C_\ell}{C_{p_v}} \Delta \left(1 - e^{-at^*}\right) \right\} \qquad \text{(B-1)}$$

This expression must be integrated numerically, but the calculation is relatively

* Symbols are defined in Appendix C and Vol. IV.

simple and can be accomplished without the use of a computer. As an example, a solution was obtained for hydrogen, assuming the following conditions:

$$p_i = 14.7 \text{ psia}$$
$$T_i = 540^{\circ}R$$
$$a = 7 \times 10^5$$
$$\dot{m}_f^* = 10^3$$

The simplified model assumed is not valid when the gas temperature nears the saturation temperature, since there is not sufficient heat transfer to vaporize all the liquid as it enters the tank. For this reason, Eq. B-1 is integrated only until the ullage vapor temperature is equal to the saturation temperature. The resulting pressure history is shown in Fig. B-5. As the ullage vapor temperature approaches the saturation temperature, the pressure will start to increase as indicated by the dashed line, since heat transfer from the tank wall to the vapor becomes more significant.

Due to the influence of the size of incoming liquid droplets on liquid evaporation rates and the resultant pressure response (as discussed in Sections 10 and 11), the critical assumption in this analysis is that incoming liquid droplets are vaporized instantaneously. This assumption implies that the initial rate of pressure rise indicated on Fig. B-5 is that which is approached when the size of the incoming droplets approaches zero. For this case Eq. (B-1) provides a simple means of estimating the initial tank pressure response.

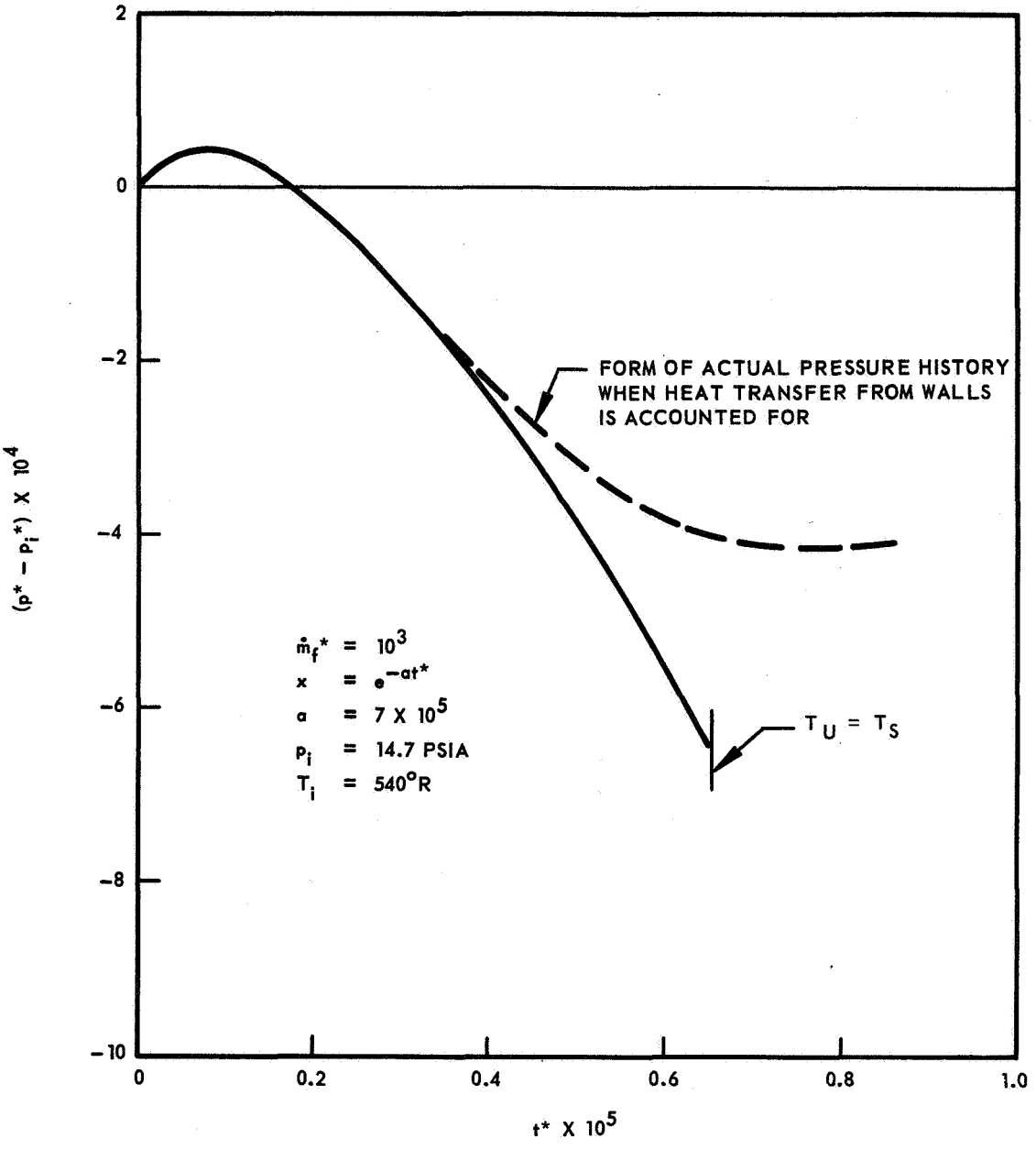


Fig. B-5. Receiver Tank Pressure With Hydrogen

INDEX

Section			Page
		FOREWORD	v
1		INTRODUCTION	1
	1.2	Task Summary	2
2		SUMMARY OF RESULTS	5
	2.1	Transfer Line Chilldown	6
	2.2	Tank Fill Thermodynamics	6
	2.3	Thermodynamic Analyses of a Complete Fill System	9
	2.4	Test Program	11
3		TRANSFER LINE ANALYSES	15
4		TANK FILL ANALYSES	17
5		DIMENSIONAL ANALYSIS	19
6		COMPUTER PROGRAMMING	21
7		MODELING LAWS	23
	7.1	Tank Fill Modeling	23
	7.2	Line Chilldown Modeling	28
	7.3	"Long" Transfer Line	29
8		FLOW PHENOMENA TESTING	31
	8.1	Quasi-Steady-State Tank Fill Tests	33
	8.1.1	Photographic Coverage	39
	8.1.2	Results of Quasi-Steady-State Fill Tests	44
	8.1.2.1	Tests Prior to Installation of Void Fraction Meter	44
	8.1.2.2	Tests Using Liquid Volume Fraction Meter	73

Section			Page
8.2		Comparison of Analytical Predictions with Experimental Data	79
	8.2.1	Tank Pressure Response	79
	8.2.2	Ullage Vapor Temperature Distribution	90
8.3		Transfer Line Tests	95
	8.3.1	Instrumentation	106
	8.3.2	Test Procedure	107
	8.3.3	Test Results	108
	8.3.3.1	Pressure and Flow Fluctuations	110
	8.3.4	Comparison of Analytical Predictions with Experimental Data	121
	8.3.4.1	Chilldown of 28-foot Line	122
	8.3.5	Correlation of NBS Data for a 200-foot Line	133
9		SCALING-LAW VERIFICATION AND COMPLETE SYSTEM TESTS	153
9.1		Transient Fill Tests with a Coupled Tank and Transfer Line	153
	9.1.1	Coupled Line and Tank Tests - Small-Size Apparatus	154
	9.1.2	Coupled Line and Tank Tests - Large-Size Apparatus	164
9.2		Correlation of Data for Coupled Line and Tank Tests	178
	9.2.1	Correlation of Data with Receiver Tank Analysis	178

Section			Page
	9.2.2	Selection of Characteristic Droplet Diameter	194
	9.2.3	Correlation of Data with Complete Fill System (CFS) Computer Program	198
	9.2.3.1	Small-Size Apparatus	198
	9.2.3.2	Large-Size Apparatus	201
10		IMPLOSION PREVENTION TECHNIQUES	211
10.2		Test Data Correlation	220
10.2.1		Screen Tests	220
10.2.2		Baffle Tests	227
10.3		Five-Foot-Diameter Tank Tests	234
10.4		Test Data Correlation	239
10.4.1		Liquid Nitrogen Tests	239
10.4.2		Liquid Hydrogen Tests	246
11		CONCLUSIONS	253
11.1		Transfer Line Thermodynamics	253
11.2		Tank Fill Thermodynamics	254
11.3		Complete Fill System Thermodynamics	255
11.4		Implosion Prevention Technique	255
12		REFERENCES	257
APPENDIX A		CALIBRATION OF LIQUID VOLUME FRACTION METER	259

Section			Page
APPENDIX B		LITERATURE SURVEY AND PRELIMINARY CALCULATIONS	273
	B.1	Literature Survey	273
	B.2	Preliminary Calculations	274
	B.2.1	Two-Phase Flow Maps	274
	B.2.2	Estimate of Tank Pressure Response	283
INDEX			287
ILLUSTRATIONS			291
TABLES			301

ILLUSTRATIONS

Figure		Page
1	Sequence of Tank Fill Conditions	20
2	Fill Rates Required to Simulate Full-Size Tanks	24
3	Vent Rates Required to Simulate Full-Size Tanks	25
4	Fill-Line Diameter Required to Simulate Full-Size Tanks	26
5	Test Setup for Quasi-Steady Flow Tests	34
6	Transparent 2-ft-Diameter Test Sphere	35
7	Transparent Tank Ready for Instrumentation	36
8	Viewing and Void Fraction Measurement Section	38
9	Early Version of Pre-Inlet Section	40
10	Image in Spherical Liquid Droplet	42
11	Photographic and Lighting Setup	43
12	Flow Phenomena Test Setup	45
13	Liquid Flow Rates and Pressures	47
14	Center Line Temperatures	48
15	Off-Center Temperatures	49
16	Inside Wall Temperatures	50
17	Drop-Diameter Histogram for Post-Inlet Flow	51
18	Reduced Flow, Quality and Drop Velocity Data	52
19	Pre-Inlet Flow	57
20	Post-Inlet Flow	58

Figure		Page
21	Liquid Flowrate and Pressure Data	60
22	Center-Line Temperatures	61
23	Off-Center Temperatures	62
24	Inside Wall Temperatures	63
25	Liquid Flowrate and Pressure Data	64
26	Center-Line Temperatures	65
27	Off-Center Temperatures	66
28	Inside Wall Temperatures	67
29	Flow Rates and Pressure Data	68
30	Centerline Temperatures	69
31	Off-Center Temperatures	70
32	Inside Wall Temperatures	71
33	Pressure, Liquid Fraction and Flowrate - Run 3-30-3	74
34	Centerline Temperatures	76
35	Off-Center Temperatures	77
36	Inside Wall Temperatures	78
37	Comparison of Pressure Data with Predictions - Two-foot Transparent Tank	80
38	Comparison of Pressure Data with Predictions - Two-foot Transparent Tank	83
39	Comparison of Pressure Data with Predictions - Two-foot Transparent Tank	84

Figure		Page
40	Comparison of Pressure Data with Predictions - Two-foot Transparent Tank	85
41	Comparison of Pressure Data with Predictions - Two-foot Transparent Tank	86
42	Comparison of Pressure Data with Predictions - Two-foot Transparent Tank	87
43	Comparison of Pressure Data with Predictions - Two-foot Transparent Tank	88
44	Comparison of Pressure Data with Predictions - Two-foot Transparent Tank	89
45	Comparison of Temperature Data with Predictions - Two-foot Transparent Tank	91
46	Comparison of Temperature Data with Predictions - Two-foot Transparent Tank	92
47	Comparison of Temperature Data with Predictions - Two-foot Transparent Tank	93
48	Assembly Drawing of One-Half Inch Transfer Line	96
49	Upstream Control Box	98
50	Standard Instrumentation Section	99
51	Liquid Volume Fraction Measuring Section, Flow Visualization section and Standard Instrumentation Section Used in 5½-foot Line Section	100
52	Location of Wall Thermocouples on Transfer Line Sections	101

Figure		Page
53	View of Supply Tank, Control Box and Two Transfer Line Sections	102
54	View of Inside of Control Box	102
55	Standard Transfer Line Instrumentation Station	103
56	Liquid Fraction Measurement and Flow Visualization Station	103
57	View of Assembled Transfer Line	104
58	Peak Line Pressures	113
59	Line Pressure Variation after Chilldown (Nominal 30 psig Tests	115
60	Line Pressure Variation after Chilldown (Nominal 10 psig Tests)	116
61	Chilldown Time vs Line Location	117
62	Measured and Calculated Wall Temperature Profiles with Saturated Liquid Nitrogen at a Driving Pressure of 44.5 psia	124
63	Measured and Calculated Wall Temperature Profiles with Subcooled Liquid Nitrogen at a Driving Pressure of 43.9 psia	125
64	Measured and Calculated Wall Temperature Profiles aith Saturated Liquid Nitrogen at a Driving Pressure of 24.7 psia	126
65	Measured and Calculated Wall Temperature Profiles with Subcooled Liquid Nitrogen at a Driving Pressure of 24.8 psia	127
66	Fluid Temperature History with Subcooled Liquid Nitrogen at a Driving Pressure of 24.8 psia	130

Figure		Page
67	Vapor Quality History with Subcooled Liquid Nitrogen at a Driving Pressure of 24.8 psia	132
68	Line Temperature History with Saturated Liquid Nitrogen at a Driving Pressure of 44.5 psia	134
69	Line Temperature History with Slightly Subcooled Liquid Nitrogen at a Driving Pressure of 43.1 psia	135
70	Line Temperature History with Subcooled Liquid Nitrogen at a Driving Pressure of 43.9 psia	136
71	Line Temperature History with Saturated Liquid Nitrogen at a Driving Pressure of 24.7 psia	137
72	Line Temperature History with Subcooled Liquid Nitrogen at a Driving Pressure of 24.8 psia	138
73	Line Temperature History with Subcooled Liquid Nitrogen at a Driving Pressure of 23.4 psia	139
74	Comparison Between Computed and Measured Line Temperature Histories with Saturated Liquid Nitrogen at a Driving Pressure of 2.5 Atm.	142
75	Comparison Between Computed and Measured Line Temperature Histories with Saturated Liquid Nitrogen at a Driving Pressure of 3.4 Atm.	143
76	Comparison Between Computed and Measured Line Temperatures Histories with Saturated Liquid Nitrogen at a Driving Pressure of 5.9 Atm.	144

Figure		Page
77	Comparison Between Computed and Measured Line Temperature Histories with Subcooled Liquid Nitrogen at a Driving Pressure of 4.2	145
78	Comparison Between Computed and Measured Line Temperature Histories with Subcooled Liquid Nitrogen at a Driving Pressure of 5.9 Atm.	146
79	Comparison Between Computed and Measured Line Temperature Histories with Saturated Liquid Hydrogen at a Driving Pressure of 5.1 Atm.	147
80	Comparison Between Computed and Measured Line Temperature Histories with Subcooled Liquid Hydrogen at a Driving Pressure of 2.5 Atm.	148
81	Comparison Between Computed and Measured Line Temperature Histories with Subcooled Liquid Hydrogen at a Driving Pressure of 5.9 Atm.	149
82	Comparison Between Computed and Measured Line Temperature Histories with Subcooled Liquid Hydrogen at a Driving Pressure of 11 Atm.	150
83	Complete System Test Setup - Small Size Apparatus	155
84	Inlet Configuration for Coupled Tests	156
85	Apparatus for Complete Fill System Tests - Small Size A Apparatus	157
86	Ullage Pressure and Supply Pressure Histories for Run 6-8-1	159

Figure		Page
87	Inlet Flowrate and Exit Quality Histories for Run 6-8-1	160
88	Transfer Line Static Pressures - Run 6-8-1	161
89	Transfer Line Fluid Temperatures-Run 6-8-1	162
90	Transfer Line Wall Temperatures - Run 6-8-1	163
91	Receiver Centerline Temperatures - Run 6-8-1	165
92	Receiver Off-Center and Wall Temperatures Run 6-8-1	166
93	Test Setup with Large Size Apparatus	167
94	Transfer Line Instrumentation - Large Size Apparatus	169
95	Five-foot Diameter Tank Prior to Installation in Test Chamber	170
96	Assembly of Three-Inch Transfer Line	171
97	Leak-Check of Three-Inch Transfer Line	172
98	Test Apparatus for Complete System Fill Tests - Large Size Apparatus	173
99	Instrumentation Location - Five Foot Diameter Tank	174
100	Comparison of Pressure Data with Predictions	180
101	Tank Wall Temperature Data	183
102	Comparison of Pressure Data with Predictions	184
103	Comparison of Pressure Data with Predictions	186
104	Comparison of Gas Temperature Data with Predictions	188
105	Comparison of Pressure Data with Predictions	189
106	Comparison of Pressure Data with Predictions	191
107	Gas Velocity Extrapolations	192

Figure		Page
108	Optimum Values of Characteristic Droplet Diameter vs Dimensionless Mass Flowrate	196
109	Liquid Volume Fraction History During Fill	199
110	Tank Pressure History During Fill	200
111	Predicted and Measured Dimensionless Mass Flowrates for Run 9-8-2	203
112	Measured and Predicted Ullage Pressure History for Run 9-8-2	204
113	Comparison of Predicted and Measured Tank Pressure Run 9-8-4	206
114	Predicted and Measured Tank Pressure for Run 9-11-1	207
115	Comparison of Predicted and Measured Tank Pressure Run 9-15-6	209
116	Sketches of Anti-Implosion Baffle and Anti-Vortex Screen	213
117a	Views of Anti-Implosion Baffle Mounted in Two-foot Tank	214
117b	View of Anti-Vortex Screen Mounted in Two-foot Tank	214
118	Comparison of Measured Pressure Responses with High Inlet Flowrates	216
119	Comparison of Measured Pressure Responses with Low Inlet Flowrates	217
120	Tank Wall Temperatures for Baffle Test - Run 4-4-67	219
121	Comparison of Pressure Data with Predictions - Two-foot Transparent Tank	221

Figure		Page
122	Comparison of Pressure Data with Predictions - Two-foot Transparent Tank	222
123	Comparison of Pressure Data with Predictions	224
124	Comparison of Pressure Data with Predictions	225
125	Comparison of Pressure Data with Predictions	226
126	Comparison of Pressure Data with Predictions	229
127	Comparison of Pressure Data with Predictions	230
128	Comparison of Pressure Data with Predictions	231
129	Comparison of Pressure Data with Predictions	232
130	Large Size Baffle Installation	235
131	Inlet Screen Attached to Instrument Probe	236
132	Inlet Baffle Attached to Instrument Probe	237
133	Instrument Probe Mounted on Tank Manhole Cover	238
134	Comparison of Pressure Data with Predictions for Run 9-11-1	240
135	Comparison of Pressure Data with Predictions for Run 9-11-2	241
136	Comparison of Gas Temperature Data with Predictions for Run 9-11-1	242
137	Comparison of Gas Temperature Data with Predictions for Run 9-11-1	243
138	Comparison of Pressure Data with Predictions for Run 9-20-3	244
139	Comparison of Pressure Data with Predictions for Run 9-15-1	247
140	Gas Velocity Extrapolations for Run 9-15-1	248
141	Comparison of Gas Temperature Data with Predictions for Run 9-15-1	250

Figure		Page
142	Comparison of Pressure Data with Predictions for Run 9-15-4	251
A-1	Schematic Diagram of Liquid Volume Fraction Measurement System	259
A-2	Arrangement of Detector, Source Tube and Shielding	261
A-3	Relationship Between Cadmium 109 Activity and High Voltage Setting	263
A-4	Cadmium 109 Spectrum with Ethanol	264
A-5	Schematic Diagram of Calibration Apparatus for Liquid Fraction Measurement System	268
A-6	Liquid Volume Fraction Meter Calibration Apparatus	269
A-7	Calibration of Volume Fraction Measurement System	270
A-8	Normalized Calibration Curve for Volume Fraction Measuring System	272
B-1	Flow Patterns	277
B-2	Baker Correlation with Adiabatic Data	278
B-3	Baker Correlation with Diabatic Data	280
B-4	Flow Map for Diabatic Two-Phase Flow	281
B-5	Receiver Tank Pressure with Hydrogen	285

TABLES

Table		Page
1	Summary of Computer Program Characteristics	7
1a	Test Program Summary	12
2	Comparison of Fluid Modeling Parameters	27
3	Summary of Quasi-Steady-State Tank Fill Tests	46
4	Summary of Small-Size Transfer Line Tests	109
5	Computed Fluid Phase Distribution at Chilldown	129
6	Test Conditions for NBS Transfer Line Tests	140
7	Summary of Large Size Tests	176
8	Summary of 60-inch Tank Tests	
9	Optimum Values of Characteristic Droplet Diameter	195
10	Summary of Small-Scale Tank Fill Tests with Baffle & Screen	215
B-1	Symbol Identification (Flow Geometry Maps)	277